CMES 2024 Symposium is supported by TUBITAK

BOOK OF FULL TEXT

ISBN-77733

8th International Conference on Computational Mathematics and Engineering Sciences

17 – 19 May 2024,
Şanlıurfa – Türkiye

Publish date: 16.05.2024

THE EIGHTH INTERNATIONAL CONFERENCE ON COMPUTATIONAL MATHEMATICS AND ENGINEERING SCIENCES (CMES-2024), ŞANLIURFA/TÜRKİYE, MAY 17-19, 2024

The **Eighth International Conference on Computational Mathematics and Engineering Sciences (CMES-2024)** will be held in Harran University from **17- to 19 May 2024 in Şanlıurfa, Türkiye.** It provides an ideal academic platform for researchers and professionals to discuss recent developments in both theoretical, applied mathematics and engineering sciences. This event also aims to initiate interactions among researchers in the field of computational mathematics and their applications in science and engineering, to present recent developments in these areas, and to share the computational experiences of our invited speakers and participants.

The Organizing Committee

Committee Chairs

Hasan Bulut, Fırat University, Türkiye
Zakia Hammouch, Ecole Normale Superierue de Meknes, Moulay Ismail University, Morocco
Ercan Çelik, Kyrgyz-Turkish Manas University, Kyrgyzstan
Haci Mehmet Baskonus, Harran University, Türkiye

MESSAGE FROM THE GENERAL CHAIRS

Dear Conference Attendees,

We are honored to welcome you to the **Eighth International Conference on Computational Mathematics and Engineering Sciences (CMES-2024)** at Harran University from 17 to 19 May 2024 in Şanlıurfa City, Türkiye.

CMES, founded in 2016 at Faculty of Science and Techniques Errachidia Moulay Ismail University Morocco is an annual intarnational conference, which was very successful in the past years by providing opportunities to the participants in sharing their knowledge and informations and promoting excellent networking among different international universities. This year, the conference includes 200 extended abstracts, several submissions were received in response to the call for papers, selected by the Program Committee. The program features keynote talks by distinguished speakers such as:

Dumitru Baleanu from Institute of Space Sciences, Magurele-Bucharest, Romania; **Yusif Gasimov** from Azerbaijan University, Azerbaijan; **Naim L. Braha** from University of Prishtina, Kosovo; **Ekrem Savas** from Usak University, Türkiye; **Mehmet Emir Köksal** from Ondokuz Mayıs University, Türkiye; **Amdulla O. Mekhrabov** from Azerbaijan Technical University, Azerbaijan. The conference also comprises contributed sessions, posters sessions and various research highlights.

We would like to thank the Program Committee members and external reviewers for volunteering their time to review and discuss submitted abstracts. We would like to extend special thanks to the Honorary, Scientific and Organizing Committees for their efforts in making CMES-2024 a successful event. We would like to thank all the authors for presenting their research studies during our conference. We hope that you will find CMES-2024 interesting and intellectually stimulating, and that you will enjoy meeting and interacting with researchers around the world.

.

***Hasan Bulut*,**

Firat University, Elazig, Türkiye.

Zakia Hammouch,

ENS Meknes, Moulay Ismail University Morocco

TOPICS

Control Theory,
Game Theory,
Applied Mathematics,
Financial Mathematics,
Artificial Intelligence,
Education Sciences,
Engineering Sciences,
Computer Science,
Information Technology,
Geometry and Its Applications,
Analysis and Its Applications,
Statistics and Its Applications,
Algebra and Its Applications,
Topology and Its Application,
Chaos and Dynamical Systems,
Cryptography and its Applications,
Fractional Calculus and Applications,
Economics and Econometric Studies,
Electrical and Electronic Engineering,
Defense industry and applications,
Mathematical Biology,
Computational Epidemiology,
Mathematical Chemistry,
Mathematics Education and Its Applications,
Numerical Methods and Scientific Programming,
Linearand Nonlinear programming and Dynamics,
Modeling of Bio-systems for Optimization and Control,
Ordinary, Partial, Stochastic and Delay Differential Equations,
Computational Fluids mechanics. Heat and Mass Transfers,
Earth Sciences,
Applied Sciences

COMMITTEE CHAIRS

Prof.Dr.Hasan Bulut, Firat University, Elazığ, Türkiye

Prof.Dr.Zakia Hammouch, ENS Meknes, Moulay Ismail University, Morocco

Prof. Dr. Ercan Çelik, Kyrgyz-Turkish Manas University, Kyrgyzstan

Prof.Dr.Haci Mehmet Baskonus, Harran University, Türkiye

COMMITTEE CO-CHAIRS

Prof.Dr. Carlo Cattani, Tuscia University, Viterbo, Italy

Prof.Dr. Mohammed Ouazzani Jamil, University Privee of Fez, Morocco

Prof. Dr. Hassan Qjidaa, Sidi Mohammed Ben Abdellah University, Fes Morocco

Prof. Dr. El Mehdi El Khattabi, Moulay Ismail University Morocco

Assoc. Prof. Dr. Tolga Aktürk, Ordu University, Türkiye

HONORARY COMMITTEE

Prof. Dr. Mehmet Tahir Güllüoğlu, Rector of Harran University, Sanliurfa, Türkiye
Prof. Dr. Fahrettin Göktaş, Rector of Firat University, Elazığ, Türkiye
Prof. Dr. Alpaslan Ceylan, Rector of Kyrgyz-Turkish Manas University, Kyrgyzstan
Prof. Dr. Vilayet M. Veliyev, Rektör of Azerbaijan Technical University, Baku, Azerbaijan
Prof. Dr. Ahmed Mouchtachi, Rector of Moulay Ismail University, Meknes Morocco
Prof. Dr. Mohammed Aziz Lahlou, President of Universite Privee of Fes, Morocco
Prof. Dr. Abdelmjid Abourriche, Vice Rector of Moulay Ismail University, Meknes Morocco
Prof. Dr. Ouazzani Jamil Mohamed, Vice President of Universite Privee of fez, Morocco
Dr. Saadat Aliyeva, Rector of Azerbaijan University, Baku, Azerbaijan
Prof. Dr. Hamdullah Şevli, Rector of Van Yüzüncü Yıl University, Türkiye
Prof. Dr. Hüseyin Yaratan, Rector of Final International University, Gime, Cyprus
Prof. Dr. Ekrem Savaş, Rectorof Uşak University,Türkiye
Prof. Dr. Bülent Çakmak, Rector of Erzurum Technical University, Erzurum, Türkiye
Prof. Dr. Orhan Baş, Rector of Ordu University, Ordu, Turkey
Prof. Dr. Subhan N. Namazov, Vice-rector .Azerbaijan Technical University, Baku, Azerbaijan
Prof. Dr. Etibar Penahh, Baku State University, Baku, Azerbaijan
Prof. Dr. Necdet Bildik, Retired Faculty Member
Prof. Dr. Mahmut Ergüt, Namık Kemal University, Tekirdağ, Türkiye
Prof. Dr.Yusif Gasimov, Azerbaijan University, Baku, Azerbaijan
Ibrahim Taşel, Final International University, Gime, Cyprus
Şevket Ertem, Final International University, Gime, Cyprus
Veysel Demirci, (Chairman of the board of Ziver Holding)
İzzettin Toraman, (Chairman of the board of Toraman Tekstil)
Selahattin Yıldız, (Chairman of the board of Hasyil Energy)

ORGANIZING COMMITTEE

Prof. Dr. Hasan Bulut, (Chair), Fırat University, Türkiye
Prof. Dr. Zakia Hammouch, (Chair), China Medical University, Taiwan
Prof. Dr. Ercan Çelik, (Chair), Kyrgyz-Turkish Manas University, Kyrgyzstan
Prof. Dr. Haci Mehmet Baskonus, (Chair), Harran University, Türkiye
Prof. Dr. Ouazzani Jamil Mohammed, (Co-Chair), Universite Privee de Fes Morocco
Prof. Dr. Hassan Qjidaa, (Co-Chair), Sidi Mohammed Ben Abdellah University, Fes Morocco
Prof. Dr. Carlo Cattani, (Co-Chair), Tuscia University, ItalyAssoc.
Prof. Dr. El Mehdi El Khattabi, (Co-Chair), Moulay Ismail University Morocco
Assoc. Prof. Dr. Tolga Aktürk, (Co-Chair), Ordu University, Türkiye
Prof. Dr. Amdulla O. Mekhrabov, Director, Azerbaijan Technical University, Azerbaijan
Prof. Dr. Mikail Et, Fırat University, Türkiye
Prof. Dr. Mahmut Işık, Harran University, Türkiye
Prof. Dr. Vedat Asil, Fırat University, Türkiye
Prof. Dr. Fevzi Erdoğan, Yüzüncüyıl University, Türkiye
Prof. Dr. Alaattin Esen, İnönü University, Türkiye
Prof. Dr. Sevilay Kırcı Serenbay, Harran University, Türkiye
Assoc. Prof. Dr. Mahmut Modanlı, Harran University, Türkiye
Assoc. Prof. Dr. Hacer Şengül Kandemir, Harran University, Türkiye
Assis. Prof. Dr. Mustafa Çağrı GÜRBÜZ, Harran University, Türkiye
Assis. Prof. Dr. Işıl BOZKURT, Harran University, Türkiye
Assoc. Prof. Dr. Fatih Özbağ, Harran University, Türkiye
Assis. Prof. Dr. N. Feyza Yalçın, Harran University, Türkiye
Assoc. Prof. Dr. Kemal Toker, Harran University, Türkiye
Res. Assist. Ömer Faruk BOYUN, Harran University, Türkiye
Assoc. Prof. Dr. Gülnur Yel, Final International University, Girne, Cyprus
Assoc. Prof. Dr. Gülay Oğuz, Harran University, Türkiye
Dr. Faculty Mem. Muhammed Yiğider, Erzurum Technic University, Türkiye

LANGUAGE EDITORIAL COMMITTEE

Suheyla Demirkol Orak (Firat University, Elazıg, Türkiye)

International Communications Consultant

Rengin AK, Kirklareli University, Kırklareli, Türkiye
ikmet Kemaloğlu, Fırat University, Elazığ, Türkiye
İlkay Açıkgöz Erkaya, Ahi evran University, Türkiye
M. Evren Aydın, Fırat University, Elazığ, Türkiye

PROCEEDINGS

Full version of submitted papers will be published in Special Volumes of reputed journals. Procedure, Guidelines and Checklist for the preparation and submission of papers to the Proceedings of CMES-2024 can be found in the journals websites. The journals in which selected and peer-reviewed full papers of CMES-2024 will be published are as follows:

1. BOOK OF ABSTRACTS [Free of charge]
If Authors submit ABSTRACT TEXTS, then, after getting referees evaluations for these abstracts, they will be published in ABSTRACT PROCEEDING BOOK of CMES-2024. For FULL TEXT PAPERS, Authors have to submit their FULL TEXT PAPERS online via submission system of CMES-2024. These FULL TEXT PAPERS will be published in FULL TEXT PROCEEDING BOOK of CMES-2024 after getting at least two positive reports.

2. CONFERENCE PROCEEDINGS [Free of charge]
At the beginning, if Authors submit FULL TEXT PAPERS, then, after getting at least two positive referee reports, FULL TEXT PAPERS will be published in FULL TEXT PROCEEDING BOOK of CMES-2024 with ISBN:77733 number. Therefore, Abstracts of these FULL TEXT PAPERS will **NOT** be published in ABSTRACT PROCEEDING BOOK of CMES-2024.

3. FRACTAL AND FRACTIONAL JOURNAL [SCI-E],
Selected papers from CMES-2024 will be published in a special issue dedicated to the Conference entitled "**Feature Papers for Mathematical Physics Section".**
https://www.mdpi.com/journal/fractalfract/special_issues/1TAP5BBZ45
This journal is indexed by SCI-E.

4. PROCEEDINGS OF THE INSTITUTE OF MATHEMATICS AND MECHANICS [E-SCI]
Selected papers from CMES-2024 will be published by https://proc.imm.az/special/

This journal is indexed by E-SCI.

5.TURKISH JOURNAL OF SCIENCE, [FREE]
Participants of CMES 2024 can submit their good quality papers to Turkish Journal of Science. After the peer review process, the papers will be published at TJOS. The authors must write "CMES 2024" as comments to the editor.
(Editor in Chief: Dr. Ahmet Ocak AKDEMİR) For on-line submission: https://dergipark.org.tr/tr/pub/tjos

6.TURKISH JOURNAL OF INEQUALITIES, [FREE]
"Participants of CMES 2024 can submit their good quality papers to Turkish Journal of Inequalities. Selected papers will be published at TJI after the peer review process. The participants can send their papers to erhanset@tjinequality.com. The authors must write "CMES 2024" as the subject.
(Editor in Chief: Prof. Dr. Erhan SET)
http://tjinequality.com/

7. MATHEMATICS IN NATURAL SCIENCE (MNS)
Authors can submit their full text paper directly to the journal by using the following link
https://www.isr-publications.com/mns

8. MATHEMATICS IN ENGINEERING, SCIENCE AND AEROSPACE (MESA), [FREE, SCOPUS]
"Selected papers will be published after peer review in the Journal of Mathematics in Engineering, Science and Aerospace (MESA)"
(Editor in Chief: Prof. Seenith Sivasundaram)
http://nonlinearstudies.com/index.php/mesa

9. APPLIED MATHEMATICS AND NONLINEAR SCIENCES, [SCOPUS]
Participants of CMES 2024 can submit their high quality full text papers to Applied Mathematics and Nonlinear Sciences by selecting CMES-2024 under the Select Article Type Menu.
https://www.editorialmanager.com/amns/default.aspx

10. MATHEMATICAL MODELLING AND NUMERICAL SIMULATION WITH APPLICATIONS (MMNSA), [TR DİZİN]
The Special Issue on "Advanced Methods of Modelling and Numerical Computation in Science and Engineering". Authors can submit their full text paper directly to the journal by using the information provided in the following link
https://mmnsa.org/index.php/mmnsa/special_issues/SI-CMES2023

11. SYMMETRY [SCI-E] ;
SPECIAL ISSUE "ADVANCES IN MATRIX TRANSFORMATIONS, OPERATORS AND SYMMETRY"
Authors can submit their full text paper directly to the journal by using the following link
https://www.mdpi.com/journal/symmetry/special_issues/Advances_Matrix_Transformations_Operators_Symmetry

12. YUZUNCU YIL UNIVERSITY JOURNAL OF THE INSTITUTE OF NATURAL AND APPLIED SCIENCES (TR-Dizin)
Authors can submit their full text paper directly to the journal by using the following link
https://dergipark.org.tr/tr/pub/yyufbed

13. PEDAGOGICAL PERSPECTIVE (PEDPER)
Pedagogical Perspective **(PedPer)** is an international, double blind reviwing, non-profit, professional scientific journal. PedPer is a journal that accepts manuscripts related to pedagogy and education. http://pedagogicalperspective.com/

PLENARY & INVITED TALKS

Generalised fractional operators with some applications

Dumitru Baleanu
Lebanese American University, Department of Computer Science and Mathematics, Beirut, Lebanon
Institute of Space Sciences, Magurele-Bucharest, Romania
dumitru.baleanu@lau.edu.lb

Abstract: We know that fractional calculus deals with the study of so-called fractional order integral and derivative operators over real or complex domains, and their applications. However, a clear definition of a generalized fractional operator is needed. In this talk I will concentrate on solving this important issue and provide some real-world applications.

Keywords: fractional calculus, generalised fractional operators

References

[1] Al-Refai, M, Baleanu, D (2022), On an extension of the operator with Mittag-Leffler kernel, Fractals, 30(5): 2240129.
[2] Anwar A, Baleanu D (2023), On two backward problems with Dzherbashian-Nersesian operator, 8(1): 887-904, AIMS Mathematics.

ON SOME INVERSE PROBLEMS IN UNTRADITIONAL FORMULATION

Yusif Gasimov
Azerbaijan University, Baku, Azerbaijan
yusif.gasimov@au.edu.az

The talk is devoted to the solution of some type of inverse problems. Usually, when solving inverse problems one has to recover the equation or boundary conditions describing the process using given additional conditions. As such conditions usually some signals received from the object may be taken. These signals in mathematical formulation are called spectral data that must satisfy some conditions. The searched objects are some functions, coefficients in the equations or in the boundary conditions.

The problems considered in the talk are different from the traditional ones. Here we consider the inverse problems for some operators and the searched object are not functions as usual but are domains. We try to identify the domain where the process is going on. To solve such problems one meets some serious mathematical problems. The first problem is the choice of additional conditions – spectral data that satisfies all necessary conditions and allows to find the domain. The second problem is to construct a constructive mathematical apparatus that allows to work with functionals of the domains. To do this the space of the domains should be developed with all necessary mechanisms.

In the work the space of the convex bounded domains is constructed and a scalar product is defined there. Then the definition of the s-functions expressed by the spectral data of the Schrodinger operator is given. A scheme is proposed to solve the following inverse spectral problem with respect to domain: Define a domain on the boundary of which the s-functions of the Schrodinger operator are equal to the given functions.

REFERENCES

1. Niftiyev A.A. Gasimov Y.S. (2004). Control by Boundaries and Eigenvalue Problems with Variable Domain. Baku University Publishing, 185p.
2. Gasimov, Y.S. (2008). Some shape optimization problems for eigenvalues. *Journal of Physics A: Mathematical and Theoretical*, *41*(5), 055202.
3. Gasimov, Y.S. (2013). On a shape design problem for one spectral functional. *Journal of Inverse and Ill-Posed Problems*, *21*(5), 629-637.

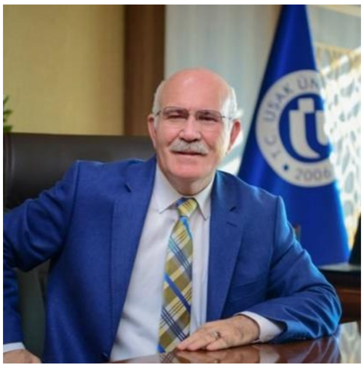

THE SECRET BEHIND WESTERN CIVILIZATION: ISLAMIC SCIENCE

Ekrem Savas[1]

[1] Department of Mathematics, Usak University, Usak, Turkey

ekremsavas@yahoo.com,

Abstract

In this study; what is the place of the Islamic Cultural world in the history of sciences? I will try to explain this. I will also explain that Western civilization is the continuation of Islamic civilization under different geographical and economic conditions.

Keywords: Islamic culture; Western civilization

REFERENCES

1. Fuat sezgin, İslam Bilim tarihi, Timaş yayınları, 2015.

Fractional Order Thinking and Proportional-Integral-Derivative (PID) Control

Mehmet Emir KÖKSAL
Department of Mathematics, Ondokuz Mayıs University, 55139 Atakum, Samsun, Turkey
mekoksal@omu.edu.tr

Abstract: The subject of fractional calculus has become very well-known and popular in recent decades. This is because fractional-order models simulate the properties of real systems better than whole order models. Therefore, fractional calculus is used as a powerful and important tool for defining, investigating, analyzing, solving, and understanding many different chemical, engineering, mathematical, physical, statistical, and social problems in real life. In this lecture, the basic concepts of fractional calculus and various common definitions of fractional integration and differentiation are introduced. Various applications in science and engineering are mentioned. In particular, the design of fractional-order proportional integral derivative controllers is emphasized. Mathematical formulations of five design specifications corresponding to the 3D drawing are presented with program implementations. The system design specifications of phase margin, gain margin, phase flatness, low-frequency output noise suppression, and high-frequency noise suppression are considered for designing controllers using the presented 3D graphical method. Each specification is represented by some surfaces that define the boundaries of the permissible parameters of PID control coefficients. The requirements are mapped in the 3D Euclid space by 3D surfaces and/or lines so that the proportional, integral, derivative control coefficients can be optimally chosen to meet the given specifications in an optimum way and to allow trade-off or compromise.

Keywords: Fractional calculus, Fractional order modeling, PID controller, FOPID controller, 3D plots.

References:

1. M.E. Koksal, Time and frequency responses of non-integer order RLC circuits, AIMS Mathematics, 4 (1) 61-75, 2019
2. M.E. Koksal, Stability analysis of fractional differential equations with unknown parameters, *Nonlinear Analysis: Modeling and Control,* 24 (2) 224-240, 2019
3. M.E. Koksal, Explicit commutativity conditions for second-order linear time-varying systems with non-zero initial conditions, *Archives of Control Sciences,* 29 (3) 413-432, 2019

Design and Development of Advanced Magnetic Materials via Computational Material Science for Technological Applications

Amdulla O. Mekhrabov[1]* and M. Vedat Akdeniz[2]

[1]Novel Materials and Nanotechnologies Institute, Azerbaijan Technical University (AzTU), Az1073, Baku, Azerbaijan, *emdulla.mehrabov@aztu.edu.az
[2]Novel Alloys Design and Development Lab (NOVALAB), Department of Metallurgical and Materials Engineering (Met E), Middle East Technical University (METU), 06800-Ankara, Turkey

Abstract: The presentation will be an overview of the main research thrusts at the "Novel Alloys Design and Development Lab" (NOVALAB) of MetE-METU and at "Novel Materials and Nanotechnologies" Institute of Azerbaijan Technical University (AzTU) in the designing, development and utilizations of advanced multicomponent magnetic materials for technological applications. Fundamental principles and main aspects of ***Computational Materials Science (CMS)*** for ***modeling and simulation based "alloy design"*** which has been developed over 45 years by Prof. Mekhrabov, will be presented.

Keywords: Modeling, Simulation, Soft Magnetic Materials, Metallic Glasses, Nanostructured alloys, Glass Formation Ability, Monte Carlo, Reverse Monte Carlo, Molecular Dinamics

REFERENCES

1. Aykol M., Mekhrabov A.O. and Akdeniz M.V., Nano-scale Phase Separation in Amorphous Fe-B Alloys: Atomic and Cluster Ordering, Acta Mater., vol. 57, 171- 81, 2009.
2. Aykol M., Akdeniz M.V. and Mekhrabov A.O., Solidification behavior, glass forming ability and thermal characteristics of soft magnetic Fe-Co-B-Si-Nb-Cu bulk amorphous alloys, Intermetallics, vol. 19, 1330-1337, 2011.
3. M.V. Akdeniz and A.O. Mekhrabov, Size dependent stability and surface energy of amorphous FePt nanoalloy, J. of Alloys and Comp., vol. 788, 787-798, 2019.

Approximation by modified (p, q)-gamma-type operators

Naim Latif Braha
nbraha@yahoo.com
Department of Mathematics and Computer Sciences, University of Prishtina, Avenue Mother Teresa,
No-5, Prishtine, 10000, Kosova and
ILIRIAS Research Institute, Janina, No-2, Ferizaj, 70000, Kosovo

Abstract
The main object of this paper is to construct a new class of modified (p, q)-Gamma-type operators. For this new class of operators, in section one, the general moments are find; in section two, the Korovkin-type theorem and some direct results are proved by considering the modulus of continuity and modulus of smoothness and their behavior in Lipschitz-type spaces. In section three, some results in the weighted spaces are given, and in the end, some shape-preserving properties are proven.

Keywords: Modified (p, q)-Gamma-type operators; Modulus of continuity; Shape-preserving approximation

References

1. Altomare, F., Campiti, M.: Korovkin-Type Approximation Theory and Its Application. Walter de Gruyter Studies in Math., vol. 17. de Gruyter & Co., Berlin (1994)

2. Atlihan, O.G., Unver, M., Duman, O.: Korovkin theorems on weighted spaces: revisited. Period. Math. Hung. 75(2), 201–209 (2017)

On solvability of cohomological equation in the space $L^2(X, \mu)$

Teubé Cyrille MBAINAISSEM[1] , Déthié DIONE [2]

[1]University of N'Djaména, N'Djaména, Chad
[2]University of Gaston Berger of Saint-Louis, Senegal

Abstract

In this paper, we carry out more research on the spectrum characteristics of the weighted composition operators denoted by $(Au)(x) = a(x)u(\alpha(x))$ or $(T_\alpha u)(x) = u(\alpha(x))$. We attempt to elucidate how the spectral features of related weighted composition operators relate to the dynamics of the mapping α. For a particular class of mappings, the operators of the form $T_\alpha - \lambda I$ in the space $L^2(X, \mu)$ are studied.The standard solvability requirements for cohomological equations in the space $L^2(X, \mu)$ are provided.

1 Introduction

Let $\mathfrak{F}(X)$ be a space of functions on a set X and α: $X \to X$ is a given mapping. Operator T_α defined in the space $\mathfrak{F}(X)$ appearance:

$$(T_\alpha u)(x) = u(\alpha(x)) \tag{1}$$

is called *composition operator*, operator A of the form:

$$(Au)(x) = a_0(x)u(\alpha(x)) \tag{2}$$

where $a(\cdot)$ is a given function, is called *weighted composition operator*.

Such operators, operator algebras generated by them and functional equations related to such operators have been studied by many authors in various functional spaces as an independent object and in relation to various applications(theory of dynamical systems, integro-functional, differential-functional, functional and difference equations, nonlocal boundary value problems etc.) (see [2], [4], [8], [10], [11], [14]).

Ones of the most important in the theory of dynamical systems are so-called *cohomological equations*, *i.e.* the equations:

$$u(x) - u(\alpha(x)) = f(x), \tag{3}$$

and more general equations:

$$\lambda u(x) - u(\alpha(x)) = f(x), \tag{4}$$

which corresponds to the composition operator T_α(see [10], [2], [9]). Such equations can be not normally solvable (see [1], [9]). We recall that following a standard terminology, an equation $Au = v$ is called *normally solvable* if

$$ImA = (KerA^\star)^\perp.$$

It is equivalent to condition the range ImA is closed. If $ImA = F$ a solution exists for any v and the equation is normally solvable.
It is clarify by G. Belitskii and Yu. Lyubich ([5], [6]) that cohomological equation (3) in the space of continuous functions $C(X)$ is normally solvable only for certain exceptional cases of mappings α.
The purpose of this paper revolves spectral properties of the composition operators and to give solvability conditions or normal solvability conditions for cohomological equations in the space $L^2(X, \mu)$ for some model classes of mappings. The main conclusion is that the cohomological equation can by normally solvable in the space $L^2(X, \mu)$.

2 Preliminary

Spectral properties of the weighted composition operators for some classes of mappings was described in the papers ([3], [12], [13]). In order to give the results in an explicit form we will consider a subclass of such mappings but it is easy to obtain a generalization.
Let X be a compact domain in $\mathbb{R}^n$, the map α: $X \to X$ is a diffeomorphism. Below we consider only the case when X inm-dimensional cube. The properties of the operator T_α depend on behavior of trajectories and on the space of functions under consideration.
We recall that the *trajectory of a point* $x \in X$ is the two-sided sequence.

$$x_n = \alpha^n(x), n \in \mathbb{Z}, \quad \alpha^n(x) = \alpha(\alpha^{n-1}(x)), \quad \alpha^0(x) \equiv x.$$

In the spaces $L^p(X)$ operator

$$U_\alpha u(x) = |J_\alpha(x)|^{\frac{1}{p}} u(\alpha(x)),$$

where $J(\alpha)$ is the Jacobian of the diffeomorphism α, is isometric. The operator A can be conveniently written in the form of $A = aU_\alpha$, where

$$a(x) = |J_\alpha(x)|^{\frac{-1}{p}} a_0(x)$$

is so-called *reduced coefficient*. We emphasize that the reduced coefficient depends on the functional space under consideration.
A map α will be called a *map of Morse-Smale type* if the set *Fix*(α) of fixed points is finite and the trajectory of every point tends to one of the fixed points as $n \to +\infty$ and tends to a different fixed points as $n \to -\infty$.
For such map a fixed point x_0 is said to be *attracting* if there exists a neighbourhood of this point,such that the trajectories of all points from this neighbourhood tend to x_0 as $n \to +\infty$. A fixed point x_0 is said be *reppeling* if there exists a neighbourhood of this point,such that the trajectories of all points from this neighbourhood tend to x_0 as

$n \to -\infty$. The rest fixed points are *saddle* : in any neighbourhood of such point there exist a point x such that its trajectory tends to some other fixed points as $n \to \pm\infty$.
The dynamic characteristic of the map α which was useful in obtaining solutions of the problem in question turned out to be an oriented graph G_α, describing the dynamics of the map.
The set *of vertices of the graph* G_α are sets $Fix(\alpha) = \{F_1, ..., F_p\}$.
An *oriented edge* $F_k \to F_j$ is included in the graph if and only if there exists a point $x \in X$ such that

$$\lim_{x \to +\infty} \alpha^n(x) = F_j, \quad \lim_{x \to -\infty} \alpha^n(x) = F_k.$$

The dynamics of α is the most simple, if there exist only two fixed points and graph $G(\alpha)$ has the form : $F_1 \to F_2$.
The use of the introduced graph permitted one to obtain a simple formulation of the important properties of weighted composition operators.
Using the coefficient a and number λ one forms two subsets of the set of vertices of the graph

$$G^+(a, \lambda) = \{F_k \in Fix(\alpha) : |a(F_k)| > |\lambda|\}, \tag{5}$$
$$G^-(a, \lambda) = \{F_k \in Fix(\alpha) : |a(F_j)| < |\lambda|\}$$

It is clear that

$$G^+(a, \lambda) \bigcap G^-(a, \lambda) = \emptyset$$

We say that subsets $G^+(a, \lambda)$ and $G^-(a, \lambda)$ give a *decomposition of the graph*, if the condition

$$G_\alpha = G^+(a, \lambda) \bigcup G^-(a, \lambda)$$

holds, ie., if

$$|a(F)| \neq |\lambda| \text{ for all } F \in Fix(\alpha)$$

The graph decomposition will be called *oriented to the right* if any edge connecting the point $F_k \in G^-(a, \lambda)$ to the point $F_j \in G^+(a, \lambda)$, is oriented from $F_k \to F_j$.
The decompostion will be called *oriented to the left* if any edge connecting the point $F_k \in G^-(a, \lambda)$ to the point $F_j \in G^+(a, \lambda)$, is oriented from $F_j \to F_k$.
The basic result in this direction in the following (see [3], [13]).

Proposition 1. *Let α be a Morse-Smale type diffeomorphism, $a \in C(X), a(x) \neq 0$ for all x and A be weighted composition operator. The operator $A - \lambda I$ is invertible from the right (left) if and only if the subsets $G^+(a, \lambda)$ and $G^-(a, \lambda)$ form a decomposition of the graph G_α which is oriented to the right (to the left).*
In particular, operator $A - \lambda I$ is invertible only at the two cases:

a) $|a(F_k)| < |\lambda|$ *for all* k*;*

b) $|a(F_k)| > |\lambda|$ *for all* k*.*

By using this theorem we describe properties of corresponding cohomological equations.

3 Spectral Properties of the composition operator on the Segment

Let be $X = [0,1]$ and $\alpha : X \to X$ a C^1-difféomorphism such that :
$Fix(\alpha) = \{0,1\}$. We remark that for such mappings the proposition was obtained earlier by *Y.I Karlovich and B.G Kravchenko* in the spaces $L^p([0,1])$ (see [11]).

Theorem 1. *Let be $X = [0,1]$ and $\alpha : X \to X$ a C^1-difféomorphism such that : $\alpha(0) = 0$, $\alpha(1) = 1$ and $x < \alpha(x)$ for $x \in]0,1[$.*

a) The spectrum of the operator $(T_\alpha u)(x) = u(\alpha(x))$ in $L^p([0,1])$ is the annulus:

$$\sigma(T_\alpha) = \left\{ \lambda \in \mathbb{C} : \frac{1}{[\alpha'(0)]^{\frac{1}{p}}} \leq |\lambda| \leq \frac{1}{[\alpha'(1)]^{\frac{1}{p}}} \right\}. \tag{6}$$

b) If $\alpha'(0) > \alpha'(1)$ and

$$\frac{1}{[\alpha'(0)]^{\frac{1}{p}}} < |\lambda| < \frac{1}{[\alpha'(1)]^{\frac{1}{p}}}$$

then the operator $T_\alpha - \lambda I$ is right-sided invertible and its kernel is infinite dimensional.

c) If $|\lambda| = \frac{1}{[\alpha'(0)]^{\frac{1}{p}}}$ or $|\lambda| = \frac{1}{[\alpha'(1)]^{\frac{1}{p}}}$ then the range of the operator $T_\alpha - \lambda I$ is nonclosed and the operator is not invertible unilaterally.

Proof 1. *Here α is the Morse- Smale type mapping with the most simple dynamics: $F_1 = 0$ is a repelling point, $F_2 = 1$ is an attracting point, saddle points do not exist, the oriented graph G_α has the form $F_1 \to F_2$.*
The reduced coefficient for T_α is given by

$$a(x) = \frac{1}{[\alpha'(1)]^{\frac{1}{p}}}$$

and $a(x) \neq 0$ for any x. Therefore we can apply proposition 1 to corresponding operators T_α. According to the proposition 1, the spectrum of operator T_α in $L^p[0,1]$ is the annulus:

$$\sigma(T_\alpha) = \{\lambda \in \mathbb{C} : r \leq |\lambda| \leq R\}.$$

where

$$R = \max\left\{ \frac{1}{[\alpha'(0)]^{\frac{1}{p}}}, \frac{1}{[\alpha'(1)]^{\frac{1}{p}}} \right\}, \quad r = \min\left\{ \frac{1}{[\alpha'(0)]^{\frac{1}{p}}}, \frac{1}{[\alpha'(1)]^{\frac{1}{p}}} \right\}.$$

From condition $x < \alpha(x)$ if $0 < x < 1$ follows that at the point $x = 0$, the function $\beta : \beta(x) = \alpha(x) - x$ is increasing and $\beta'(0) = \alpha'(0) - 1 \geq 0$ and $\alpha'(0) \geq 1$. Similarly at the point and $x = 1$, the function $\beta : \beta(x) = \alpha(x) - x$ is decreasing and $\alpha'(1) \leq 1$.

Therefore,

$$\max\left\{\frac{1}{[\alpha'(0)]^{\frac{1}{p}}}, \frac{1}{[\alpha'(1)]^{\frac{1}{p}}}\right\} = \frac{1}{[\alpha'(1)]^{\frac{1}{p}}}$$

$$\min\left\{\frac{1}{[\alpha'(0)]^{\frac{1}{p}}}, \frac{1}{[\alpha'(1)]^{\frac{1}{p}}}\right\} = \frac{1}{[\alpha'(0)]^{\frac{1}{p}}}$$

and the spectrum $\sigma(T_\alpha)$ is given by ([6]).
For the reduced coefficient $a(\cdot)$ we have

$$|a(0)| \leq |a(1)|$$

therefore, for $\lambda \in \sigma(T_\alpha)$ the corresponding decomposition of G_α into subset $G^+(a,\lambda)$ and $G^-(a,\lambda)$ can not be oriented to the left and operator $T_\alpha - \lambda I$ can not be left-sided invertible. If $\alpha'(0) \neq \alpha'(1)$ then there are numbers λ such that :

$$\frac{1}{[\alpha'(0)]^{\frac{1}{p}}} \leq |\lambda| \leq \frac{1}{[\alpha'(1)]^{\frac{1}{p}}}$$

For such λ, the decomposition of G_α into subset $G^+(a,\lambda)$ and $G^-(a,\lambda)$ is oriented to the right, operator $T_\alpha - \lambda I$ is right-sided invertible and its kernel is infinite- dimensional. Right-sided inverse operator can be given by expression

$$R(\lambda) = \sum_{-\infty}^{-1} \lambda^k T^{-k-1} P \sum_{k=0}^{+\infty} \lambda^k T^{-k-1}(I-P)$$

where P is a projection in $L^p[0,1]$ acting by

$$P_q u(x) = \begin{cases} u(x) & x \leq q \\ 0 & x > q. \end{cases}$$

◄

Corollary 1. *For this class of applications of segment , the cohomological equation (3) is normaly solvable in $L^p[0,1]$ if and only if $p < +\infty$ and $\alpha'(0) > 1 > \alpha'(1)$. Under these conditions, the equation (3) is solvable for all function $f \in L^p[0,1]$ and the space of solutions of homogeneous equation has infinite dimension.*

We remark that the same results can be obtained for any α such that there exist only two fixed points and the graph $G(\alpha)$ has the form $F_1 \to F_2$.

4 Influence of the saddle points on the Spectral Properties

Let $X = \{x \in \mathbb{R}^m : 0 \leq x_k \leq 1; 1 \leq k \leq m\}$ be m-dimensional cube. At this section, we give description of the spectral properties of the operator T_α for a classes of diffeomorphisms $\alpha : X \to X$.

4.1 Diagonal mappings

Let γ be a diffeomorphism of a segment $[0,1]$ into itself acting as α in section 3: $\gamma(0) = 0, \gamma(1) = 1$ and $\gamma(x) > x$ for $x \in (0,1)$. Assume that $\gamma'(0) > 1 > \gamma'(1)$. We consider diffeomorphism $\alpha : X \to X$ definite by expression:

$$\alpha(x_1, ..., x_m) = (\gamma(x_1), \gamma(x_2), ..., \gamma(x_m)) \tag{7}$$

Theorem 2.
- *a) The spectrum of the operator $(T_\alpha u)(x) = u(\alpha(x))$ in $L^2([0,1])$ is the annulus:*

$$\sigma(T_\alpha) = \left\{ \lambda \in \mathbb{C} : \frac{1}{\sqrt{\gamma'^m(0)}} \leq |\lambda| \leq \frac{1}{\sqrt{\gamma'^m(1)}} \right\}.$$

- *b) If the resonance condition holds:*

$$|\lambda| = \frac{1}{\sqrt{\gamma'^{m-k_0}(0)\gamma'^{k_0}(1)}}$$

  for some k_0 with $0 \leq k_0 \leq m$, then the range of the operator $T_\alpha - \lambda I$ is nonclosed, in particular, this operator can not be unilaterally invertible.

- *c) If $\lambda \in \sigma(T_\alpha)$ and that $|\lambda| \neq \frac{1}{\sqrt{\gamma'^{m-k}(0)\gamma'^k(1)}}; k = 0, 1, ..., m$*

  then the operator $T_\alpha - \lambda I$ is right-sided invertible and its kernel is infinite dimensional.

Proof 2. *The fixed points of α are the tops of the cube X :*

$$Fix(\alpha) = \{\Omega = (\omega_1, \omega_2, ..., \omega_m) : \omega_k \in \{0, 1\}\}.$$

For $t \in [0,1]$ we put

$$\omega^+(t) = \lim_{n \to +\infty} \gamma^n(t) = \begin{cases} 1 & 0 < t \leq 1 \\ 0 & t = 0 \end{cases}$$

$$\omega^-(t) = \lim_{n \to -\infty} \gamma^n(t) = \begin{cases} 1 & t = 1 \\ 0 & 0 \leq t < 1 \end{cases}$$

Let us consider the trajectory of a point $x = (x_1, x_2, ..., x_m) \in X$.
We have that

$$\lim_{n \to \pm\infty} \alpha^n(x) = (\omega^\pm(x_1), \omega^\pm(x_2), ..., \omega^\pm(x_m)) = \omega^\pm(x).$$

It follows from this that α is a Morse-Smale type mapping and oriented edge $\omega \to \tilde{\omega}$ is included to oriented graph $G(\alpha)$ if and only if $\omega_k \leq \tilde{\omega_k}$ for all k.

In particular, the point $(0, 0, ..., 0)$ is repelling, the point $(1, 1, ..., 1)$ is attracting and the rest fixed points are saddle.

The reduced coefficient for the operator $(T_\alpha u)(x) = u(\alpha(x))$ is function of the form:

$$a(x) = [\gamma'(x_1), \gamma'(x_2)..., \gamma'(x_m)]^{-\frac{1}{2}}$$

That is why

$$a(\omega) = \frac{1}{\sqrt{[\gamma'(0)]^{m-|\omega|}[\gamma'(1)]^{|\omega|}}},$$

where $|\omega| = \omega_1 + \omega_2 + ... + \omega_m$. *In particular,*

$$\max_{\omega}\{|a(\omega)|\} = \frac{1}{\sqrt{\gamma'^m(1)}} > 1,$$

$$\min_{\omega}\{|a(\omega)|\} = \frac{1}{\sqrt{\gamma'^m(0)}} < 1,$$

and $a(\omega)$ monotonic *as a function on the oriented graph* $G(\alpha)$*:*
if $\omega \to \tilde{\omega}$ *then* $a(\omega) < a(\tilde{\omega})$.

Now we can obtain the conclusion of the theorem 2 from proposition 1. Assertion than the subsets $G^+(a,\lambda)$ *and* $G^-(a,\lambda)$ *form a decomposition of the graph* G_α *which is oriented to the right, follows from the monotonicity of* $a(\omega)$.

◀

Corollary 2. *For map* α *of the form (7) the equation (3) is normally solvable in* $L^2(X)$ *if and only if*

$$|\gamma'(0)|^{m-k}|\gamma'(1)|^{m-k} \neq 1$$

for all $k = 0, 1, ..., m$. *If these conditions are satisfied then equation (3) is solvable for all function* $f \in L^2(X)$ *and the solution space of equation* $u(\alpha(x)) - u(x) = 0$ *has infinite dimensional.*

4.2 A Morse-Smale type diffeomorphism of cube

There exist a lot of diffeomorphisms of cube for with the dynamical properties are similar to the properties of diffeomorphism (7):
$Fix(\alpha) = \Omega$ and the oriented graph $G(\alpha)$ is the same. But for such diffeomorphism the function

$$a(\omega) = \frac{1}{\sqrt{|J_\alpha(\omega)|}}$$

can be not monotonic on the oriented graph $G(\alpha)$ and conclusions of the theorem 2 do not hold. Spectral properties of the composition operators for this more general situation can be described as follows.

Theorem 3. *a) The spectrum of operator* $(T_\alpha u)(x) = u(\alpha(x))$ *in* $L^p(X)$ *is the annulus:*

$$\sigma(T_\alpha) = \{\lambda \in \mathbb{C} : r \leq |\lambda| \leq R\}$$

Where

$$R = \max\{|a(\omega)| : \omega \in \Omega\}. \quad r = \min\{|a(\omega)| : \omega \in \Omega\}.$$

b) If $|\lambda| = |a(\omega)|$ *for some* $\omega \in \Omega$ *then the range of the operator* $T_\alpha - \lambda I$ *is a nonclosed, in particular, this operator can not be unilaterally invertible.*

c) Let $\lambda \in \sigma(T_\alpha)$ and $|\lambda| \neq |a(\omega)|$ for any $\omega \in \Omega$.

The operator $T_\alpha - \lambda I$ is right-side invertible if and only if it does not exist an oriented edge $\omega \to \tilde{\omega}$ such that $|a(\omega)| > |\lambda| > |a(\tilde{\omega})|$.

In the opposite case the range of the operator $T_\alpha - \lambda I$ is nonclosed.

Corollary 3. *Under condition of the theorem the cohomological equation (3) is normally resolvable in $L^2(X)$ if and only if*

i) $|a(\omega)| \neq 1$ for all $\omega \in \Omega$

ii) it does not exist an oriented edge $\omega \to \tilde{\omega}$ such that $|a(\omega)| > 1 > |a(\tilde{\omega})|$.

If these conditions are satisfied then equation (3) is solvable for all function $f \in L^2(X)$

Example. Let $X = \{x \in \mathbb{R}^2 : 0 \leq x_1 \leq 1; 0 \leq x_2 \leq 1\}$ be 2-dimensional cube and diffeomorphism $\alpha : X \to X$ defined by expression

$$\alpha(x_1, x_2) = (x_1 + \frac{3}{100}(2 - x_2)x_1(1 - x_1), x_2 + \frac{1}{100}x_2(1 - x_2)).$$

Let us consider the corresponding functional equations

$$u(\alpha(x)) - \lambda u(x) = f(x) \tag{8}$$

in the space $L^2(X)$.

There are four fixed points here, the values of the reduced coefficient at the fixed points are

$$a(0,0) = \frac{100}{\sqrt{10706}}, a(0,1) = \frac{100}{\sqrt{10197}}, a(1,0) = \frac{100}{\sqrt{9494}}, a(1,1) = \frac{100}{\sqrt{9603}}$$

We can see that $a(\omega)$ is not monotonic the oriented edge $(1,0) \to (1,1)$ below to graph $G(\alpha)$ but $(1,0) > (1,1)$.

It follows from the theorem 3 that

$$\sigma(T_\alpha) = \{\lambda \in \mathbb{C} : \frac{100}{\sqrt{10706}} \leq, |\lambda| \leq \frac{100}{\sqrt{9494}}\};$$

if

$$\frac{100}{\sqrt{10706}} < |\lambda| < \frac{100}{\sqrt{10197}} \text{ and if } \frac{100}{\sqrt{10197}} < |\lambda| < \frac{100}{\sqrt{9603}}$$

a solution of (8) exists for any $f \in L^2(X)$;

$$\text{if } \frac{100}{\sqrt{9603}} \leq |\lambda| \leq \frac{100}{\sqrt{9494}} \text{ and if } |\lambda| < \frac{100}{\sqrt{10197}}$$

the equation (8) is not normally solvable.

Acknowledgement

The authors thank Professeur A.B. Antonevich of Belorussian University and University of Bialystok in Poland, for his valuable comments and several helpful remarks.

References

[1] Anosov D.V. *The additive functional homology equation that is connected with an ergodic rotation of the circle.*Izv.Akad.Nauk SSSR Ser. Mat 37(1973),n,6,1259-1274(russian);English transl.in Math.URSS IZv.(1973).

[2] A. B. Antonevich. *Linear functional Equations. Operator approach [in Russian].* Universitetskoe, Mins, 1988. English Transl. Operator theory : Advances and Applications, Vol. 83, Birkhäuser, 1996.

[3] A.Antonevich and J.Jakubowska (Makowska). *On properties of weighted shift operators generated by mapping with saddle points.* Complex analysis and operator theory. 2008-V2 p. 215-240.

[4] A. Antonevich and V.A. Lebedev. *Functional Differentiel Equations I. C^*-theory* Harlow: Longman, 1994.

[5] G.Belitskii and Y.Lyubich. *On the normal solvability of cohomological equations on locally compact topological spaces.* Non linear analysis and related problems. Tr. Inst. Mat. Minsk,2(1999) 44-51 .

[6] G.Belitskii and Y.Lyubich. *On the normal solvability of cohomological equations on topological spaces.* Operator theory: Advances and applications 103, 75-87 (1998).

[7] A. Bottcher and H. Heidler. *Algebraic compositions operators.* Integral equations and operator theory 15 (1992), 389-411.

[8] C. Chicone and Y. Latushkin. *Evolution semi-group in dynamical systems and differential equations.* Providence, AMS, RI, 1999.

[9] Gordon A.Ya. *A sufficient condition for the nonsolvability of the additive functional homological equation associated with an ergodic rotation of the circle.*Functional.anal.Appl.9(1975).

[10] A. Katok A., B. Hasselblatt.*Introduction to the modern theory of dynamical systems.*Cambridge. Cambridge University Press.1998.
katok

[11] V. G. Kravchenko and G. S. Litvinchuk. *Introduction to the theory of singular integral operators with shift.* Dordrecht. Kluver Acad. Publ. 1994.

[12] J. Makowska *On spectral properties of weighted shift operators generated by mappings with saddle points in L_p,*Proceedings of the XXVII Workshop on Geometric Methods in Physic(BiaE,owieEja), American Institute of Physics, 2008, 96-101.

[13] J. Makowska *One sided-invertibility of the weighted shift operators,*Proceedings of the XXIX Workshop on Geometric Methods in Physic (Poland, 2010, June 27-July 3), American Institute of Physics, 2010, 101-105.

[14] D. Przeworska and D. Rolewicz.*Equations with transformed argument* Elsevier Scientific Publ. Comp. and Polish Scientific Publishers,Amsterdam and WARSAW 1973.

LOCAL ROUGH EQUALITIES AND LOCAL ROUGH EQUIVALENCES OF SETS

Mustafa BEYDAĞI[1] , A. Fatih ÖZCAN[2], İlhan İÇEN[3]

[1]Department of Mathematics, Faculty of Arts and Sciences, Inonu University, Malatya, Turkey

mbeydagi23@gmail.com

[2]Department of Mathematics, Faculty of Arts and Sciences, Inonu University, Malatya, Turkey

abdullah.ozcan@inonu.edu.tr

[3]Department of Mathematics, Faculty of Arts and Sciences, Inonu University, Malatya, Turkey

ilhan.icen@inonu.edu.tr

ABSTRACT

Since the concept of equality of sets used in classical set theory cannot be applied in general terms for rough sets, the concept of "rough equality" has been defined. Later, this concept was expanded and the concept of “rough equivalence”, which reached a higher level than rough equality, emerged. In this paper, the concepts of rough equality and rough equivalence are transferred to the local rough set theory, which gives clearer results than rough sets, and their properties are stated for the first time. Also, the given example shows that by dividing big data into groups in the local rough set, the elements are presented more concretely with local lower and local upper approaches, and the concepts of local rough equality and local rough equivalence will have better-defined boundaries.

Keywords: Equality of Rough Sets, Equivalence of Rough Sets, Equivalence of Local Rough Sets, Equivalence of Local Rough Sets.

1. INTRODUCTION

The rough set theory put forward by Pawlak has been a tool for solving various problems such as identifying sets that cannot be determined with the help of approaches and reasoning based on incomplete information [1]. Pawlak's work is extremely important because many of the traditional tools for reasoning and computation in situations of uncertainty are not applicable in real life.

In classical set theory, the equality of two sets consists of elements with clearly defined boundaries. The concept of rough equality given by Pawlak and Novotny [2-4] is based on combining uncertain information. Since it is known that concrete information about the equality of the two sets cannot be obtained in some cases, it is possible to say that the two sets are approximately equal or indistinguishable with limited information.

Later, it was seen that the concept of approximate equality of the sets was also insufficient, and rough equivalence concepts were introduced by Tripathy, Mitra, and Ojha [5,6], which capture the approximate equality of the two sets at a higher and general level.

In this study, firstly, the properties of the concepts of rough equality and rough equivalence are presented. In addition, a local rough set definition is given [7,8]. Later, the concepts of local rough equality and local rough equivalence were introduced with their properties for the first time. According to the results obtained, it has been seen that the concept of local rough equivalence can make more clear comparisons with better-defined boundaries.

2. ROUGH EQUALITY OF SETS

Definition 2.1: Let (U, R) be the approximation space and $X, Y \subset U$. Let be the lower approximation $\underline{R}(X)$ of X set and the upper approximation $\overline{R}(X)$ of X set in the (U, R) approximation space [9].

i) If $\underline{R}(X) = \underline{R}(Y)$, the sets X, and Y are *roughly bottom equal* in (U, R) and are denoted by $X \eqsim Y$.

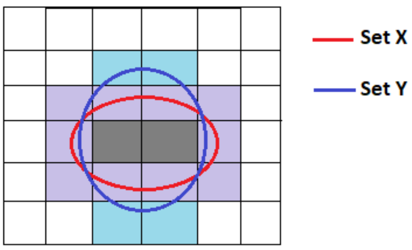

Fig. 1: For roughly bottom equal sets.

ii) If $\overline{R}(X) = \overline{R}(Y)$, the sets X, and Y are *roughly top equal* in (U, R) and are denoted by $X \simeq Y$.

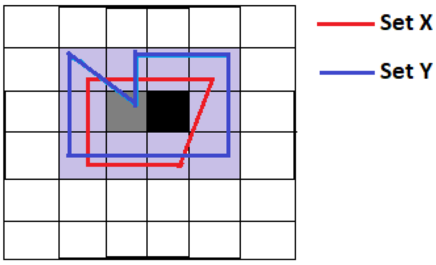

Fig. 2: For roughly top equal sets.

iii) If $\underline{R}(X) = \underline{R}(Y)$ and $\overline{R}(X) = \overline{R}(Y)$, the sets X and Y are *roughly equal* in (U, R) and are denoted by $X \approx Y$.

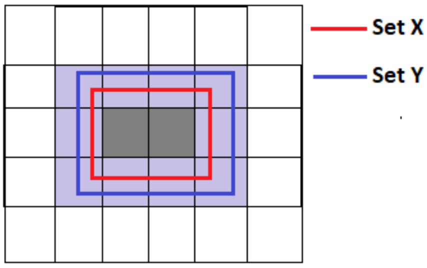

Fig. 3: For roughly equal sets.

The following properties are true for (U, R) approximation space, and $X, Y \subset U$ [9].

1) $X \eqsim Y \Leftrightarrow X \cap Y \eqsim X$ or $X \cap Y \eqsim Y$.
2) $X \simeq Y \Leftrightarrow X \cup Y \simeq X$ or $X \cup Y \simeq Y$.
3) If $X \simeq X'$ and $Y \simeq Y'$, then $X \cup Y \simeq X' \cup Y'$.
4) If $X \eqsim X'$ and $Y \eqsim Y'$,then $X \cap Y \eqsim X' \cap Y'$.
5) $X \eqsim Y \Rightarrow X - Y \eqsim \emptyset$.
6) $X = Y \Rightarrow X - Y \eqsim \emptyset$.
7) $X \eqsim Y \Rightarrow -(-X) \eqsim Y$.
8) $X \simeq Y \Rightarrow -(-X) \simeq Y$.
9) $X \approx Y \Rightarrow -(-X) \approx Y$.
10) $X \simeq Y \Rightarrow X \cup (-Y) \simeq U$
11) $X \simeq Y \Rightarrow X \cap (-Y) \eqsim \emptyset$.

Definition 2.2: Let (U, R) be the approximation space and $X \subset U$ [9].

i) If $X \simeq U$, the set X is called *dense* in the (U, R) approximation space.

ii) If $X \eqsim \emptyset$, the set X is called *co-dense* in the (U, R) approximation space.

iii) If $X \simeq U$ and $X \eqsim \emptyset$, the set X is called *dispersed* in the (U, R) approximation space.

The following properties are true for (U, R) approximation space, and $X, Y \subset U$ [9].

1) If $X \subset Y$ and $Y \eqsim \emptyset$, then $X \eqsim \emptyset$.
2) If $X \subset Y$ and $X \simeq U$, then $Y \simeq U$.
3) İf $X \simeq U$, then $(-X) \eqsim \emptyset$.
4) If $X \eqsim \emptyset$, then $(-X) \simeq U$.
5) If $X \eqsim -X$ and $X \simeq -X$, then $X \approx -X$.
6) If $X \simeq U$ and $Y \simeq U$, then $X \simeq Y$.
7) If $X \eqsim \emptyset$ and $Y \eqsim \emptyset$, then $X \eqsim Y$.
8) If X, Y are both dispersed, then $X \approx Y$ dir.
9) If $X \eqsim \emptyset$, then $\underline{R}(X) = \emptyset$.
10) If $X \simeq \emptyset$, then $X = \emptyset$.
11) If $X \eqsim U$, then $X = U$.
12) If $X \simeq U$, then $\overline{R}(X) = U$.
13) $\overline{R}(X)$ is the union of all sets Y such that $X \simeq Y$.
14) $\underline{R}(X)$ is the intersection of all sets Y such that $X \eqsim Y$.

3. ROUGH EQUIVALENCES OF SETS

Definition 3.1: Let (U, R) be the approximation space and $X, Y \subset U$ [10].

i) The set X is called *bottom roughly equivalent* to the set Y if both $\underline{R}(X)$ and $\underline{R}(Y)$ are equal to $\emptyset$ or both are different from $\emptyset$.

ii) The set X is called *top roughly equivalent* to the set Y if both $\overline{R}(X)$ and $\overline{R}(Y)$ are equal to U or both are different from U.

iii) If the set X is both the bottom roughly equivalent and the top roughly equivalent to the set Y, the set X is called *roughly equivalent* to set Y.

Although the rough equivalence of two sets has similar properties to the rough equality, these properties are satisfied under certain conditions. Therefore, it is necessary to specify concepts such as rough inclusions and rough comparisons.

Definition 3.2: Let (U, R) be the approximation space and $X, Y \subset U$ [10].

i) If $\underline{R}(X) \subset \underline{R}(Y)$, then the set X is the *bottom roughly included* in the set Y and is denoted by $X \underset{\sim}{\subset} Y$.

ii) If $\overline{R}(X) \subset \overline{R}(Y)$, then the set X is *top roughly included* in the set Y and is denoted by $X \overset{\sim}{\subset} Y$.

iii) If both $\underline{R}(X) \subset \underline{R}(Y)$ and $\overline{R}(X) \subset \overline{R}(Y)$, then the set X is *roughly included* in the set Y and is denoted by $X \overset{\sim}{\underset{\sim}{\subset}} Y$.

Definition 3.3: Let (U, R) be the approximation space and $X, Y \subset U$ [10].

i) If $X \underset{\sim}{\subset} Y$ or $Y \underset{\sim}{\subset} X$, then the sets X and Y are *bottom rough comparable.*
ii) If $X \overset{\sim}{\subset} Y$ or $Y \overset{\sim}{\subset} X$, then the sets X and Y are *top rough comparable.*
iii) If $X \overset{\sim}{\underset{\sim}{\subset}} Y$ or $\overset{\sim}{\underset{\sim}{\subset}} X$, the sets X and Y are roughly *comparable.*

Definition 3.4: Let (U, R) be the approximation space. The all rough subset family of the set $X \subset U$ is called the *rough power set* and is denoted by $P(X)\left(P_{\underline{R}}(X), P_{\overline{R}}(X)\right)$ [9]. Thus,

$$P_{\underline{R}}(X) = \{Y : Y \underset{\sim}{\subset} X\}$$

$$P_{\overline{R}}(X) = \{Y : Y \overset{\sim}{\subset} X\}$$

$$P(X) = \{Y : Y \overset{\sim}{\underset{\sim}{\subset}} X\}$$

The following properties are true for (U, R) approximation space, and $X, Y \subset U$ [9].

1) If $X \eqsim Y$, then $P_{\underline{R}}(X) = P_{\underline{R}}(Y)$.
2) If $X \simeq Y$, then $P_{\overline{R}}(X) = P_{\overline{R}}(Y)$.
3) If $X \approx Y$, then $P(X) = P(Y)$.
4) If $X \underset{\sim}{\subset} Y$, then $P_{\underline{R}}(X) \subset P_{\underline{R}}(Y)$.
5) If $X \overset{\sim}{\subset} Y$, then $P_{\overline{R}}(X) \subset P_{\overline{R}}(Y)$.
6) If $X \overset{\sim}{\underset{\sim}{\subset}} Y$, then $P(X) \subset P(Y)$.

The following properties are true for (U, R) approximation space, and $X, Y \subset U$ [9].

1) If $X \subset Y$, then $X \underset{\sim}{\subset} Y$, $X \overset{\sim}{\subset} Y$ and $X \overset{\sim}{\underset{\sim}{\subset}} Y$.
2) If $X \underset{\sim}{\subset} Y$ and $Y \underset{\sim}{\subset} X$, then $X \eqsim Y$.
3) If $X \overset{\sim}{\subset} Y$ and $Y \overset{\sim}{\subset} X$, then $X \simeq Y$.
4) $X \overset{\sim}{\underset{\sim}{\subset}} Y$ and $Y \overset{\sim}{\underset{\sim}{\subset}} X$, then $X \approx Y$.
5) If $X \overset{\sim}{\subset} Y$, then $X \cup Y \simeq Y$.
6) If $X \underset{\sim}{\subset} Y$, then $X \cap Y \eqsim X$.
7) If $X \subset Y$, $X \eqsim X'$ and $Y \eqsim Y'$, then $X' \underset{\sim}{\subset} Y'$.
8) If $X \subset Y$, $X \simeq X'$ and $Y \simeq Y'$, then $X' \overset{\sim}{\subset} Y'$.
9) If $X \subset Y$, $X \approx X'$ and $Y \approx Y'$, then $X' \overset{\sim}{\underset{\sim}{\subset}} Y'$.
10) If $X' \overset{\sim}{\subset} X$ and $Y' \overset{\sim}{\subset} Y$, then $X' \cup Y' \overset{\sim}{\subset} X \cup Y$.
11) If $X' \underset{\sim}{\subset} X$ and $Y' \underset{\sim}{\subset} Y$, then $X' \cap Y' \underset{\sim}{\subset} X \cap Y$.

4. LOCAL ROUGH EQUALITY OF SETS

It has been observed that the equality properties in the rough sets are satisfied under certain conditions for the local rough sets.

Definition 4.1: Let $\boldsymbol{\mathcal{U}}$=$\{(U_i, R_i) : i \in I, U_i \subset U$ finite set of objects, $R_i \subset U_i \times U_i$ equivalence relation$\}$ family be the local approximation space and $X, Y \subset U_i$. For the pair $(U_i, R_i) \in \boldsymbol{\mathcal{U}}$, let the local lower approximation of the set X is $\underline{R_l}(X)$ and the local upper approximation is $\overline{R_l}(X)$.

i) If $\underline{R_l}(X) = \underline{R_l}(Y)$, the sets X, and Y will be named *local roughly bottom equal* and will be denoted by $X \eqsim_l Y$.

ii) If $\overline{R_l}(X) = \overline{R_l}(Y)$, the sets X and Y will be named *local roughly top equal* and will be denoted by $X \simeq_l Y$.

iii) If $\underline{R_l}(X) = \underline{R_l}(Y)$ and $\overline{R_l}(X) = \overline{R_l}(Y)$, the sets X and Y will be named *local roughly equal* and will be denoted by $X \approx_l Y$.

Theorem 4.1: The following properties are true for $\boldsymbol{\mathcal{U}}$ local approximation space and

$X, Y \subset U_i$.

i) $X = Y \Longrightarrow X \eqsim_l Y$.

ii) $X = Y \Longrightarrow X \simeq_l Y$.

iii) $X = Y \Longrightarrow X \approx_l Y$.

Proof. i) Let $X = Y$. If $\forall x \in \underline{R_l}(X)$, then $[x]_l \subseteq X$. Since $x \in [x]_l$, $x \in X$ is obtained. When $X = Y$, it becomes $x \in Y$. For $[x]_l \subseteq Y$, $x \in \underline{R_l}(Y)$ is obtained. Thus, $\underline{R_l}(X) \subseteq \underline{R_l}(Y)$.

If $\forall y \in \underline{R_l}(Y)$, then $[y]_l \subseteq Y$. Since $y \in [y]_l$, $y \in Y$ is obtained. When $X = Y$, $y \in X$, it becomes. For $[y]_l \subseteq X$, $y \in \underline{R_l}(X)$ is obtained. Thus, $\underline{R_l}(Y) \subseteq \underline{R_l}(X)$.

So if $X = Y$, then $\underline{R_l}(X) = \underline{R_l}(Y)$ is found.

Theorems ii) and iii) can also be easily proven.

Theorem 4.2: The following properties are true for $\boldsymbol{\mathcal{U}}$ to be the local approximation space and $X, Y \subset U_i$.

i) Let $X \eqsim Y$. If $\underline{R_l}(X) - \underline{R}(X) = \emptyset$ and $\underline{R_l}(Y) - \underline{R}(Y) = \emptyset$, then $X \eqsim_l Y$.

ii) Let $X \simeq Y$. If $\overline{R}(X) - \overline{R_l}(X) = \emptyset$ and $\overline{R}(Y) - \overline{R_l}(Y) = \emptyset$, then $X \simeq_l Y$.

iii) Let $X \approx Y$. If $\underline{R_l}(X) - \underline{R}(X) = \emptyset$, $\underline{R_l}(Y) - \underline{R}(Y) = \emptyset$, $\overline{R}(X) - \overline{R_l}(X) = \emptyset$, and $\overline{R}(Y) - \overline{R_l}(Y) = \emptyset$, then $X \approx_l Y$.

Proof. i) Let $\forall x \in \underline{R}(X)$. Since $\underline{R_l}(X) - \underline{R}(X) = \emptyset$, $\underline{R_l}(X) = \underline{R}(X)$ is obtained. Thus, $\forall x \in \overline{R_l}(X)$ is found. Since $\forall x \in \underline{R}(Y)$ and $\underline{R_l}(Y) - \underline{R}(Y) = \emptyset$ for $\underline{R}(X) = \underline{R}(Y)$, $\forall x \in \overline{R_l}(Y)$. Thus, $\underline{R_l}(X) = \underline{R_l}(Y)$. So $X \eqsim_l Y$ is written.

Theorems ii) and iii) can also be easily proven.

Let $\boldsymbol{U}$ be the local approximation space and $X, Y \subset U_i$. X and Y sets, which satisfy the properties in Theorem 4.1 and Theorem 4.2, provide the following properties as in the rough equality.

1) If $X \eqsim_l Y$, then $X \cap Y \eqsim_l X$ or $X \cap Y \eqsim_l Y$.
2) If $X \simeq_l Y$, then $X \cup Y \simeq_l X$ or $X \cup Y \simeq_l Y$.
3) If $X \eqsim_l Y$, then $X - Y \eqsim_l \emptyset$.
4) If $X \eqsim_l Y$, then $-(-X) \eqsim_l Y$.
5) If $X \simeq_l Y$, then $-(-X) \simeq_l Y$.
6) If $X \approx_l Y$, then$-(-X) \approx_l Y$.
7) If $X \simeq_l Y$, then $X \cup (-Y) \simeq_l U_i$
8) If $X \simeq_l Y$, then $X \cap (-Y) \eqsim_l \emptyset$.

Definition 4.2: Let $\boldsymbol{U}$ be the local approximation space and $X, Y \subset U_i$.

i) If $X \simeq_l U_i$, that is, the set X is local externally indefinable or the local totally indefinable [7], the set X will be named *dense* in the $\boldsymbol{U}$ local approximation space.
ii) If $X \eqsim_l \emptyset$, that is, the set X is local internally indefinable or the local totally indefinable [7], the set X will be named *co-dense* in the $\boldsymbol{U}$ local approximation space.
iii) If $X \simeq_l U_i$ and $X \eqsim_l \emptyset$, that is, the set X is local totally indefinable [7], the set X will be named *dispersed* in the $\boldsymbol{U}$ local approximation space.

The following properties are true for $\boldsymbol{U}$ be the local approximation space and $X, Y \subset U_i$.

1) If $X \subset Y$ and $Y \eqsim_l \emptyset$, then $X \eqsim_l \emptyset$.
2) If $X \subset Y$ and $Y \simeq_l U_i$, then $\underline{R_l}(X) \subset \underline{R_l}(Y)$ and $\overline{R}_l(X) \subset \overline{R}_l(Y)$.
3) If $X \simeq_l U_i$ and $\underline{R_l}(X) \neq \emptyset$, then $(-X) \eqsim_l \emptyset$.
4) If $X \eqsim_l \emptyset$ and $\overline{R}_l(X) = U_i$, then $(-X) \eqsim_l \emptyset$ and $(-X) \simeq_l U_i$.
5) For $X = Y \neq \emptyset, X \simeq_l U_i$ and $Y \simeq_l U_i$, then $X \simeq_l Y$.
6) For $X = Y = \emptyset, X \eqsim_l \emptyset$ and $Y \eqsim_l \emptyset$, then $X \eqsim_l Y$.
7) If $X \eqsim_l \emptyset$, then $\underline{R_l}(X) = \emptyset$.
8) If $X \simeq_l \emptyset$, then $X = \emptyset$.
9) If $X \eqsim_l U_i$, then $X = U_i$.
10) If $X \simeq_l U_i$, then $\overline{R}_l(X) = U_i$.

5. LOCAL ROUGH EQUIVALENCES OF SETS

Definition 5.1 : Let $\boldsymbol{\mathcal{U}}$=$\{(U_i, R_i) : \ i \in I \ , U_i \subset U$ finite set of objects, $R_i \subset U_i \times U_i$ equivalence relation$\}$ family be the local approximation space and $X, Y \subset U_i$.

i) The set X will be named *bottom local roughly equivalent* to the set Y if both $\underline{R_l}(X)$ and $\underline{R_l}(Y)$ are equal to $\emptyset$ or both are different from $\emptyset$.

ii) The set X will be named *top local roughly equivalent* to the set Y if both $\overline{R_l}(X)$ and $\overline{R_l}(Y)$ are equal to U or both are different from U.

iii) If both $\underline{R_l}(X)$ and $\underline{R_l}(Y)$ are both equal to $\emptyset$ or both different from $\emptyset$ and both $\overline{R_l}(X)$ and $\overline{R_l}(Y)$ are equal to U or both are different from U, set X will be named *local roughly equivalent* to set Y.

Definition 5.2: Let $\boldsymbol{\mathcal{U}}$=$\{(U_i, R_i) : \ i \in I, U_i \subset U$ finite set of objects, $R_i \subset U_i \times U_i$ equivalence relation$\}$ family be the local approximation space and $X, Y \subset U_i$. For the pair $(U_i, R_i) \in \boldsymbol{\mathcal{U}}$**,** let the local lower approximation of the set X is $\underline{R_l}(X)$ and the local upper approximation is $\overline{R_l}(X)$.

i) If $\underline{R_l}(X) \subset \underline{R_l}(Y)$, then the set X will be named *bottom local roughly included* in the set Y and will be denoted by $X \subsetneq_l Y$.

ii) If $\overline{R_l}(X) \subset \overline{R_l}(Y)$, then the set X will be named *top roughly local included* in the set Y and will be denoted by $X \,\tilde{\subset}_l\, Y$.

iii) If $\underline{R_l}(X) \subset \underline{R_l}(Y)$ and $\overline{R_l}(X) \subset \overline{R_l}(Y)$, then the set X will be named *local roughly included* in the set Y and will be denoted by $X \,\tilde{\subsetneq}_l\, Y$.

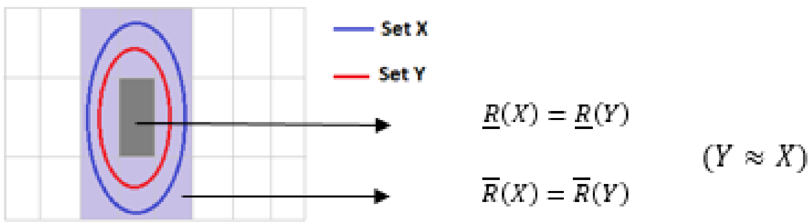

Fig. 4. Rough Equality of Sets.

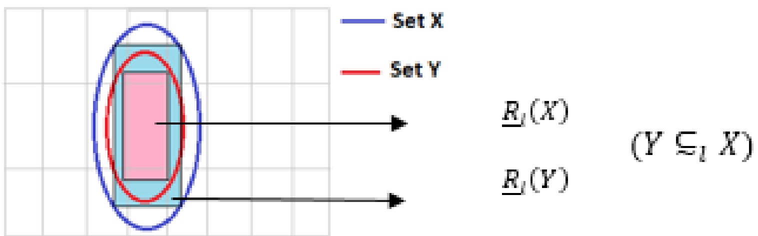

Fig. 5. Bottom-local roughly included.

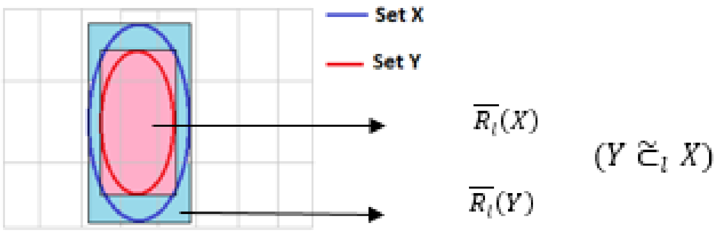

Fig. 6. Top-local roughly included.

The sets X and Y for $Y \subset X$ are roughly equal in Fig. 4 ($Y \approx X$). When these sets are reduced to the local without changing, they are the bottom-local roughly equivalent in Fig. 5 ($Y \underset{\sim}{\subset}_l X$) and they are top-local roughly equivalent in Fig. 6 ($Y \overset{\sim}{\subset}_l X$).

Lemma 5.1 : Roughly equal sets may be local roughly equivalent.

$$\text{If } Y \approx X, \text{ then } Y \overset{\sim}{\underset{\sim}{\subset}}_l X.$$

Definition 5.3 : Let $\mathcal{U}$=$\{(U_i, R_i) :\ i \in I\ , U_i \subset U$ finite set of objects, $R_i \subset U_i \times U_i$ equivalence relation$\}$ family be the local approximation space and $X, Y \subset U_i$.

i) If $X \underset{\sim}{\subset}_l Y$ or $Y \underset{\sim}{\subset}_l X$, then the sets X and Y will be named *bottom-rough comparable.*
ii) If $X \overset{\sim}{\subset}_l Y$ or $Y \overset{\sim}{\subset}_l X$, then the sets X and Y will be named *top-rough comparable.*
iii) If $X \overset{\sim}{\underset{\sim}{\subset}}_l Y$ or $Y \overset{\sim}{\underset{\sim}{\subset}}_l X$, then the sets X and Y will be named *rough comparable.*

The following properties are true for $\mathcal{U}$ to be the local approximation space and $X \subset Y \subset U_i$.

1) If $X \underset{\sim}{\subset}_l Y$, then $X \overset{\sim}{\subset}_l Y$ and $X \overset{\sim}{\underset{\sim}{\subset}}_l Y$.

2) If $X \eqsim Y$, then $X \underset{\sim}{\subset}_l Y$.

3) If $X \simeq Y$, then $X \overset{\sim}{\subset}_l Y$.

4) If $X \approx Y$, then $X \overset{\sim}{\underset{\sim}{\subset}}_l Y$.

5) If $X \overset{\sim}{\subset}_l Y$, then $X \cup Y \simeq_l Y$.

6) If $X \underset{\sim}{\subset}_l Y$, then $X \cap Y \eqsim_l X$.

7) If $X \underset{\sim}{\subset}_l X'$ and $Y \underset{\sim}{\subset}_l Y'$, then $X' \underset{\sim}{\subset}_l Y'$.

8) If $X \overset{\sim}{\subset}_l X'$ and $Y \overset{\sim}{\subset}_l Y'$, then $X' \overset{\sim}{\subset}_l Y'$ dir.

9) If $X \underset{\sim}{\subset}_l X'$ and $Y \underset{\sim}{\subset}_l Y'$, then $X \cap Y \underset{\sim}{\subset}_l X' \cap Y'$.

10) If $X \overset{\sim}{\subset}_l X'$ and $Y \overset{\sim}{\subset}_l Y'$, then $X \cup Y \overset{\sim}{\subset}_l X' \cup Y'$.

6. EXAMPLES

In this section, let's show the sets that are roughly equivalent and local roughly equivalent with an example from daily life. Let's also calculate the saliency levels of these sets and compare them.

Example 6.1: Let the sets of animals of four different kind be as follows.
$Cow = \{c_1, c_2, c_3, c_4\}, Sheep = \{s_1, s_2, s_3\}, Goat = \{g_1, g_2, g_3, g_4\}, Duck = \{\, d_1, d_2, d_3\}$ Let $U = \{c_1, c_2, c_3, c_4, s_1, s_2, s_3, g_1, g_2, g_3, g_4, d_1, d_2, d_3\}$ set of objects,
$A = \{Cow, Sheep, Goat, Duck\}$ set of properties, $V_1 = \{\, 1,2,3,4 \,\}$, $V_2 = \{\, 1,2,3 \,\}$, $V_3 = \{\, 1,2,3,4 \,\}$, $V_4 = \{\, 1,2,3 \,\}$ be set of values.
Let $R(x) = \{x, y\epsilon U\colon\ xRy, x \text{ and } y$ being animals of the same kind$\}$ be an equivalence relation on U. Let the set of animals owned by two people be $X = \{c_1, c_2, c_3, c_4, s_1, g_3\}$ and $Y = \{\, d_1, d_2, d_3, g_1, s_3\}$, respectively.
According to the equivalence (indistinguishability) relations, let's show the lower approximation, the upper approximation and the measure of completeness (saliency levels) of the X and Y sets.
$\underline{R}(X) = \{c_1, c_2, c_3, c_4\} \neq \emptyset$, $\overline{R}(X) = \{c_1, c_2, c_3, c_4, s_1, s_2, s_3, g_1, g_2, g_3, g_4\} \neq U$
$\underline{R}(Y) = \{\, d_1, d_2, d_3\} \neq \emptyset$, $\overline{R}(Y) = \{d_1, d_2, d_3, g_1, g_2, g_3, g_4, s_1, s_2, s_3\} \neq U$
Here it is seen that two persons own some kind of animal and also all animals of a particular kind. So, X and Y are equivalent.
Also, measure of completeness $\alpha_R(X) = \frac{|\underline{R}(X)|}{|\overline{R}(X)|} = \frac{4}{11} \cong 0{,}36$ and $\alpha_R(Y) = \frac{|\underline{R}(Y)|}{|\overline{R}(Y)|} = \frac{3}{10} = 0{,}30$

Example 6.2: Let's apply the same example for the local rough set. Let $U = \{c_1, c_2, c_3, c_4, s_1, s_2, s_3, g_1, g_2, g_3, g_4, d_1, d_2, d_3\}$ set of objects, $A = \{Cow, Sheep, Goat, Duck\}$ set of properties, $V_1 = \{\, 1,2,3,4 \,\}$, $V_2 = \{\, 1,2,3 \,\}$, $V_3 = \{\, 1,2,3,4 \,\}$, $V_4 = \{\, 1,2,3 \,\}$ be set of values.
Let $R(x) = \{x, y\epsilon U\colon\ xRy, x \text{ and } y$ being animals of the same kind$\}$ be an equivalence relation on U.
For the subset $U_l \subseteq U$, let the equivalence relation $R_l \subseteq U_l \times U_l$ and $U = \cup\, U_l$.
Let $\boldsymbol{U}$=$\{(U_i, R_i) :\ i \in I, U_i \subset U$ finite set of objects, $R_i \subset U_i \times U_i$ equivalence relation$\}$ family be the local approximation space. Also, Let , $U_1 = \{c_1, c_2, c_3, c_4, d_1, d_2, d_3, s_1, g_1\}$ and $U_2 = \{s_2, s_3, g_2, g_3, g_4\}$ subsets be given pairs (U_1, R_1) and (U_2, R_2), selected from the local approximation space family.

For $U_1 = \{c_1, c_2, c_3, c_4, d_1, d_2, d_3, s_1, g_1\} \subseteq U$, according to the equivalence (indistinguishability) relations, let's show the local lower approximation, the local upper approximation and the local measure of completeness (local saliency levels) of the X and Y sets.

$\underline{R_l}(X) = \{c_1, c_2, c_3, c_4\} \neq \emptyset$, $\overline{R_l}(X) = \{c_1, c_2, c_3, c_4, s_1\} \neq U_1$

$\underline{R_l}(Y) = \{d_1, d_2, d_3\} \neq \emptyset$, $\overline{R_l}(Y) = \{d_1, d_2, d_3, g_1\} \neq U_1$

Here it is seen that two persons own some kind of animal and also all animals of a particular kinds. So, X and Y are local equivalent.

Measure of completeness $\alpha_{R_l}(X) = \frac{|\underline{R_l}(X)|}{|\overline{R_l}(X)|} = \frac{4}{4} = 1$ and $\alpha_{R_l}(Y) = \frac{|\underline{R_l}(Y)|}{|\overline{R_l}(Y)|} = \frac{3}{3} = 1$

Comparatively, the completeness measures of the elements can be seen more clearly on the following figures.

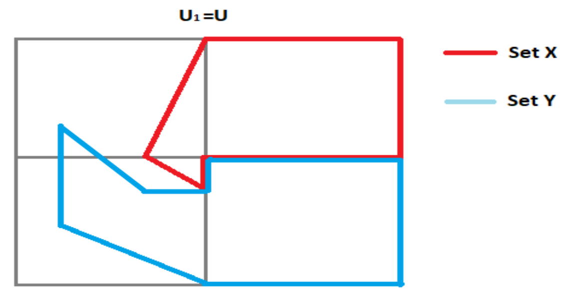

$$\alpha_R(X) = \frac{|\underline{R}(X)|}{|\overline{R}(X)|} = \frac{4}{11} \cong 0{,}36$$

$$\alpha_R(Y) = \frac{|\underline{R}(Y)|}{|\overline{R}(Y)|} = \frac{3}{10} = 0{,}30$$

Fig. 7. Completeness measures of rough equivalent sets.

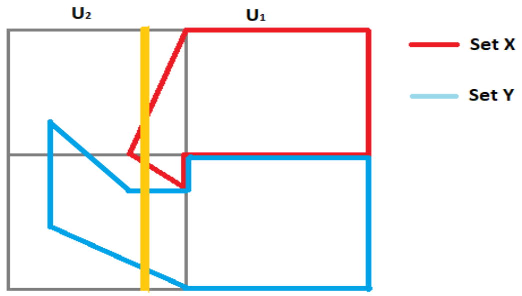

$$\alpha_{R_l}(X) = \frac{|\underline{R_l}(X)|}{|\overline{R_l}(X)|} = \frac{4}{5} = 0{,}80$$

$$\alpha_{R_l}(Y) = \frac{|\underline{R_l}(Y)|}{|\overline{R_l}(Y)|} = \frac{3}{4} = 0{,}75$$

Fig. 8. According to the U_1, completeness measures of local rough equivalent sets.

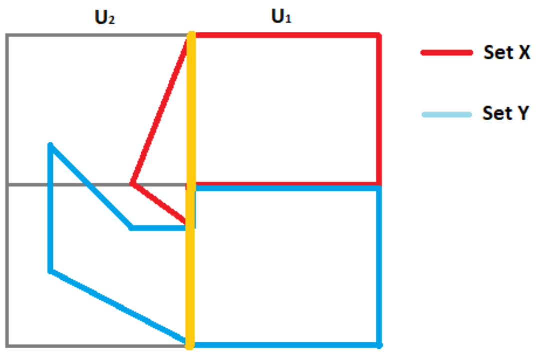

$$\alpha_{R_l}(X) = \frac{|\underline{R_l}(X)|}{|\overline{R_l}(X)|} = 1$$

$$\alpha_{R_l}(Y) = \frac{|\underline{R_l}(Y)|}{|\overline{R_l}(Y)|} = 1$$

Fig. 9. According to the U_1, completeness measures of local rough equivalent sets.

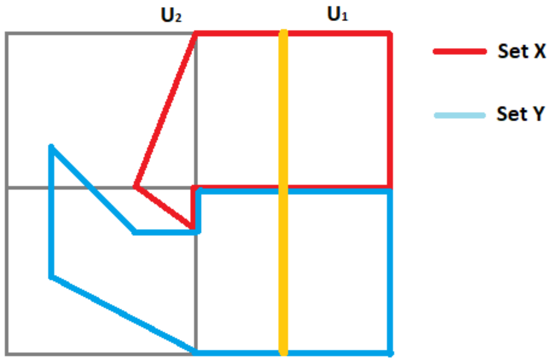

$$\alpha_{R_l}(X) = \frac{|\underline{R_l}(X)|}{|\overline{R_l}(X)|} = 1$$

$$\alpha_{R_l}(Y) = \frac{|\underline{R_l}(Y)|}{|\overline{R_l}(Y)|} = 1$$

Fig. 10. According to the U_1, completeness measures of local rough equivalent sets.

The completeness measures of the X and Y rough equivalent sets were 36% and 30%, respectively. However, for the X and Y sets, which are equivalent to the local rough equivalent, the completeness of the elements increased to 80% and 75%, respectively. Moreover, it has been observed that this rate reaches 100% when the local borders are narrowed.

7. CONCLISUON

It may be said that rough equal sets can be local rough equivalent. If X=Y, then these two sets can be equal to the local rough equal. In addition, it has been noticed that rough equal sets and local rough equal sets can be represented topologically, but it is not appropriate on examples from daily life. It provides more detailed information about the elements of the sets that are local rough equivalent than the rough equivalent. It has been determined that the workload is lightened when the rough sets are grouped and localized. It has also been revealed that the local rough set will have more distinct elements when the boundaries are narrowed.

8. REFERENCES

[1] Pawlak, Z. Rough Sets – theoretical aspects of reasoning about data, Boston, London, Dordrecht: Kluwer Academic Publishers (1991)

[2] M. Novotny and Z. Pawlak, "Characterization of Rough Top equalities and Rough Bottom Equalities", Bull. Polish Acad. Sci. Math., 33, (1985), pp.91-97.

[3] M. Novotny and Z. Pawlak, "On Rough Equalities", Bull. Polish Acad. Sci. Math., 33, (1985), pp.99-104.

[4] M. Novotny and Z. Pawlak, "Black Box Analysis and Rough Top Equality", Bull. Polish Acad. Sci. Math., 33, (1985), pp.105-113.

[5] B.K.Tripathy, A.Mitra and J.Ojha, “On Rough Equalities and Rough Equivalences of Sets”, RSCTC 2008- Akron, U.S.A., Springer-Verlag Berlin Heidelberg (2008), LNAI 5306, pp. 92–102.

[6] B.K.Tripathy, A.Mitra and J.Ojha, ”Rough Equivalence and Algebraic properties of Rough Sets”, International Journal of Artificial Intelligence and Soft Computing, (Switzerland), vol.1, nos.2/3/4, (2009)

[7] Taşbozan, H. (2017). Lokal Rough Kümeler ve Rough Altgrupoidler, Ph. D. Thesis, İnönü University, Malatya, Turkey.

[8] A.F. Özcan, M.M. Beydağı, İ. İçen, “Comparison of Rough Sets and Local Rough Sets in Data Analysis”, New Trends in Mathematical Sciences (2022) vol:10 pp:1-13

[9] Pawlak, Z. Rough Sets, “International Journal of Computer and Information Sciences (1982) Vol.11, No.5

[10] Tripathy, B.K., “An Analysis of Approximate Equalities based on Rough Set Theory”, International Journal of Advanced Science and Technology Vol. 31, June, 2011.

MODERN SET THEORIES

FUZZY, ROUGH, SOFT, NEAR SETS AND THE RELATIONSHIPS BETWEEN THEM

Semih GEÇEN[1], İlhan İÇEN[2], A. Fatih ÖZCAN[3]

[1]Department of Topology,Graduate School of Nature and Applied Sciences,Inonu University,Malatya,semihgecen44@gmail.com

[2],Department of Topology,Graduate School of Nature and Applied Sciences,Inonu University,Malatya,ilhan.icen@inonu.edu.tr

[3]Department of Topology,Graduate School of Nature and Applied Sciences,Inonu University,Malatya,abdullah.ozcan@inonu.edu.tr

Abstract

Fuzzy set, rough set, soft set and near set theories have given modern mathematics the facility to re-express itself with a new direction, perspective and an up-to-date language. In this way, alternative methods have been introduced for the solution of incomplete and imprecise problems. In this study, these set theories are discussed together, unique examples are given and the relationships between them are examined.

Keywords : Fuzzy set, Rough set, Soft set, Near set

1.Introduction

The uncertainties in nature and especially the complex and uncertain problems of modern times have not only attracted the attention of thinkers, but also entered the agenda of scientists dealing with mathematics and logic. The classical medhods of mathematics were insufficient to solve some of the uncertainty problems of the modern age. In order to overcome this situation, set theories, which G.Cantor, added a new perspective to mathematics, found the facility to Express itself again and in a new language, and presented alternative solution medhods to the problems of uncertainty situations:

L. A. Zadeh breathed new life into the world of science by introducing Fuzzy Set Theory in 1965 [1]. Then, in 1982, Z. Pawlak introduced the “Rough set” theory for modeling inconsistencies in information systems [2].

D. A. Molodtsov introduced the “Soft set” theory in 1999, which gave a new perspective to the concepts of exactness and precision in mathematics [3]. This theory proposes more specific and easier to classify solutions by parameterizing some incomplete and imprecise concepts encountered in pratical life.

In 2002, J. F. Peters introduced the “Near set” theory, which is a more generalized version of Rough sets [4]. In near sets, data is obtained not in the form of information tables, which is the working method of Rough sets,but by using real-valued functions, which is a simpler and more pratical method.

2. FUZZY SET THEORY

Fuzzy set theory, which reveals a wider structure than classical set theories, deals with sets with imprecise boundaries. In classical sets, an element is either an element (1) or not an element (0) of a set. However, a Fuzzy set, unlike a classical set, allows partial membership of the elements of the set. In fuzzy sets, the membership degree of an element can theoretically take infinite values in the range of [0,1]. In classical set theory, it is desired for a set to have well-defined properties that do not allow for ambiguity; however, we may not always find precise and well-defined properties in set definitions in the new world, and Fuzzy set theory has emerged precisely from this need.

2.1. Fuzzy Sets: L. A. Zadeh brought a new breath to the world of science by introducing the Fuzzy set theory in 1965 [1].

Definition 2.1.1: U is a non-empty set and A is a Fuzzy set at U; it is given by the function $\forall\, x \in U$ için $\mu_A\colon U \longrightarrow I = [0,1]$. μ_A is called the membership function corresponding to the Fuzzy set. The Fuzzy set A is the set formed by each element in U together with its membership degree, so $A = \{(x, \mu_A(x)) : x \in U\}$. The degree of belonging or membership of x to A is μ_A. Every membership function is a function that corresponds to a number in the range [0,1] of the elements of a classical universal set. For example $\mu_A(x) = 0.5$ means x is fifty percent element of set A. The concept of fuzzy set is in many ways parallel to the framework used for classical sets, but it provides a suitable starting point for the construction of a more general conceptual framework than the classical set and has a wider application area [1].

The fuzzy set theory is formulated based on the terms complement, union and intersection of the fuzzy set, which are given below, respectively [1]:

- $\mu_{U-A}(x) = 1 - \mu_A(x),\ x \in U$
- $\mu_{A\cup B}(x) = \max\{\mu_A(x), \mu_B(x)\},\ x \in U$
- $\mu_{A\cap B}(x) = \min\{\mu_A(x), \mu_B(x)\},\ x \in U.$

Example 2.1.1. Let's consider whether a car brand belongs to a country within the framework of the classic set: We know that the classical set works with precise and well-defined properties. For example "A TOGG brand vehicle is either manufactured in Türkiye (1) or not produced in Türkiye (0). It want to make a judgment as "if all parts of the vehicle are produced in Türkiye, it is a Turkish brand (1) or if all parts are not produced in Türkiye, it is not a Turkish brand (0). But we know that real life is not always clear and well-defined. At this stage, Fuzzy set theory comes into play and provides us with the possibility of multiple grading in the [0,1] range, dilemma, with the help of the membership function for definitions with unclear boundaries. Accordingly, external support can be obtained for certain parts of the TOGG brand vehicle or for certain design stages and this does not prevent TOGG from becoming a brand of Türkiye.

Definition 2.1.2. Let X be a set. The $R\colon X \times X \longrightarrow [0,1]$ transform that satisfies the following properties is called a similarity relation:

(i) Reflection: $\forall\, x \in X$ için $R(x,x) = 1$
(ii) Symmetry: $\forall\, x, y \in X$ için $R(x,y) = R(y,x)$
(iii) Transitive: $\forall\, x, y, z \in X$ için $R(x,z) \geq \min\{R(x,y), R(y,z)\}$

With this relation defined, (X, R) pair is called Fuzzy approximation space [5].

A Fuzzy set is defined by assigning each element of the study area a value that represents the degree of membership in the set mathematically. This value expresses the degree of belonging of the related element to the Fuzzy set according to the determined criteria.The membership degree can take a value between 0 and 1. Full membership and non-member status are met by the numbers 1 and 0, respectively, in Fuzzy sets, so the classical set concept can be considered as a special case of the Fuzzy set concept reduced to these two values. Although mathematical structures built on Fuzzy sets have a more explanator power than classical mathematics, their usability depends on the construction of appropriate membership functions for the concepts we encounter in the application areas [5].

A Fuzzy set A is fully characterized by an ordered set of pairs $A = \{(x, \mu_A(x))\colon x \in U\}$. A Fuzzy set can be associated with a crisp family of sets through the concept of a α-level set. The α-level set of a Fuzzy set A is defined by $A(\alpha) = \{x \in U\colon \mu_A(x) \geq \alpha\}$, where $\alpha \in [0,1]$. The α value can be chosen arbitrarily, but is usually set as one of the membership degrees seen in the fuzzy set in question. α-level sets can be used to describe a family of nested subsets of U. On the other hand, a fuzzy set A can be reconstructed from any family of α-level sets using the following formula (F-1): $\mu_A(x) = \sup\{\alpha : x \in A(\alpha)\}$ [6].

Example 2.1.2. X being the set of trees; suppose there are 6 different alternatives in the $X = \{h_1, h_2, h_3, h_4, h_5, h_6\}$ set and "age of trees" is selected as a single parameter. We can define the set of terms T(age) = {very old, middle-aged, young, very young} fort his varible. Each term can be associated with its own Fuzzy set. Two of them can be defined as:

$$A_{very\ old} = \{(h_1, 0.3), (h_2, 0.6), (h_5, 0.9), (h_6, 1.0)\} \quad \text{or}$$
$$A_{very\ young} = \{(h_1, 0.9), (h_2, 0.4), (h_3, 0.9), (h_4, 1.0), (h_5, 0.2)\}$$

For example, when interpreting the set $A_{very\ old}$, we infer that the h_1, h_2, h_5, h_6 trees are very old, at a ratio of 0.3, 0.6, 0.9, 1.0 respectively. In this case, we get the facility to compare the elements of the set according to the specified parameter.

3. ROUGH SET THEORY

The Rough set theory was introduced by Z. Pawlak in 1982 [7]. This theory is a method of dealing with the uncertainty and incomprehensibility of imprecise information. The basis of classification of objects in Rough set theory is based on equivalence classes. The purpose of this theory is to characterize a universal set with lower approximation and upper approximation when given any subset. Rough set theory has been a tool for defining sets that cannot be determined with available information, with the help of approaches and for solving various problems such as reasoning based on incomplete information [7].

This theory, which is a new mathematical method for imprecise information, has found many applications such as artificial intelligence, medicine, machine teaching and data mining.

3.1 Rough Set

Definition 3.1.1. U is the universal set of a finite number of objects, a relation on U corresponds to any subset R of the product set $U \times U$. If the relation R provides the properties of being reflexive, symmetric and transitive, it is called an equivance relation. In this situation U is called the universal set, R is called the indiscernibility relation. If R is an equivalence relation over U, then the (U, R) pair is called the approximation space [8].

Definition 3.1.2. Let U be a non-empty finite universal set of objects and R be an equivalence relation over U. For $x \in U$, the set $R(x) = [x]_R = \{ y \in U : xRy \}$ is defined as the equivalence class of x. These equivalence classes form bits of information for a full understanding of the given information [9].

Definition 3.1.3. Let (U, R) be the approximation space and $\emptyset \neq X \subseteq U$.

$$\underline{R}(X) = \{ x : [x]_R \subseteq X \}$$

The set (U, R) is called the lower approximation of the set X in the approximation space. Accordingly, the lower approximation of X consists of a combination of equivalence classes completely covered by X. Or it is the set of elements in equivalence class X [10].

Definition 3.1.4. Let (U, R) be the approximation space and $\emptyset \neq X \subseteq U$

$$\overline{R}(X) = \{ x : [x]_R \cap X \neq \emptyset \}$$

set (U, R) is called the upper approximation of X set in approximation space. The upper approximation of X is the set formed by the equivalence class and the elements of X whose intersection is different from the empty [10].

$\overline{R}(X)$ consists of elements that are likely to be in set X. Here for $x \notin X$ it can be$[x]_R \cap X \neq \emptyset$. That is, an element in the upper approximation of set X may not be an element of set X. With the help of the equivalence classes determined according to the equivalence relation on a set, the lower and upper approximations of the given set can be understood more easily from the figure below [5].

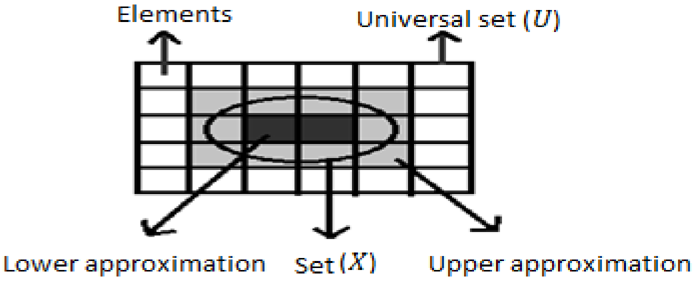

Shape 3.1 Lower and upper approximation of a set

Definition 3.1.5. Let (U, R)be the approximation space and $X \subseteq U$. $BndR(X)$, the boundary region of the set X, is the difference between the upper and lower approximations. So $BndR(X) = \overline{R}(X) - \underline{R}(X)$ [7].

Definition 3.1.6. If the boundary region of the set X is the empty set, the set X is called a complete set according to the R relation. So, $BndR(X) = \emptyset \Leftrightarrow \underline{R}(X) = \overline{R}(X)$.
In this case, the complete set gives the concept of the classical set. [7].

Definition 3.1.7. If the boundary region of the set X is different from the empty, the set X is called a rough set according to the R relation. So, $BndR(X) \neq \emptyset \Leftrightarrow \underline{R}(X) \neq \overline{R}(X)$ [7].

Example 3.1.1. The following information table is given, where $U = \{ x_1, x_2, x_3, x_4, x_5, x_6, x_7, x_8, x_9, x_{10}, x_{11}, x_{12} \}$ is set of objects, $A = \{ a_1, a_2, a_3, a_4 \}$ is the set of properties, $V_1 = \{ 1,2,3\}$, $V_2 = \{ 1,2,3.4 \}$, $V_3 = \{ 1,2,3,4,5\}$, value sets and the equivalence relation on U is $R(x_i) = \{ x_j : x_j ,$ have the same dimensions as the x_i's, $1 \leq i,j \leq 12 \}$;

U	a_1	a_2	a_3	a_4
x_1	2	1	3	4
x_2	3	2	1	3
x_3	2	1	3	4
x_4	5	2	3	1
x_5	3	5	4	2
x_6	1	2	3	5
x_7	3	2	1	3
x_8	3	5	4	2

x_9	3	2	1	3
x_{10}	2	1	3	4
x_{11}	1	2	3	5
x_{12}	3	5	4	2

The indiscernibility relation of this table is as follows:

$$R(x_1) = R(x_3) = R(x_{10}) = \{ x_1, x_3, x_{10} \}$$
$$R(x_2) = R(x_7) = R(x_9) = \{ x_2, x_7, x_9 \}$$
$$R(x_4) = \{ x_4 \}$$
$$R(x_5) = R(x_8) = R(x_{12}) = \{ x_5, x_8, x_{12} \}$$
$$R(x_6) = R(x_{11}) = \{ x_6, x_{11} \}$$

With the help of these equivalence classes, for a set $X = \{ x_1, x_3, x_4, x_5, x_8, x_9, x_{12} \}$ on U

$$\underline{R}(X) = \{x_4, x_5, x_8, x_{12}$$
$$\overline{R}(X) = \{x_1, x_2, x_3, x_4, x_5, x_7, x_8, x_9, x_{10}, x_{12} \}$$
$$BndR(X) = \overline{R}(X) - \underline{R}(X) = \{x_1, x_2, x_3, x_7, x_9, x_{10}\}$$

obtained. Then the set X cannot be defined with these properties, that is, it is a rough set.

Definition 3.1.8. Let $X \neq \emptyset$ be a set and $|X|$ be the cardinality (number of elements) of the set X. Accuracy of approximation (measure of completeness) in the rough set X in the approximation space (U, R) is $\alpha_R(X) = \frac{|\underline{R}(X)|}{|\overline{R}(X)|}$ [7].

3.2. Approximate Membership Function in Rough Set

In full set theory, the membership of an element to the set takes values of 1 and 0, whereas in rough sets, the membership function notation is different. Rough sets can also be defined by taking the approximation membership function $\mu_X^R : U \rightarrow [0,1]$ instead of approximations. In the approximate membership function, the $[x]_R$ equivalence class of the element x and the degree of overlap of the set X are measured.

Definition 3.2.1. Let $X \neq \emptyset$ be a set. Cardinality (number of elements) of the set, $|X|$ The approximate membership function on a rough set X of the approximation space (U, R) is defined as: It is the ratio of the number of elements of the intersection of the set X and the equivalence classes $[x]_R$ to the number of elements of the equivalence class $[x]_R$, and

$$\mu_X^R(x) = \frac{| X \cap [x]_R |}{| [x]_R |}$$

is displayed as [5].

The approximate membership function is provided as follows

$$\text{If } X \cap [x]_R = \emptyset \text{ then } \mu_X^R(x) = 0,$$
$$\text{If } X \cap [x]_R \neq \emptyset \text{ then } 0 < \mu_X^R(x) < 1,$$
$$\text{If } [x]_R \subseteq X \text{ then } \mu_X^R(x) = 1$$

Lower, upper approaches, and boundary regions of a rough set X are defined by approximate membership function as follows;

$$\underline{R}(X) = \{x \in U : \mu_X^R(x) = 1 \}$$

$$\overline{R}(X) = \{x \in U : \ \mu_X^R(x) > 0\}$$

$$BndR(X) = \overline{R}(X) - \underline{R}(X) = \{x \in U : 0 < \mu_X^R(x) < 1\}$$ [5].

The membership functions satisfy the following properties

1. $\mu_X^R(x) = 1 \Leftrightarrow x \in \underline{R}(X)$
2. $\mu_X^R(x) = 0 \Leftrightarrow x \in U - \overline{R}(X)$
3. $0 < \mu_X^R(x) < 1 \Leftrightarrow x \in BndR(X)$
4. $\mu_{U-X}^R(x) = 1 - \mu_X^R(x), x \in U$
5. $\mu_{X\cup Y}^R(x) \geq \max\{\mu_X^R(x), \mu_Y^R(x)\}, x \in U$
6. $\mu_{X\cap Y}^R(x) \leq \min\{\mu_X^R(x), \mu_Y^R(x)\}, x \in U$ [5].

Example 3.2.1. Using the data of Example 3.1.1, the membership values of each element of set X are as follows:

$$\mu_X^R(x_1) = \mu_X^R(x_3) = \mu_X^R(x_{10}) = \tfrac{2}{3},$$

$$\mu_X^R(x_2) = \mu_X^R(x_7) = \mu_X^R(x_9) = \tfrac{1}{3},$$

$$\mu_X^R(x_4) = 1$$

$$\mu_X^R(x_5) = \mu_X^R(x_8) = \mu_X^R(x_{12}) = 1$$

$$\mu_X^R(x_6) = \mu_X^R(x_{11}) = 0$$

Accordingly, with the help of the membership function, the following can be easily written:

$$\underline{R}(X) = \{x_4, x_5, x_8, x_{12}\}$$

$$\overline{R}(X) = \{x_1, x_2, x_3, x_4, x_5, x_7, x_8, x_9, x_{10}, x_{12}\}$$

$$BndR(X) = \{x_1, x_2, x_3, x_7, x_9, x_{10}\}.$$

4. SOFT SET THEORY

Soft set theory defined by D.A. Molodtsov has found wide repercussion in modern mathematics. After the introduction of soft set theory, which gives a new perspective to the precision concepts in mathematics, it has been studied topologically, categorically and algebraically by many mathematicians [11-13]. In this section, soft set theory defined by D.A. Molodtsov in 1999 is given [3].

4.1 Soft Sets

Let the set of all subsets of X be $P(X)$ and $A \subset E$, where X is a universal set and E is the set of parameters. Thus, the definition of a soft set is given as follows:

Definition 4.1.1. The pair (F, A) given with any $F : A \longrightarrow P(X)$ transformation is called a **soft set** on X [4]. For the above definition, it can be said that a soft set on X is a parameterized family of subsets of the universal set X. For $\alpha \in A$, the $F(\alpha)$ family can be defined as a set of α approximation elements of the soft set (F, A) [3].

Here, for convenience, a soft set (F, A) on X will sometimes be denoted by (X, F, A).

Example 4.1.1. Let the universal set X be the set of trees. Also, let the set of E parameters be defined as $E = \{$apricot, plane tree, old, beautiful, young, pine, walnut, tall$\}$. In this case, a soft set to be defined; will indicate trees such as apricot trees, walnut trees, pine trees, plane trees, … etc.
Suppose there are six trees in the universal set $X = \{h_1, h_2, h_3, h_4, h_5, h_6\}$.
For the set $A = \{e_1, e_2, e_3, e_4, e_5\}$, e_1 parameter is 'apricot', e_2 parameter is 'plane tree', e_3 parameter is 'old', e_4 parameter is 'beautiful', e_5 parameter is 'young' and
$F(e_1) = \{h_1, h_3\}$, $F(e_2) = \{h_2, h_4\}$, $F(e_3) = \{h_2, h_3, h_5\}$, $F(e_4) = \{h_1, h_2, h_4\}$, $F(e_5) = \{h_1\}$
be defines as. Here;

$F(e_1) = \{h_1, h_3\}$ apricot trees, $F(e_2) = \{h_2, h_4\}$ plane trees, $F(e_3) = \{h_2, h_3, h_5\}$ old trees, $F(e_4) = \{h_1, h_2, h_4\}$ beautiful trees, $F(e_5) = \{h_1\}$ young trees.
Accordingly, the soft set (F, A) is a parameterized $\{F(e_i)$, i = 1, 2, 3, 4, 5$\}$ family of subsets of the universal set X.
Thus, the (F, A) soft set $(F, A) = \{$apricot trees = $\{h_1, h_3\}$, plane trees = $\{h_2, h_4\}$, old trees = $\{h_2, h_3, h_5\}$, beautiful trees = $\{h_1, h_2, h_4\}$, young trees = $\{h_1\}\}$.

Note 4.1.1. As the number of simıltaneously selected parameters in a soft set increases, the uncertainty level of subsets classified with these parameters decreases. If a single "apricot" parameter is used in example 4.1.1., only "apricot trees" will be classified.

However, if the "apricot, young and beautiful" parameters are selected at the same time, trees suitable for these three characteristics are classified, reduces uncertainty about the properties of trees and the resulting soft sets are better defined. In this context, the number of parameters selected and the uncertainty level of the set are inversely proportional

Definition 4.1.2. For two soft sets (F, A) and (H, B) over a common universe X, we say that (H, B) is a **soft subset** of (F, A) if

- **i.** $B \subset A$.
- **ii.** $\forall \alpha \in B$, $H(\alpha)$ and $F(\alpha)$ are identical approximations.

We write $(H, B) \tilde{\subset} (F, A)$ [14].

Definition 4.1.3. Two soft sets (F, A) and (H, B) over a common universe X are said to be **soft equal** if (F, A) is a soft subset of (H, B) and (H, B) is a soft set of (F, A) [15].

Example 4.1.2. Let X be universal set and E set of parameters as given in example 4.1.1. and $B = \{e_1, e_3\} \subset E$ and $A = \{e_1, e_3, e_4\} \subset E$. It is clear that $B \subset A$. Also, let the (F, A) and (H, B) soft sets be given as

$H(e_1) = \{h_1, h_3\}$, $H(e_3) = \{h_2, h_3, h_5\}$, $F(e_1) = \{h_1, h_3\}$, $F(e_3) = \{h_2, h_3, h_5\}$, $F(e_4) = \{h_1, h_2, h_4\}$, on the $X = \{h_1, h_2, h_3, h_4, h_5, h_6\}$ universal. In this case it is clear that $(H, B) \tilde{\subset} (F, A)$.

Definition 4.1.4. Let $E = \{e_1, e_2, e_3, \ldots e_n\}$ be a set of parameters. The NOT set of E denoted by $\urcorner E$ is defined by $\urcorner E = \{\urcorner e_1, \urcorner e_2, \urcorner e_3, \ldots \urcorner e_n\}$ where $\urcorner e_i = e_i$-, $\forall i$ [14].

The following results are obvious.

Proposition 4.1.1. [14]

i. $\urcorner(\urcorner A) = A$.

ii. $\urcorner(A \cup B) = (\urcorner A \cup \urcorner B)$.

iii. $\urcorner(A \cap B) = (\urcorner A \cap \urcorner B)$.

Example 4.1.3. Considering example 4.1.1. $\urcorner E$ = {not apricot, not plane tree, not old, not beautiful, not young, not pine, not walnut, not tall}.

Definition 4.1.5. The complement of a soft set (F, A) is denoted by $(F, A)^c = (F^c, \urcorner A)$, where, $\forall\, \alpha \in \urcorner A$, $F^c: \ \urcorner A \longrightarrow P(X)$

$$\alpha \mapsto F^c(\alpha) = X - F(\urcorner\alpha) \ [14].$$

Let us call F^c to be soft complement function of F. The following equations can be easily written: $(F^c)^c = F$, $((F, A)^c)^c = (F, A)$ [14].

Example 4.1.4. Consider the soft set (F, A) given in example 4.1.1. Its complement is obtained as a soft set defined as $(F, A)^c$ = {trees other than apricots = { h_2, h_4, h_5, h_6 }, trees other than plane tree = {h_1, h_3, h_5, h_6 }, trees other than old = { h_1, h_4, h_6 }, trees other than beautiful = {h_3, h_5, h_6 }, trees other than young = { h_2, h_3, h_4, h_5, h_6 }}.

Definition 4.1.6. A soft set (F, A) over X is said to be a **Null** soft set denoted by ϕ, if $\forall\, \alpha \in A$, $F(\alpha) = \emptyset$ [14].

Definition 4.1.7. A soft set (F, A) over X is said to be **absolute** soft set denoted by $\tilde{A}$, if , $\forall\, \alpha \in A$, $F(\alpha) = X$. Clearly, $\tilde{A}^{\,c} = \emptyset$ and $\phi^c = \tilde{A}$ [14].

Definition 4.1.8. A soft set (F, A) defined on $X \times X$ is called a **soft relation** on set X [15].

Definition 4.1.9. Let the soft set (F, A) be a soft relation on the set X, and let $F(\alpha) \neq \emptyset$ be for $\forall\, \alpha \in A$, if $F(\alpha)$ is an equivalence relation on the set X, then (F, A) is called a **soft equivalence relation** on the set X [15].

5. NEAR SET THEORY

It can be said that near set theory emerged from the problem of comparing similarities between digital images, especially with the development of computer-based technologies. For example, subimages of one digital image class may have similar definitions as subimages of another digital image class. This theory, proposed by J. F. Peters in 2002, should be understood as a generalization of the rough set theory put forward by Z. Pawlak [2]. Near set theory provides that similar information obtained from objects in discrete sets can be used as a method. That is, near set theory is used to observe, compare and classify objects [16]. For this, first, functions are assigned to the properties of the observed objects. In near set theory, inference functions that represent the distinguishing properties of objects are defined from an object to a real number corresponding to the value of the observable properties. [17].

5.1. Near Set

Definition 5.1.1. Real-valued functions that represent the distinguishing features of perceptual objects are called probe functions. [17, 18].

Probe functions establish similarities between objects as well as between sets of similar objects. [19]. An probe function measures the observed physical characteristics of objects around us. Accordingly, an probe function is a partial function that measures a property. Each of them can be considered as a sensor that detects the physical feature to be measured and creates its real-valued counterpart.

Each feature can be assigned an probe function, or a feature can be measured with more than one probe function. The set of probe functions and the set of perceptual objects form the basis of the near set [20].

Axiom 5.1.1. An object is perceivable if, and only if the object is describable [20].

Definition 5.1.2. A perceptual system $\langle O, \mathscr{F} \rangle$ consists of a sample space O containing a finite, non-empty set of sensed sample objects and a non-empty, countable set $\mathscr{F}$ containing probe functions representing object features [20].

Probe functions can be real-valued functions as well as non-real-valued functions. That is, any set where V is not empty, $X \subseteq O$ is the set of perceptual objects, the probe function can be defined as $\varphi: X \longrightarrow V$ [21].

Symbol	Interpretation
$\mathbb{R}$	Set of real numbers,
$\boldsymbol{O}$	Set of perceptual objects,
$\boldsymbol{X}$	$X \subseteq O$, set of sample objects,
$\boldsymbol{x}$	$x \in O$, sample object,
$\mathscr{F}$	A set of functions representing object features,
$\boldsymbol{B}$	$B \subseteq \mathcal{F}$,
$\boldsymbol{L}$	Description length,
$\boldsymbol{i}$	$i \leq L, L \in \mathbb{Z}^{+}$,
$\boldsymbol{\varphi_{\mathrm{i}}}$	$\varphi_{\mathrm{i}} : O \longrightarrow \mathbb{R}$, probe function,
$\boldsymbol{\Phi}$	$\Phi: O \longrightarrow \mathbb{R}^{L}$, Object description
$\boldsymbol{\Phi\ (x)}$	$\Phi\ (x)=(\varphi_1(x), \varphi_2(x), \varphi_3(x), \dots, \varphi_{\mathrm{i}}(x), \dots, \varphi_L(x))$

Table-1

In order for computer systems to perceive physical objects existing in the perceptual system, these objects must have some mathematical definitions. The definition of an $x \in X$ object is determined by the function $\Phi(x)$ determined with the help of probe functions. One of the important issues here is the selection of the $\varphi_{\mathrm{i}} \in B$ probe functions by considering the properties of the objects to be measured. Let $B \subseteq \mathcal{F}$ be the set of features to be measured, let the features in set $\mathbb{R}$ represent the distinguishing features of $x \in X$ objects.

Let $\varphi_{\mathrm{i}} \in B$ be $\varphi_{\mathrm{i}} : O \longrightarrow \mathbb{R}$. Considering the combination of these probe functions $\Phi: O \longrightarrow \mathbb{R}^{L}$ object description is obtained. This means; $\Phi(x)=(\varphi_1(x), \varphi_2(x), \varphi_3(x), \dots, \varphi_{\mathrm{i}}(x), \dots, \varphi_L(x))$ is the object description with description length $|\varphi_{\mathrm{i}}| = L$. The intuition underlying a description $\Phi\ (x)$ is a recording of measurements from sensors, where each sensor is modelled by a function φ_{i} [17].

Example 5.1.1. (Behavioral description in mountaineers)

x_i	s	a	$p(s,a)$	r
x_1	0	1	0.1	0.60
x_2	0	2	0.1	0.60
x_3	1	3	0.02	0.1
x_4	2	1	0.027	0.1
x_5	2	4	0.036	0.70
x_6	0	2	0.01	0.75
x_7	2	4	0.03	0.8

Table-2

The mathematical modeling of the climbing behaviors that can be observed in mountaineers is possible by using the probe functions assigned to these behaviors. Let $X = \{x_1, x_2, x_3, x_4, x_5, x_6, x_7\} \subseteq O$ be a set of climbers and $B = \{s, a\ p, r\} \subseteq \mathcal{F}$ be a set of functions.

$s: X \longrightarrow \{0,1,2\}$ the different state values of the state function going to the top of the mountain and $a: X \longrightarrow \{1,2,3,4\}$, the action functions modeling the different action styles going to the top of the mountain are as shown in Table-3. Let's assume that $r: X \longrightarrow [0,1]$ is the reward function and $p(s,a): S \text{ x } A \longrightarrow [0,1)$ is the preference function.

Accordingly, the behavior description can be represented by the probe functions $\{s, a, p(s,a), r\}$. Here {s,a,p(s,a),r} respectively; means functions that represent state, action, preference for climbing at a state, and reward as a result of climbing. A reward r is observed in state s and results from an action a performed in the previous state.

The preferred action a in state s is calculated using $p(s,a) + \beta\delta(r,s)$. Here β is the ratio of each climber's climbing ability and $\delta(r,s)$ is used to evaluate the quality of an a action. In this case, the behavior description of the $x \in X$ climber can be modeled as $\Phi(x) = \{s(x), a(x), V(s(x)), r(x)\}$.

The variety or number of an probe function can be increased or decreased to solve the problem under consideration.

Symbol	interpretation
$\sim_B$	$\sim_B = \{(x,x') : f(x) = f(x'), \forall f \in B\}$, indiscernibility relation
$[x]_B$	$[x]_B = \{x' \in X : x \sim_B x'\}$, elementary set (class)
$O/\sim_B$	$O/\sim_B = \{[x]_B\, x \in O\}$, quotient set
ξ_B	$\xi_B = O/\sim_B$
Δ_{φ_i}	$\Delta_{\varphi_i} = \lvert\varphi_i(x') - \varphi_i(x)\rvert$, probe function difference

Table-3

Sample objects $X \subseteq O$ are near each other if, and only if the objects have similar descriptions. Each φ indicates a distinctive feature of an object. In this case, with $x, x' \in O$; Δ_{φ_i} difference $\Delta_{\varphi_i} = |\varphi_i(x') - \varphi_i(x)|$ is defined as. Δ_{φ_i} difference determines the indiscernibility relation defined by Z. Pawlak [22].

Definition 5.1.3. (indiscernibility relation): Let $x, x' \in O$ and $B \subseteq \mathcal{F}$. The relation defined as $\sim_B = \{(x, x') \in O \times O : \forall \varphi_i \in B, \Delta_{\varphi_i} = 0\}$ is called the indiscernibility relation on O, where $i \leq |\Phi|$ (description length) [17].

Definition 5.1.4. (Weak nearness relation): Let $\langle O, \mathscr{F} \rangle$ be a perceptual system and let $X, Y \subseteq O$. A set X is weakly near to a set Y within the perceptual system $\langle O, \mathscr{F} \rangle$ ($X \underline{\bowtie}_{\mathcal{F}} Y$) iff there are $x \in X$ and $y \in Y$ and there is $B \subseteq \mathcal{F}$ such that $x \sim_B y$ [23].

Definition 5.1.5. (Nearness Description Principle) Let $B \subseteq \mathcal{F}$ be a set of functions representing features of objects $x, x' \in O$. Objects x, x' are minimally near each other if, and only if there exists $\varphi_i \in B$ such that $x \sim_{\{\varphi_i\}} x'$ i.e. $\Delta_{\varphi_i} = 0$ [17].

Definition 5.1.6. (measure of object nearness): Let $B \subseteq \mathcal{F}$ be a set of functions representing features of objects in O. Let $X, X' \subseteq O$ denote a set of objects of interest and set of test objects, respectively. Let $\varphi_i \in B$, where $i \leq |B|$. Let $\mu_X^B : P(O) \longrightarrow [0, 1]$ denote a capacity function defined by

$$\mu_X^B(X') = \frac{\left|\{\varphi_i \in B : x \sim_{\{\varphi_i\}} x', x \in X, x' \in X'\}\right|}{|B|}$$

[17].

Example 5.1.2. Let O be a set of sample vehicles. Let the sets $X_K, X_L \subseteq O$ be the set of cars produced in factory K and minibuses produced in factory L, respectively. Let's assume that the probe functions $\varphi_i \in B \subseteq \mathcal{F}$ represent the distinguishing features of the vehicles in O. Also, let $i \leq |B| = 7$ and $x \in X_K$ car and $x' \in X_L$ minibuse be indiscernible only in terms of φ_i. In this case, since $x \sim_{\{\varphi_i\}} x'$ for an $x \in X_K$ car and an $x' \in X_L$ minibuse, $\mu_{X_K}^B(X_L) = \frac{1}{7}$.

The basic idea for object recognition in the near-set approach is the comparison of object descriptions. Accordingly, sets X and X' are close to each other if they contain objects with partially identical descriptions.

Definition 5.1.7. Let $X, X' \subseteq O$ and $B \subseteq \mathcal{F}$. Set X is near X' if, and only if there exists $x \in X$, $x' \in X'$, $\varphi_i \in B$ such that $x \sim_{\{\varphi_i\}} x'$ [17].

6. RELATIONS BETWEEN FUZZY SET, ROUGH SET, SOFT SET AND NEAR SET

While classical set theories produced solutions for complete and precise problems, the nature of the problems has changed in the modern period, and rather incomplete and imprecise problems have emerged. As there are differences between fuzzy, rough, soft and near set theories, which are put forward to overcome these uncertainties, there are undoubtedly similarities and transitions in many respects. In this section, these similarities and transitions will be revealed.

6.1. The relationship between fuzzy set and soft set

Proposition 6.1.1. Every fuzzy set can be expressed as a soft set [6].

Proof : Let $A = \{(x,\ \mu_A(x)): x\ \in U\}$ be a fuzzy set and μ_A a fuzzy membership function defined from the universal set U to the closed interval [0,1]. For the function μ_A defined by $\mu_A(x) = \sup\{\alpha: x \in\ A(\alpha)\}$, consider the family of α -level sets $A(\alpha) = \{x \in U: \mu_A(x) \geq \alpha\}$. Accordingly, if the A family is known, the $\mu_A(x)$ functions can be found with the equation $\mu_A(x) = \sup\{\alpha: x \in A(\alpha)\}$. In this case, every fuzzy set A can also be expressed as a soft set as $(A, [0,1])$.

Example 6.1.1 Consider the fuzzy set A in Example 2.1.2:

$$A_{very\ old}(0.3) = \{h_1, h_2, h_5, h_6\}, A_{very\ old}(0.6) = \{h_2, h_5, h_6\},$$

$$A_{very\ old}(0.9) = \{h_5, h_6\}, A_{very\ old}(1.0) = \{h_6\}$$

$D = \{0.3, 0.6, 0.9, 1.0\} \subseteq [0,1]$ values can be treated as a parameter set such that the mapping $A_{very\ old}: D \longrightarrow P(X)$ gives approximate sets of values $A_{very\ old}(\alpha)$ for $\alpha \in D$

Accordingly, the relevant soft set can be written as:

$(A_{very\ old}, [0,1]) = \{(0.3, \{h_1, h_2, h_5, h_6\}), (0.6, \{h_2, h_5, h_6\}), (0.9, \{h_5, h_6\}), (1.0, \{h_6\})\}$.

6.2. Relationship between rough set and near set

Proposition 6.2.2. Every Rough set can be expressed as a Near set [24].

Proof: Let $\langle O, \mathscr{F}\rangle$ be the perceptual system containing perceptual objects, and $\mathscr{F}$ represent the properties of objects in O. Also, let $O_{\sim B}$ be all classes in the quotient of O defined by $\sim B$ for $B \subseteq F$. We know that $X_{\sim B}$ means equivalence classes of $x \in\ O$. For $X \subseteq O, B \subseteq F$, an example perceptual particle X can be defined with B - lower approximation $\underline{B}$and B - upper approximation $\overline{B}$.

$$\underline{B}(X) = \bigcup_{[x]_{B \subseteq X}} [x]_B$$

$$\overline{B}(X) = \bigcup_{[x]_{B \cap X \neq \emptyset}} [x]_B$$

Let $BndB(X) = \overline{B}(X) - \underline{B}(X)$ mean the boundary approximation. A set X is a rough set if $BndB(X)$ is not empty. Accordingly, if $\overline{B}(X) - \underline{B}(X) \neq \emptyset$ is valid as long as $\underline{B}(X)$ is a subset of $\overline{B}(X)$. That is, sample X is classified as conjugate and X is considered as a rough set. From the definition of the weakly nearness relation $\underline{B}(X) \bowtie_B X$ and $\overline{B}(X) \bowtie_B X$.
Because it is one of the approximation classes of X that contains objects that match the definition of at least one object in X. Therefore, $(\overline{B}(X), X))$ and ($\underline{B}(X), X)$ pairs are examples of near sets.

6.3. Relationship between rough set and soft set

Proposition 6.3.1. Every rough set can be expressed as a soft set. [6].

Proof: Let us consider an X set in the universe U and the $R(X)$ rough set of X with an equivalence relation R. Let's write $p_1(x)$ for $[x]_R \subseteq X$ and $p_2(x)$ for $[x]_R \cap X\ \neq \emptyset$. In this case, the conditions $p_1(x)$ and $p_2(x)$ can be treated as elements of a parameter set;

ie $E = \{ p_1(x), p_2(x)\}$ then $F: E \longrightarrow P(U); F\big(p_i(x)\big) = \{x \in U\colon\ p_i(x)\ doğru\}$, the function $i \in \{1, 2\}$ can be written. Therefore, every $R(X)$ rough set of X can be expressed as a soft set as $F(E) = \{(p_1(x), \underline{R}(X), (p_2(x), \overline{R}(X)\}$.

Example 6.3.1. Let's consider example 3.1.1: $E = \{ p_i(x), p_j(x)\}$ parameter set and let $p_i(x) = [x_i]_R, i \in \{4,5\}$ for $[x]_R \subseteq X$ and $p_j(x) = \left[x_j\right]_R, j \in \{1,2,4,5\}$ for $[x]_R \cap X \neq \emptyset$.

$F: E \longrightarrow P(U)$; For the function $F\big(p_*(x)\big) = \{x \in U\colon\ p_*(x)\ is\ true\}, * \in \{i, j\}$, each $R(X)$ rough set of X can be expressed as a soft set as $F(E) = \{(p_i(x), \underline{R}(X), (p_j(x), \overline{R}(X)\}$.

6.4. Relationship between near set and soft set

Proposition 6.4.1 Every family of neighborhoods may be considered a soft set [25].

Proof: Let $N_r(B)(X)$ be a family of neighbourhoods of X in the universe O with respect to the equivalence relation R and probe fuctions r. The neighbourhoods of X is defined by a lower approximation $N_r(\underline{B})(X) \neq \emptyset$ and upper approximation $N_r(\overline{B})(X) \neq \emptyset$. Consider the precidates $p_1(x) = \{h_1, h_2, \dots, h_{|B|}\}$ which stands for $[x]_R \subseteq X$ is not empty for $r \leq |B|$ and $p_2(x)$ which stands for $[x]_R \cap X \neq \emptyset$. Also $Bnd_{N_r(B)}(X) \geq 0$.

The conditions $p_1(x)$ and $p_2(x)$ may be treated as elements of a parameter set; that is $E = \{ p_1(x), p_2(x)\}$. Then we can write the function $F: E \longrightarrow P(U)$, $F\big(p_i(x)\big) = \{x \in U\colon\ p_i(x)\ is\ true\}, i \in \{1, 2\}$.

Thus every family of neighbourhoods $N_r(B)(X)$ of X may also be considered a soft set with the representation $(F, E) = \{(p_1(x), N_r\big(\underline{B}\big)(X), (p_2(x), N_r\big(\overline{B}\big)(X)\}$.

7. Conclusions

In this study, Fuzzy Set, Rough Set, Soft Set and Near Set theories, which are set theories about the solution of complex problems of modern periods, are discussed. Although each set theory was put forward to solve a certain problem, it is clear that they also have common points. In this study, the similarities and transitions between these set theories are examined and unique examples are given.

References

[1] L. A. Zadeh, Fuzzy Sets, **İnformation and Control**, 8, 338-353, (1965).

[2] Z. Pawlak, Rough sets, **Int. J. Comput. Inform. Sci.,** 11:5, 341-356, (1982).

[3] D. A. Molodtsov, *Soft set theory-First results,* **Comput. Math. Appl.,** 37, 19-31, (1999).

[4] Z. Pawlak and J. F. Peters, Jak Blisko (how near), **Systemy Wspomagania Decyzji** I, 57, 109, ISBN: 83-920730-4-5, (2002-2007).

[5] H., Aktas¸, N., Çağman, Fuzzy and Rough sets, Cankaya University, **Journal of Arts and Sciences**, May, 13-25, (2005).

[6] H. Aktas and N. Cagman, *Soft sets and soft groups,* **Inform.Sci.,** 177, 2726-2735, (2007).

[7] Z. Pawlak, Rough Sets – theoretical aspects of reasoning about data, Boston, London, Dordrecht: **Kluwer Academic Publishers** (1991).

[8] Z. Suraj, An Introduction to Rough Set Theory and Its Application, Cairo, Egypt, **ICENCO'2004**, December, 27-30, (2004).

[9] H. Taşbozan, Local Rough sets and Rough Subgroupoids, Ph. D. Thesis, İnönü University, Malatya, Türkiye, (2017).

[10] X. Liang, D. Li, On Rough Subgroup of a Group, **Formalized Mathematics**, 17, 213-217, (2009).

[11] G. Oguz, M. H. Gursoy and I. Icen, On Soft Topological Categories, **Hacet. J. Math. Stat**. ,(2008).

[12] G. Oguz, I.Icen and M. H. Gursoy, Action of Groups, Commun. Fac. Sci. Univ. Ank. Ser. A 1 Math. Stat. Volume 68, Number 1, Pages 1163-1174 (2019).

[13] S. Gecen, I.Icen and A. F. Ozcan, Reflections of global action on soft set theory, **master's thesis** İnönü University, Malatya, Turkey, (2021).

[14] P. K. Maji, R. Biswas and R. Roy, *Soft set theory,* **Comput. Math. Appl. ,** 45(4-5) ,555-562, (2003).

[15] M. I. Ali, *A note on soft sets, rough soft sets and fuzzy soft sets,* **Appl.Soft Comput. ,** 11, 3329-3332, (2011).

[16] M. Pawel, Fundamentals of pattern recognition, 2nd Ed. N. Y., **Marcel Dekker**, Inc., (1993).

[17] J. F. Peters, Near sets. General theory about nearness of objects, **Appl. Math. Sci.,** 1: 53-56, 2609-2629, (2007).

[18] J. F. Peters, Classification of perceptual objects by means of features, **Int. J. Info. Technol. Intell. Comput.,** 3:2, 1-35, (2008).

[19] J. F. Peters and S. Ramanna, Affinities between perceptual granules: Foundations and perspectives. In Human-centric information processing through granual modelling sci 182, Eds. A. Bargiela and W. Pedrycz, Springer-Verlag, Berlin, (2009).

[20] S. K. Pal and J. F. Peters, Rough fuzzy Image Analysis. **Foundations and Methodologies**, CRC Press, Taylor- Francis Group, ISBN 13:9781439803295 ISBN 10: 1439803293, (2010).

[21] L. Polkowski, Rough Sets, Mathematical Foundations, Springer-Verlag, Heidelberg, (2002).

[22] Z. Pawlak, Classification of objects by means of attributes, **Institute for Computer Science, Polish Academy of Sciences**, Report 429, (1981).

[23] J. F. Peters, P. Wasilewski, Foundations of near sets, **Information Sciences,** 179,3091-3109, (2009).

[24] M. Durna, Near sets and the fundamental properties of near sets, Master thesis, cumhuriyet University, sivas, (2014).

[25] H. Taşbozan, İ. İçen, N. Bağırmaz, A. F. Özcan, Soft Sets and Soft Topology on Nearness Approximation Spaces, **Published by Sciences and Mathematics**, Serbia, 31: 13, 4117-4125, (2017).

Solving A System Of Partial Differential Equations Via A Hybrid Method Between Homotopy Analytical Method And Chaotic Sine Cosine Algorithm

Aytekin Enver [1] Mostafa Raed Najeeb [2] Fatma Ayaz [3] Omar Saber Qasim[4] Ahmed Entesar[5]

[2, 4, 5] Department of Mathematics, College of Computer Sciences and Mathematics, University of Mosul, Mosul, Iraq

[1,3]Department of Mathematics, Gazi University, Teknikokullar, Ankara, Turkey

[1]aytekin.enver@gazi.edu.tr [2]mostafa.csp115@student.uomosul.edu.iq [3]fayaz@gazi.edu.tr
[4] omar.saber@uomosul.edu.iq [5]ahmed_entesar84@uomosul.edu.iq

Abstract.

In this paper, a hybrid method was proposed between the homotopy analysis method (HAM) and the chaotic sine cosine algorithm (CSCA) for solving systems of partial differential equations (PDEs) of two types linear and nonlinear. The chaotic cosine algorithm (CSCA) was used to obtain a better value for the homotopy parameter h by relying on a suitable fitness function representing the series of solutions for the HAM. The chaotic maps were also adopted in the sine cosine algorithm to obtain stability of solutions during processing operations. The proposed method (HAM-CSCA) gives a solution that detects reliability and efficiency corresponding to the hypothetical HAM method as well as for the HAM-SCA method by computing the maximum absolute error (MAE), mean squared error (MSE), and L^2-Norm of Error.

Keywords: Homotopy analytical method, Sine cosine algorithm, Linear and nonlinear partial differential equations, Swarm intelligent, Chaotic maps, Adomian Polynomials.

1. Introduction.

All-natural, physical, engineering, and other phenomena are expressed by modeling them into the linear and nonlinear differential equation, these equations differential in the method of solution, a few of them can be solved directly, so it was necessary to use approximate methods to address problems and arrive at the solution, as the HAM is one of these methods [1, 2].

In 1992 the scientist Liao Shijun discovered the Homotopy Analysis Method (HAM) [3, 4], which is known as a semi-analytical method based on the use of the symmetry principle to obtain a convergent series solution of different types of equations, such as ordinary differential equations, partial differential equations, integral equations, Difference Equations and many Other linear and nonlinear equations, as this is done by relying on the Homotopy-Maclaurin series. HAM is an expansion method that does not depend directly on any parameter small or large, as it uses a parameter only at the theoretical level to demonstrate that a nonlinear system can be divided into an infinite set of linear systems. It also has the freedom to choose the type of equation in the auxiliary function, the initial approximation, and the basic functions, and this enables it to ensure the convergence of the series of solutions in solving various equations [5, 6]. The method of homotopy analysis describes a kind of continuous difference or distortion in mathematics, for example, that a circle can be continuously deformed into a square or oval shape, and a cup of coffee can be distorted continuously into a cake shape. In general, the concept of homotopy connects the different things in mathematics that have common properties in some of the features[7].

SCA was introduced by Seyedali Mirjalili in 2016 [8], it is a population-based intelligent optimization algorithm. SCA divides the optimization process into two phases: exploration versus exploitation [8]. In the exploration stage, the algorithm groups random solutions into the solution set, accompanied by a high rate of randomness, to find the best area in the search space. As for the exploitation stage, the focus is on the remaining solution area from the previous stage and researched. The random variations of solutions in the exploitation phase are much less than those in the exploration phase [8]. In the sine cosine algorithm, the position update equations for the exploration and exploitation phases are proposed as follows [9]:

$$X_i^{t+1} = \begin{cases} X_i^t + r_1 \sin(r_2) | r_3\, p_i^t - X_i^t \,| & , \quad r_4 < 0.5 \\ X_i^t + r_1 \cos(r_2) | r_3\, p_i^t - X_i^t | & , \quad r_4 \geq 0.5 \end{cases} \tag{1}$$

Whereas, X_i^t is the position of the solution in the i-th dimension at iteration t, p_i^t represents the position of the destination point in the i-th dimension and that r_1, r_2, r_3 and r_4 represent parameters with random values, where the parameter r_1 determines the regions of the next position which can be either in the distance between the solution and the destination or outside it and the parameter r_2 determines the extent to which the movement should be towards the destination or outwards, The parameter r_3 gives random destination weights for random confirmation (r_3> 1) or de-focus (r_3 <1) for the destination effect when a distance is specified. Finally, the parameter r_4 performs equal switching between the sine cosine components of function (1) [8, 10]. The exploration and exploitation processes in SCA can be represented in **Figure 1:**

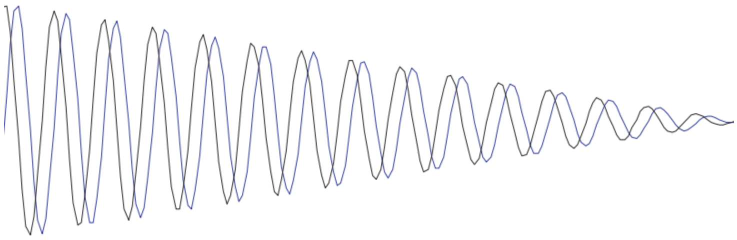

Figure 1: Shows how the SCA works

Chaotic is defined as a phenomenon that occurs as a result of a simple change in the initial state of the system, which will lead to an unstable change in the behavior of that phenomenon in the future [11]. This random behavior results from non-linear systems and functions that have values and elementary parameters that have a great impact on the occurrence of this Chaotic. The unusual (chaotic) behavior of some systems has attracted the attention of many researchers in various scientific fields. These chaotic unstable behaviors have been observed in various fields of application. From sciences such as engineering, medicine, economics, communications, climate, etc. [12, 13]. Chaotic maps are one of the modern algorithms or methods that rely on the idea of converting variable parameters from hypothetical random values to values that are generated in one of the chaotic ways during the search for an optimal solution [14 ,8]. Chaotic phenomenon contains three important basic characteristics through which the process of controlling dispersion or Chaotic occurring in any given system is interpreted, which are the probability of finding a solution, regularity, and random characteristics [15, 16]. Recently, chaotic systems have been used instead of random processes in many areas, where optimization theory is one of them. The role of randomness in optimization algorithms can be played by Chaotic theory, as experimental studies confirm that using chaotic diagrams instead of random values gives results that are often clear, stable, and quick to reach the optimal solution, although this has not been proven mathematically yet [8, 17].

2. General Concepts.

In this paragraph, we will mention some important definitions that will be covered in this paper

2.1 Definition (1).

The maximum absolute errors MAE is determined by the following formula

$$\|z_{Exact}(y)-\alpha_i(y)\|_\infty = \max_{a\le x\le b}\{|z_{Exact}(y)-\alpha_i(y)|\} \tag{2}$$

here $\alpha_i(y), i = 1,2,\ldots$ are the successive estimates of the solution $z\ (y)$ [18].

2.2 Definition (2).

Let's have the vectors $\vec{x_i}$ wher $i = 1,2,\ldots$, the MSE is a sum of the square of the exact solution Exact (y_i) minus the approximate solution divided by the number of iterations k which is as follows [19].

$$MSE = \frac{1}{k}\sum_{i=1}^{k}(Exact\ (y_i) - \emptyset(y_i))^2 \tag{3}$$

2.3 Definition (3).

The L^2-Norm of Error is defined as [20]:

$$\|\cdot\|_2 = \left(\int_a^b [y_{Exact}(t) - \phi_n(t)]^2 dt\right)^{1/2} \tag{4}$$

2.4 Adomian Polynomials.

Will use the Adomian method to solve the non-linear terms from the ordinary DEs [21].

When $f(u) = uu''$ [22, 23]. (5)

can use the Adomian method to extend the nonlinear term to the $f(u) = uu''$ document using

$$x_0 = u_0\, u_0''$$
$$x_1 = u_1\, u_0'' + u_0\, u_1''$$
$$x_2 = u_2\, u_0'' + u_1\, u_1'' + u_0\, u_2''$$
$$x_3 = u_3\, u_0'' + u_2\, u_1'' + u_1\, u_2'' + u_0\, u_3''$$
$$x_4 = u_4\, u_0'' + u_3\, u_1'' + u_2\, u_2'' + u_1\, u_3'' + u_0\, u_4''$$
$$x_5 = u_5\, u_0'' + u_4\, u_1'' + u_3\, u_2'' + u_2\, u_3'' + u_1\, u_4'' + u_0\, u_5''$$
$$\vdots$$
$$x_n = \sum_{i=0}^{n} u_i\, u_{n-i}'', \quad n \ge i, \quad n = 0, 1, 2, \cdots$$

3. Basic Ideas of Homotopy Analysis Method.

Let we have $\mathcal{N}[u(t)] = g(t),$ (6)

where $\mathcal{N}$ is a non-linear operator, t denotes the independent variable, $u(t)$ is an unknown function and $g(t)$ is a known analytic function. By applying the traditional homotopy method we have [24]:

$$(1-q)\mathcal{L}[\phi(t;q)-u_0(t)] = qh\{\mathcal{N}[\phi(t;q)]-g(t)\} \tag{7}$$

where $q \in [0,1]$ is an embedding parameter, h is a non-zero auxiliary function, $\mathcal{L}$ is an auxiliary linear operator, $u_0(t)$ is an initial guess of $u(t)$ and $\phi(t;q)$ is an unknown function. The HAM method has great freedom in choosing the auxiliary function, q, h, $\mathcal{N}$, and $\mathcal{L}$.

when $q = 0$ we have $\phi(t;0) = u_0(t)$

and when $q = 1$ we have $\phi(t;1) = u(t)$

This means that as q increases from 0 to 1, the solution $\phi(t;q)$ differs from the initial guess $u_0(t)$ to the solution $u(t)$. Then by using Taylor's Sequence

$$\phi(t;q) = u_0(t) + \sum_{m=1}^{+\infty} u_m(t)q^m, \tag{8}$$

where

$$u_m = \frac{1}{m!}\frac{\partial^m \phi(t;q)}{\partial q^m}\bigg|_{q=0}, \tag{9}$$

If the auxiliary linear operator, the initial guess, the auxiliary parameter h, and the auxiliary function are so properly chosen, then the series (8) converges at $q = 1$ and we get

$$\phi(t;1) = u_0(t) + \sum_{m=1}^{+\infty} u_m(t),$$

Hence, we substitute for $h = 1$

$$(1-q)\mathcal{L}[\phi(t;q)-u_0(t)] + q\{\mathcal{N}[\phi(t;q)]-g(t)\} = 0, \tag{10}$$

After deriving equation (9) m-times and adjusting the parameter q and then dividing it by $m!$ we obtain the m deformation equation

$$\mathcal{L}[u_m(t) - \chi_m u_{m-1}(t)] = hR_m\left(\vec{u}_{m-1}(t)\right) \tag{11}$$

where

$$R_m(\vec{u}_{m-1}(t)) = \frac{1}{(m-1)!}\frac{\partial^{m-1}\{\mathcal{N}[\phi(t;q)]-g(t)\}}{\partial q^{m-1}}\bigg|_{q=0} \tag{12}$$

and

$$\chi_m = \begin{cases} 0, & m \leq 1, \\ 1, & m > 1. \end{cases} \tag{13}$$

4. The Proposed Method HAM-CSCA.

The proposed method HAM-CSCA is based on solving a system of linear and nonlinear, homogeneous and non-homogeneous partial differential equations by using the HAM method with the CSCA algorithm, Whereas the hybridization process between SCA and Chaotic maps was used to select the best value for auxiliary homotopy parameter and us it in the calculations of the HAM method.

5. Some Applications of HAM-CSCA.

We will solve three examples of partial differential equations as a linear and non-linear system by using the proposed method (HAM-CSCA).

5.1 Example [25].

$$\begin{aligned} u_t(x,t) + v(x,t)u_x(x,t) + u(x,t) - 1 = 0 \\ v_t(x,t) + u(x,t)v_x(x,t) + v(x,t) - 1 = 0 \end{aligned} \quad ,0 < x \leq 1 \ ,0 < t \leq 1$$

and the exact solution

$$u_{exact}(x,t) = e^{x-t}$$
$$v_{exact}(x,t) = e^{-x+t}$$

and pick out the initial approximation

$$u_0(x,t) = e^{x}$$
$$v_0(x,t) = e^{-x}$$

then the linear operator (which represents the general solution)

$$\mathcal{L}_1[\beta_1(x,t;q)] = \frac{\partial \beta_1(x,t;q)}{\partial t} = \mathcal{L}[c_1 + c_2 t] = 0$$
$$\mathcal{L}_2[\beta_2(x,t;q)] = \frac{\partial \beta_2(x,t;q)}{\partial t} = \mathcal{L}[c_1 + c_2 t] = 0$$

and the non-linear operator will look like this

$$\mathcal{N}_1[\beta(x,t;q)] = \frac{\partial \beta_1(x,t;q)}{\partial t} + \beta_2(x,t;q)\frac{\partial \beta_1(x,t;q)}{\partial x} + \beta_1(x,t;q) - 1 = 0$$
$$\mathcal{N}_2[\beta(x,t;q)] = \frac{\partial \beta_2(x,t;q)}{\partial t} + \beta_1(x,t;q)\frac{\partial \beta_2(x,t;q)}{\partial x} + \beta_2(x,t;q) - 1 = 0$$

and the initial condition

$$u(x,0) = e^{x}$$
$$v(x,0) = e^{-x}$$

by using an Adomian polynomial we expanding the nonlinear term vu_x, by the following formula:

$$\sum_{j=0}^{m-1} v_j(x,t) \ \ u'_{m-1-j}(x,t)$$

and the nonlinear term uv_x is as follows:

$$\sum_{j=0}^{m-1} u_j(x,t) \ \ v'_{m-1-j}(x,t)$$

where

$$R_{m,1}\left(u_{i,m-1}^{\rightarrow}(x,t)\right) = u_t(x,t) + \sum_{i=0}^{j-1} v_j(x,t)\ u_{j-1-i}'(x,t)\ + u(x,t) - 1(1-\chi)$$
$$R_{m,2}\left(v_{i,m-1}^{\rightarrow}(x,t)\right) = v_t(x,t) + \sum_{i=0}^{j-1} u_j(x,t)\ v_{j-1-i}'(x,t)\ + v(x,t) - 1(1-\chi)$$

by using the m-order deformation equation, we get the following iterative formula

$$u_m(x,t) = \chi_{m-1}\, u_{m-1}(x,t) + h\, L^{-1}R_m\left(u_{m-1}^{\rightarrow}(x,t)\right)$$
$$v_m(x,t) = \chi_{m-1}\, v_{m-1}(x,t) + h\, L^{-1}R_m\left(v_{m-1}^{\rightarrow}(x,t)\right)$$

after substituting for the value of $m = 1,2,3,\cdots$ we get the following iterations

$$u_1(x,t) = he^x t$$
$$v_1(x,t) = -he^{-x} t$$
$$u_2(x,t) = he^x t + \tfrac{1}{2}\, h^2 e^x t^2 + h^2 e^x t$$
$$v_2(x,t) = -he^{-x} t + \tfrac{1}{2}\, h^2 e^{-x} t^2 - h^2 e^{-x} t$$
$$u_3(x,t) = he^x t + h^2 e^x t^2 + 2h^2\, e^x t + \tfrac{1}{6}\, h^3 t^3 e^x + h^3 t^2 e^x + h^3 t e^x$$
$$v_3(x,t) = -he^{-x} t + h^2 e^{-x} t^2 - 2h^2 e^{-x} t - \frac{1}{6}\, h^3 t^3 e^{-x} + h^3 t^2 e^{-x} - h^3 t e^{-x}$$

$\vdots$

by collect the previous iterations we get

$$u(x,t) \approx \sum_{s=0}^{m} u_s(x,t) \approx he^x t + he^x t + \tfrac{1}{2}\, h^2 e^x t^2 + h^2 e^x t + he^x t + h^2 e^x t^2 + 2h^2\, e^x t + \tfrac{1}{6}\, h^3 t^3 e^x + h^3 t^2 e^x + h^3 t e^x + \cdots \qquad (14)$$

$$v(x,t) \approx \sum_{s=0}^{m} v_s(x,t) \approx -he^{-x} t - he^{-x} t + \tfrac{1}{2}\, h^2 e^{-x} t^2 - h^2 e^{-x} t - he^{-x} t + h^2 e^{-x} t^2 - 2h^2 e^{-x} t - \tfrac{1}{6}\, h^3 t^3 e^{-x} + h^3 t^2 e^{-x} - h^3 t e^{-x} + \cdots \qquad (15)$$

The HAM method selects a random value for the auxiliary homotopy parameter h, let $h = -1$. We also use SCA to modify the parameter h and get the following results $h^{SCA} = -9.9698$ and $h^{SCA} = -1.0030$ for $u(x,t)$ and $v(x,t)$ respectively. We will also choose another value for the parameter h, and get the following results $h^{CSCA} = -0.8005$ and $h^{CSCA} = -1.1267$ for $u(x,t)$ and $v(x,t)$ respectively after using CSCA. Then we substitute h^{HAM}, $h^{\mathrm{HAM-SCA}}$, and $h^{\mathrm{HAM-CSCA}}$ into equations (14) and (15). The comparison of the results for $u^{\mathrm{HAM}}(x,t)$, $u^{\mathrm{HAM-SCA}}(x,t)$ and

$u^{\mathrm{HAM-CSCA}}(x,t)$ is shown in **Table 1** and **Figure 2**. And the comparison of the results for $v^{\mathrm{HAM}}(x,t)$, $v^{\mathrm{HAM-SCA}}(x,t)$ and $v^{\mathrm{HAM-CSCA}}(x,t)$ is shown in **Table 2** and **Figure 3**.

Table 1: Comparison of MAE, MSE and L^2-Norm for $u^{HAM}(x,t)$, $u^{HAM-SCA}(x,t)$ and $u^{HAM-CSCA}(x,t)$.

$u^{HAM-CSCA}(x,t)$	$u^{HAM-SCA}(x,t)$	$u^{HAM}(x,t)$	
$1.554491E-6$	$2.068691E-4$	$2.272966E-4$	**MSE**
$3.104170E-3$	$3.653315E-2$	$3.817935E-2$	**MAE**
$1.001665E-2$	$9.403242E-2$	$9.899985E-2$	**L^2-Norm**

Table 2: Comparison of MAE, MSE and L^2-Norm for $v^{HAM}(x,t)$, $v^{HAM-SCA}(x,t)$ and $v^{HAM-CSCA}(x,t)$.

$v^{HAM-CSCA}(x,t)$	$v^{HAM-SCA}(x,t)$	$v^{HAM}(x,t)$	
$1.978733E-6$	$3.034935E-4$	$3.237543E-4$	**MSE**
$3.915195E-3$	$4.533904E-2$	$4.670332E-2$	**MAE**
$9.199385E-3$	$1.108964E-1$	$1.150131E-1$	**L^2-Norm**

Figure 2: Comparison of MAE, MSE and L^2-Norm for $v^{HAM}(x,t)$, $v^{HAM-SCA}(x,t)$ and $v^{HAM-CSCA}(x,t)$ for $v(x,t)$

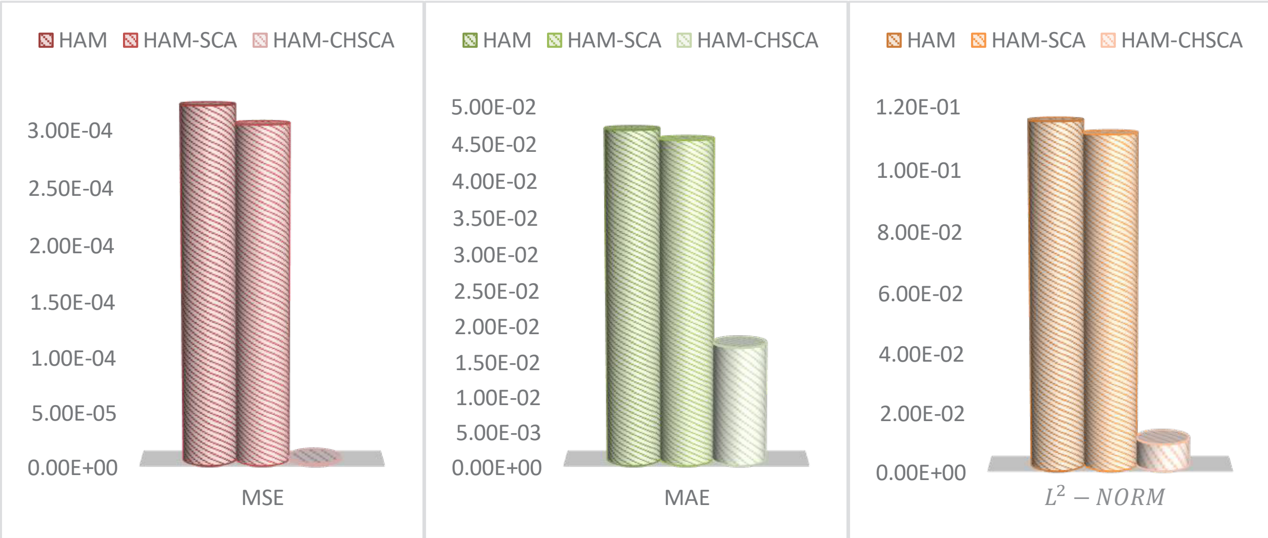

Figure 3: Comparison of MAE, MSE and L^2-Norm for $u^{HAM}(x,t)$, $u^{HAM-SCA}(x,t)$ and $u^{HAM-CSCA}(x,t)$.

5.2 Example [25].

$$\begin{aligned} u_t(x,t) - v_x(x,t) - \big(u(x,t) - v(x,t)\big) &= -2 \\ v_t(x,t) - u_x(x,t) - \big(u(x,t) - v(x,t)\big) &= -2 \end{aligned} \quad , \quad 0 < x \le 1, 0 < t \le 1$$

and the exact solution

$$u_{exact}(x,t) = 1 + e^{x+t}$$
$$v_{exact}(x,t) = -1 + e^{x-t}$$

and pick out the initial approximation

$$u_0(x,t) = 1 + e^{x}$$
$$v_0(x,t) = -1 + e^{x}$$

then the linear operator (which represents the general solution)

$$\mathcal{L}_1[\beta_1(x,t;q)] = \frac{\partial \beta_1(x,t;q)}{\partial t} = \mathcal{L}[c_1 + c_2 t] = 0$$
$$\mathcal{L}_2[\beta_2(x,t;q)] = \frac{\partial \beta_2(x,t;q)}{\partial t} = \mathcal{L}[c_1 + c_2 t] = 0$$

and the non-linear operator will look like this

$$\mathcal{N}_1[\beta_1(x,t;q)] = \frac{\partial \beta_1(x,t;q)}{\partial t} - \frac{\partial \beta_2(x,t;q)}{\partial x} - \big(\beta_1(x,t;q) - \beta_1(x,t;q)\big) + 2\,(1-\chi)$$
$$\mathcal{N}_2[\beta_2(x,t;q)] = \frac{\partial \beta_2(x,t;q)}{\partial t} - \frac{\partial \beta_1(x,t;q)}{\partial x} - \big(\beta_1(x,t;q) - \beta_1(x,t;q)\big) + 2\,(1-\chi)$$

and the initial condition

$$u(x,0) = 1 + e^x$$
$$v(x,0) = -1 + e^x$$

then

$$R_{m,1}\left(u_{i,m-1}^{\rightarrow}(x,t)\right) = u_t(x,t) - v_x(x,t) - \big(u(x,t) - v(x,t)\big) + 2(1-\chi)$$
$$R_{m,2}\left(v_{i,m-1}^{\rightarrow}(x,t)\right) = v_t(x,t) - u_x(x,t) - \big(u(x,t) - v(x,t)\big) + 2(1-\chi)$$

by using the m-order deformation equation, we get the following iterative formula

$$u_m(x,t) = \chi_{m-1}\, u_{m-1}(x,t) + h\, L^{-1} R_m\big(u_{m-1}^{\rightarrow}(x,t)\big)$$
$$v_m(x,t) = \chi_{m-1}\, v_{m-1}(x,t) + h\, L^{-1} R_m\big(v_{m-1}^{\rightarrow}(x,t)\big)$$

after substituting for the value of $m = 1,2,3,\cdots$ we get the following iterations

$$u_1(x,t) = -h\,t\,e^x$$
$$v_1(x,t) = -h\,t\,e^x$$
$$u_2(x,t) = -h\mathrm{e}^x t - h^2\mathrm{e}^x t + \frac{1}{2}h^2\mathrm{e}^x t^2$$
$$v_2(x,t) = -h\mathrm{e}^x t - h^2\mathrm{e}^x t + \frac{1}{2}h^2\mathrm{e}^x t^2$$
$$\vdots$$

by collect the previous iterations we get

$$u(x,t) \approx \sum_{s=0}^{m} u_s(x,t) \approx e^x + 1 - h\,t\,e^x - he^x t - h^2 e^x t + \frac{1}{2}h^2 e^x t^2 - he^x t - 2h^2 e^x t + h^2 e^x t^2 - \frac{1}{6}h^3 e^x t^3 + h^3 e^x t^2 - h^3 e^x t + \cdots \quad (16)$$

$$v(x,t) \approx \sum_{s=0}^{m} v_s(x,t) \approx e^x - 1 - h\,t\,e^x - he^x t - h^2 e^x t + \frac{1}{2}h^2 e^x t^2 - he^x t - 2h^2 e^x t + h^2 e^x t^2 - \frac{1}{6}h^3 e^x t^3 + h^3 e^x t^2 - h^3 e^x t + \cdots \quad (17)$$

The HAM method selects a random value for the auxiliary homotopy parameter h, let $h = -1$. We also use SCA to modify the parameter h and get the following results $h^{SCA} = -1.3025$ and $h^{SCA} = -0.0001$ for $u(x,t)$ and $v(x,t)$ respectively. We will also choose another value for the parameter h, and get the following results results $h^{CSCA} = -1.1267$ and $h^{CSCA} = -0.0001$ for $u(x,t)$ and $v(x,t)$

respectively after using CSCA. Then we substitute h^{HAM}, $h^{HAM-SCA}$, and $h^{HAM-CSCA}$ into equations (16) and (17). The comparison of the results for $u^{\mathrm{HAM}}(x,t)$, $u^{\mathrm{HAM-SCA}}(x,t)$ and $u^{\mathrm{HAM-CSCA}}(x,t)$ is shown in **Table 3** and **Figure 4**. And the comparison of the results for $v^{\mathrm{HAM}}(x,t)$, $v^{\mathrm{HAM-SCA}}(x,t)$ and $v^{\mathrm{HAM-CSCA}}(x,t)$ is shown in **Table 4** and **Figure 5**.

Table 3: Comparison of MAE, MSE and L^2-Norm for $u^{HAM}(x,t)$, $u^{HAM-SCA}(x,t)$ and $u^{HAM-CSCA}(x,t)$.

$u^{HAM-CSCA}(x,t)$	$u^{HAM-SCA}(x,t)$	$u^{HAM}(x,t)$	
$2.465653E-6$	$3.060266E-5$	$4.829846E-4$	**MSE**
$4.370446E-3$	$1.408139E-2$	$5.704357E-2$	**MAE**
$1.026907E-2$	$4.359946E-2$	$1.404773E-1$	**L^2-Norm**

Table 4: Comparison of MAE, MSE and L^2-Norm for $v^{HAM}(x,t)$, $v^{HAM-SCA}(x,t)$ and $v^{HAM-CSCA}(x,t)$.

$v^{HAM-CSCA}(x,t)$	$v^{HAM-SCA}(x,t)$	$v^{HAM}(x,t)$	
$1.713244E-1$	$1.713586E-1$	1.695472	**MSE**
$6.321205E-1$	$6.321837E-1$	2.299017	**MAE**
3.949587	3.989936	11.919946	**L^2-Norm**

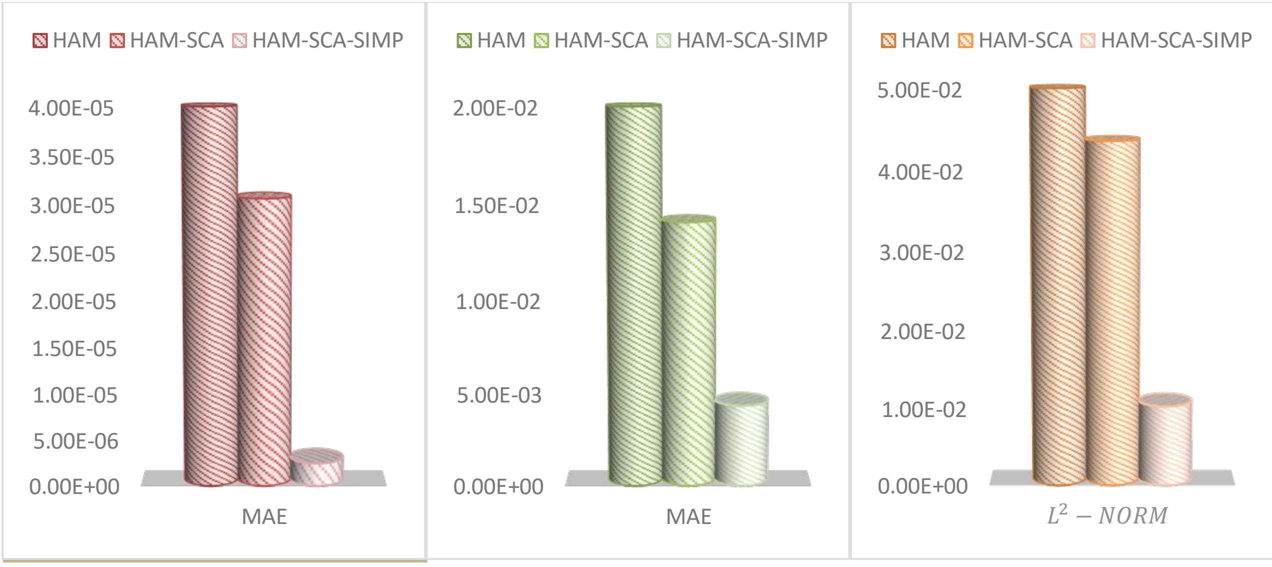

Figure 4: Comparison of MAE, MSE and L^2-Norm for $v^{HAM}(x,t)$, $v^{HAM-SCA}(x,t)$ and $v^{HAM-CSCA}(x,t)$ for $v(x,t)$

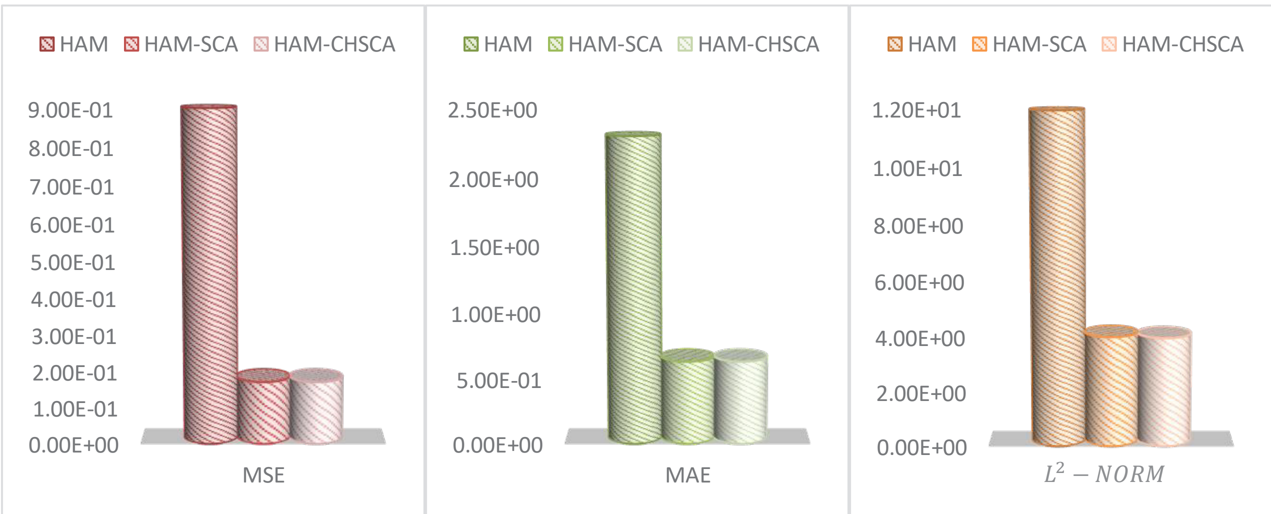

Figure 5: Comparison of MAE, MSE and L^2-Norm for $u^{HAM}(x,t)$, $u^{HAM-SCA}(x,t)$ and $u^{HAM-CSCA}(x,t)$.

5.3 Example [26].

$$
\begin{aligned}
&u_t(x,y,t) + u_x(x,y,t) + 2w(x,y,t) = 0 \\
&v_t(x,y,t) + v_x(x,y,t) + 2u(x,y,t) \ = 0 \quad ,0 < x,y,t \le 1 \\
&w_t(x,y,t) + w_x(x,y,t) - 2u(x,y,t) = 0
\end{aligned}
$$

and the exact solution

$u_{exact}(x, y, 0) = sin(x + y + t)$
$v_{exact}(x, y, 0) = cos(x + y + t)$
$w_{exact}(x, y, 0) = -cos\,(x + y + t)$

and pick out the initial approximation

$u_0(x, y, t) = sin(x + y)$
$v_0(x, y, t) = cos(x + y)$
$w_0(x, y, t) = -cos\,(x + y)$

then the linear operator (which represents the general solution)

$\mathcal{L}_1[\beta_1(x, y, t; q)] = \frac{\partial\beta_1(x,y,t;q)}{\partial t} = \mathcal{L}[c_1 + c_2 t] = 0$
$\mathcal{L}_2[\beta_2(x, y, t; q)] = \frac{\partial\beta_2(x,y,t;q)}{\partial t} = \mathcal{L}[c_1 + c_2 t] = 0$
$\mathcal{L}_3[\beta_3(x, y, t; q)] = \frac{\partial\beta_3(x,y,t;q)}{\partial t} = \mathcal{L}[c_1 + c_2 t] = 0$

and the non-linear operator will look like this

$\mathcal{N}_1[\beta_1(x, y, t; q)] = \frac{\partial\beta_1(x,y,t;q)}{\partial t} + \frac{\partial\beta_1(x,y,t;q)}{\partial x} + 2\beta_3(x, y, t; q) = 0$
$\mathcal{N}_2[\beta_2(x, y, t; q)] = \frac{\partial\beta_2(x,y,t;q)}{\partial t} + \frac{\partial\beta_2(x,y,t;q)}{\partial x} + 2\beta_1(x, y, t; q) = 0$
$\mathcal{N}_3[\beta_3(x, y, t; q)] = \frac{\partial\beta_3(x,y,t;q)}{\partial t} + \frac{\partial\beta_3(x,y,t;q)}{\partial x} - 2\beta_2(x, y, t; q) = 0$

then

$R_{m,1}\left(u_{\vec{i,m-1}}(x, y, t)\right) = u_t(x, y, t) + u_x(x, y, t) + 2w(x, y, t)$
$R_{m,2}\left(v_{\vec{i,m-1}}(x, y, t)\right) = v_t(x, y, t) + v_x(x, y, t) + 2u(x, y, t)$
$R_{m,3}\left(w_{\vec{i,m-1}}(x, y, t)\right) = w_t(x, y, t) + w_x(x, y, t) - 2u(x, y, t)$

by using the m-order deformation equation, we get the following iterative formula

$u_m(x, y, t) = \chi_{m-1}\, u_{m-1}(x, y, t) + h\, L^{-1} R_{m,1}\left(u_{\vec{m-1}}(x, y, t)\right)$
$v_m(x, y, t) = \chi_{m-1}\, v_{m-1}(x, y, t) + h\, L^{-1} R_{m,2}\left(v_{\vec{m-1}}(x, y, t)\right)$ after substituting for the value of
$w_m(x, y, t) = \chi_{m-1}\, w_{m-1}(x, y, t) + h\, L^{-1} R_{m,3}\left(w_{\vec{m-1}}(x, y, t)\right)$

when $m = 1,2,3, \cdots$ we get the following iterations

$u_1(x, y, t) = -htcos\,(x)cos\,(y) + htsin\,(x)sin\,(y)$

$v_1(x, y, t) = htsin\,(x)cos\,(y) + htcos\,(x)sin\,(y)$

$w_1(x,y,t) = -htsin\,(x)cos\,(y) - htcos\,(x)sin\,(y)$

$u_2(x,y,t) = -htcos\,(x)cos\,(y) + htsin\,(x)sin\,(y) - \frac{1}{2}t^2h^2sin\,(x)cos\,(y) - \frac{1}{2}t^2h^2cos\,(x)sin\,(y) - h^2tcos\,(x)cos\,(y) + h^2tsin\,(x)sin\,(y)$

$v_2(x,y,t) = htsin\,(x)cos\,(y) + htcos\,(x)sin\,(y) - \frac{1}{2}t^2h^2cos\,(x)cos\,(y) + \frac{1}{2}t^2h^2sin\,(x)sin\,(y) + h^2tsin\,(x)cos\,(y) + h^2tcos\,(x)sin\,(y)$

$w_2(x,y,t) = -htsin\,(x)cos\,(y) - htcos\,(x)sin\,(y) + \frac{1}{2}t^2h^2cos\,(x)cos\,(y) - \frac{1}{2}t^2h^2sin\,(x)sin\,(y) - h^2tsin\,(x)cos\,(y) - h^2tcos\,(x)sin\,(y)$

$u_3(x,y,t) = -htcos\,(x)cos\,(y) + htsin\,(x)sin\,(y) - t^2h^2sin\,(x)cos\,(y) - t^2h^2cos\,(x)sin\,(y) - 2h^2tcos\,(x)cos\,(y) + 2h^2\,tsin(x)\,sin(y) + \frac{1}{6}t^3h^3\,cos(x)\,cos(y) - \frac{1}{6}t^3h^3\,sin(x)\,sin(y) - t^2h^3\,sin(x)\,cos(y) - t^2h^3\,cos(x)\,sin(y) - h^3\,tcos(x)\,cos(y) + h^3\,tsin(x)\,sin(y)$

$v_3(x,y,t) = htsin\,(x)cos\,(y) + htcos\,(x)sin\,(y) - t^2h^2cos\,(x)cos\,(y) + t^2h^2sin\,(x)sin\,(y) + 2h^2tsin\,(x)cos\,(y) + 2h^2tcos\,(x)sin\,(y) - \frac{1}{6}t^3h^3sin\,(x)cos\,(y) - \frac{1}{6}t^3h^3cos\,(x)sin\,(y) - t^2h^3cos\,(x)cos\,(y) + t^2h^3sin\,(x)sin(y) + h^3tsin\,(x)cos\,(y) + h^3tcos\,(x)sin\,(y)$

$w_3(x,y,t) = -htsin\,(x)cos\,(y) - htcos\,(x)sin\,(y) + t^2h^2cos\,(x)cos\,(y) - t^2h^2sin\,(x)sin\,(y) - 2h^2tsin\,(x)cos\,(y) - 2h^2tcos\,(x)sin\,(y) + \frac{1}{6}t^3h^3sin\,(x)cos\,(y) + \frac{1}{6}t^3h^3cos\,(x)sin\,(y) + t^2h^3cos\,(x)cos\,(y) - t^2h^3sin\,(x)sin\,(y) - h^3tsin\,(x)cos\,(y) - h^3tcos\,(x)sin\,(y)$

$\vdots$

by collect the previous iterations we get

$$u(x,y,t) \approx \sum_{s=0}^{m} u_s(x,t) \approx -htco\,s(x)\,co\,s(y) + htsi\,n(x)\,si\,n(y) - htcos\,(x)cos\,(y) + htsin\,(x)sin\,(y) - \frac{1}{2}t^2h^2sin\,(x)cos\,(y) - \frac{1}{2}t^2h^2cos\,(x)sin\,(y) - h^2tcos\,(x)cos\,(y) + h^2tsin\,(x)sin\,(y) + \cdots \quad (16)$$

$$v(x,y,t) \approx \sum_{s=0}^{m} v_s(x,t) \approx htsin\,(x)cos\,(y) + htcos\,(x)sin\,(y)htsin\,(x)cos\,(y) + htcos\,(x)sin\,(y) - \frac{1}{2}t^2h^2cos\,(x)cos\,(y) + \frac{1}{2}t^2h^2sin\,(x)sin\,(y) + h^2tsin\,(x)cos\,(y) + h^2tcos\,(x)sin\,(y) + \cdots \quad (17)$$

$w(x,y,t) \approx \sum_{s=0}^{m} w_s(x,t) \approx -htsin\,(x)cos\,(y) - htcos\,(x)sin\,(y) - htsin\,(x)cos\,(y) - htcos\,(x)sin\,(y) + \frac{1}{2}t^2h^2cos\,(x)cos\,(y) - \frac{1}{2}t^2h^2sin\,(x)sin\,(y) - h^2tsin\,(x)cos\,(y) - h^2tcos\,(x)sin\,(y) + \cdots$ (18)

The HAM method selects a random value for the auxiliary homotopy parameter h, let $h = -1$. We use SCA to modify the parameter h and get the following results $h^{SCA} = -9.7861$, $h^{SCA} = -8.7001$ and $h^{SCA} = -1.0009$ for $u(x,y,t), v(x,y,t)$ and $w(x,\ y,t)$ respectively. We will also choose another value for the parameter h, and get the following results $h^{CSCA} = -0.9767, h^{CSCA} = -1.0973$ and $h^{CSCA} = -1.0090$ for $u(x,y,t), v(x,y,t)$ and $w(x,y,t)$ respectively after using CSCA. Then we substitute h^{HAM}, $h^{HAM-SCA}$, and $h^{HAM-CSCA}$ into equations (16), (17), and (18). The comparison of the results for $u^{\mathrm{HAM}}(x,y,t)$, $u^{\mathrm{HAM-SCA}}(x,y,t)$ and $u^{\mathrm{HAM-CSCA}}(x,y,t)$ is shown in **Table 5** and **Figure 6**. And the comparison of the results for $v^{\mathrm{HAM}}(x,y,t)$, $v^{\mathrm{HAM-SCA}}(x,y,t)$ and $v^{\mathrm{HAM-CSCA}}(x,\ y,t)$ is shown in **Table 6** and **Figure 7**. And also, the comparison of the results for $w^{\mathrm{HAM}}(x,t)$, $w^{\mathrm{HAM-SCA}}(x,y,t)$ and $w^{\mathrm{HAM-CSCA}}(x,y,t)$ is shown in **Table 7** and **Figure 8**.

Table 5: Comparison of MAE, MSE and L^2-Norm for $u^{HAM}(x,y,t)$, $u^{HAM-SCA}(x,y,t)$ and $u^{HAM-CSCA}(x,y,t)$

$\boldsymbol{u^{HAM-CSCA}(x,t)}$	$\boldsymbol{u^{HAM-SCA}(x,t)}$	$\boldsymbol{u^{HAM}(x,t)}$	
$2.434385E-6$	$3.510310E-6$	$3.688611E-5$	**MSE**
$4.689733E-3$	$5.602275E-3$	$1.958227E-2$	**MAE**
$9.380722E-3$	$1.070448E-2$	$3.812055E-2$	$\boldsymbol{L^2}$**-Norm**

Table 6: Comparison of MAE, MSE and L^2-Norm for $v^{HAM}(x,y,t)$, $v^{HAM-SCA}(x,y,t)$ and $v^{HAM-CSCA}(x,y,t)$.

$\boldsymbol{v^{HAM-CSCA}(x,t)}$	$\boldsymbol{v^{HAM-SCA}(x,t)}$	$\boldsymbol{v^{HAM}(x,t)}$	
$1.900183E-5$	$8.668543E-5$	$2.216491E-4$	**MSE**
$1.256750E-2$	$2.606506E-2$	$3.788224E-2$	**MAE**

$2.934731E-2$	$5.682170E-2$	$9.721195E-2$	**L^2-Norm**

Table 7: Comparison of MAE, MSE and L^2-Norm for $w^{HAM}(x,y,t)$, $w^{HAM-SCA}(x,y,t)$ and $w^{HAM-CSCA}(x,y,t)$.

$w^{HAM-CSCA}(x,t)$	$w^{HAM-SCA}(x,t)$	$w^{HAM}(x,t)$	
$2.792484E-12$	$9.453630E-12$	$1.096570E-11$	**MSE**
$2.733426E-7$	$1.368468E-6$	$1.815104E-6$	**MAE**
$1.601926E-5$	$3.242005E-5$	$3.546038E-5$	**L^2-Norm**

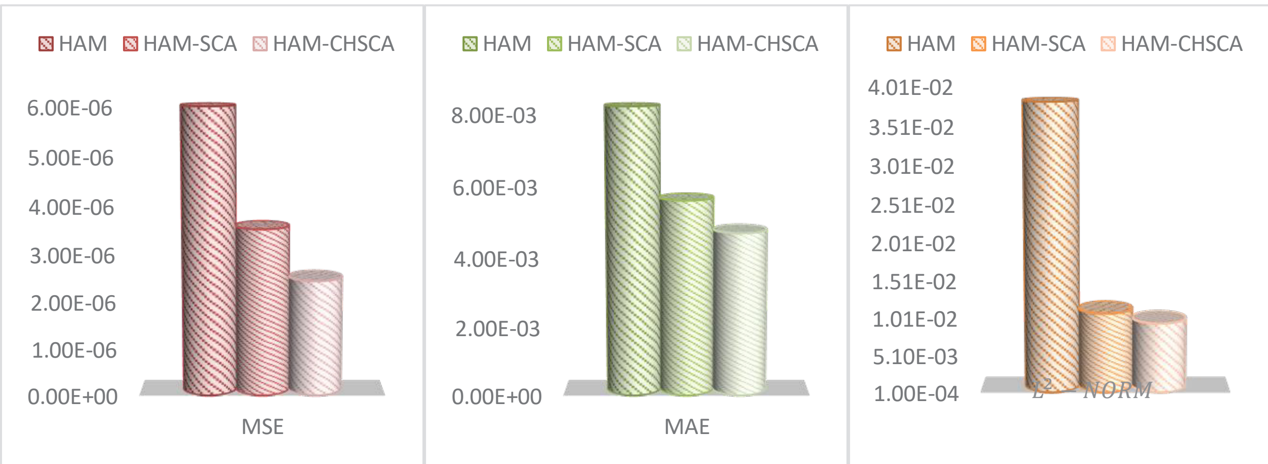

Figure 6: Comparison between $u^{HAM}(x,y,t)$, $u^{HAM-SCA}(x,y,t)$ and $u^{HAM-CSCA}(x,y,t)$

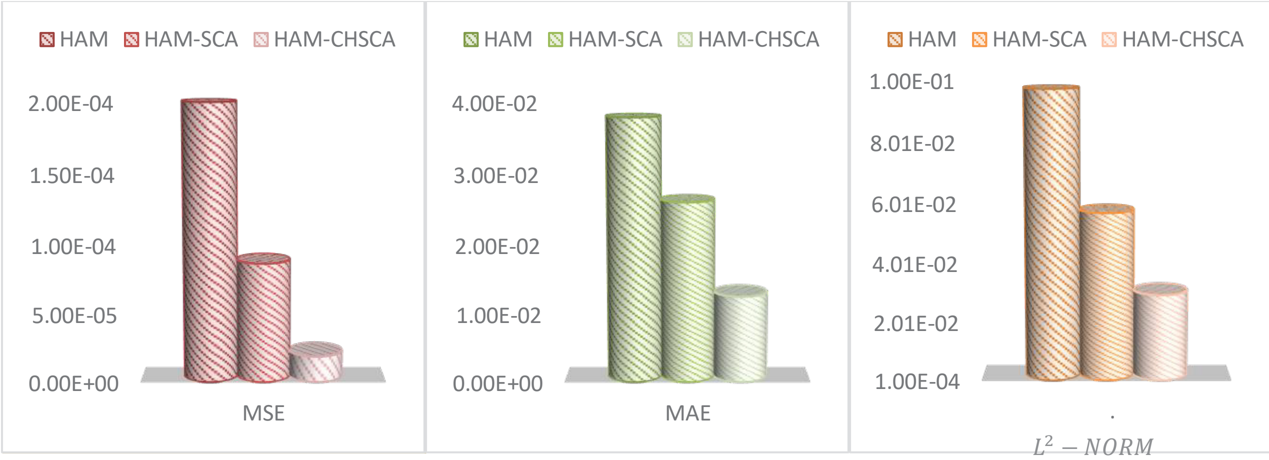

Figure 7: Comparison between L^2 for $v^{HAM}(x,y,t)$, $v^{HAM-SCA}(x,y,t)$ and $v^{HAM-CSCA}(x,y,t)$

Figure 8: Comparison between $w^{HAM}(x,y,t)$, $w^{HAM-SCA}(x,y,t)$ and $w^{HAM-CSCA}(x,y,t)$

6. Conclusion

In this paper, three examples as systems of partial differential equations of two types linear and nonlinear are solved by using the hybridization process between HAM and CSCA. The SCA cosine algorithms were combined with Chaotic maps to determine the best value of the auxiliary homotopy parameter h from the random solution set by relying on a suitable fitness function that represented the solution chain for HAM. The reliability and efficiency of the proposed HAM-CSCA method was demonstrated by computing a set of measures shown in **Tables (1-7)** and **Figures (2-8)**, in which the maximum absolute error (MAE), mean square error (MSE), and standard error L^2 criterion were calculated.

References

[1] A. Sami Bataineh, M. S. M. Noorani, and I. Hashim, "Solving systems of ODEs by homotopy analysis method," *Communications in Nonlinear Science and Numerical Simulation,* vol. 13, no. 10, pp. 2060-2070, 2008, doi: 10.1016/j.cnsns.2007.05.026.

[2] A. Entesar and O. S. Qasim, "Solve fractional differential equations via a hybrid method between variational iteration method and gray wolf optimization algorithm," *Asian-European Journal of Mathematics,* p. 2150144, 2020.

[3] F. Abidi and K. Omrani, "The homotopy analysis method for solving the Fornberg–Whitham equation and comparison with Adomian's decomposition method," *Computers & Mathematics with Applications,* vol. 59, no. 8, pp. 2743-2750, 2010.

[4] G. Akram and M. Sadaf, "Application of homotopy analysis method to the solution of ninth order boundary value problems in AFTI-F16 fighters," *Journal of the Association of Arab Universities for Basic and Applied Sciences,* vol. 24, pp. 149-155, 2017.

[5] A. S. Bataineh, M. S. M. Noorani, and I. Hashim, "Homotopy analysis method for singular IVPs of Emden–Fowler type," *Communications in Nonlinear Science and Numerical Simulation,* vol. 14, no. 4, pp. 1121-1131, 2009.

[6] A. S. Bataineh, M. S. M. Noorani, and I. Hashim, "Solving systems of ODEs by homotopy analysis method," *Communications in Nonlinear Science and Numerical Simulation,* vol. 13, no. 10, pp. 2060-2070, 2008.

[7] A. El-Ajou, Z. Odibat, S. Momani, and A. Alawneh, "Construction of Analytical Solutions to Fractional Differential Equations Using Homotopy Analysis Method," *International Journal of Applied Mathematics,* vol. 40, no. 2, 2010.

[8] S. Mirjalili, "SCA: a sine cosine algorithm for solving optimization problems," *Knowledge-based systems,* vol. 96, pp. 120-133, 2016.

[9] S. M. Mirjalili, S. Z. Mirjalili, S. Saremi, and S. Mirjalili, "Sine cosine algorithm: theory, literature review, and application in designing bend photonic crystal waveguides," *Nature-inspired optimizers,* pp. 201-217, 2020.

[10] M. A. Tawhid and V. Savsani, "Multi-objective sine-cosine algorithm (MO-SCA) for multi-objective engineering design problems," *Neural Computing and Applications,* vol. 31, no. 2, pp. 915-929, 2019.

[11] K. T. Alligood, T. D. Sauer, and J. A. Yorke, *Chaos*. Springer, 1996.

[12] A. Abbott, *Chaos of disciplines*. University of Chicago Press, 2010.

[13] Z. S. Al-Talib and S. F. AL-Azzawi, "Projective synchronization for 4D hyperchaotic system based on adaptive nonlinear control strategy," *Indonesian Journal of Electrical Engineering and Computer Science,* vol. 19, no. 2, pp. 715-722, 2020.

[14] S. Al-Azzawi, L. Patria, A. Sambas, and W. Sanjaya, "Stability of Lorenz system at the second equilibria point based on Gardano's method," in *Journal of Physics: Conference Series*, 2020, vol. 1477, no. 2: IOP Publishing, p. 022009.

[15] L. Bing and J. Weisun, "Chaos optimization method and its application [J]," *Control Theory & Applications,* vol. 4, 1997.

[16] S. Al-Azzawi, M. Mohamed, H. Rubiani, M. Mamat, and J. Titaley, "Chaotic Lorenz system and it's suppressed," *Journal of Advanced Research in Dynamical and Control Systems,* vol. 12, no. 2, pp. 548-555, 2020.

[17] D. Yang, Z. Liu, and J. Zhou, "Chaos optimization algorithms based on chaotic maps with different probability distribution and search speed for global optimization," *Communications in Nonlinear Science and Numerical Simulation,* vol. 19, no. 4, pp. 1229-1246, 2014.

[18] L. Shijun, *Advances in the Homotopy Analysis Method*. World Scientific, 2013.

[19] F. Wang, X. Yuan, S. C. Liew, and D. J. I. t. o. i. t. Guo, "Wireless MIMO switching: Weighted sum mean square error and sum rate optimization," vol. 59, no. 9, pp. 5297-5312, 2013.

[20] O. S. Qasim, A. Entesar, and W. Al-Hayani, "Solving nonlinear differential equations using hybrid method between Lyapunov's artificial small parameter and continuous particle swarm optimization," *Numerical Algebra, Control & Optimization,* p. 0, 2019.

[21] E. Babolian and J. Biazar, "On the order of convergence of Adomian method," *Applied Mathematics and Computation,* vol. 130, no. 2-3, pp. 383-387, 2002.

[22] A.-M. J. A. M. Wazwaz and computation, "A new algorithm for calculating Adomian polynomials for nonlinear operators," vol. 111, no. 1, pp. 33-51, 2000.

[23] W. Al-Hayani, L. Alzubaidy, and A. J. A. M. I. S. Entesar, "Solutions of singular IVP's of Lane–Emden type by homotopy analysis method with genetic algorithm," vol. 11, no. 2, pp. 407-416, 2017.

[24] S. Liao, *Beyond perturbation: introduction to the homotopy analysis method*. CRC press, 2003.

[25] A. S. Bataineh, M. Noorani, and I. Hashim, "Approximate analytical solutions of systems of PDEs by homotopy analysis method," *Computers & Mathematics with Applications,* vol. 55, no. 12, pp. 2913-2923, 2008.

[26] T. Zubair, M. Usman, U. Ali, and S. T. Mohyud-Din, "Homotopy analysis method for system of partial differential equations," *International Journal of Modern Engineering Sciences,* vol. 1, no. 2, pp. 67-79, 2012.

Diverse new solitons and other exact solutions for the 3-D generalized Zakharov–Kuznetsov equation using the generalized (G'/G)-expansion method

Ceylan Çelik[1] and Ebru Cavlak Aslan[2]

[1,2] Fırat University, Science Faculty, Department of Mathematics, 23119, Elazig, Turkey

ebrucavlak@hotmail.com, c.celik23.ce@gmail.com

Abstract

In this paper, the generalized G'/G-expansion method is employed to extract new solitary wave solutions for the generalized Zakharov–Kuznetsov equation in three dimensions. The proposed technique are discovered recently to derive the exact solutions for many other NLPDE that arising in various branches of science and usually give good results. By applying this method, we obtain novel solutions, which are expressed in terms hyperbolic, periodic and trigonometric wave solutions.

Keywords :The nonlinear partial differential equation, The Generalized G'/G-Expansion Method, The Zakharov-Kuznetsov equation.

1 Introduction

Partial differential equations describe various nonlinear phenomena in natural and applied sciences such as, fluid dynamics, plasma physics, solid state physics, biology, mathematical finance, etc. It is significant importance to solve the nonlinear partial differential equations (NLPDEs) from both theoretical and applied fields. One of the most significant nonlinear phenomenon is the Soliton wave. This wave from was first proposed in the process of studying fluid physics. In 1834, John Scott Russell made a remarkable scientific discovery about water waves when he was conducting experiments to determine the most efficient design for canal boats. In later years, ıt was named the Solitary wave by D. Korteweg and G. de Vries. In 1965, Zabusky and Kruskal improved the Korteweg de Vries equation (KdV) and found its stable wave solutions. Also, they showed that these solutions preserve their shape and velocities after two of them collide, interact and then spread apart again. Because of these, they named such wave the Solitons. In the past decades, many powerful methods for solving NLPDEs have been developed, such as the extended F-expansion method [1, 2], the Hirota's bilinear method [3], the Jacobi elliptic function expansion method [4, 5], the extended mapping approach [6], the rational sine–Gordon method [7], the sine-Gordon expansion method [8], the improved $tan(\phi(\eta)/2)$-expansion approach [9], Fan sub-equation method [10], the Exp-function method [11], the modified simple equation method [12], modified Kudryashov method [13], the Sardar sub-equation method [14], the unified method [15], etc.

The weakly nonlinear ion-acoustic waves in strongly magnetized lossleas plasma in two-dimension are described by the Zakharov Kuznetsov equation (ZK). The ZK equation as follow

$$u_t + auu_x + (u_{xx} + u_{yy})_x = 0$$

In the present paper, we will seek exact solutions of the following the generalized Zakharov-Kuznetsov equation in three dimensions given as

$$\Upsilon_t + \alpha_1 \Upsilon^2 \Upsilon_x + \beta_1 \Upsilon_{xxx} + \beta_2 \Upsilon_{xyy} + \beta_3 \Upsilon_{xzz} + \alpha_2 \Upsilon \Upsilon_x + \beta_4 \Upsilon_{txx} = 0 \quad (1.1)$$

where $\alpha_i, \beta_j (i = 1, 2; j = 1, ..., 4)$ as real constans. Adjusting $\alpha_1 = \beta_2 = \beta_3 = \beta_4 = 0$ reduces Eq. (1.1) to the KdV equation, while $\beta_1 = \beta_3 = \alpha_2 = 0$ reduces Eq. (1.1) to the (2+1)-dimensional ZK-MEW equation and the setting $\beta_2 = \beta_3 = \beta_4 = 0$ reduces Eq. (1.1) to the Gardner equation. In addition, If $\beta_3 = \alpha_2 = \beta_4 = 0$, then Eq. (1.1) is the mZK equation [16, 18].

In this work, the generalized (G'/G)-expansion method is used to the new solitons and other solutions for the proposed model [19, 20]. This method provide a wide variety of solutions. The rest of the paper is organized as follows. Section 2, brief of the generalized (G'/G)-expansion method is given. Section 3, solitons and other exact solutions for the governing equation are obtained.

2 Explanation of the generalized (G'/G)-expansion method

Let us consider a general NPDE given by

$$G(\Upsilon, \Upsilon_t, \Upsilon_x, \Upsilon_y, \Upsilon_z, \Upsilon_{tt}, \Upsilon_{xx}, \Upsilon_{yy}, \Upsilon_{zz}...) = 0 \tag{2.1}$$

which can be converted into an the ordinary differential equation (ODE) of the following form:

$$H(q, q', q'', ...) = 0 \tag{2.2}$$

by using the following transformation;

$$\Upsilon(x, y, z, t) = q(\xi) \tag{2.3}$$

where $\xi = x + y + z - vt$.

We assume that Eq. (2.3) has a solution of the following form

$$q(\xi) = a_0 + \sum \left\{ a_i \left(\frac{G'}{G}\right)^i + b_i \left(\frac{G'}{G}\right) \sqrt{\sigma \left(1 + \frac{1}{\mu}\left(\frac{G'}{G}\right)^2\right)} + c_i \left(\frac{G'}{G}\right)^{-i} \right\}$$

$$+d_i \frac{\left(\frac{G'}{G}\right)^{-i+1}}{\sqrt{\sigma\left(1 + \frac{1}{\mu}\left(\frac{G'}{G}\right)^2\right)}} \tag{2.4}$$

where $a_0, a_i, b_i, c_i, d_i (i = 1, 2, 3, ...)$ are contants to be determined later. In (2.4), $\sigma = \pm 1$ and $G = G(\xi)$ satisfies the following second order linear ordinary differential equation

$$G'' + \mu G = 0 \tag{2.5}$$

where μ is a constant. The positive integer n can be find out by homogeneous balance method between the nonlinear term and the highest order derivative of Eq. (2.2) collecting the exponents with the same power of $(\frac{G'}{G})^k, (\frac{G'}{G})^k\sqrt{\sigma(1 + \frac{1}{\mu})(\frac{G'}{G})^2}$, and then equating them zero seperately, we will get system of equations for $a_0, a_i, b_i, c_i, d_i (i = 1, 2, ..., n)$ and v. The general solution of Eq.(2.5) has possible solutions as below

Case 2.1 *Trigonometric solution for* $\mu > 0$

$$\frac{G'(\xi)}{G(\xi)} = \sqrt{-\mu} \frac{A_1 \sinh(\sqrt{-\mu}\xi) + A_2 \cosh(\sqrt{-\mu}\xi)}{A_1 \cosh(\sqrt{-\mu}\xi) + A_2 \sinh(\sqrt{-\mu}\xi)}. \tag{2.6}$$

Case 2.2 *Hyperbolic solution for* $\mu < 0$

$$\frac{G'(\xi)}{G(\xi)} = \sqrt{\mu}\frac{A_1\cos(\sqrt{\mu}\xi) - A_2\sin(\sqrt{\mu}\xi)}{A_1\sin(\sqrt{\mu}\xi) + A_2\cos(\sqrt{\mu}\xi)}. \tag{2.7}$$

Case 2.3 *Rational solution for* $\mu = 0$

$$\frac{G'(\xi)}{G(\xi)} = \frac{A_1}{A_1\xi + A_2}. \tag{2.8}$$

In Eq.(2.6), (2.7) and (2.8), A_1, A_2 are constants.

3 Mathematical Computation

Substituting Eq.(2.3) into Eq.(1.1), we get

$$(v - q(\alpha_1 q + \alpha_2))q' - (\beta_1 + \beta_2 + \beta_3 - v\beta_4)q''' = 0. \tag{3.1}$$

This, after integrating of Eq.(3.1) yields

$$vq - \frac{1}{3}\alpha_1 q^3 - \frac{1}{2}\alpha_2 q^2 - (\beta_1 + \beta_2 + \beta_3 - v\beta_4)q'' = 0. \tag{3.2}$$

In Eq. (3.2), the homogeneous balancing constant $n = 1$ between q'' and q^3. Thus, the solution is given as follows;

$$q(\xi) = a_0 + a_1\left(\frac{G'}{G}\right) + b_1\sqrt{\sigma\left(1 + \frac{1}{\mu}\left(\frac{G'}{G}\right)^2\right)} + c_1\left(\frac{G'}{G}\right)^{-1} + d_i\frac{1}{\sqrt{\sigma\left(1 + \frac{1}{\mu}\left(\frac{G'}{G}\right)^2\right)}}. \tag{3.3}$$

Substituting Eq.(3.3) along with Eq.(2.5) into Eq.(3.2), and all coefficients of each order $(\frac{G'}{G})^k$ and $(\frac{G'}{G})^k\sqrt{\sigma(1+\frac{1}{\mu})(\frac{G'}{G})^2}$, yields a set of over determined algebraic equation system. We can obtain the following results:

Family 1: $\alpha_1 \neq 0, \alpha_2 = 0, v = \frac{2(\beta_1\mu+\beta_2\mu+\beta_3\mu)}{2\beta_4\mu+1}, 1 + 2\beta_4\mu \neq 0, a_0 = a_1 = b_1 = d_1 = 0, c_1 = \pm\frac{i\sqrt{3}\sqrt{\mu}\sqrt{v}}{\sqrt{\alpha_1}}, \gamma = \sqrt{\frac{\beta_1\mu+\beta_2\mu+\beta_3\mu}{2\beta_4\mu+1}}$, we obtain the solutions

When $\mu < 0$,

$$\Upsilon_{1,1}(x,y,z,t) = \frac{i\sqrt{6}\sqrt{\mu}\gamma\left(A_2\sinh\left(\sqrt{-\mu}(x+y+z-vt)\right)+A_1\cosh\left(\sqrt{-\mu}(x+y+z-vt)\right)\right)}{\sqrt{\alpha_1}\sqrt{-\mu}\left(A_1\sinh\left(\sqrt{-\mu}(x+y+z-vt)\right)+A_2\cosh\left(\sqrt{-\mu}(x+y+z-vt)\right)\right)}. \tag{3.4}$$

When $\mu > 0$

$$\Upsilon_{1,2}(x,y,z,t) = \frac{i\sqrt{6}\gamma\left(A_1\sin\left(\sqrt{\mu}(x+y+z-vt)\right)+A_2\cos\left(\sqrt{\mu}(x+y+z-vt)\right)\right)}{\sqrt{\alpha_1}\left(A_1\cos\left(\sqrt{\mu}(x+y+z-vt)\right)-A_2\sin\left(\sqrt{\mu}r\right)\right)}. \tag{3.5}$$

Family 2: $\mu = \frac{\alpha_2^2}{4\left(\alpha_2^2\beta_4+6\alpha_1\beta_1+6\alpha_1\beta_2+6\alpha_1\beta_3\right)}, v = \frac{4(\beta_1\mu+\beta_2\mu+\beta_3\mu)}{4\beta_4\mu-1}, \alpha_2 \neq 0, a_0 = \frac{3v}{\alpha_2}, a_1 = b_1 = d_1 = 0, c_1 = \pm i a_0\sqrt{\mu}$, we obtain the solutions

When $\mu < 0$, for $\gamma_1 = \sqrt{-\frac{\alpha_2^2}{\alpha_2^2\beta_4+6\alpha_1(\beta_1+\beta_2+\beta_3)}}$

$$\Upsilon_{2,1}(x,y,z,t) = \frac{1}{2\alpha_1\gamma_1((A_1\sinh((\frac{1}{2}\gamma_1(-\mathrm{vt}+x+y+z)))+A_2\cosh((\frac{1}{2}\gamma_1(-\mathrm{vt}+x+y+z)))}$$

$$-(\alpha_2((A_1\left(\gamma_1\sinh((\frac{1}{2}\gamma_1(-\mathrm{vt}+x+y+z)\right)+i\gamma_1\cosh((\frac{1}{2}\gamma_1(-\mathrm{vt}+x+y+z)))$$

$$+A_2((\gamma_1\cosh((\frac{1}{2}\gamma_1(-\mathrm{vt}+x+y+z)))+i\gamma_1\sinh((\frac{1}{2}\gamma_1(-\mathrm{vt}+x+y+z))))). \tag{3.6}$$

When $\mu > 0$, for $\gamma_2 = \sqrt{\alpha_2^2\beta_4+6\alpha_1\left(\beta_1+\beta_2+\beta_3\right)}$

$$\Upsilon_{2,2}(x,y,z,t) = -\frac{\alpha_2\left(A_1+iA_2\right)e^{\frac{1}{2}i\sqrt{\frac{\alpha_2^2}{\gamma_2}}(-\mathrm{vt}+x+y+z)}}{2\alpha_1\left(A_1\cos\left(\frac{\alpha_2(-\mathrm{vt}+x+y+z)}{2\gamma_2}\right)-A_2\sin\left(\frac{1}{2}\sqrt{\frac{\alpha_2^2}{\gamma_2}}(-\mathrm{vt}+x+y+z)\right)\right)}. \tag{3.7}$$

5

Family 3: $\beta_1 = 1, \alpha_2 = 0, v = \frac{8(\beta_2\mu+\beta_3\mu+\mu)}{8\beta_4\mu+1}, a_0 = b_1 = d_1 = 0, a_1 = \pm\frac{\sqrt{6}\sqrt{-\beta_2-\beta_3+\beta_4 v-1}}{\sqrt{\alpha_1}}, c_1 = \frac{a_1\mu(-16\beta_2\mu-16\beta_3\mu-16\mu+16\beta_4\mu v-v)}{3v}, \gamma_1 = \sqrt{-\frac{\beta_2+\beta_3+1}{8\beta_4\mu+1}}$, we obtain the solutions

When $\mu < 0$,

$$\Upsilon_{3,1}(x,y,z,t) = \frac{1}{\sqrt{\alpha_1}\left(2A_1A_2\cos\left(2\sqrt{\mu}(-\mathrm{vt}+x+y+z)\right)+\left(A_1^2+A_2^2\right)\sinh\left(2\sqrt{-\mu}(-\mathrm{vt}+x+y+z\right.\right.}$$

$$2\sqrt{6}\gamma_1\sqrt{-\mu}\left(\left(A_1^2+A_2^2\right)\cos\left(2\sqrt{\mu}(-\mathrm{vt}+x+y+z)\right)+2A_1A_2\sinh\left(2\sqrt{-\mu}(-\mathrm{vt}+x+y+z)\right)\right). \tag{3.8}$$

When $\mu > 0$,

$$\Upsilon_{3,2}(x,y,z,t) = \frac{1}{\sqrt{\alpha_1}\left(\left(A_1^2-A_2^2\right)\sin\left(2\sqrt{\mu}(-\mathrm{vt}+x+y+z)\right)+2A_1A_2\cos\left(2\sqrt{\mu}(-\mathrm{vt}+x+y+z)\right)\right)}$$

$$2\gamma_1\sqrt{6\mu}\left(\left(A_1^2-A_2^2\right)\cos\left(2\sqrt{\mu}(-\mathrm{vt}+x+y+z)\right)-2A_1A_2\sin\left(2\sqrt{\mu}(-\mathrm{vt}+x+y+z)\right)\right). \tag{3.9}$$

Family 4: $\beta_1 = -\beta_2-\beta_3, \alpha_2 = 0, \mu = -\frac{1}{2\beta_4}, a_0 = a_1 = b_1 = d_1 = 0, c_1 = \frac{i\sqrt{3}\sqrt{\mu}\sqrt{v}}{\sqrt{\alpha_1}}$, we obtain the solutions

When $\mu < 0$,

$$\Upsilon_{4,1}(x,y,z,t) = \frac{i\sqrt{-\frac{1}{\beta_4}}\sqrt{3v}\left(A_2\sinh\left(\frac{-\mathrm{vt}+x+y+z}{\sqrt{2\beta_4}}\right)+A_1\cosh\left(\frac{-\mathrm{vt}+x+y+z}{\sqrt{2\beta_4}}\right)\right)}{\sqrt{\frac{\alpha_1}{\beta_4}}\left(A_1\sinh\left(\frac{-\mathrm{vt}+x+y+z}{\sqrt{2\beta_4}}\right)+A_2\cosh\left(\frac{-\mathrm{vt}+x+y+z}{\sqrt{2\beta_4}}\right)\right)}. \tag{3.10}$$

When $\mu > 0$,

$$\Upsilon_{4,2}(x,y,z,t) = \frac{i\sqrt{\frac{3v}{\alpha_1}}\left(A_1\sin\left(\frac{\sqrt{-\frac{1}{\beta_4}}(-\mathrm{vt}+x+y+z)}{\sqrt{2}}\right)+A_2\cosh\left(\frac{-\mathrm{vt}+x+y+z}{\sqrt{2\beta_4}}\right)\right)}{A_1\cosh\left(\frac{-\mathrm{vt}+x+y+z}{\sqrt{2\beta_4}}\right)-A_2\sin\left(\frac{\sqrt{-\frac{1}{\beta_4}}(-\mathrm{vt}+x+y+z)}{\sqrt{2}}\right)}. \tag{3.11}$$

6

Family 5: $\beta_1 = -\beta_2 - \beta_3, \mu = \frac{1}{4\beta_4}, v = -\frac{\alpha_2^2}{6\alpha_1}, a_0 = \frac{3v}{\alpha_2}, a_1 = b_1 = d_1 = 0, c_1 = ia_0\sqrt{\mu}$, we obtain the solutions

When $\mu < 0$,

$$\Upsilon_{5,1}(x,y,z,t) = \frac{\alpha_2\left(-1 - \frac{i\sqrt{\frac{1}{\beta_4}}\left(A_1\cos\left(\frac{-\mathrm{vt}+x+y+z}{2\sqrt{\beta_4}}\right)+A_2\sinh\left(\frac{1}{2}\sqrt{-\frac{1}{\beta_4}}(-\mathrm{vt}+x+y+z)\right)\right)}{A_2\sqrt{-\frac{1}{\beta_4}}\cos\left(\frac{-\mathrm{vt}+x+y+z}{2\sqrt{\beta_4}}\right)-\frac{A_1\sin\left(\frac{-\mathrm{vt}+x+y+z}{2\sqrt{\beta_4}}\right)}{\sqrt{\beta_4}}}\right)}{2\alpha_1}. \tag{3.12}$$

When $\mu > 0$,

$$\Upsilon_{5,2}(x,y,z,t) = -\frac{\alpha_2\left(A_1 + iA_2\right)e^{\frac{1}{2}i\sqrt{\frac{1}{\beta_4}}(-\mathrm{vt}+x+y+z)}}{2\alpha_1\left(A_1\cos\left(\frac{-\mathrm{vt}+x+y+z}{2\sqrt{\beta_4}}\right) - A_2\sin\left(\frac{1}{2}\sqrt{\frac{1}{\beta_4}}(-\mathrm{vt}+x+y+z)\right)\right)}. \tag{3.13}$$

Family 6: $\beta_2 = -\beta_3 - 1, \beta_1 = 1, \alpha_2 = 0, \mu = \frac{1}{4\beta_4}, a_0 = b_1 = d_1 = 0, a_1 = \frac{\sqrt{6}\sqrt{\beta_4}\sqrt{v}}{\sqrt{\alpha_1}}, c_1 = \frac{1}{3}a_1\mu\left(16\beta_4\mu - 1\right)$, we obtain the solutions

When $\mu < 0$,

$$\Upsilon_{6,1}(x,y,z,t) = \sqrt{\frac{3}{2}}\left(A_1^2 - A_2^2\right)\sqrt{v}\Bigg/\left(\left(A_1\sinh\left(\frac{1}{2}\sqrt{-\frac{1}{\beta_4}}(-\mathrm{vt}+x+y+z)\right)\right.\right.$$

$$\left.A_2 + \cosh\left(\frac{1}{2}\sqrt{-\frac{1}{\beta_4}}(-\mathrm{vt}+x+y+z)\right)\right)\left(A_1\cosh\left(\frac{1}{2}\sqrt{-\frac{1}{\beta_4}}(-\mathrm{vt}+x+y+z)\right)\right.$$

$$\left.\left.A_2\sinh\left(\frac{1}{2}\sqrt{-\frac{1}{\beta_4}}(-\mathrm{vt}+x+y+z)\right)\right)\sqrt{\alpha_1}\sqrt{-\frac{1}{\beta_4}}\sqrt{\beta_4}\right). \tag{3.14}$$

7

When $\mu > 0$,

$$\Upsilon_{6,2}(x,y,z,t) = \frac{\sqrt{6}\left(A_1^2 + A_2^2\right)\sqrt{\frac{1}{\beta_4}}\sqrt{\beta_4}\sqrt{v}}{\sqrt{\alpha_1}\left(\left(A_1^2 - A_2^2\right)\sin\left(\frac{-\mathrm{vt}+x+y+z}{\sqrt{\beta_4}}\right) + 2A_1A_2\cos\left(\frac{-\mathrm{vt}+x+y+z}{\sqrt{\beta_4}}\right)\right)}. \tag{3.15}$$

Family 7: $\beta_1 = 1, \alpha_2 = 0, \mu = \frac{1}{4\beta_4}, v = \frac{8}{9}\left(\beta_2 + \beta_3 + 1\right)\mu\left(16\beta_4\mu - 1\right), a_0 = b_1 = d_1 = 0, a_1 = \frac{\sqrt{6}\sqrt{-\beta_2-\beta_3+\beta_4 v-1}}{\sqrt{\alpha_1}}, c_1 = \frac{a_1\mu(-16\beta_2\mu-16\beta_3\mu-16\mu+16\beta_4\mu v-v)}{3v}$, we obtain the solutions

When $\mu < 0$,

$$\begin{aligned}\Upsilon_{7,1}(x,y,z,t) = {} & \left(A_1^2 + A_2^2\right)\cos\left(\frac{-\mathrm{vt}+x+y+z}{\sqrt{\beta_4}}\right) + 2A_1A_2\sinh\left(\sqrt{-\frac{1}{\beta_4}}(-\mathrm{vt}+x+y+z)\right) \\ & \sqrt{-\beta_2-\beta_3-1}\sqrt{-\frac{2}{\beta_4}}(1/\sqrt{\alpha_1}(2A_1A_2\cos(\frac{-\mathrm{vt}+x+y+z}{\sqrt{\beta_4}}) \\ & +(A_1^2 + A_2^2)\sinh(\sqrt{-\frac{1}{\beta_4}}(-\mathrm{vt}+x+y+z))))\end{aligned} \tag{3.16}$$

When $\mu > 0$,

$$\begin{aligned}\Upsilon_{7,2}(x,y,z,t) = {} & \left(A_1^2 - A_2^2\right)\cos\left(\frac{-\mathrm{vt}+x+y+z}{\sqrt{\beta_4}}\right) - 2A_1A_2\sin\left(\sqrt{\frac{1}{\beta_4}}(-\mathrm{vt}+x+y+z)\right) \\ & \sqrt{-\beta_2-\beta_3-1}\sqrt{\frac{2}{\beta_4}}(\sqrt{\alpha_1}(2A_1A_2\cos(\frac{-\mathrm{vt}+x+y+z}{\sqrt{\beta_4}}) \\ & +(A_1^2 - A_2^2)\sin(\sqrt{\frac{1}{\beta_4}}(-\mathrm{vt}+x+y+z))))\end{aligned} \tag{3.17}$$

4 Conclusion

In this paper, a generalized (G'/G) -expansion method is used to obtain more general exact solutions of the generalized Zakharov-Kuznetsov equation. As a result, exact wave solutions are obtained including hyperbolic function solutions, trigonometric function solutions and periodic solutions. The paper shows that the generalized (G'/G) -expansion method is direct, effective and can be used for many other NLEEs in mathematical physics.

Acknowledgement

This study is related to the Master's thesis of the first author.

References

[1] M. Borg, N. M. Badra, H. M. Ahmed, W. B. Rabie, "Solitons behavior of Sasa-Satsuma equation in birefringent fibers with Kerr law nonlinearity using extended F-expansion method," Ain Shams Engineering Journal, 15 (102290), 1-12, 2023.

[2] W. B. Rabie and H. M. Ahmed, "Cubic-quartic solitons perturbation with couplers in optical metamaterials having triple-power law nonlinearity using extended F-expansion method," Optik, 262(169255), 169255, 2022.

[3] M.Rahman et al., "Rational solutions and some interactions phenomena of a (3+1)-dimensional BLMP equation in incompressible fluids: A Hirota bilinear method and dimensionally reduction approach," Results in Physics, 56 (107269), 1-13, 2024.

[4] E. Cavlak Aslan, L. Gürgöze, "Soliton and Other Function Solutions of The Potential KdV Equation with Jacobi Elliptic Function Method," International Journal of Innovative Engineering Applications 6 (2), 183-188, 2022.

[5] E. Cavlak Aslan, D. Deniz, M. Inc, "Analysing of different wave structures to the dissipative NLS equation and modulation instability," Optical and Quantum Electronics, 56 (254), 1-15, 2024.

[6] CL. Zheng, J. Fang, L. Chen, "New variable separation excitations of (2 + 1)-dimensional dispersive long-water wave system obtained by an extended mapping approach," Chaos, Solitons and Fractals, 23 (5), 1741-1748, 2005.

[7] B. Kemaloğlı, G. Yel and H Bulut, "An application of the rational sine–Gordon method to the Hirota equation," Optical and Quantum Electronics, 55(658), 1-10, 2022.

[8] K. K. Ali, M. S. Osman, and M. Abdel-Aty, "New optical solitary wave solutions of Fokas-Lenells equation in optical fiber via Sine-Gordon expansion method," Alex. Eng. J., 59(3), 1191–1196, 2020.

[9] S. Arshed et al., "New soliton solutions of nonlinear Kudryashov's equation via Improved $tan(\phi(\eta)/2)$-expansion approach in optical ber,"Kuwait J.Sci.,49(3), 1-16, 2022.

[10] K. U. Tariq, et al., "Construction of new exact solutions of the resonant fractional NLS equation with the extended Fan sub-equation method", Journal of King Saud University - Science, 33(8), 101643, 2021.

[11] J.-H. He and X.-H. Wu, "Exp-function method for nonlinear wave equations," Chaos Solitons Fractals, 30(3), 700–708, 2006.

[12] G. Bakicierler, S. Alfaqeih, and E. Misirli, "Application of the modified simple equation method for solving two nonlinear time-fractional long water wave equations," Rev. Mexic. Fis., 67(6), 2021.

[13] M. Ali Akbar et al., "Soliton solutions to the Boussinesq equation through sine-Gordon method and Kudryashov method," Results Phys., 25(104228), 104228, 2021.

[14] M. Cinar, A. Secer, M. Ozisik, M. Bayram, "Derivation of optical solitons of dimensionless Fokas-Lenells equation with perturbation term using Sardar sub-equation method," Optical and Quantum Electronics, 54(4029), 2022.

[15] M. S. Ullah, et al., "Application of the unified method to solve the Biswas–Arshed model," Results in Physics, 42(105946), 1-6, 2022.

[16] C. M. Khalique, O. D. Adeyemo, "Langrangian formulation and solitary wave solutions of a generalized Zakharov–Kuznetsov equation with dual power-law nonlinearity in physical sciences and engineering," Journal of Ocean Engineering and Science, 8, 152-168, 2023.

[17] E. H. M. Zahran, et al., "New diverse exact optical solutions of the three dimensional Zakharov–Kuznetsov equation," Optical and Quantum Electronics, 55 (817), 1-20, 2023.

[18] O. D. Adeyemo, L. Zhang, C. M. Khalique, "Optimal solutions of Lie subalgebra, dynamical system, travelling wave solutions and conserved currents of (3+1)-dimensional generalized Zakharov–Kuznetsov equation type I," European Physical Journal Plus, 137(954), 1-37, 2022.

[19] K. K. Ali, N. Al-Harbi, A. Abdel-Aty, "Traveling wave solutions to (3 + 1) conformal time derivative generalized q-deformed Sinh-Gordon equation," Alexandria Engineering Journal, 65, 233–243, 2023.

[20] S. Zhang, W. Wang, J.-L. Tong, "A generalized (G'/G)-expansion method and its application to the (2 +1)-dimensional Broer–Kaup equations," Applied Mathematics and Computation 209, 399–404, 2009.

Enhancing Microgrid Stability with Fuzzy Logic Controller

Abdulkadir Eren[1], Ahmet Kaysal[2]

[1]Department of Electrical Engineering, University of Afyon Kocatepe, Afyonkarahisar, Turkey

[2]Department of Electrical and Electronics Engineering, University of Afyon Kocatepe, Afyonkarahisar, Turkey

abdulkadir0436@gmail.com, akaysal@aku.edu.tr

Abstract

As populations expand, meeting the increasing need for electrical energy is becoming increasingly difficult. Electrical energy obtained from fossil fuels causes environmental pollution. Additionally, the load increase makes main grid control difficult. In this study, the DC microgrid design, which consists of distributed generation units, has been implemented. The designed DC microgrid feeds three different loads, including the critical load. For DC bus voltage regulation, a fuzzy logic controller is proposed in the control structure of DC/AC converters. This control strategy is evaluated against conventional P, PI, and PID control structures. It is observed that the fuzzy logic controller performs more effectively when the DC microgrids operate standalone or grid-connected with the main grid.

Keywords: DC microgrid system, Fuzzy logic, DC bus voltage, PID

1. INTRODUCTION

Energy is of great importance for the survival of the human race. As the population increases rapidly, electrical energy needs also increase [1]. Electrical energy is generally obtained from fossil fuels such as coal, oil and natural gas. It is rapidly depleting due to the constant use of fossil fuels [2,3]. In addition, using these fuels increases the emission of carbon dioxide and other greenhouse gases and further deepens the global warming problem [3-5]. Renewable energy sources (RES) offer an alternative solution to energy needs and climate change problems. RESs such as solar, wind, geothermal, and hydroelectric are frequently preferred due to their ease of accessibility. These sources are environmentally friendly as they provide clean energy, but their intermittency may cause some difficulties for the grid [6-8].

Microgrids (MGs) consist of distributed energy resources (DERs), energy storage systems, and a variety of load types. In remote or geographically challenging areas where the main grid is inaccessible, MGs, equipped with photovoltaic (PV) panels, wind turbines (WT), and diesel generators (DG), can independently satisfy the energy demands of those areas [9,10]. Additionally, MGs, which operate in grid-connected and standalone modes, are particularly advantageous as they can be installed proximate to consumers [11]. MGs are categorized into two primary types: AC and DC. In AC MGs, a significant portion of the power transferred to consumers is consumed by the converters. Comparatively, DC MGs are noted for their simpler control structures and generally higher efficiency [12]. The lack of a reactive component in DC

MGs results in lower line losses than in AC MGs. DER units are only connected to the DC bus, so each can be controlled more efficiently [13].

In MGs, the electrical energy production of DER units and the energy demand of consumers vary. Therefore, it isn't easy to balance the power produced and consumed. This situation causes voltage fluctuations in MGs. To ensure the voltage stability of MGs, the most appropriate control methods should be applied, considering the characteristics of DERs and energy storage systems (ESS) [14]. Recently, researchers have been working to improve these control methods. Recent research has focused on enhancing these control strategies. Yousuf et al. compared a self-tuning fuzzy PID controller with a conventional PID controller for frequency stabilization in MGs, finding that the fuzzy PID controller offered superior performance in managing frequency deviations [15]. In another study, Sun designed a fuzzy neural PID controller with particle swarm optimization to provide voltage control of DC MGs. According to the simulation results, it has been observed that the proposed controller performs better than the conventional PID controller [16]. Hussein et al. designed a fuzzy PI controller for voltage control in islanded DC MGs. The proposed controller has been tested in different voltage references, and successful results have been obtained [17].

In this study, an islanded DC MG containing various loads, fed by PV arrays, WT, DG, and ESS, has been created. A total of 3 loads have been determined, one of which was the critical load. By using energy management systems, the uninterrupted feeding of the critical load is ensured. In addition, it is aimed to keep the DC bus voltage regulation, which is an important parameter in MGs, optimally within critical limits. Thus, fuzzy logic controller (FLC) is proposed in the control structure of the DC/AC converter. The proposed controller is compared with conventional P, PI and PID controllers.

2. DC MICROGRID SYSTEM

In this study, an islanded DC MG has been established, incorporating PV arrays, WT, DG, ESS, and loads. Each power source is connected to the DC bus: PV arrays via DC/DC converters, WTs through AC/DC converters, ESS via bidirectional DC/DC converters, and DGs using AC/DC converters. Three AC loads, including one critical load, are powered using a DC/AC converter connected to the DC bus. The configuration of the DC MG is depicted in Figure 1. Additionally, the specifications of the DC bus and the loads are detailed in Table 1.

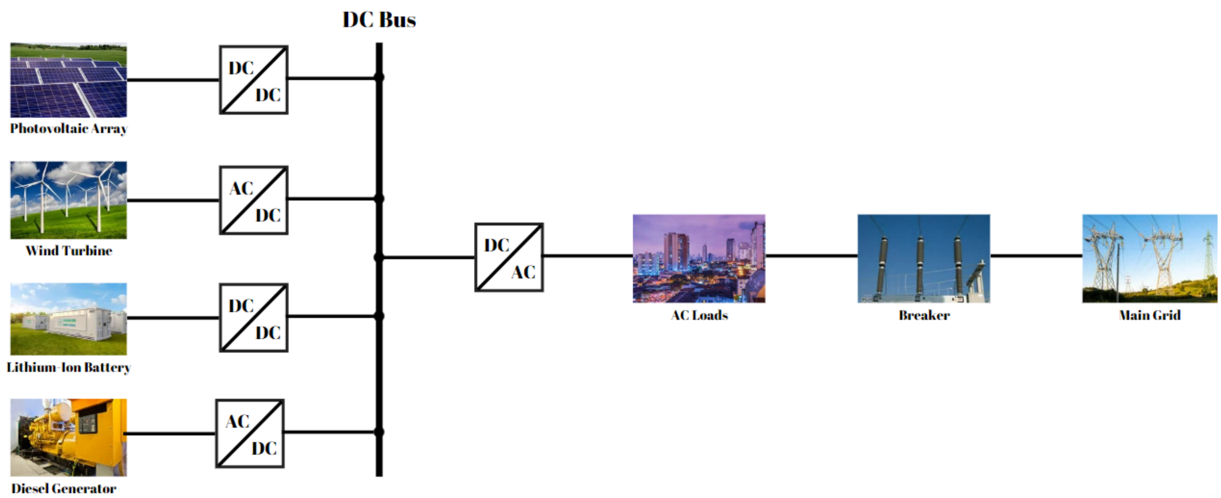

Fig. 1. Block diagram of the designed DC MG system

Table 1. Parameters of DC microgrid and loads

Equipment	Parameter	Value
DC grid	DC bus voltage	$V_{ref} = 400V$
	Line resistance	$R_{li} = 0.01\Omega$
Loads	Critical load act. pwr	$P_{crt} = 4kW$
	Critical load react. pwr	$Q_{Lcrt} = 100VAR$
	Load1 act. pwr	$P_1 = 5kW$
	Load1 react. pwr	$Q_{C1} = 100VAR$
	Load2 active pwr	$P_2 = 6kW$
	Load2 reactive pwr	$Q_{L2} = 250VAR$

2.1. Photovoltaic Array

PV cells consist of a combination of a current source, series and parallel connected resistors and a diode. These cells convert sunlight into electrical current. PV arrays occur when PV cells come together [18]. The output current of the PV array is specified in Equation 1 [19].

$$I_{PV} = N_p I_{ph} - N_p I_o \left[e^{\left(\frac{V_{PV} + I_{PV} R_{seq}}{\alpha N_s V_t} \right)} - 1 \right] - \frac{V_{PV} + I_{PV} R_{seq}}{R_{sheq}} \tag{1}$$

In this equation, I_{PV} is the output current of the PV array, I_o is the saturation current, I_{ph} is the current produced by solar radiation, V_{PV} is the voltage of the PV array, V_t is the thermal voltage, N_p is the number of parallel cells, N_s is the number of series cells, α is the ideality factor, R_{seq} is the series shunt internal resistance and R_{sheq} represents the parallel internal resistance. The characteristics of the PV array used for DC MG are given in Table 2.

Table 2. Parameters of photovoltaic array

Parameter	Value
Voltage at the mpp	$V_{mpp} = 54.7V$
Current at the mpp	$I_{mpp} = 5.49A$
Maximum power at 1000 W/m^2 solar irradiance	$P_{pv} = 6kW$
Cell per module	$N_s = 20$
Light-generated current	$I_L = 5.9004A$
Short-circuit current	$I_{SC} = 5.87A$
Open circuit voltage	$V_{OC} = 64V$
Diode saturation current	$I_0 = 6.2104e^{-11}A$

2.2. Wind Turbine

Various generators can be employed in wind turbines, among which the Permanent Magnet Synchronous Generator (PMSG) is a notable option. The absence of a brush mechanism and winding losses characterizes this generator type. Due to these advantages, the PMSG has been selected for use in our DC Microgrid (MG) system. The output power of the wind turbine utilizing a PMSG is expressed in Equation 2 [20].

$$P_w = \frac{1}{2} \rho A_w \vartheta_w^3 C_p \tag{2}$$

In this equation, P_w represents the rotor output power, A_w represents the blade swept area, ρ represents the air density, and ϑ_w represents the wind speed. C_p power coefficient affects the rotor performance of wind turbines. The properties of WT used for DC MG are given in Table 3.

Table 3. Parameters of wind turbine

Parameter	Value
Nominal rotor speed	$n_s = 2000rpm$
Mechanical torque	$T_m = 8N.m$
Stator phase resistance	$R_w = 0.9585\Omega$
Armature inductance	$L_w = 5.25mH$

2.3. Diesel Generator

DGs are a secondary power source for internal combustion used for peak energy demands and power outages. In MG systems, in cases where RES are insufficient, DGs are used to meet the energy demand of the loads. The efficiency of the DG also decreases at low loads. Therefore, DGs should not be operated in no-load and low-load situations [21,22]. The properties of the DG used for DC MG are given in Table 4.

Table 4. Parameters of diesel generator

Parameter	Value
Nominal power rate	$P_d = 8.1kVA$
Nominal voltage	$V_d = 400V$
Nominal frequency	$f_d = 50Hz$

2.4. Energy Storage System

Batteries store electrical energy and allow it to be used when needed. Dimensions, weights and shapes of batteries are parameters that affect their storage capacity [23]. Lithium-ion batteries, which are high-tech products that provide higher energy than their size, are frequently preferred [24]. Lithium-ion batteries have been used in our system because they have low internal resistance, can be charged quickly, can provide load power density and are reliable. The technical specifications of the ESS used for DC MG are given in Table 5.

Table 5. Parameters of ESS

Parameter	Value
Nominal voltage	$V_b = 200V$
Rated capacity	$Q_{nom} = 30Ah$
Nominal discharge current	$I_{dis} = 13.0435A$
Internal resistance	$R_b = 0.0667\Omega$

3. MICROGRID CONTROL METHODS

3.1. PID Controller

The PID controller is comprised of three components: a proportional controller (P), an integral controller (I), and a derivative controller (D). The proportional parameter diminishes both the rise time and the steady-state error, yet it may increase the overshoot and impact the settling time. The integral parameter effectively eliminates the steady-state error but also causes an increased overshoot. Conversely, the derivative parameter is instrumental in reducing the overshoot and the settling time while only marginally influencing the rise time and steady-state error. The output of the PID controller is articulated in Equation 3 [25,26].

$$u(t) = K_p e(t) + K_i \int e(t)dt + K_d \frac{de(t)}{dt} \quad (3)$$

Where $u(t)$ is the output of the PID controller, K_p is the ratio coefficient, K_i is the integral coefficient, K_d is the derivative coefficient, and $e(t)$ is the error signal. The Ziegler-Nichols method was used when calculating the coefficients in our DC MG system.

3.2. Fuzzy Logic Controller

Some systems are poorly defined, change over time, and have complex structures. In such systems, expert opinion is often used. The expert controls the system using linguistic expressions used in daily life. FLC convert these linguistic expressions into mathematical expressions and transfer them to the computer environment. Fuzzy logic controllers consist of four basic components: knowledge base, fuzzification, defuzzification and decision-making units [27,28].

FLC has been implemented in the control structure of the DC/AC converter to increase the efficiency of the DC MG system and ensure DC bus voltage stability. The controller has two inputs: the error signal e(t) and the de(t)/dt, which expresses the change of the error signal with time. The rule base of the FLC system is given in Table 6.

Table 6. Fuzzy logic controller rules set

DeltaE / Error	NNB	NNK	SS	PPK	PPB
NNB	NNB	NNB	NNK	NNK	SS
NNK	NNB	NNK	NNK	SS	PPK
SS	NNB	NNK	SS	PPK	PPB
PPK	NNK	SS	PPK	PPK	PPB
PPB	SS	PPK	PPK	PPB	PPB

4. RESULTS

In this study, P, PI, PID and FLC structures are compared in the DC MG system. DC bus voltage graphs for each control structure are given in Figure 2. The FLC has a much faster response and recovery time than traditional controllers. It is seen that the voltage fluctuation in the system is less when the FLC structure is used when the DC MG system is operating at full load. In addition, it is clearly seen that with the recommended controller structure, voltage drops and voltage rises are less during mains connection and disconnection. Additionally, system frequency graphs for each controller structure are given in Figure 3.

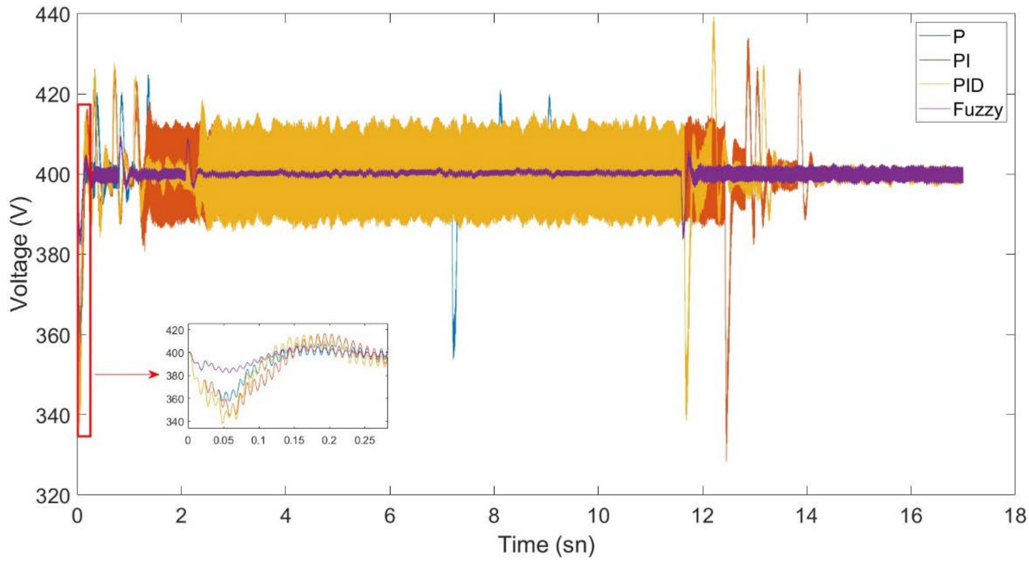

Fig. 2. DC bus voltage

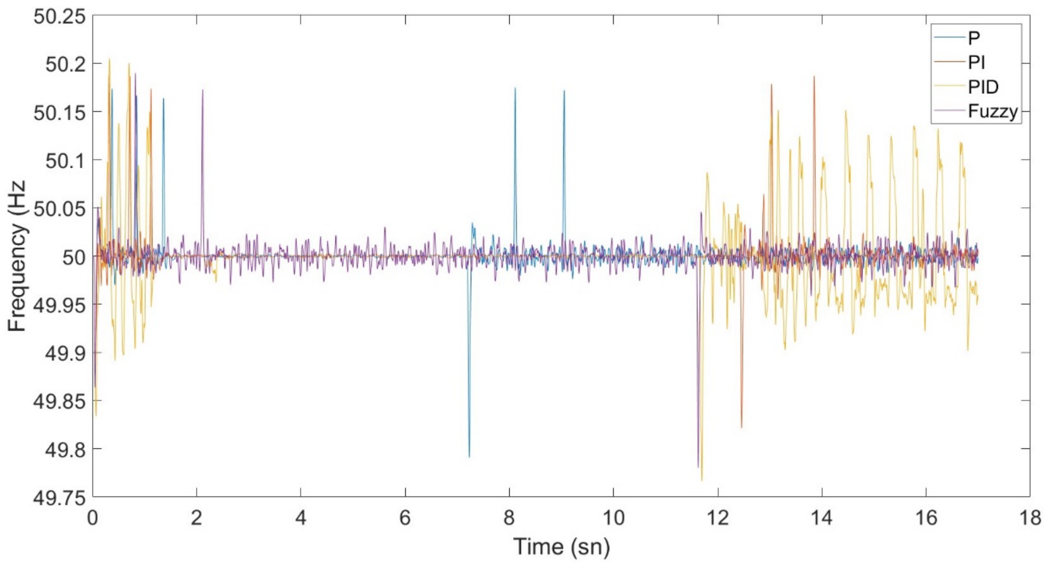

Fig. 3. DC MG frequency

As seen in Figure 3, P, PI, and FLC controllers ensure the system frequency is kept in the desired range. The PID controller disrupts the system frequency when connected to the main grid.

5. CONCLUSIONS

In this study, the DC MG system has been designed. Conventional controllers P, PI and PID controllers are used in the control structure of the DC/AC converter. Additionally, the designed FLC has been compared with conventional controllers. According to the results obtained, it was concluded that the FLC is more suitable for this system than conventional controllers. Future studies intend to compare the DC bus and frequency profiles of the DC MG system using different control structures.

REFERENCES

[1] I. El Kafazi, R. Bannari, A. Abouabdellah, M. Aboutafail & J.M. Guerrero, Energy production: a comparison of forecasting methods using the polynomial curve fitting and linear regression. International Renewable and Sustainable Energy Conference pp. 1-5, 2017.

[2] N. Abas, A. Kalair, N. Khan, Review of fossil fuels and future energy technologies, Futures 69, 31–49, 2015.

[3] F. O. Hocaoğlu, K. Kaysal, ve A. Kaysal, Hybrid Model for Load Forecasting (ANN and Regression), APJES, 3(2), 2015, 33–39.

[4] H. Heidari, S.T. Katircioğlu, L. Saeidpour, Economic growth, CO2 emissions, and energy consumption in the five ASEAN countries, Int. J. Electr. Power Energy Syst. 64, 785–791, 2015.

[5] M.O. Faruque, M.A.J. Rabby, M.A. Hossain, M.R. Islam, M.M.U. Rashid, S. Muyeen, A comparative analysis to forecast carbon dioxide emissions, Energy Rep. 8, 8046–8060, 2022.

[6] E. Kötter, L. Schneider, F. Sehnke, K. Ohnmeiss, R. Schröer, The future electric power system: Impact of Power-to-Gas by interacting with other renewable energy components, J. Energy Storage 5, 113–119, 2016.

[7] G. Pleßmann, M. Erdmann, M. Hlusiak, C. Breyer, Global energy storage demand for a 100% renewable electricity supply, Energy Procedia 46, 22–31, 2014.

[8] P. Colbertaldo, S.B. Agustin, S. Campanari, J. Brouwer, Impact of hydrogen energy storage on California electric power system: Towards 100% renewable electricity, Int. J. Hydrogen Energy 44 (19), 9558–9576, 2019.

[9] M Carpintero-Rentería, D Santos-Martín, J M Guerrero, Microgrids literature review through a layer's structure. Energies, 12:4381, 2019.

[10] MN Alam, S Chakrabarti, A Ghosh. Networked microgrids: state-of-the-art and future perspectives. IEEE Trans Ind Informatics, 15:1238–50, 2015.

[11] L Mehigan, JP Deane, BPO Gallachoir',' V Bertsch, A review of the role of distributed generation (DG) in future electricity systems. Energy, 163:822–36, 2018.

[12] R. Lasseter and P. Paigi, Microgrid: a conceptual solution, Power Electron. Specialists Conf., vol. 6, pp. 4285–4290, 2004.

[13] C. Byers and A. Botterud, Additional capacity value from the synergy of variable renewable energy and energy storage, IEEE Trans. Sustain. Energy, vol. 11, no. 2, pp. 1106–1109, 2020.

[14] A. Parisio, E. Rikos, L. Glielmo, A model predictive control approach to microgrid operation optimization, IEEE Transactions on Control Systems Technology, 22(5), 1813-1827, 2014.

[15] Y. Yousuf, J. Dhillon, S. Mishra, Frequency control of an islanded microgrid using self-tuning fuzzy PID controller, International Conference on Artificial Intelligence and Applications (ICAIA) Alliance Technology Conference (ATCON-1) (pp. 1-5), 2023.

[16] J. Sun, Voltage control of DC microgrid based on fuzzy neural network and improved particle swarm optimization algorithm. In 2022 First International Conference on Cyber-Energy Systems and Intelligent Energy (ICCSIE) (pp. 1-5), 2023.

[17] H. Hussein, A. Aghmadi, O.A. Mohammed, Design and Analysis of Voltage Control for Islanded DC Microgrids Based on a Fuzzy-PI Controller. Green Technologies Conference (GreenTech) (pp. 229-233), 2023.

[18] B. Bendib, H. Belmili, F. Krim, A survey of the most used MPPT methods: Conventional and advanced algorithms applied for photovoltaic systems. Renewable and Sustainable Energy Reviews, 45, 637-648, 2015.

[19] S. Batiyah, N.Zohrabi, S. Abdelwahed, R. Sharma, An MPC-based power management of a PV/battery system in an islanded DC microgrid, Transportation Electrification Conference and Expo (ITEC) (pp. 231-236), 2018.

[20] A. Kaysal, S. Köroğlu, Y. Oğuz, Hierarchical energy management system with multiple operation modes for hybrid DC microgrid, International Journal of Electrical Power & Energy Systems, 141, 108149, 2022.

[21] H. Borhanazad, S. Mekhilef, V.G. Ganapathy, M. Modiri-Delshad, A. Mirtaheri, Optimization of micro-grid system using MOPSO, Renewable energy, 71, 295-306, 2014.

[22] M.A. Ramli, HREH. Bouchekara, AS. Alghamdi, Optimal sizing of PV/wind/diesel hybrid microgrid system using multi-objective self-adaptive differential evolution algorithm, Renewable energy, 121, 400-411, 2018.

[23] Bacha, B., Ghodbane, H., Dahmani, H., Betka, A., Toumi, A., & Chouder, A., Optimal sizing of a hybrid microgrid system using solar, wind, diesel, and battery energy storage to alleviate energy poverty in a rural area of Biskra, Algeria. Journal of Energy Storage, 84, 110651, 2024.

[24] Kaysal, K., Hocaoğlu, F., & Kaysal, A. Design and Experimental Implementation of Passive Battery Management Systems Using ARM-Based Microprocessors. Gazi University Journal of Science Part C: Design and Technology, 9 (1), 26-39, 2021.

[25] Kothakotla, V., & Kumar, B. Analysis and design of robust PID controller for grid voltage control of islanded microgrid using genetic algorithm. In 2021 5th International Conference on Intelligent Computing and Control Systems (ICICCS) pp. 719-726, 2021.

[26] Kamel, H. A. Laboratuarda gerçek zamanda klasik PID kontrolörlerin matlab simulink uygulamasının PLC uygulaması ile karşılaştırılması (Doctoral dissertation, Yüksek Lisans Tezi, İstanbul Demirel Üniversitesi Fen Bilimleri Enstitüsü, İstanbul, 44-49), 2016.

[27] Lee, C. C. Fuzzy logic in control systems: fuzzy logic controller. I. IEEE Transactions on systems, man, and cybernetics, 20(2), 404-418, 1990.

[28] Bai, Y., & Wang, D. Fundamentals of fuzzy logic control—fuzzy sets, fuzzy rules and defuzzifications. Advanced fuzzy logic technologies in industrial applications, 17-36, 2006.

Forecasting Seasonal Energy Production with K-Nearest Neighbours Regression Method

Abdulkadir Eren[1] Hayriye Sarısoy[1] Kübra Kaysal[2]

[1]Department of Electirical Engineering, University of Afyon Kocatepe, Afyonkarahisar, Turkey

[2]Department of Electrical and Electronics Engineering, University of Afyon Kocatepe, Afyonkarahisar, Turkey

abdulkadir0436@gmail.com hayriyesarisoy@gmail.com kkaysal@aku.edu.tr

Abstract

With the increasing demand for energy and the rapid depletion of fossil resources, accurate energy production has become even more important. In this study, seasonal forecasting was made using hourly energy production data between 2014 and 2023. The data is divided into one dependent and two independent variables. In estimation, k-nearest neighbour regression, one of the most commonly used machine learning methods, was used. The neighbourhood coefficient was tested using odd numbers between 3 and 11. It was observed that the best prediction results were obtained for K value 3. R-squared and RMSE performance metrics for four seasons were found and compared separately. The best forecasting result was calculated as R-squared 0.995 and RMSE 288.007 in the autumn season for k value 3. It was concluded that K-nearest neighbour regression gives successful results in seasonal forecasting.

***Keywords*:** K-nearest neighbours, Energy production, Forecasting, Machine learning.

1. INTRODUCTION

Humanity's need for energy is directly related to the population growth rate. As we know, under normal conditions, population growth will not decrease, and therefore, electricity demand will be much higher in the future [1]. Most of the world's energy is derived from fossil resources such as oil, coal, and natural gas, known as non-renewable resources. The rapid depletion of fossil resources, their negative environmental effects, and the pollution of water resources during processing compel humanity to seek sustainable and renewable energy sources [2].

Production capacities of some energy resources vary depending on the seasons. In spring, Hydroelectric Power Plants (HEPPs) hold more water and can produce more electrical energy. During the summer months, evaporation increases due to the effect of hot weather; therefore, the production capacity of HEPPs decreases. Additionally, the amount of energy demanded varies depending on the seasons, with factors such as the use of cooling systems in summer and the revival of the tourism sector leading to an increase in energy demand [3]. Therefore, seasonal changes have significant effects on the supply-demand balance in energy production. It is crucial to maintain this balance with successful forecasting models.

Many studies have been conducted using prediction algorithms. According to literature studies, Sahoo et al. utilized K-nearest neighbours regression (KNN) and Light GBM algorithms for wind energy forecasting. The results of their studies showed that both algorithms yielded successful results [4]. In another study, Haque and colleagues predicted the energy consumption of an apartment using various machine learning models such as KNN and multiple linear regression. As a result, they recommended employing diverse machine-learning algorithms with more extensive data [5]. Johannesen and colleagues also utilized random forest regression, k-nearest neighbour regression, and linear regression algorithms to study the forecasting of electrical energy demand in urban areas. They observed that random forest regression provided more accurate results in forecasting short-term electrical energy, while they recommended using KNN regression for long-term predictions [6].

In this study, estimates were derived using hourly electricity production data from 2014 to 2023. The total production data was categorized into two main variables: fossil fuel resources and renewable energy resources. The K-nearest neighbour algorithm was employed with the acquired data, and the study observed the seasonal success of this algorithm in forecasting electricity production.

2. MATERIAL and METHOD

2.1. K-Nearest Neighbor Regression

The K-nearest neighbour (KNN) regression model stands out as one of the easiest to understand, most popular, and widely used forecasting methods among machine learning algorithms. This regression predicts a new object based on similar objects in the training set [7,8]. In the KNN algorithm, training data is recorded in a dataset known as the training set, which comprises data points containing the properties of each object. A new object is stored in a dataset referred to as the test set. The Euclidean distance is the most commonly used calculation method in the KNN regression model and is represented by Equation 1 [9].

$$d(xi, xj) = \sqrt{\sum_{k=1}^{p} (x_{ik} - x_{jk})^2} \tag{1}$$

In this equation, the p value represents the number of input features, the x_{ik} value represents the k input features for i observation and the x_{jk} value represents k features for j observations. After the distances are calculated, KNN regression determines the k neighbours with the closest distance.

2.2. PERFORMANCE METRICS

2.2.1. R-Square

R-squared error is a measure of fit that shows the total variation value of the regression line relative to the true value in the data. It is desired that the R-square value be close to 1. The R-squared formula is given in Equation 2.

$$R^2 = 1 - \frac{\sum_{i=1}^{n}(y_i - \hat{y}_i)^2}{\sum_{i=1}^{n}(y_i - \bar{y}_i)^2} \tag{2}$$

Here, n value is the number of samples, y value is the required value, $\hat{y}$ value is the forecasting value of the machine learning algorithm and $\bar{y}$ value is the average of y values. [10]

2.2.2. Root Mean Square Error (RMSE)

RMSE is a metric that shows the deviation between the data values obtained by the algorithm as a result of forecasting and the real values. The closer the RMSE value approaches zero, the lower the error rate of the algorithm. [11,12]. The RMSE value was calculated in Equation 3.

$$RMSE = \sqrt{\frac{1}{n}\sum(y_i - \hat{y}_i)^2} \tag{3}$$

Here, the n value is the number of data points, the y value is the actual value and the $\hat{y}$ value is the forecast value of the algorithm.

2.3. Data Collection and Preprocessing

The data preprocessing stage has an important position in data mining and machine learning applications. The processes performed at this stage are the process of cleaning the data by getting rid of errors, deficiencies and inconsistencies in the data. In this way, it is aimed to increase the model's success [13].

In this study, hourly electricity production data between 2014 and 2023 was obtained from EPİAŞ (Energy Markets Management Joint Stock Company). The data set used is given in Figure 1.

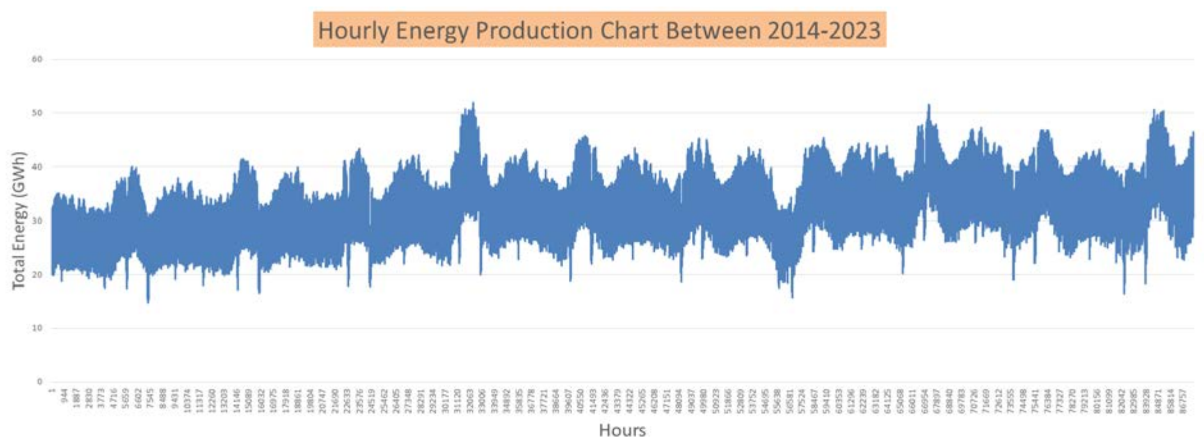

Şekil 1. Hourly Energy Production

The dataset consists of two variables: fossil and renewable energy sources. The total data was divided into seasons to observe the algorithm's seasonal success. For each season, 80%

of the data set is divided as training data and 20% as test data. The k neighbourhood coefficient chosen in the estimation was tested with odd numbers between 3-11 for each season. Normalization was performed on the data to make the forecasting more accurate. The normalization formula is given in Equation 4 [14].

$$x_{new} = \frac{x - x_{min}}{x_{max} - x_{min}} \tag{4}$$

Here, x_{new} value shows the value obtained as a result of normalization. The x value represents the real value of the number. While x_{min} value shows the smallest number of the data set, x_{max} value shows the largest number of the data set.

3. RESULTS

In this study, 86,745 hourly data points were analyzed across four seasons: winter, spring, summer, and autumn. Simultaneously, the data were categorized into one dependent variable, named "Total," representing hourly energy production data, and two independent variables: "Fossil resources" and "RES." Fossil resources consist of methane, brown coal, foreign coal, and heating oil. Renewable energy sources (RES) include dammed, river, wind, solar, geothermal, biomass, and waste heat.

The entire dataset was partitioned into seasons, and the efficacy of k-nearest neighbour regression was assessed seasonally. A total of 69,396 data points were used as training data, while 17,349 were utilized as test data. The selection of the k neighbourhood coefficient at the optimum value is a crucial criterion for forecasting. To determine this, the algorithm was tested with odd numbers between k values of 3 to 11, revealing more accurate results for k value 3. The forecast results, categorized by seasons, are illustrated in Figure 2(a-d).

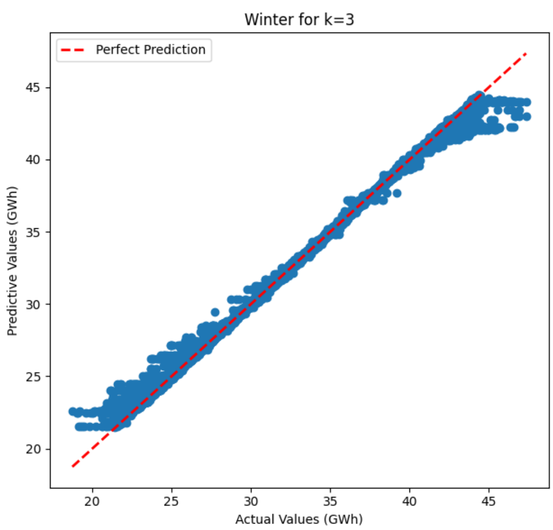

Şekil 2.a Winter prediction performance

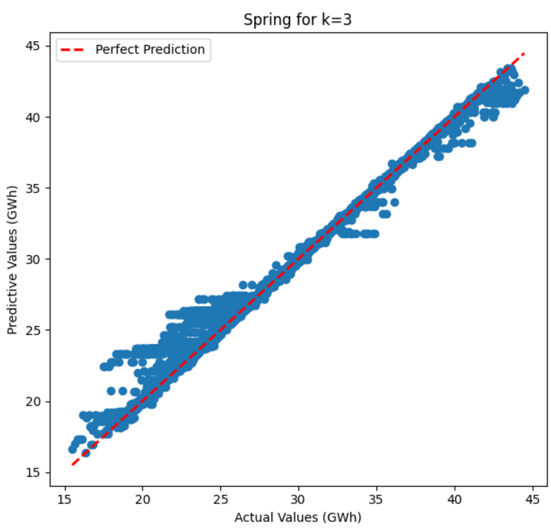

Şekil 2.b Spring prediction performance

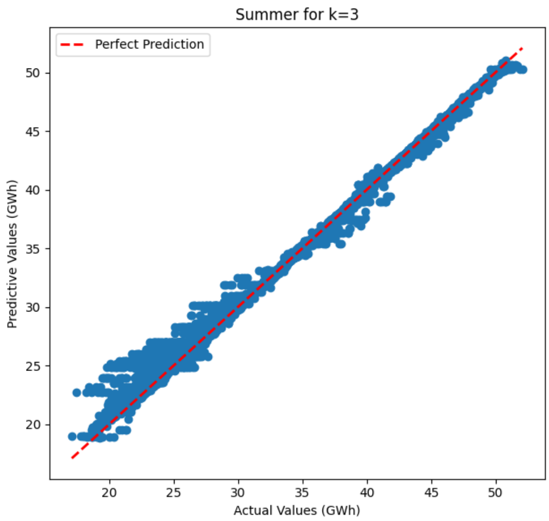

Şekil 2.c Summer prediction performance

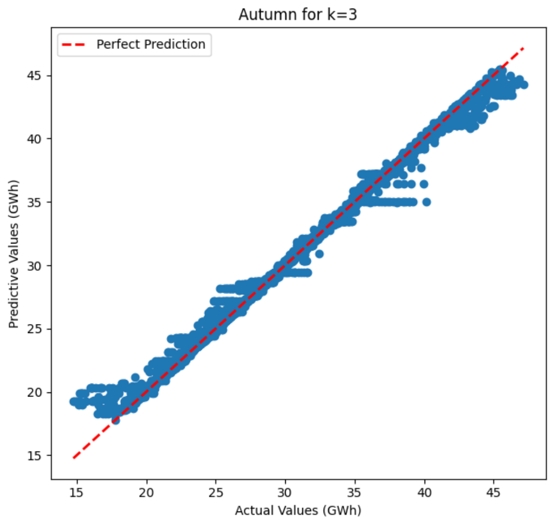

Şekil 2.d Autumn prediction performance

R-square and RMSE values found according to the K-nearest neighbor algorithm are given in Table 1.

Tablo 1. Performance metrics results

SEASONS		***R^2***	***RMSE(GWh)***
Winter	k=3	0,995	294,32
	k=5	0.995	306,64
	k=7	0.994	320,17
	k=9	0.994	330,70
	k=11	0.994	340,66
Spring	k=3	0,984	473,06
	k=5	0,982	491,65
	k=7	0,981	511,22
	k=9	0,980	523,35
	k=11	0,979	535,34
Summer	k=3	0,992	421,20
	k=5	0,992	427,97
	k=7	0,992	435,74
	k=9	0,991	443,97
	k=11	0,991	451,74
Autumn	**k=3**	**0,995**	**288,00**
	k=5	0,995	296,23
	k=7	0,995	299,56
	k=9	0,995	303,86
	k=11	0,995	309,84

Considering Figure 2(a-d) and Table 1, it was observed that the most successful results were obtained in the autumn season and neighbourhood value k = 3 for the k-nearest neighbour regression in seasonal, hourly energy production. Additionally, it has been observed that the error rate increases as the k value increases for this data set.

4. DISCUSSION

In this study, the results indicate that k-nearest neighbour regression has proven effective in handling high-volume data and seasonal forecasting. However, it was observed that K-nearest neighbour regression may exhibit overlearning issues in multivariate data. The features in the dataset were grouped into two categories: fossil resources (including natural gas, lignite, imported coal, fuel oil, asphaltite coal, and hard coal) and RES (comprising dammed, river, wind, solar, geothermal, biomass, and waste heat). This categorization aimed to prevent overlearning problems.

The overlearning problem typically arises when the number of independent variables is three or more. Therefore, it is advisable not to exceed two independent variables for this study. Subsequent research should consider making comparisons for seasonal forecasting using alternative machine learning methods.

REFERENCES

[1] El Kafazi, I., Bannari, R., Abouabdellah, A., Aboutafail, M. O., & Guerrero, J. M. Energy production: a comparison of forecasting methods using the polynomial curve fitting and linear regression. In 2017 International Renewable and Sustainable Energy Conference, pp. 1-5, IEEE, 2017.

[2] Jahanshahi, A., Jahanianfard, D., Mostafaie, A. and Kamali, M. An Auto Regressive Integrated Moving Average (Arıma) Model for prediction of energy consumption by household sector in Euro area. AIMS Energy, 7(2), 2019.

[3] Elma, I. and Yılmaz, O. Güneydoğu Anadolu bölgesi gerilim çökme problemlerinin değerlendirilmesi. Elektrik-Elektronik ve Bilgisayar Mühendisliği Sempozyumu, 29, 2012.

[4] Pattanaik, S. S., Sahoo, A. K. and Panda, R. A Comparative Analysis of KNN and Light GBM Algorithms for Wind Energy Forecasting. In 2023 1st International Conference on Circuits, Power and Intelligent Systems, pp. 1-4., IEEE, 2023.

[5] Haque, H., Chowdhury, A. K., Khan, M. N. R. and Razzak, M. A. Demand analysis of energy consumption in a residential apartment using machine learning. In 2021 IEEE International IOT, Electronics and Mechatronics Conference, pp. 1-6., IEEE, 2021.

[6] Johannesen, N. J., Kolhe, M., and Goodwin, M. Relative evaluation of regression tools for urban area electrical energy demand forecasting. Journal of cleaner production, 218, 555-564, 2019.

[7] Naghibi, S. A. and Dashtpagerdi, M. M. Evaluation of four supervised learning methods for groundwater spring potential mapping in Khalkhal region (Iran) using GIS-based features. Hydrogeology journal, 25(1), 169, 2017.

[8] Kılınç, D., Borandağ, E., Yücalar, F., Tunali, V., Şimşek, M., and Özçift, A. KNN algoritması ve r dili ile metin madenciliği kullanılarak bilimsel makale tasnifi. Marmara Fen Bilimleri Dergisi, 28(3), 89-94, 2016.

[9] Türkoğlu, M. and Hanbay, D. Apricot Disease Identification Based On Attributes Obtained From Deep Learning Algorithms. International Conference On Artificial Intelligence And Data Processing, Malatya, Turkey, 2018.

[10] Hacıbeyoglu, M., Çelik, M. and Çiçek, Ö. E. K En Yakın Komşu Algoritması ile Binalarda Enerji Verimliliği Tahmini. Necmettin Erbakan Üniversitesi Fen ve Mühendislik Bilimleri Dergisi, 5(2), 28-37, 2023.

[11] Gezmez, K. Ç. Bir İlin Elektrik Tüketim Verilerinin Makine Öğrenmesi Yöntemleri İle Analizi (Master's Thesis, Başkent Üniversitesi Fen Bilimler Enstitüsü), 2023.

[12] Kaysal, A., Köroglu, S., Oguz, Y. and Kaysal, K. Artificial Neural Networks and Adaptive Neuro-Fuzzy Inference Systems Approaches to Forecast the Electricity Data for Load Demand, an Analysis of Dinar District Case. In 2018 2nd International Symposium on Multidisciplinary Studies and Innovative Technologies, pp. 1-6, IEEE, 2018.

[13] Demirtaş, M., Akkoyun, N., Akkoyun, E. and Çetinbaş, İ. The probabilistic prediction of solar energy power production based on time in smart grids. Gazi University Journal of Science Part C: Design and Technology, 7(2), 411-424, 2019.

[14] Yavuz, S. and Deveci, M. İstatiksel normalizasyon tekniklerinin yapay sinir ağin performansina etkisi. Erciyes Üniversitesi İktisadi ve İdari Bilimler Fakültesi Dergisi, (40), 167-187, 2012.

IMPROVING α-PARAMETER NEW ITERATIVE METHOD WITH DANDELION OPTIMIZER FOR SOLVING PARTIAL DIFFERENTIAL EQUATIONS OF FRACTAL ORDER

Mustafa Raed Najeeb[1, a] **Omar Saber Qasim**[2, b]

[1,2] Department of Mathematics, College of Computer Sciences and Mathematics, University of Mosul, Mosul, Iraq.

[a] mostafa.csp115@student.uomosul.edu.iq [b] omar.saber@uomosul.edu.iq

Abstract

In this paper, the α-Parameter New Iterative Method (α-PNIM) with approximate analytical solutions is used to solve Partial Differential Equations of Fractal Order (F-PDEs), which arise from the development of the New Iterative Method (NIM), by introducing a linear Combination to the final formulation of NIM, this linear combination works with parameter α, which works to synthesize solutions and adjust them for the exact solution. Additionally, we seek to enhance the effectiveness of α-PDTM by incorporating the Dandelion Optimizer (DO). The DO plays a crucial role in optimizing the parameter α, ensuring its adjustment and modification to secure the most favorable value, this improvement leads to a more accurate approximation compared to traditional methods of choosing the α value. The proposed method, referred to as (α^{DO}-PNIM), demonstrates a reliable and efficient solution without any discrimination or restrictive assumptions by calculating Maximum Absolute Error (MAE) and Mean Square Errors (MSE) for a set of examples of Linear and Non-Linear F-PDEs that will be solve.

Keywords: α -Parameter New Iterative Method; New Iterative Method; Dandelion Optimizer; Partial Differential Equations; Meta Heuristic.

1.INTRODUCTION

Recently, interest in F-PDEs has increased with their wide applications in various scientific fields and their representation of many phenomena. It is generally difficult to find a universal method that provides exact solutions for all partial differential equations, as only a limited subset can be treated effectively by direct methods. As a result, approximate methods have become prevalent, yielding results that are often considered acceptable and manageable., such as the variable iteration method (VIM) [1], Homotopy Analysis Method (HAM) [2],, New Iterative Method (NIM), and others.

This paper is organized as follows for the remaining sections: In Section 2, he iterative NIM method is explained. Section 3, General framework of α-PNIM conditional on the parameter α. Section 4, provides an in-depth explanation of the smart DO algorithm. The section 5 also explains Some important definitions that will be used in this research, all results obtained in this study are covered in Section 6 Finally, in Section 7, the most important general conclusions are drawn.

2. NEW UTERATIVE METHOD (NIM)

In 2006, Daftardar and Jafari proposed a New Iterative Method namely (NIM) or (DJM) [3, 4]. The NIM used by many researchers for solving many problem such as linear and nonlinear ordinary and partial differential equations, algebraic equations [5], and used in various problems such as linear and nonlinear wave diffusion equations[6], and many other problems. In NIM the solution is obtained by successive approximations that converge to the exact solution (if one exists). for a specific problem. The main goal of this research is to obtain the analytical solution that is very close to the exact solution.

2.1. BASIC IDEA OF NIM

Consider the following general functional equation

$$u(x,t) = N(u) + f(x,t), x \in [a,b] \tag{1}$$

Where N is known as the Non-Linear operator and f is known function. The goal is to obtain a solution to equation (1), which will be in the form of a set of iterations of the following form [7]

$$u(x) = \sum_{i=0}^{\infty} u_i(x,t) \tag{2}$$

The nonlinear operator N can be decomposed as

$$N\left(\sum_{i=0}^{\infty} u_i\right) = N(u_0) + \sum_{i=1}^{\infty} \left(N\left(\sum_{j=0}^{\infty} u_j\right) - N\left(\sum_{j=0}^{\infty} u_j\right)\right) \tag{3}$$

From the above equations (2) and (3), we get

$$\sum_{i=0}^{\infty} u_i = f(x,t) + N(u_0) + \sum_{i=1}^{\infty} \left(N\left(\sum_{j=0}^{\infty} u_j\right) - N\left(\sum_{j=0}^{\infty} u_j\right)\right) \tag{4}$$

The frequencies are determined by the following formula

$$u_0(x,t) = f(x,t) \tag{5}$$

$$u_1(x,t) = N\big(u_0(x,t)\big) \tag{6}$$

$$u_2(x,t) = N\big(u_0(x,t) + u_1(x,t)\big) - N\big(u_0(x,t)\big) \tag{7}$$

$$\vdots$$

$$u_{n+1}(x,t) = N\big(u_0(x,t) + \cdots + u_n(x,t)\big) - N\big(u_0(x,t) + \cdots + u_{n-1}(x,t)\big), n = 1,2,3 \ldots \tag{8}$$

Then

$$\big(u_0(x,t) + \cdots + u_{n+1}(x,t)\big) = N\big(u_0(x,t) + \cdots + u_n(x,t)\big), n = 1,2,3 \ldots \tag{9}$$

$$u(x,t) = \sum_{i=0}^{\infty} u_i(x,t) = f(x,t) + N\left(\sum_{i=0}^{\infty} u_i(x,t)\right) \tag{10}$$

3. THE GENERAL FRAMEWORDK OF α-PNIM

In this part of this paper, we will talk about developing NIM and obtaining the proposed method α-PNIM. A new term has been added to the final formulation of NIM, called linear combination, as:

$$u(x,t) = \sum_{i=0}^{\infty} u_i(x,t)(x - x_\alpha)^i \tag{11}$$

where

$$x_\alpha = a\alpha + (1-b)\alpha \tag{12}$$

As shown in the equations above, the linear Combination $\boldsymbol{x_\alpha}$ is in terms of the parameter α, and that a and b represent the interval to which the differential equation belongs. the parameter α works to synthesize the final approximate solution of NIM and adjust it relative to the exact solution. Thus, we obtain a lower amount of Error for the proposed method compared to NIM, as shown in the examples that will be solved.

4. DANDELION OPTIMIZER (DO)

4.1. BASIC PRINCIPLES

The DO algorithm presented by the scientist Shiji Zhao[8] is considered one of the famous algorithms that outperform many other algorithms in terms of the quality of solutions and speed of convergence [9]. DO is classified as a Meta-Heuristic algorithm [10] that continuously works to find a solution based on Exploration and Exploitation [11], Consideration must be given to two crucial factors. An algorithm can become challenging to solve with excessive exploration, and prioritizing exploitation may result in the convergence of solutions, the DO algorithm is among those inspired by dandelion seeds, which disperse over long distances with the aid of wind. The growth process of dandelion dandelion is segmented into three stages. Planting dandelion seeds is divided into several stages. The first stage involves an upward movement, where the wind helps the seeds spread to remote areas during sunny conditions with wind or drift in cloudy conditions with rain. Then the seeds move to the landing stage, where they gradually decrease after the seed reaches a certain height. Finally, In the next stage specifically, and the seeds settle somewhere after being affected by weather and wind conditions, starting a new generation of dandelion plants, Based on these three stages, the dandelion optimization algorithm updates individuals' positions. In the bull phase, there are instances of exploration and exploitation, influenced by randomly generated numbers. Furthermore, the adjuster of length is employed to control the fluctuation In seed positions. Dandelion Optimizer depends on two primary parameters, seed dispersion radius η and local search Coefficient ξ. These parameters change over time continuously in each iteration. Specifically, η determines the global search step length, while ξ dictates the local search step length [9].

4.2. INITIALIZATION STAGE

A population matrix of the identified seed set with N individuals is defined in space d. We represent any seed with the symbol $X_v = [X_i^1, X_i^2, \dots X_i^d]$ wher $v = 1,2,3, \dots$ to initialize the population use

$$X_i = lb + r_v(ub - lb) \tag{13}$$

Let r_v denote a randomly generated number according to a normal distribution within the interval $(0,1)$. Here, the highest value of the decision space will be represented by the symbol ub, the lowest value of the decision space will be represented by the symbol lb, N indicates the number of least rows in the population matrix, and d represents the columns of the population matrix. In subsequent sections, these parameters remain with the same symbols.[9].

4.3. UPWARD STAGE

In the bottom-up phase, we determine what we will do (global search or local exploitation) based on r, which is a random number with a normal distribution

- If $r < 1.5$ if the cut is clear, the following equation is used to determine the new seed location:

$$X_{t+1} = X_t + \eta\, v_x v_y\, ln(Y)\,(X_s - X_t) \quad (14)$$

Where X_s is the initial seed position, v_x acd v_y Represents the two wind directions (horizontal and vertical), η represents the seed dispersal radius, and $ln(Y)$ represents the lognormal distribution with mean 0 and variance 1.

$$X_s = rand(1,d)(ub - lb) + lb \quad (15)$$

$$\eta = rand(\,)(\tfrac{1}{T^2}t^2 - \tfrac{2}{T}t + 1) \quad (16)$$

$$v_x = r\cos(\theta) \quad (17)$$

$$v_y = r\sin(\theta) \quad (18)$$

Where $r = \frac{1}{e^{\theta}}$, $\theta \in [-\pi, \pi]$, T represents the total number of iterations, and t is the current iteration.

- If $r \geq 1.5$, it indicates rainy weather, then the next location of the seed is determined

$$X_{t+1} = X_t\, \xi\, 1 \quad (19)$$

Where the local search factor ξ appears in the formula

$$\xi = 1 - rand(\,)\, q \quad (20)$$

$$q = \frac{1}{T^2-2T-1}t^2 - \frac{2}{T^2-2T-1}t + 1 + \frac{1}{T^2-2T-1} \quad (21)$$

4.4. DESCENDING STAGE

The algorithm descends when it reaches a certain level of height, and through Brownian motion the seeds are in their position determined by the following equation. [9].

$$X_{t+1} = X_t - \eta\, \beta_t (X_{meant} - \eta\, \beta_t X_t) \quad (22)$$

$$X_{meant} = \frac{1}{n}\sum_{i=1}^{n} X_i \quad (23)$$

4.5. LAND STAGE Stage

In the landing stage, the position of the seeds is as shown in the following formula

$$X_{t+1} = X_{elite} + leve(\lambda)\, \eta\, (X_{elite} - X_t\, \tfrac{2t}{T}) \quad (24)$$

$$leve(\lambda) = \frac{s(w \times \sigma)}{|t|^{\frac{1}{\beta}}} \quad (25)$$

$$\sigma = \left(\Gamma(\,1+\beta)\, sin\left(\frac{\pi\beta}{2}\right)\right)\,(\Gamma\left(\frac{1+\beta}{2}\right)\beta\, 2^{\left(\frac{\beta-1}{2}\right)}\,) \quad (26)$$

Where $s = 0.01$, $\beta = 1.5$, Where the gamma function is defined by the symbol Γ [9].

5. GENERAL CONCEPTS

We will discuss some important definitions that we will use in this research.

5.1. DEFINITION (1)

The Maximum Absolute Errors (MAE) is defined by

$$\|exact\ solution - T_i(y)\|_\infty = \max_{a \le x \le b}\{|W_{Exact}(y) - T_i(y)|\} \tag{27}$$

where $T_i(y)$ is the approximate solution [12].

5.2. DEFINITION (2)

The Mean Square Errors (MSE) is defined by

$$MSE = \frac{1}{n}\ exact\ solution - T_i(y))^2 \tag{28}$$

where $T_i(y)$ is the approximate solution [13].

5.2. RIEMANN-LIOUVILLE FRACTIONAL FOR INTEGRAL

The Riemann-Liouville0fractional0integral properties [14]

1- $J^k z(t) = \frac{1}{\Gamma(k)}\int_0^t (t-x)^{k-1} z(x)dx\ ,t > 0$ (29)

2- $J^0 z\ (t) = z(t)$ (30)

3- For $z(t) \in C_\mu, \mu \ge -1, \alpha, \beta \ge 0, \gamma \ge -1$ Properties of the operator J^k (31)

4- $J^k\ J^\beta z(t) = \ J^\beta\ J^k\ z(t)$ (32)

5- $J^k\ t^\gamma = \frac{\Gamma(\gamma+1)}{\Gamma(k+\gamma+1)} t^{k+\gamma}$ (33)

5.3. DEVRATIVE CAPUTO FRACTIONAL

The Devative Caputo Fractional properties [14]

1- $D_t^k z(t) = \ J^{n-k} D^n z(t) = \frac{1}{\Gamma(n-k)}\int_0^t (t-x)^{n-k-1} z^{(n)}(x)dx.$ (34)

2- For $z(t) \in C_\mu^n, \mu \ge -1, k, \beta \ge 0, \gamma \ge -1, n-1 < k \le n, n \in \mathbb{N}$ Properties of the operator

3- $D_t^k D_t^k\ D_t^\beta z(t) = \ D_t^{k+\beta} z(t) = \ D_t^\beta\ D_t^k\ z(t)$ (35)

4- $D_t^k\ t^\gamma = \frac{\Gamma(1+\gamma)}{\Gamma(1+\gamma-k)}\ t^{\gamma-k}, t > 0$ (36)

6. THE PROPOSED METHOD α^{DO}-PNIM

The proposed method α^{DO}-PNIM finds a set of approximate solutions for NIM in terms of linear Combination parameter α that improves the results. The intelligent DO algorithm will also be used to find the best value for the parameter α based on the fitness function resulting from the approximate solution of α-PNIM. We will solve a set of examples of F-PDEs using α-PNIM and compare the results with the exact solution by calculating the MSE and MAE.

6.1. EXAMPLE [15]

Consider the Linear time-fractional partial diffusion equation, with the initial conditions

$$\frac{\partial^\tau}{\partial t^\tau} y(x,t) = \frac{\partial^2}{\partial x^2} y(x,t), \quad x,t \in [0,1]\,, 0 < \tau \le 1 \tag{37}$$

$$y(x,0) = sin\,(x) \tag{38}$$

And the exact solution when

$$y(x,t) = \left(1 - \frac{t^{3-2\tau}}{\Gamma(4-2\tau)} + \frac{3t^{2-\tau}}{\Gamma(3-\tau)} - \frac{2t^{3-\tau}}{\Gamma(4-\tau)} - 3t + \frac{3t^2}{2} - \frac{t^3}{6}\right) sin\,(x) \tag{39}$$

Integration from both sides of equation (37) by using Riemann-Liouville Fractional For Integral

$$y(x,t) = \int_0^t 0\,dt + J^\tau \left(\frac{\partial^2 y(x,t)}{\partial x^2}\right) \tag{40}$$

By using the initial conditions, we get the Initial iteration. From definition of NIM get the others iterations

$$y_0(x,t) = sin\,(x)$$

$$y_1(x,t) = N\big(y_0(x,t)\big) = -sin(x)\left(\frac{\Gamma(1+1)t^{(\tau+1)}}{\Gamma(\tau+1+1)}\right)$$

$$\begin{aligned} y_2(x,t) &= N\big(y_0(x,t) + y_1(x,t)\big) - N\big(y_0(x,t)\big) \\ &= \left(-\left(\frac{\Gamma(1+1)t^{(\tau+1)}}{\Gamma(\tau+1+1)}\right) + \frac{1}{2}\left(\frac{\Gamma(2+1)t^{(\tau+2)}}{\Gamma(\tau+2+1)}\right)\right) sin(x) + \left(\left(\frac{\Gamma(1+1)t^{(\tau+1)}}{\Gamma(\tau+1+1)}\right) sin(x)\right) \end{aligned}$$

$$\begin{aligned} y_3(x,t) &= N\big(y_0(x,t) + y_1(x,t) + y_2(x,t)\big) - N\big(y_0(x,t) + y_1(x,t)\big) \\ &= \left(-\left(\frac{\Gamma(1+1)t^{(\tau+1)}}{\Gamma(\tau+1+1)}\right) + \frac{1}{2}\left(\frac{\Gamma(2+1)t^{(\tau+2)}}{\Gamma(\tau+2+1)}\right) - \frac{1}{6}\left(\frac{\Gamma(3+1)t^{(\tau+3)}}{\Gamma(\tau+3+1)}\right)\right) sin(x) \\ &\quad - \left(-\left(\frac{\Gamma(1+1)t^{(\tau+1)}}{\Gamma(\tau+1+1)}\right) + \frac{1}{2}\left(\frac{\Gamma(2+1)t^{(\tau+2)}}{\Gamma(\tau+2+1)}\right)\right) sin(x) \end{aligned}$$

$$\begin{aligned} y_4(x,t) &= N\big(y_0(x,t) + y_1(x,t) + y_2(x,t) + y_3(x,t)\big) - N\big(y_0(x,t) + y_1(x,t) + y_2(x,t)\big) \\ &= \left(-\left(\frac{\Gamma(1+1)t^{(\tau+1)}}{\Gamma(\tau+1+1)}\right) + \frac{1}{2}\left(\frac{\Gamma(2+1)t^{(\tau+2)}}{\Gamma(\tau+2+1)}\right) - \frac{1}{6}\left(\frac{\Gamma(3+1)t^{(\tau+3)}}{\Gamma(\tau+3+1)}\right) + \frac{1}{24}\left(\frac{\Gamma(4+1)t^{(\tau+4)}}{\Gamma(\tau+4+1)}\right)\right) sin(x) \end{aligned}$$

$$-\left(-\left(\frac{\Gamma(1+1)t^{(\tau+1)}}{\Gamma(\tau+1+1)}\right) + \frac{1}{2}\left(\frac{\Gamma(2+1)t^{(\tau+2)}}{\Gamma(\tau+2+1)}\right)\right) sin(x) \left(-\left(\frac{\Gamma(1+1)t^{(\tau+1)}}{\Gamma(\tau+1+1)}\right) + \frac{1}{2}\left(\frac{\Gamma(2+1)t^{(\tau+2)}}{\Gamma(\tau+2+1)}\right) - \frac{1}{6}\left(\frac{\Gamma(3+1)t^{(\tau+3)}}{\Gamma(\tau+3+1)}\right)\right) sin(x)$$

$y_\alpha(x,t) = \sum_{m=0}^{4} y_m(x,t)(t-t_\alpha)^m$, Where $t_\alpha = a\alpha + (1-b)\alpha = 1-\alpha$

$$y_\alpha(x,y) = sin(x) - \frac{t^\tau sin(x)(t+\alpha)}{\Gamma(\tau+1)} + \left(\left(-\frac{t^\tau}{\Gamma(\tau+1)} + \frac{t^{(\tau+1)}}{\Gamma(\tau+2)}\right) sin(x) + \frac{t^\tau sin\,(x)}{\Gamma(\tau+1)}\right)(t+\alpha)^2 + \left(\left(-\frac{t^\tau}{\Gamma(\tau+1)} + \frac{t^{(\tau+1)}}{\Gamma(\tau+2)} - \frac{t^{(\tau+2)}}{\Gamma(\tau+3)}\right) sin(x) - \left(-\frac{t^\tau}{\Gamma(\tau+1)} + \frac{t^{(\tau+1)}}{\Gamma(\tau+2)}\right) sin(x)\right)(t+\alpha)^3 \tag{41}$$

Using the DO algorithm, we will calculate the best value of α for different values of order τ, Given that equation (41) is the fitness function for $y(x,t)$ after subtracting it from the exact solution, then we will obtain the final approximate solution of α^{DO}-PNIM, for which we will calculate the MSE and MAE when $t = 0.01$ and $x \in [0,1]$ and compared with values for α that were adopted randomly, as shown in Table (1) and Figure (1).

Table 1: Comparison MSE and MAE for NIM and α-PNIM

When $\tau = 1$	$\alpha^{0.025}$-PNIM	$\alpha^{0.25}$-PNIM	$\alpha^{0.5}$-PNIM	$\alpha^{DO=1.8009}$-PNIM
MSE	$8.0495E-5$	$7.5758E-5$	$6.0490E-5$	$1.9934E-7$
MAE	$1.9346E-2$	$1.7161E-2$	$1.4697E-2$	$6.2846E-3$
When $\tau = 0.75$	**$\alpha^{0.025}$-PNIM**	**$\alpha^{0.25}$-PNIM**	**$\alpha^{0.5}$-PNIM**	**$\alpha^{DO=1.5923}$-PNIM**
MSE	$6.0333E-4$	$5.5747E-4$	$4.1678E-4$	$1.5049E-7$
MAE	$5.4736E-2$	$4.7206E-2$	$3.8723E-2$	$6.9214E-3$
When $\tau = 0.5$	**$\alpha^{0.025}$-PNIM**	**$\alpha^{0.25}$-PNIM**	**$\alpha^{0.5}$-PNIM**	**$\alpha^{DO=1.2342}$-PNIM**
MSE	$3.2236E-3$	$2.8591E-3$	$1.8444E-3$	$1.1615E-9$
MAE	$1.3475E-1$	$1.1002E-1$	$7.5048E-2$	$6.1525E-4$
When $\tau = 0.25$	**$\alpha^{0.025}$-PNIM**	**$\alpha^{0.25}$-PNIM**	**$\alpha^{0.5}$-PNIM**	**$\alpha^{DO=1.0739}$-PNIM**
MSE	$2.1438E-2$	$1.8426E-2$	$1.0622E-2$	$1.8603E-11$
MAE	$3.1035E-1$	$2.8479E-1$	$1.9854E-1$	$1.9578E-5$

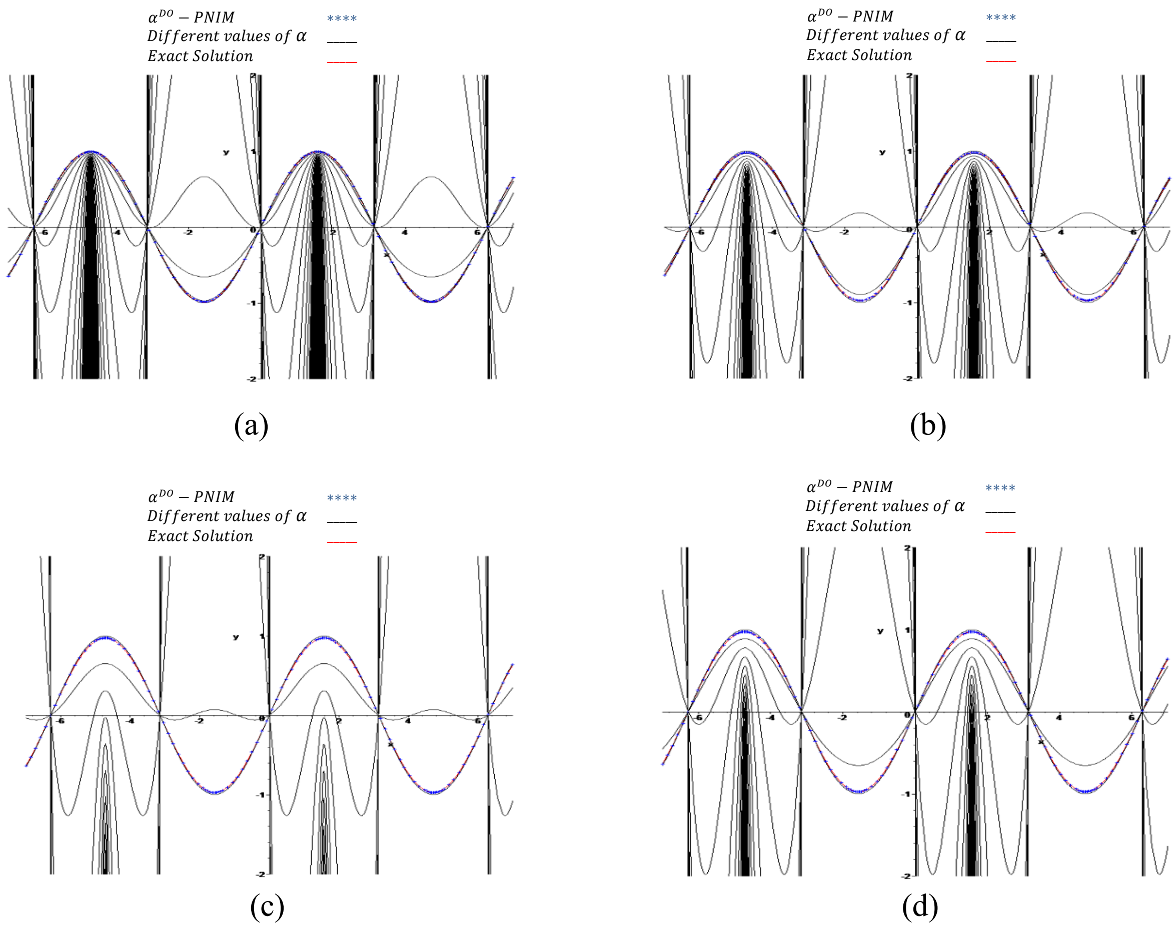

Figure 1: Shows the difference between Exact solution, α^{DO}-PNIM and different values of α, when τ =1 in (a),τ =0.75 in (b), τ =0.5 in (c), τ =0.25 in (d).

6.2. EXAMPLE [16]

Consider the following Non-Linear time-fractional equation, with the initial conditions

$$\frac{\partial^{\tau} y(x,t)}{\partial t^{\tau}} + y(x,t)y_x(x,t) = x + xt^2\,, \quad x,t \in [0,1] \quad ,0 < \tau \leq 1 \tag{42}$$

$$y(x,0) = 0 \tag{43}$$

And the exact solution

$$y(x,t) = xt \tag{44}$$

Form equation (42) we have

$$\frac{\partial^{\tau} y(x,t)}{\partial t^{\tau}} = -y(x,t)y_x(x,t) + x + xt^2 \tag{45}$$

Integration from both sides of equation (32) by using Riemann-Liouville Fractional For Integral

$$y(x,t) = J^{\tau}(x + xt^2) + J^{\tau}\big(-y(x,t)y_x(x,t)\big) \tag{46}$$

Where $f(x,t) = x + xt^2$ and $N\big(y(x,t)\big) = y(x,t)y_x(x,t)$

Then we get the initial iteration

$$y_0(x,t) = x\frac{\Gamma(0+1)t^{(k+0)}}{\Gamma(k+0+1)} + x\frac{\Gamma(2+1)t^{(k+2)}}{\Gamma(k+2+1)} = x\left(t + \frac{1}{3}t^3\right)$$

$$y_1(x,t) = N\big(y_0(x,t)\big)$$

$$= x\left(\frac{\Gamma(0+1)t^{(k+0)}}{\Gamma(k+0+1)} + \frac{1}{3}\frac{\Gamma(3+1)t^{(k+3)}}{\Gamma(k+3+1)}\right) = \left(\frac{1}{2}t^2 + \frac{1}{12}t^4\right)^2 x$$

$$y_2(x,t) = N\big(y_0(x,t) + y_1(x,t)\big) - N\big(y_0(x,t)\big)$$

$$= \left(\left(\frac{\Gamma(1+1)t^{(k+1)}}{\Gamma(k+1+1)} + \frac{1}{3}\frac{\Gamma(3+1)t^{(k+3)}}{\Gamma(k+3+1)} + \left(\frac{1}{2}\frac{\Gamma(2+1)t^{(k+2)}}{\Gamma(k+2+1)} + \frac{1}{12}\frac{\Gamma(4+1)t^{(k+4)}}{\Gamma(k+4+1)}\right)^2\right)\right)^2 x - \left(t_1 + \frac{1}{3}\frac{\Gamma(3+1)t^{(k+3)}}{\Gamma(k+3+1)}\right)^2 x$$

$$y_3(x,t) = N\big(y_0(x,t) + y_1(x,t) + y_2(x,t)\big) - N\big(y_0(x,t) + y_1(x,t)\big)$$

$$= \left(\frac{\Gamma(1+1)t^{(k+1)}}{\Gamma(k+1+1)} + \frac{\Gamma(3+1)t^{(k+3)}}{3\Gamma(k+3+1)} + \left(\frac{\Gamma(2+1)t^{(k+2)}}{2\Gamma(k+2+1)} + \frac{\Gamma(4+1)t^{(k+4)}}{12\,\Gamma(k+4+1)} + \left(\frac{\Gamma(3+1)t^{(k+3)}}{6\,\Gamma(k+3+1)} + \frac{\Gamma(5+1)t^{(k+5)}}{60\,\Gamma(k+5+1)}\right)^2\right)^2\right)$$

$$\left(\frac{\Gamma(0+1)t^{(k+0)}}{\Gamma(k+0+1)} + \frac{\Gamma(3+1)t^{(k+3)}}{3\,\Gamma(k+3+1)} + \left(\frac{\Gamma(2+1)t^{(k+2)}}{2\,\Gamma(k+2+1)} + \frac{\Gamma(4+1)t^{(k+4)}}{12\,\Gamma(k+4+1)}\right)^2\right)x$$

$$-\left(\frac{\Gamma(1+1)t^{(k+1)}}{\Gamma(k+1+1)} + \frac{\Gamma(3+1)t^{(k+3)}}{3\,\Gamma(k+3+1)} + \left(\frac{\Gamma(2+1)t^{(k+2)}}{2\,\Gamma(k+2+1)} + \frac{\Gamma(4+1)t^{(k+4)}}{12\,\Gamma(k+4+1)}\right)^2\right)^2 x$$

The solution by using α^{DO}-PNIM will be

$$y_\alpha(x,t) = \sum_{m=0}^{4} y_m(x,t)(t - t_\alpha)^m, \text{ Where } t_\alpha = a\alpha + (1-b)\alpha = 1 - \alpha$$

$$y_\alpha(x,t) = \frac{xt^{\tau}}{\Gamma(\tau+1)} + \frac{2xt^{(\tau+2)}}{\Gamma(\tau+3)} + \left(\frac{t^{(\tau+1)}}{\Gamma(\tau+2)} + \frac{2t^{(\tau+3)}}{\Gamma(\tau+4)}\right)^2 x(t+\alpha) + \left(\left(\frac{t^{(\tau+1)}}{\Gamma(\tau+2)} + \frac{2t^{(\tau+3)}}{\Gamma(\tau+4)} + \left(\frac{t^{(\tau+2)}}{\Gamma(\tau+3)} + \frac{2t^{(\tau+4)}}{\Gamma(\tau+5)}\right)^2\right)x - \left(\frac{t^{(\tau+1)}}{\Gamma(\tau+2)} + \frac{2t^{(\tau+3)}}{\Gamma(\tau+4)}\right)^2 x\right)(t+\alpha)^2 + \left(\frac{t^{(\tau+2)}}{\Gamma(\tau+3)} + \frac{2t^{(\tau+4)}}{\Gamma(\tau+5)} + \left(\frac{t^{(\tau+3)}}{\Gamma(\tau+4)} + \frac{2t^{(\tau+5)}}{\Gamma(\tau+6)}\right)^2\right)\left(\frac{t^{\tau}}{\Gamma(\tau+1)} + \frac{2t^{(\tau+3)}}{\Gamma(\tau+4)} + \left(\frac{t^{(\tau+2)}}{\Gamma(\tau+3)} + \frac{2t^{(\tau+4)}}{\Gamma(\tau+5)}\right)^2\right)x\left(\frac{t^{(\tau+1)}}{\Gamma(\tau+2)} + \frac{2t^{(\tau+3)}}{\Gamma(\tau+4)} + \left(\frac{t^{(\tau+1)}}{\Gamma(\tau+2)} + \frac{2t^{(\tau+3)}}{\Gamma(\tau+4)} + \left(\frac{t^{(\tau+2)}}{\Gamma(\tau+3)} + \frac{2t^{(\tau+4)}}{\Gamma(\tau+5)}\right)^2\right)x\right)(t+\alpha)^3 + \cdots \tag{47}$$

Using the DO algorithm, we will calculate the best value of α for different values of order τ, Given that equation (47) is the fitness function for $y(x,t)$ after subtracting it from the exact solution, then we will obtain the final approximate solution of α^{DO}-PNIM, for which we will calculate the MSE and MAE when $t = 0.01$ and $x \in [0,1]$ and compared with values for α that were adopted randomly, as shown in Table (2) and Figure (2).

Table 2: Comparison MSE and MAE for NIM and α-PNIM

When $\tau = 1$	$\alpha^{0.025}$-PNIM	$\alpha^{0.25}$-PNIM	$\alpha^{0.5}$-PNIM	$\alpha^{DO=2.2908}$-PNIM
MSE	$1.0578E-13$	$1.4076E-16$	$2.0966E-14$	$5.1153E-22$
MAE	$5.4975E-7$	$2.0054E-8$	$2.4475E-7$	$3.8230E-11$
When τ*=0.75*	$\alpha^{0.025}$*-PNIM*	$\alpha^{0.25}$*-PNIM*	$\alpha^{0.5}$*-PNIM*	$\alpha^{DO=-6.5232}$*-PNIM*
MSE	$2.0832E-4$	$2.0844E-4$	$2.0851E-4$	$1.0621E-13$
MAE	$2.4397E-2$	$2.4404E-2$	$2.4407E-2$	$5.5089E-7$
When τ*=0.5*	$\alpha^{0.025}$*-PNIM*	$\alpha^{0.25}$*-PNIM*	$\alpha^{0.5}$*-PNIM*	$\alpha^{DO=-4.6763}$*-PNIM*
MSE	$3.6911E-2$	$3.6975E-2$	$3.7008E-3$	$2.3098E-12$
MAE	$1.0269E-1$	$1.0278E-1$	$1.0282E-1$	$2.5689E-6$
When $\tau = 0.25$	$\alpha^{0.025}$-PNIM	$\alpha^{0.25}$-PNIM	$\alpha^{0.5}$-PNIM	$\alpha^{DO=-3.1009}$-PNIM
MSE	$3.9793E-2$	$4.0036E-2$	$4.0159E-2$	$8.3003E-11$
MAE	$3.3718E-1$	$3.3821E-1$	$3.3873E-1$	$1.5399E-5$

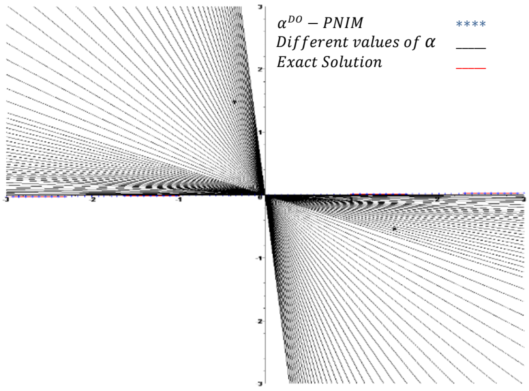

(a)

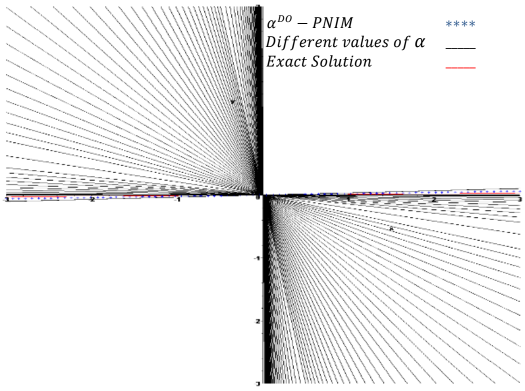

(b)

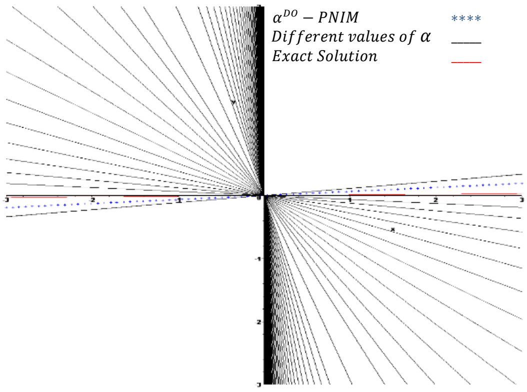

(c)

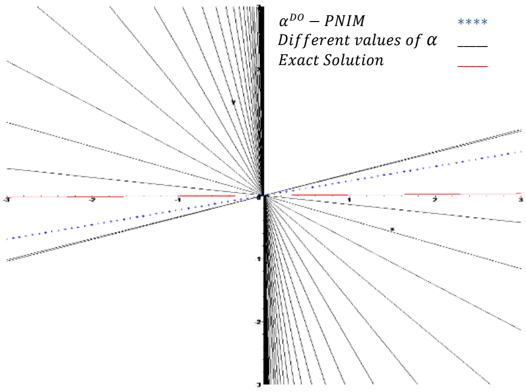

(d)

Figure 2: Shows the difference between exact solution, α^{DO}-PNIM and different values of α, when τ =1 in (a),τ =0.75 in (b), τ =0.5 in (c), τ =0.25 in (d).

6.3. EXAMPLE [17]

Consider the following Non-Linear FPDE

$$D_t^\tau u(x,t) = y_{xx}(x,t) + y(x,t)y_x(x,t)\,,\quad x,t \in [0,1]\quad ,0 < \tau \le 1 \tag{48}$$

With the initial conditions

$$y(x,0) = 2 - x \tag{49}$$

And the exact solution

$$y(x,t) = \frac{2-x}{1+t} \tag{50}$$

Integration from both sides of equation (48) by using Riemann-Liouville Fractional for Integral

$$y(x,t) = \int_0^t 0\,dt + J^\tau(y_{xx} + yy_x\,) \tag{51}$$

Where $f(x,t) = 0$ and $N\big(y(x,t)\big) = u_{xx} + uu_x$

By using the initial conditions, we get the Initial iteration

$$y_0(x,t) = 2 - x$$

From the definition of NIM we get the required iterations

$$y_1(x,t) = N\big(y_0(x,t)\big)$$
$$= (2-x)\frac{\Gamma(0+1)t^{(k+0)}}{\Gamma(k+0+1)}$$

$$y_2(x,t) = N\big(y_0(x,t) + y_1(x,t)\big) - N\big(y_0(x,t)\big)$$
$$= \left(\frac{1}{2} - \frac{x}{4}\right)\frac{\Gamma(4+1)t^{(k+4)}}{\Gamma(k+4+1)} + (2-x)\frac{\Gamma(2+1)t^{(k+2)}}{\Gamma(k+2+1)}$$

$$y_3(x,t) = N\big(y_0(x,t) + y_1(x,t) + y_2(x,t)\big) - N\big(y_0(x,t) + y_1(x,t)\big)$$
$$= \left(\frac{1}{2} - \frac{x}{4}\right)\frac{\Gamma(6+1)t^{(k+6)}}{30\Gamma(k+6+1)} + (2-x)\frac{\Gamma(4+1)t^{(k+4)}}{\Gamma(k+4+1)}\left(\frac{1}{7200} - \frac{1x}{14400}\right)\frac{\Gamma(12+1)t^{(k+12)}}{12\,\Gamma(k+12+1)} + \left(\frac{1}{360} - \frac{1x}{720}\right)t_{10}$$
$$+ \left(\frac{11}{360} - \frac{11x}{720}\right)\frac{\Gamma(8+1)t^{(k+8)}}{\Gamma(k+8+1)} + \left(\frac{1}{5} - \frac{1x}{10}\right)\frac{\Gamma(6+1)t^{(k+6)}}{\Gamma(k+6+1)} + \left(\frac{1}{3} - \frac{1x}{6}\right)\frac{\Gamma(4+1)t^{(k+4)}}{\Gamma(k+4+1)}$$

$$y_4(x,t) = N\big(y_0(x,t) + y_1(x,t) + y_2(x,t) + y_3(x,t)\big) - N\big(y_0(x,t) + y_1(x,t) + y_2(x,t)\big)$$
$$= -0.604540218010^{-5}(2-x)\left(\frac{1}{7200} - \frac{x}{14400}\right)\left(-\frac{1}{235872000} + \frac{x}{471744000}\right)t^{40.25} +$$
$$0.4184160989\left(-\left(\frac{1}{47520} - \frac{x}{95040}\right)\left(-\frac{1}{235872000} + \frac{x}{471744000}\right) + \frac{(2-x)\left(\frac{1}{7200} - \frac{x}{14400}\right)}{6227020800}\right)t^{32.25} + \cdots$$

The solution by using α^{DO}-PNIM will be

$$y_\alpha(x,t) = \sum_{m=0}^{4} y_m(x,t)(t-t_\alpha)^m,\quad \text{Where } t_\alpha = a\alpha + (1-b)\alpha = 1-\alpha$$

$$y_\alpha(x,t) = 2 - x + \frac{(2-x)t^\tau(t-1+\alpha)}{\Gamma(\tau+1)} + \left(\frac{24\left(\frac{1}{2}-\frac{x}{4}\right)t^{(\tau+4)}}{\Gamma(\tau+5)} + \frac{2(2-x)t^{(\tau+2)}}{\Gamma(\tau+3)}\right)(t-1+\alpha)^2 + \left(\frac{24\left(\frac{1}{2}-\frac{x}{4}\right)t^{(\tau+6)}}{\Gamma(\tau+7)} + \right.$$
$$\frac{958003200(2-x)t^{(\tau+4)}\left(\frac{1}{7200}-\frac{x}{14400}\right)t^{(\tau+12)}}{\Gamma(\tau+5)\Gamma(\tau+13)} + \frac{3628800\left(\frac{1}{360}-\frac{x}{720}\right)t^{(\tau+10)}}{\Gamma(\tau+11)} + \frac{40320\left(\frac{11}{360}-\frac{11x}{720}\right)t^{(\tau+8)}}{\Gamma(\tau+9)} +$$
$$\left.\frac{720\left(\frac{1}{5}-\frac{x}{10}\right)t^{(\tau+6)}}{\Gamma(\tau+7)} + \frac{24\left(\frac{1}{3}-\frac{x}{6}\right)t^{(\tau+4)}}{\Gamma(\tau+5)}\right)(t-1+\alpha)^3 + \cdots \tag{52}$$

Using the DO algorithm, we will calculate the best value of α for different values of order τ, Given that equation (52) is the fitness function for $y(x,t)$ after subtracting it from the exact solution, then we will obtain the final approximate solution of α^{DO}-PNIM, for which we will calculate the MSE and MAE when $t = 0.01$ and $x \in [0,1]$ and compared with values for α that were adopted randomly, as shown in Table (3) and Figure (3).

Table 2: Comparison MSE and MAE for NIM and α-PNIM

When $\tau = 1$	$\alpha^{0.025}$-PNIM	$\alpha^{0.25}$-PNIM	$\alpha^{0.5}$-PNIM	$\alpha^{DO=-0.00013168}$-PNIM
MSE	$1.4840E-7$	$1.4701E-5$	$5.8775E-5$	$1.0079E-21$
MAE	$5.0260E-4$	$5.0023E-3$	$1.0002E-2$	$8.8580E-11$
When $\tau = 0.75$	$\alpha^{0.025}$-PNIM	$\alpha^{0.25}$-PNIM	$\alpha^{0.5}$-PNIM	$\alpha^{DO=0.70224}$-PNIM
MSE	$1.2759E-3$	$5.6895E-4$	$1.1378E-4$	$2.9346E-15$
MAE	$2.3301E-2$	$1.5559E-2$	$1.3916E-2$	$7.0684E-8$
When $\tau = 0.5$	$\alpha^{0.025}$-PNIM	$\alpha^{0.25}$-PNIM	$\alpha^{0.5}$-PNIM	$\alpha^{DO=0.90225}$-PNIM
MSE	$2.3023E-2$	$1.2728E-2$	$4.8411E-3$	$5.6618E-13$
MAE	$1.9796E-1$	$1.4719E-1$	$9.0776E-2$	$9.8170E-7$
When $\tau = 0.25$	$\alpha^{0.025}$-PNIM	$\alpha^{0.25}$-PNIM	$\alpha^{0.5}$-PNIM	$\alpha^{DO=0.96162}$-PNIM
MSE	$2.5089E-1$	$1.4483E-1$	$6.0948E-2$	$1.7032E-13$
MAE	$6.5349E-1$	$4.9651E-1$	$3.2209E-1$	$5.3844E-7$

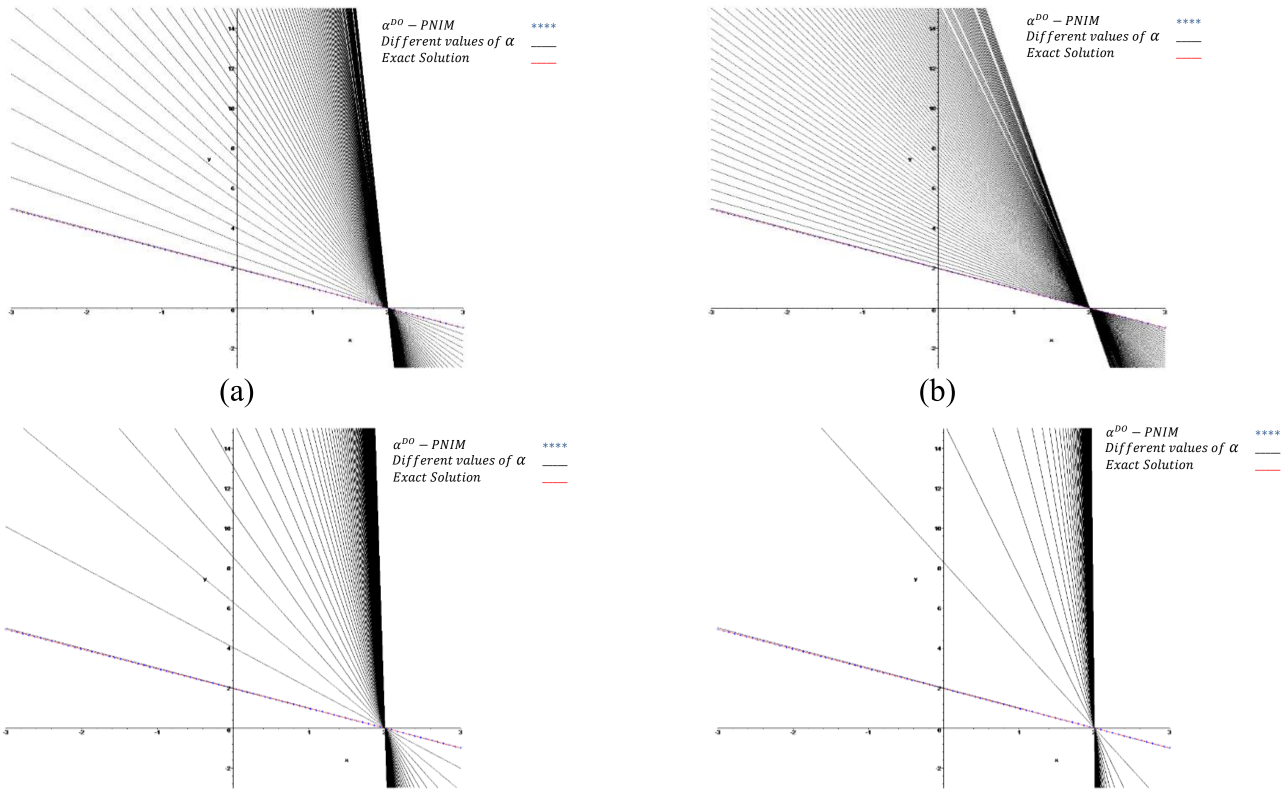

Figure 3: Shows the difference between exact solution, α^{DO}-PNIM and different values of α, when τ =1 in (a),τ =0.75 in (b), τ =0.5 in (c), τ =0.25 in (d).

7. CONCLUSIONS

In this Paper, the NIM was developed by combining it with linear combination. This linear combination is in terms of the parameter α, where α works to combine the solutions and adjust them with respect to the exact solution. The intelligent DO algorithm was also used to choose the appropriate value for the parameter α by relying on the final approximate solution for α-PDTM as a fitness function after subtracting from the exact solution. The results of the α-PNIM (Which contains a random value for the parameter α) were compared with αDO-PDTM (Which contains the parameter α chosen by DO) through three examples of F-PDEs shown in Tables (1-3) and Figures (1-3), where α^{DO}-PDTM shows superior results on α-PDTM by calculating MSE and MAE.

REFERENCES

[1] M. A. S. Murad, "Modified integral equation combined with the decomposition method for time fractional differential equations with variable coefficients," *Applied Mathematics-A Journal of Chinese Universities,* vol. 37, no. 3, pp. 404-414, 2022.

[2] M. R. Najeeb, A. Entesar, and O. S. Qasim, "Improving homotopy analytical method with sine cosine algorithm and Simpson integrative method for solving fractional ordinary differential equations," in *AIP Conference Proceedings*, 2022, vol. 2398, no. 1: AIP Publishing.

[3] S. Bhalekar and V. Daftardar-Gejji, "Convergence of the new iterative method," *International journal of differential equations,* vol. 2011, 2011.

[4] V. Daftardar-Gejji and H. Jafari, "An iterative method for solving nonlinear functional equations," *Journal of mathematical analysis and applications,* vol. 316, no. 2, pp. 753-763, 2006.

[5] M. Yaseen, M. Samraiz, and S. Naheed, "Exact solutions of Laplace equation by DJ method," *Results in physics,* vol. 3, pp. 38-40, 2013.

[6] M. Al-Jawary, "Exact solutions to linear and nonlinear wave and diffusion equations," *International Journal of Applied Mathematics Research,* vol. 4, no. 1, p. 106, 2015.

[7] M. A. Ramadan and M. S. Al-luhaibi, "New iterative method for solving the fornberg-whitham equation and comparison with homotopy perturbation transform method," *British Journal of Mathematics & Computer Science,* vol. 4, no. 9, pp. 1213-1227, 2014.

[8] S. Zhao, T. Zhang, S. Ma, and M. Chen, "Dandelion Optimizer: A nature-inspired metaheuristic algorithm for engineering applications," *Engineering Applications of Artificial Intelligence,* vol. 114, p. 105075, 2022.

[9] Z. Wang, F. Yu, D. Wang, T. Liu, and R. Hu, "Multi-threshold segmentation of breast cancer images based on improved dandelion optimization algorithm," *The Journal of Supercomputing,* pp. 1-26, 2023.

[10] Z. Beheshti and S. M. H. Shamsuddin, "A review of population-based meta-heuristic algorithms," *Int. j. adv. soft comput. appl,* vol. 5, no. 1, pp. 1-35, 2013.

[11] Z. Wang, Y. Li, H. Zhang, C. Liu, and Q. Chen, "Sampling-based optimal motion planning with smart exploration and exploitation," *IEEE/ASME Transactions on Mechatronics,* vol. 25, no. 5, pp. 2376-2386, 2020.

[12] L. Shijun, *Advances in the Homotopy Analysis Method*. World Scientific, 2013.

[13] F. Wang, X. Yuan, S. C. Liew, and D. J. I. t. o. i. t. Guo, "Wireless MIMO switching: Weighted sum mean square error and sum rate optimization," vol. 59, no. 9, pp. 5297-5312, 2013.

[14] A. Entesar and O. S. Qasim, "Solve fractional differential equations via a hybrid method between variational iteration method and gray wolf optimization algorithm," *Asian-European Journal of Mathematics,* p. 2150144, 2020.

[15] H. Günerhan, M. Yiğider, J. Manafian, and O. A. Ilhan, "Numerical solution of fractional order logistic equations via conformable fractional differential transform method," *Journal of Interdisciplinary Mathematics,* vol. 24, no. 5, pp. 1207-1220, 2021.

[16] S. Momani and Z. Odibat, "A novel method for nonlinear fractional partial differential equations: combination of DTM and generalized Taylor's formula," *Journal of Computational and Applied Mathematics,* vol. 220, no. 1-2, pp. 85-95, 2008.

[17] V. Daftardar-Gejji and S. Bhalekar, "Solving fractional boundary value problems with Dirichlet boundary conditions using a new iterative method," *Computers & Mathematics with Applications,* vol. 59, no. 5, pp. 1801-1809, 2010.

PERFORMANCE COMPARISON OF OBJECT DETECTION ALGORITHMS FOR SHIP DETECTION AND CLASSIFICATION FROM SATELLITE IMAGERY

Mehmet Sami Türker [1], Enes Ayan [2]

[1,2]Department of Computer Engineering, University of Kirikkale, Kirikkale, Turkey

mehmetsamiturker@gmail.com, enesayan@kku.edu.tr

Abstract

Automatic detection and classification of ships from satellite imagery is an important research area that can be used to monitor maritime traffic, environmental pollution, drug trafficking, migrant smuggling, border violations and other crimes. Convolutional Neural Networks (CNNs), one of the deep learning algorithms that has become popular in recent years, has achieved successful results in computer vision problems such as object detection and classification. In this study, the ship detection and classification performances of three different versions (YOLOv5, YOLOv7, YOLOv9) of the CNN-based object detection algorithm You Only Look Once (YOLO) were compared in satellite images. The advantages and disadvantages of the available YOLO-based architectures for detecting ships using satellite imagery are discussed. According to the test results, YOLOv5l architecture was more successful in ship detection and classification than other YOLO architectures, achieving 0.984 precision, 0.984 recall, 0.991 mAP and 0.984 F1 score values, respectively. The results show that YOLO-based architectures can provide promising benefits for the maritime industry and security applications.

Keywords: Remote Sensing, Ship Classification, Object Detection, YOLO.

1.INTRODUCTION

Automatic detection and classification of ships is an increasingly important research area in maritime security. The ability to detect ships and obtain information about their maneuvers and behaviors is crucial for the management of ship traffic and the control of port entrances and exits [1]. Moreover, security forces employ ship detection technologies to monitor and investigate criminal activities such as environmental pollution, drug trafficking, migrant smuggling, and border violations. The automatic detection of security breaches by computers prevents the loss of labor and the occurrence of false alarms due to potential human error. A variety of imaging techniques are employed to identify maritime ships. The first of these is synthetic aperture radar (SAR) imagery. SAR images are preferred over other types of images because they are less affected by weather conditions and time [2], [3], [4]. Additionally, SAR images can be utilized to ascertain the velocity of moving objects [3]. However, SAR images often contain high levels of speckles. In addition, it is insensitive to wooden materials and is difficult to interpret by humans [5]. Another imaging method is high-resolution optical satellite images. In contrast to SAR, optical satellite imagery is often the preferred method for ship detection and classification, as it can provide more detailed information, especially for the detection of small targets and the recognition of ships [6], [7], [8]. Although high-resolution images have been obtained with the developments in remote sensing technology, the detection of ships from optical satellite images remains a challenging task due to various conditions, including fog, waves, and sunlight reflection. So, there is a clear need for further studies in this field [8]. While classical machine learning methods were previously employed for object detection and classification tasks, they have now been superseded by deep learning algorithms [9]. In particular, convolutional neural networks (CNNs), which have demonstrated remarkable success in numerous computer vision applications, have emerged as a promising avenue for addressing ship detection and classification tasks [8]. A number of studies in the literature are as follows. In 2019, Scholler et al. [10] conducted a study on object detection at sea using Long Wavelength Infrared (LWIR) images. In the study, the RetinaNet, YOLO and Faster RCNN models are employed to focus on detecting ships and mines on the sea surface. Ophoff et al. [11], compared the strengths and weaknesses of four different YOLO ONLY LOOK (YOLO) models, namely YOLOV2, YOLOV3, YOLT and D-YOLO, on a dataset specifically created for vehicle and ship detection. The results of this study indicated that the YOLT model was more successful than YOLOV3 and D-YOLO in detecting ships. Atik and İpbüker [12] achieved an accuracy rate of 99.17% in the classification of ships using the Mask-R CNN architecture with the ResNet-101 model using the AIRBUS Ship Detection dataset. In another study conducted by Patel et al. in 2022 [13], the authors employed a Graphical Neural Network (GNN) and the YOLOv7 model to detect ships using the HRSID dataset. The results indicated that the YOLOv7 algorithm achieved a 93.4% success rate. A further study by Patel et al. [14] compared the performance of different versions of the YOLO algorithm, including YOLOv3, YOLOv4 and YOLOv5, after training on a large satellite image dataset of the Airbus Ship Challenge using the Airbus dataset, which consists of approximately 40,000 satellite images. The study found that the YOLOv5 object detection algorithm demonstrated superior performance in terms of success rate compared to the other YOLO versions. YOLOv5 achieved a 99% success rate, while YOLOv4 achieved a 98% success rate and YOLOv3 achieved a 97% success rate. Kızılkaya et al. [7] trained the YOLOv4 algorithm for the detection and classification of ship types using a dataset created with Google Earth images. The YOLOv4 model achieved an accuracy of 84.31% and a F1 score of 75.34% in the recognition of ships.

A review of the literature reveals that the YOLO algorithm is employed in object detection and that it yields successful results. However, to the best of our knowledge, no study has evaluated newer YOLO architectures for ship detection and classification from satellite images. The YOLO algorithm is a CNN-based object detection algorithm developed for real-time object detection [15]. Since its initial release, the algorithm has undergone continuous development, resulting in multiple versions, including V1 to V9 [16], [17], [18]. This study evaluates the performance of three versions of the algorithm, namely YOLOv5 [18], YOLOv7[16] and YOLOv9[17], in detecting and classifying ships from optical satellite images.

2.GENERAL PROPERTIES OF METHOD

The objective of this study is to compare the performance of three different versions of YOLO algorithms in detecting and classifying ships from optical satellite images. In the study, four YOLOv5 version, two YOLOv7 version and one YOLOv9 version was utilized. Figure 1 presents a visual representation of the overall study.

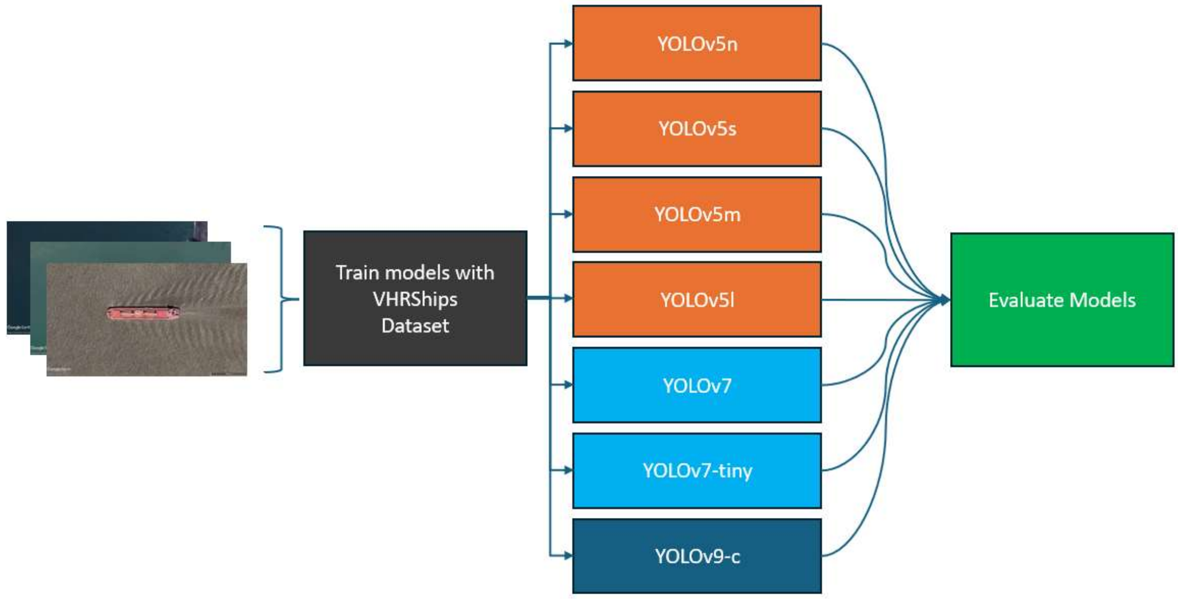

Figure 1 Flowchart of the study.

2.1 Dataset

The open-source datasets utilized in the literature for the detection of ships are generated through the cropping of images sourced from Google Earth and various satellites. There isn't any standard database, and many datasets are not shared as open source. This study utilizes the Very High-Resolution Ships (VHRShips) dataset created by Kızılkaya et al. [7]. The VHRShips dataset includes a total of 6,312 images with a resolution of 720x1280, obtained from Google Earth. Of these, 1,000 lack any floating elements. The remaining 5,312 images contain at least one ship. The data set comprises 34 different classes and is currently divided into training and test sets [21]. Table 1 presents the class distributions and total number of classes for the training and test groups. Figure 2 also includes some examples from the dataset.

Table 1 The class distributions of the training and test groups in the dataset.

S.N.	Class Name	Numbers of Training Data	Numbers of Test Data
1	Aircraft	35	6
2	Auxilary	164	40
3	Barge PonToon	737	138
4	Bulk Carrier	678	128
5	Coast Guard	40	10
6	Coaster	346	55

7	Container	580	111
8	Cruiser	68	14
9	Destroyer	91	17
10	Dredger Revlamation	268	54
11	Dredging	195	42
12	Drill	34	6
13	Ferry	99	17
14	Fishing	37	6
15	Floating Dock	52	12
16	Frigate	71	11
17	General Cargo	655	131
18	Landing	34	9
19	LPG	33	7
20	Offshore	127	25
21	Oil Tanker	592	118
22	Ore Carrier	771	159
23	Other	27	6
24	Passanger	144	27
25	Patrol Force	102	13
26	Roro	102	20
27	Service Craft	151	10
28	Small Boat	944	177
29	Small Passanger	418	72
30	Submarine	50	6
31	Tanker	779	148
32	Tug	854	171
33	Undefined	435	83
34	Yatch	1620	326
Total		5312	1075

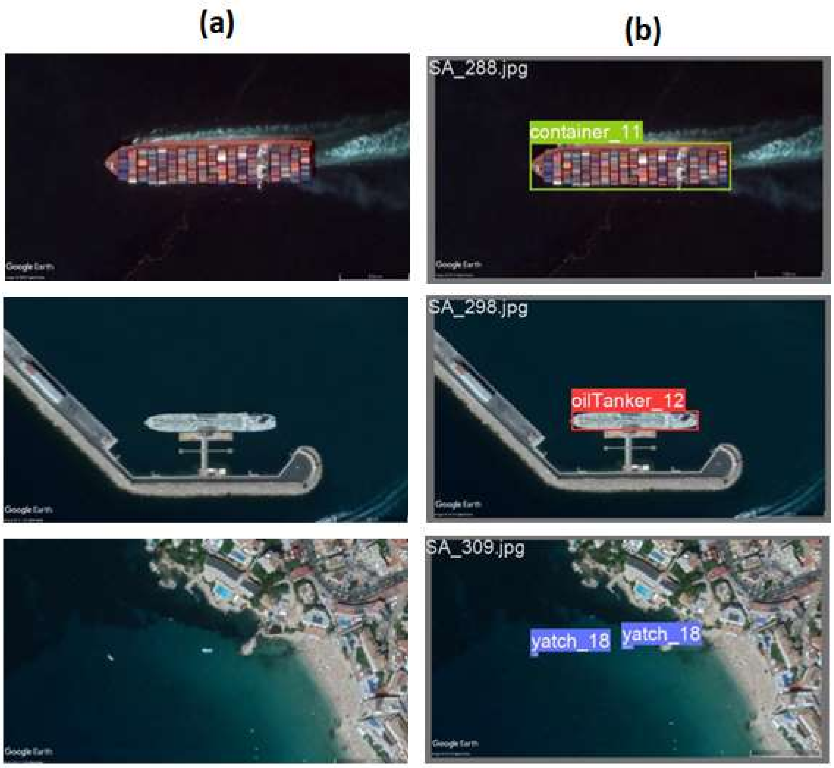

Figure 2 Example images from the dataset: (a) the original image and (b) the labelled image.

2.2 YOLO

Object detection and classification is a significant challenge in the field of computer vision. To address this issue, researchers have developed a range of algorithms over time. Recently, CNN-based object detection algorithms have gained prominence due to the rise of deep learning techniques. Among these algorithms, YOLO stands out for its high detection speed and compact model size. The initial version of YOLO was introduced by Reademon et al. in 2015 [15]. In contrast to two-step object detection algorithms, YOLO performs bounding box detection and classification in a single step. Over the years, various versions of YOLOv2, YOLOv3, YOLOv4, YOLOv5, YOLOv6, YOLOv7, YOLOv8, and YOLOv9 have been developed. In this study, the YOLOv5, YOLOv7, and YOLOv9 models are evaluated.

2.2.1 YOLOv5

YOLOv5 was presented by Glenn et al. in 2020 [19]. The architecture consists of input, backbone, neck, and head (prediction) modules as in other YOLO models. The model can take 640X640 or 1280x1280 images as input. YOLOv5 was developed using PyTorch development environment instead of Darknet development environment like older versions. The number of parameters included in the model determines the scale of the architecture, which is reflected in the nomenclature: YOLOv5n, YOLOv5s, YOLOv5m, YOLOv5l, and YOLOv5x. In this study, the YOLOv5n, YOLOv5s, YOLOv5m, YOLOv5l models were employed.

2.2.2 YOLOv7

YOLOv7 was developed by Wang et al. in 2022 [20]. The model architecture contains several modifications, including improvements to the loss function, backbone network and activation function. These modifications resulted in a model with 40% fewer parameters than other object detection algorithms, while simultaneously demonstrating enhanced classification speed and performance. YOLOv7 comprises input, backbone, neck, and head modules like older versions. The model is capable of processing images with a resolution of either 640×640 or 1280×1280. The most significant advancement brought about by the YOLOv7 architecture is the Extended Efficient Layer Aggregation Network (E-ELAN) module incorporated into the neck. E-ELAN modules provide a framework that enables the network to continuously enhance its learning capacity through the utilization of extend, mix, merge links, thereby improving the learning capacity of the operational network without disrupting the original gradient path. The YOLOv7 architecture comprises a number of scale models, including YOLOv7tiny, YOLOv7 and YOLOv7w6. In this study, the YOLOv7tiny and YOLOv7 models were utilized.

2.2.3 YOLOv9

The latest version of the YOLO architecture was developed by Chang et al. in 2024 [17]. The authors introduced two novel techniques: Programmable Gradient Information (PGI) and Generalized Efficient Layer Aggregation Network (GELAN). PGI prevents data loss and ensures accurate gradient updates, while GELAN enables the optimization of lightweight models through gradient path planning. The combination of PGI and the adaptive GELAN architecture in YOLOv9 not only enhances the learning capabilities of the model but also guarantees the preservation of vital information throughout the detection process. YOLOv9 is presented with four models ordered by the number of parameters: v9-S, v9-M, v9-C and v9-E. The YOLOV9-C model with shared weight values was used in this study.

2.3 The Evaluation Criteria

In this study, a comprehensive set of evaluation metrics is employed to assess the ship detection performance of the models. These metrics include precision (P), recall (R), mean average precision (mAP), and F1 score were calculated according to the following formulas:

$$P = \frac{TP}{TP+FP} \tag{1}$$

$$R = \frac{TP}{TP+FN} \tag{2}$$

$$mAP = \int_0^1 P(R)dR \tag{3}$$

$$F1\ Score = 2\text{x}\frac{\text{P x R}}{\text{P+R}} \tag{4}$$

In the equations, TP represents correctly detected ships, FP represents incorrectly detected ships, and FN represents undetected ships.

2.4 Development Environment and Training Parameters

All experiments in this study were conducted on Ubuntu 20.04, PyTorch 2.0.0, CUDA 11.8, Python 3.8, NVIDIA RTX 1080 Ti GPU with 12 GB VRAM and 2 Intel(R) Xeon(R) CPUs. All models were trained with the default training parameters to ensure an equal comparison. The transfer learning method was employed to train the models. The training parameters of the models are presented in Table 2.

Table 2 Model training parameters

Parameter Name	Value
Epoch	200
Batch Size	16
IOU	0.50
Confidence	0.20
Optimizer	Stochastic Gradient Descent
Learning Rate	0.01
Momentum	0.93
Weight Decay	0.0005
Input size	640x640x3

3.APPLICATIONS

The ship detection and classification performances of the models evaluated within the scope of the study are presented in Table 3. According to test results the YOLOv5l model has been the most successful model, with precision, recall, mAP and F1 score values of 0.984, 0.984, 0.991 and 0.984, respectively. The most successful model is followed by the YOLOv5m, YOLOv9-c, YOLOv5s, YOLOv7-tiny, YOLOv7 and YOLOv5n models in terms of performance, respectively.

Table 3 Model performances of the test data

Model	Precision (All classes)	Recall (All classes)	mAP50 (All classes)	F1-Score
YOLOv5n	0.888	0.835	0.889	0.860
YOLOv5s	0.966	0.975	0.978	0.970
YOLOv5m	0.983	0.984	0.991	0.983
YOLOv5l	**0.984**	**0.984**	**0.991**	**0.984**
YOLOv7tiny	0.911	0.832	0.901	0.869
YOLOv7	0.896	0.815	0.872	0.853
YOLOv9-c	0.98	0.962	0.983	0.970

Table 4 presents the total number of layers, the number of parameters, the number of Giga Floating Point Operations (GFLOPS), and the total memory allocation for the models. The data presented in Table 4 indicates that the YOLOv5n model, with the lowest detection performance, also has the least number of total parameters. However, it is not possible to conclude that the opposite is true. The YOLOv9-c model, with the highest number of parameters, ranks third in terms of performance, as shown in Table 4. Nevertheless, this indicates that there is a correlation between the size of the model and its success, with the successful model having the second highest total parameter count in the ranking.

Table 4 Model sizes

Model	Layers	Parameters	GFLOPS	Size
YOLOv5n	157	1,805,167	4.3	3.9 MB
YOLOv5s	157	7,101,823	16.1	14.5 MB
YOLOv5m	212	20,986,287	48.4	42.4 MB
YOLOv5l	267	46,285,983	108.4	93.1 MB
YOLOv7tiny	208	6,096,894	13.4	12.4 MB
YOLOv7	314	36,659,774	103.9	75.1 MB
YOLOv9-c	604	50,774,508	237.0	102.9 MB

Table 5 presents the performance metrics of the YOLOv5l model on a class-by-class basis. Upon examination of Table 5, it can be observed that a significant number of classes are detected with 100% accuracy by the model. Additionally, it is determined that the classes with the lowest detection performance of the model are 'yacht' with a recall value of 0.855 and 'small boat' with 0.901. The probable causes are the extremely small dimensions of these types of ships. Various studies have indicated that in remote sensing problems with optical satellite imagery, the detection performance of small objects is low [22], [23], [24]. Consequently, it is understandable that models have a low performance in detecting small ships. Figure 3 illustrates the detections made by the model on the test data.

Table 5 Performance results of the YOLOv5l model by class

Class	Instances	P	R	mAP
All	2175	0.984	0.984	0.991
Aircraft	6	0.958	1	0.995
Auxilary	40	0.988	1	0.995
Barge PonToon	138	0.992	0.956	0.977
Bulk Carrier	128	1	0.996	0.995
Coast Guard	10	0.975	1	0.995
Coaster	55	1	0.979	0.994
Container	111	0.997	1	0.995
Cruiser	14	0.977	1	0.995
Destroyer	17	0.987	1	0.995
Dredger Revlamation	54	0.993	1	0.995
Dredging	42	0.991	1	0.995
Drill	6	0.95	1	0.995
Ferry	17	0.984	1	0.995
Fishing	6	0.964	1	0.995
Floating Dock	12	0.991	1	0.995
Frigate	11	0.984	1	0.995
General Cargo	131	0.997	1	0.995

Landing	9	0.976	1	0.995
LPG	7	0.962	1	0.995
Offshore	25	0.986	1	0.995
Oil Tanker	118	1	1	0.995
Ore Carrier	159	0.993	0.987	0.995
Other	6	0.969	1	0.995
Passanger	27	0.989	0.963	0.966
Patrol Force	13	0.977	1	0.995
Roro	20	0.986	1	0.995
Service Craft	10	1	0.943	0.995
Small Boat	177	0.982	0.901	0.974
Small Passanger	72	1	0.961	0.994
Submarine	6	0.968	1	0.995
Tanker	148	1	0.965	0.991
Tug	171	0.997	0.988	0.987
Undefined	83	0.976	0.976	0.994
Yatch	326	0.969	0.855	0.957

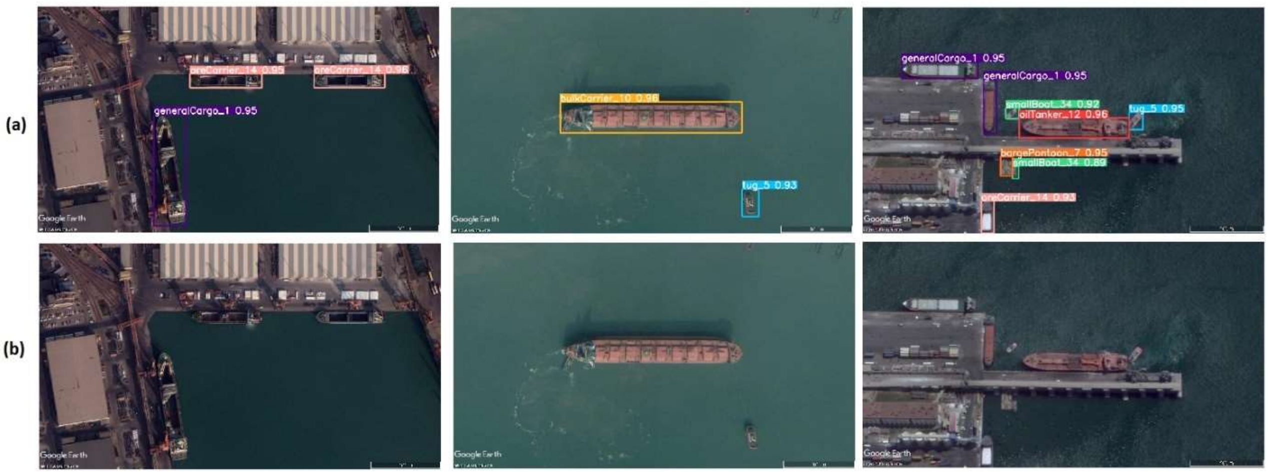

Figure 3 (a) predictions made by YOLOv5l (b) original images.

To the best of our knowledge, there is only one study in the literature that utilized the same VHRShips dataset and compared the ship detection and classification performances of object detection models [7]. In the study, Kızılkaya et al. employed their self-created VHRShips dataset for training the YOLOv4 algorithm. According to the training results, they expressed the ship recognition performance of the YOLOv4 algorithm as 71.34 F1 score. The result obtained in our study is a 98.4 F1 score value. Even the YOLOv5n model, which showed the lowest performance in the study, achieved an F1 score of 86, surpassing YOLOv4. The success of larger models in the study may be considered a disadvantage in terms of their usage in embedded systems. It is anticipated that this issue can be addressed through the incorporation of attention mechanisms into smaller models. The introduction of attention mechanisms may result in enhanced detection capabilities for small objects.

4.CONCLUSIONS

In this study, three different YOLO architectures were evaluated with regard to their performance in ship detection and classification from optical satellite imagery. The YOLOv5l model emerged as the most successful, with a 0.991 mAP value. The study's findings indicate that YOLO-based object detection algorithms are effective in detecting and classifying ships from optical satellite imagery. The study revealed that ships in classes that could not be detected by the models were smaller than others. Consequently, future research directions include expanding the dataset, adding attention mechanisms to the architecture for detecting small ships, and making improvements aimed at enhancing the performance of smaller models.

REFERENCES

1. H. İ. Şenol, "Gelişmiş Deniz Gözlemi: SAR Tabanlı Gemi Tespiti için CNN Algoritmalarının Kullanımı," Türkiye Lidar Dergisi, vol. 5, no. 1, pp. 1–7, 2023.

2. K. Eldhuset, "An automatic ship and ship wake detection system for spaceborne SAR images in coastal regions," IEEE transactions on Geoscience and Remote Sensing, vol. 34, no. 4, pp. 1010–1019, 1996.

3. M. V. Dragosevic and P. W. Vachon, "Estimation of ship radial speed by adaptive processing of RADARSAT-1 fine mode data," IEEE Geoscience and Remote Sensing Letters, vol. 5, no. 4, pp. 678–682, 2008.

4. X. Li and J. Chong, "Processing of Envisat alternating polarization data for vessel detection," IEEE Geoscience and Remote Sensing Letters, vol. 5, no. 2, pp. 271–275, 2008.

5. S. Mirghasemi, H. Sadoghi Yazdi, and M. Lotfizad, "A target-based color space for sea target detection," Appl Intell, vol. 36, no. 4, pp. 960–978, Jun. 2012, doi: 10.1007/s10489-011-0307-y.

6. A. Mehran, S. Tehsin, and M. Hamza, "An effective deep learning model for ship detection from satellite images," Spat. Inf. Res., vol. 31, no. 1, pp. 61–72, Feb. 2023, doi: 10.1007/s41324-022-00482-1.

7. S. Kızılkaya, U. Alganci, and E. Sertel, "VHRShips: An extensive benchmark dataset for scalable deep learning-based ship detection applications," ISPRS International Journal of Geo-Information, vol. 11, no. 8, p. 445, 2022.

8. B. Li, X. Xie, X. Wei, and W. Tang, “Ship detection and classification from optical remote sensing images: A survey,” Chinese Journal of Aeronautics, vol. 34, no. 3, pp. 145–163, Mar. 2021, doi: 10.1016/j.cja.2020.09.022.

9. J. Chai, H. Zeng, A. Li, and E. W. T. Ngai, “Deep learning in computer vision: A critical review of emerging techniques and application scenarios,” Machine Learning with Applications, vol. 6, p. 100134, Dec. 2021, doi: 10.1016/j.mlwa.2021.100134.

10. F. E. T. Schöller, M. K. Plenge-Feidenhans’l, J. D. Stets, and M. Blanke, “Assessing Deep-learning Methods for Object Detection at Sea from LWIR Images,” IFAC-PapersOnLine, vol. 52, no. 21, pp. 64–71, Jan. 2019, doi: 10.1016/j.ifacol.2019.12.284.

11. T. Ophoff, S. Puttemans, V. Kalogirou, J.-P. Robin, and T. Goedemé, “Vehicle and vessel detection on satellite imagery: A comparative study on single-shot detectors,” Remote Sensing, vol. 12, no. 7, p. 1217, 2020.

12. S. Atik and C. Ipbuker, “Uydu Görüntülerinden Örnek Segmentasyonu ile Gemi Tespiti (Ship Detection from Satellite Images with Instance Segmentation),” presented at the 18. Türkiye Harita Bilimsel ve Teknik Kurultayı, Ankara: TMMOB Harita ve Kadastro Mühendisleri Odası, May 2021, pp. 1–5. [Online]. Available: https://www.researchgate.net/profile/Saziye-Atik/publication/354708449_Uydu_Goruntulerinden_Ornek_Segmentasyonu_ile_Gemi_Tespiti_Ship_Detection_from_Satellite_Images_with_Instance_Segmentation/links/6149048ca595d06017dd332f/Uydu-Goeruentuelerinden-Oernek-Segmentasyonu-ile-Gemi-Tespiti-Ship-Detection-from-Satellite-Images-with-Instance-Segmentation.pdf

13. K. Patel, C. Bhatt, and P. L. Mazzeo, “Improved ship detection algorithm from satellite images using YOLOv7 and graph neural network,” Algorithms, vol. 15, no. 12, p. 473, 2022.

14. K. Patel, C. Bhatt, and P. L. Mazzeo, “Deep learning-based automatic detection of ships: An experimental study using satellite images,” Journal of imaging, vol. 8, no. 7, p. 182, 2022.

15. J. Redmon, S. Divvala, R. Girshick, and A. Farhadi, “You Only Look Once: Unified, Real-Time Object Detection.” arXiv, May 09, 2016. doi: 10.48550/arXiv.1506.02640.

16. R. Hasan, R. Hassoo, and I. Aboud, “Yolo Versions Architecture: Review,” International Journal of Advances in Scientific Research and Engineering, vol. 09, pp. 73–92, Jan. 2023, doi: 10.31695/IJASRE.2023.9.11.7.

17. C.-Y. Wang, I.-H. Yeh, and H.-Y. M. Liao, “YOLOv9: Learning What You Want to Learn Using Programmable Gradient Information.” arXiv, Feb. 28, 2024. doi: 10.48550/arXiv.2402.13616.

18. J. Terven and D. Cordova-Esparza, “A Comprehensive Review of YOLO Architectures in Computer Vision: From YOLOv1 to YOLOv8 and YOLO-NAS,” MAKE, vol. 5, no. 4, pp. 1680–1716, Nov. 2023, doi: 10.3390/make5040083.

19. J. Glen, “YOLOv5.” Accessed: Apr. 22, 2024. [Online]. Available: https://github.com/ultralytics/yolov5

20. C.-Y. Wang, A. Bochkovskiy, and H.-Y. M. Liao, “YOLOv7: Trainable bag-of-freebies sets new state-of-the-art for real-time object detectors.” arXiv, Jul. 06, 2022. doi: 10.48550/arXiv.2207.02696.

21. S. Kızılkaya, “VHRShips.” Apr. 17, 2024. Accessed: Apr. 22, 2024. [Online]. Available: https://github.com/radres333/VHRShips

22. J. Rabbi, N. Ray, M. Schubert, S. Chowdhury, and D. Chao, “Small-object detection in remote sensing images with end-to-end edge-enhanced GAN and object detector network,” Remote Sensing, vol. 12, no. 9, p. 1432, 2020.

23. X. Wang, Q. Zhao, P. Jiang, Y. Zheng, L. Yuan, and P. Yuan, “LDS-YOLO: A lightweight small object detection method for dead trees from shelter forest,” Computers and Electronics in Agriculture, vol. 198, p. 107035, 2022.

24. W. Nina, W. Condori, V. Machaca, J. Villegas, and E. Castro, “Small Ship Detection on Optical Satellite Imagery with YOLO and YOLT,” in Advances in Information and Communication, K. Arai, S. Kapoor, and R. Bhatia, Eds., Cham: Springer International Publishing, 2020, pp. 664–677. doi: 10.1007/978-3-030-39442-4_49.

Torsional Buckling Behaviour of Propeller Shaft: Comparative Investigation of Experimental and Numerical Analysis

Serdar Kaan Hortooğlu [1], **Efe Işık** [1], **Sedat Tarakçı** [1]

[1] Tirsan Kardan San. ve Tic. A.Ş. Manisa Türkiye,

s.hortooglu@tirsankardan.com.tr,

Abstract

This study aims to analyse the torsional buckling behaviour of propeller shaft with different tube profiles and to compare numerical analysis methods with experimental test results. The study reveals that propeller shaft made of E355+C material enter the torsional buckling mode when loaded above the specified torque capacity. The experimental tests for Sample 1 and Sample 2 were repeated three times for data validation and the results were compared with FEA analysis. High agreement was obtained between the results with a margin of error of 1.97% for Sample 1 and 8.6% for Sample 2. These results emphasise the importance of material selection and structural parameters used in the design and engineering calculations of propeller shaft. Furthermore, this study has the potential to raise the safety standards in the automotive industry and suggests a more detailed investigation of the effects of parameters such as the material of the tubes, swaging profiles and thickness of the tubes on the torsional buckling mode for future studies.

Keywords: Torsional Buckling, Propeller shaft analysis, Finite element method,

1. INTRODUCTION

In engineering applications, the structural reliability of elements such as propeller shaft is one of the important criteria in terms of design and functionality. Especially in automotive industry, the durability and performance of these elements are critical for safety and efficiency. This study addresses the buckling phenomenon, one of the most critical failure modes of propeller shaft and combines experimental tests and numerical analysis methods for the detection of these modes.

The focus of this study is to investigate the torsional buckling behaviour of two propeller shaft with different tube profiles and to verify these behaviours by numerical modelling. These propeller shafts, which are made of E355+C material, have non-linear material properties and the main objective of this study is to understand how they will behave under the loads they may encounter in real world conditions. The general view of the propeller shaft is shown in Figure 1. The most likely part of the propeller shaft where vibration may occur is the tube. Test results and FEA analysis show that the tube determines the natural frequency of the system.

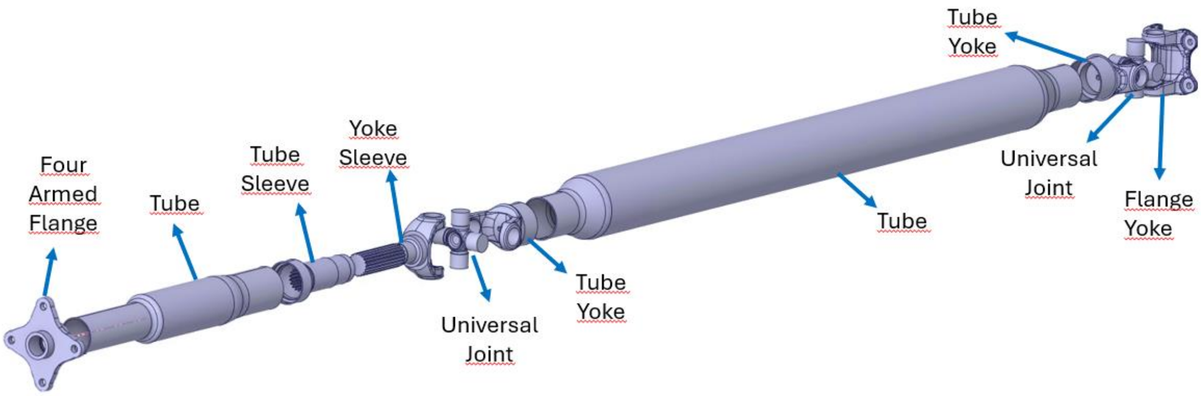

Figure 1 Propeller shaft

In case of loading more than the permissible torque capacity of the vehicle, torsional buckling mode is observed in the tube. The methodology of the research aims to integrate the theoretical knowledge and practical applications encountered in the field of engineering by correlating experimental tests and numerical analysis. This integration will contribute to the optimisation of engineering designs and to make structural elements more reliable. The study of two different tube profiles will not only reveal the strengths and weaknesses of the methodology, but also the effects of different design parameters on buckling.

Mahmood M. et al. the effect of boundary conditions and the stacking sequence of the composite layers on the strength of the drive shaft is studied. The study is shown that increasing of the applied torque on the shaft reduces the natural frequency.

Nie et al. element method is used and a four-node Shell-type element is chosen to predict buckling modes of the tubular beams. The computational results are compared with that of theoretical model and experimental data.

Dr. Borrvall, discusses a heuristic approach to alleviate transverse shear locking in hexahedra with poor aspect ratios, introducing two new solid element types in LS-DYNA, which are demonstrated to be practical through various examples.

Nedelcu and Cucu introduce an innovative method utilizing Generalized Beam Theory (GBT) for the identification of fundamental buckling modes in isotropic thin-walled members through shell finite element analysis (FEA), offering a quantitative evaluation of coupled instability without the constraints of cross-sectional shape, loading, or boundary conditions.

2. METHODOLOGY

In this comprehensive study, the buckling modes of two propeller shaft with different tube profiles have been determined in detail using both experimental tests and numerical analysis methods. The static test results of the investigated propeller shaft clearly show that the initial damage is caused by the buckling mode on the tube.

In order to accurately determine the buckling mode in the numerical analysis model, a non-linear material definition is mandatory. In this context, the stress-strain graph obtained from the non-linear material data of the E355+C tube material was obtained to be used in the analysis model.

In the validation phase of the research, two different tube profiles were analysed: The first one has a straight profile without swaging, while the other has a Ø60-Ø80 swaging profile. These two different

profiles will show different deformation modes to prove the accuracy of the analysis and test results, reinforcing the reliability of the methodology.
Loading of the propeller shaft under torsion was continued until fracture. These tests were repeated on at least three different specimens, ensuring reliability and proving the reproducibility of the results.
The model created using Ansys Ls-Dyna software was prepared after defining the geometry of the tubes, material properties, boundary conditions and loading conditions. In the numerical analysis model, the tubes were modelled as solid and an explicit analysis model was created. The same analysis parameters were applied for Sample 1 and Sample 2.
The parameters examined to verify the numerical analysis and test results are the torque value at which the buckling mode occurs and the shape of the torsional buckling mode.
By comparing these two parameters, the accuracy of the analysis results was confirmed, and this process supports the reliability of the research.

2.1. Material Properties

As the tubes are produced using the cold extrusion method, test specimens for E355+C tubes were not made from raw steel, but rather from the tube itself. According to the ASTM E8 - M standard, a dog bone profile was obtained from the sample tube. The stress-strain graph was obtained by connecting the sensor on the device's head to the tensile specimen at two points, which was later confirmed by measurements taken on the device itself. Figure 2 depicts the test arrangement.

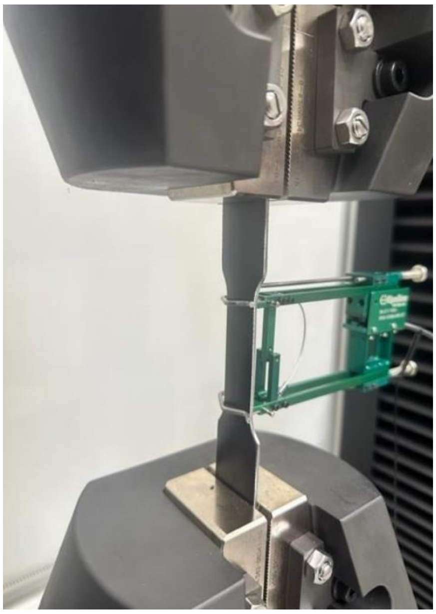

Figure 2 Tensile test machine

The test samples were secured to the test apparatus by means of clamping with the hydraulic head. The samples were subjected to tensile testing and the results are displayed in Figure 3. Upon examination of the samples, fractures were observed at the central regions. Stress-strain diagrams were plotted and the material properties were derived, as depicted in Figure 4.

Figure 3 Sample after test

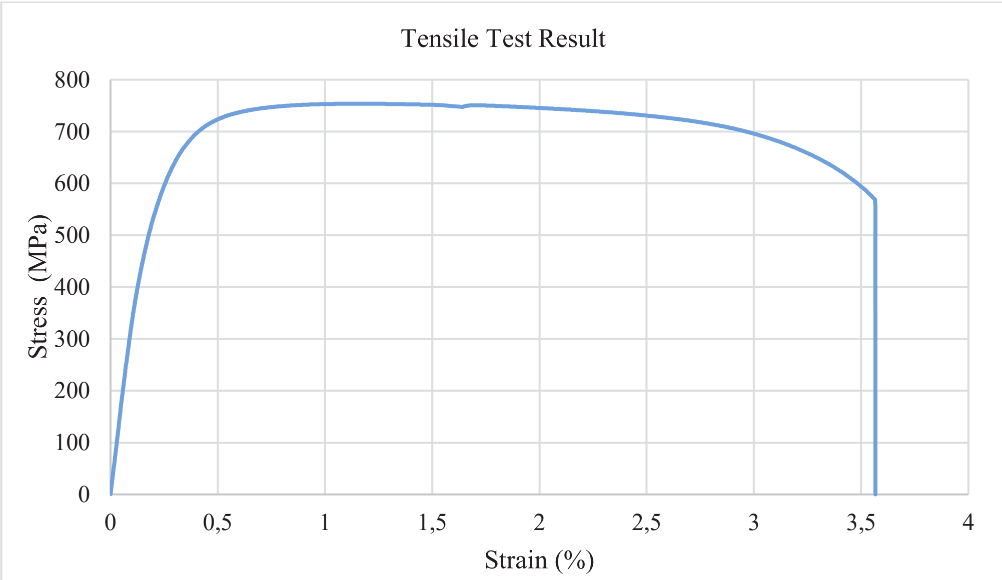

Figure 4 Strain-stress curves of the tube sample

As a result of the tensile tests, the average strengths of the specimens were calculated and are shown in Table 1. The yield stress and tensile stress are 708 MPa and 765,8 MPa respectively. To investigate the deformation mode of the tube, it is necessary to establish a non-linear analysis model. Consequently, Ls-Dyna software created a "024_piecewise_linear_plasticity" material card with a non-linear material model.

Table 1 Mechanical Properties of E355+C Test Sample

Sample	Young Modulus (GPa)	Poisson Ratio	Yield Strength (MPa)	Tensile Strength (MPa)	Elongation at Break (%)
1	198	0,33	708,8	765,8	8,18

3. METHODOLOGY

3.1. Geometric Description

In this study, two different propeller shaft with different swaging profiles were studied. In the first model, the tube with a straight profile is used, in the second model, the tube has a swaging profile between Ø60-Ø80. The technical drawing of the first sample propeller shaft is shown in Figure 5, the technical drawing of the second sample propeller shaft is shown in Figure 6.

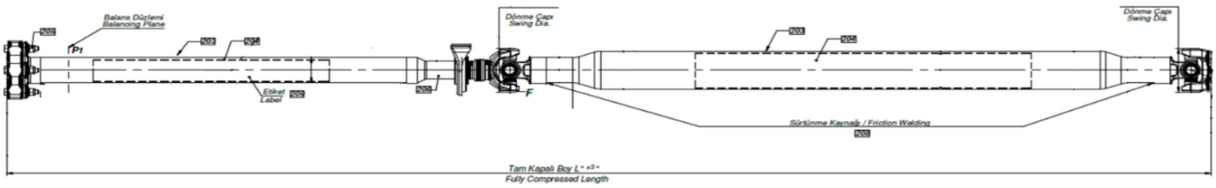

Figure 5 Technical illustration of Sample 1

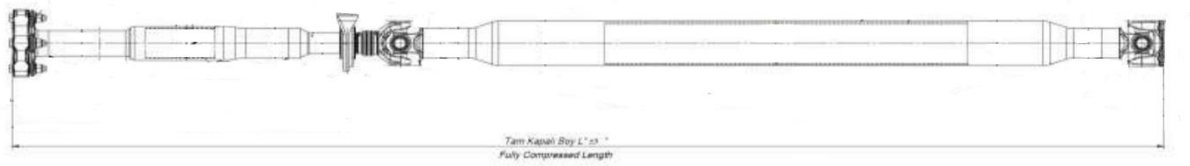

Figure 6 Technical illustration of Sample 2

3.2. Finite Element Model

The numerical analysis model was created using the Ls-Dyna programme. The analysis method was modelled as open analysis method. "Automatic_surface_surface" contact was used in the analysis model. The material card "024_piecewise_linear_plasticity" was used and the material data was obtained from the extracted tensile samples. The geometry of the tube, material properties, loading conditions and boundary conditions were defined in accordance with the experimental setup. The meshing of the tube was performed with element geometric solid using "Hexa8" and "Tetra4" element types. The mesh properties used in Sample 1 and Sample 2 models are shown in Table 2.

Table 2 Mesh properties

	Sample 1	**Sample 2**
Nodes Number	224.862	176.933
Element Number	747.376	547.020

Figure 7 and Figure 8 shows the finite element analysis (FEA) boundary conditions. In the region marked with 'A', the loading condition specified in Table 3 was applied and torque loading was performed. In the region marked with 'B', fixed support is defined. In region 'A', displacement (dx) and rotation (Rx) movements are allowed.

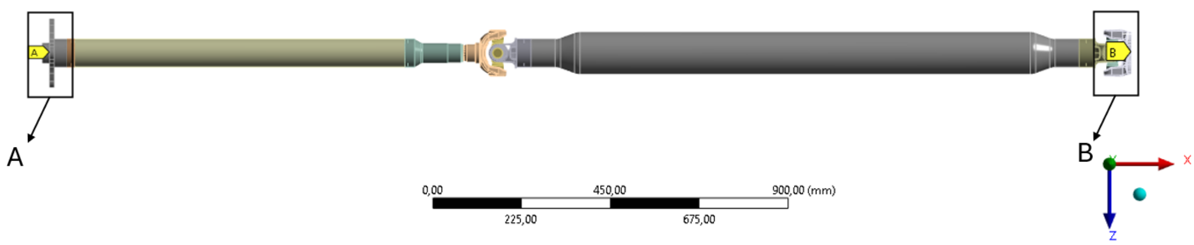

Figure 7 FEA Boundary conditions for Sample 1

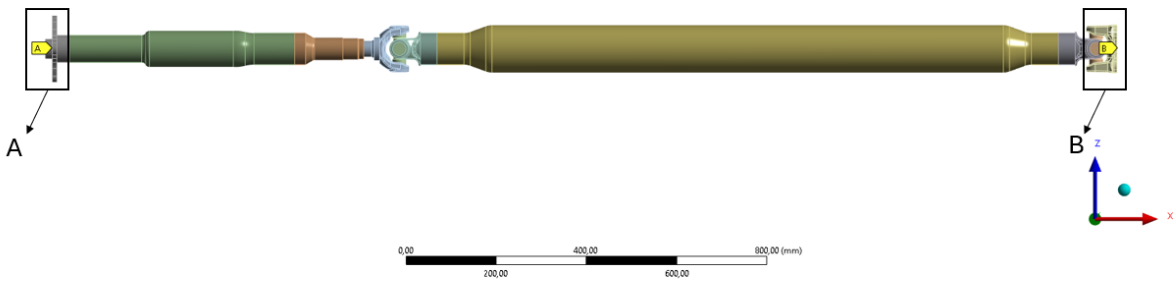

Figure 8 FEA Boundary conditions for Sample 2

Table 3 Fea load conditions

Time (Second)	Applied Torque (Nm)
0	0
0.1	6000

4. RESULT AND DISCUSSIONS

According to the results of the FEA analysis model, an image of the FEA analysis results of the Sample 1 propeller shaft is presented at Figure 9 likewise, the detailed visualisation of the torsional buckling mode occurring in Sample 1 is shown in Figure 10.

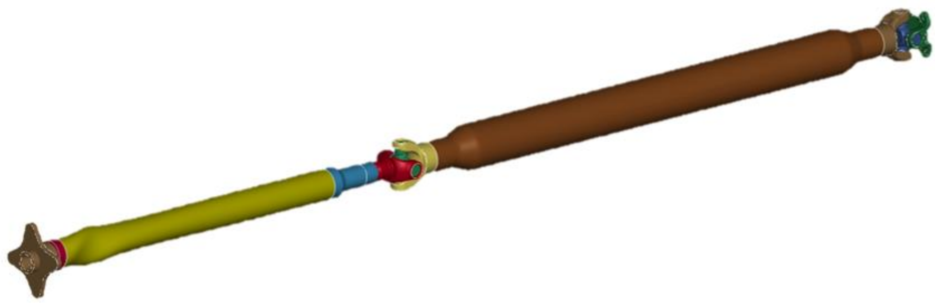

Figure 9 FEA analysis results of the Sample 1

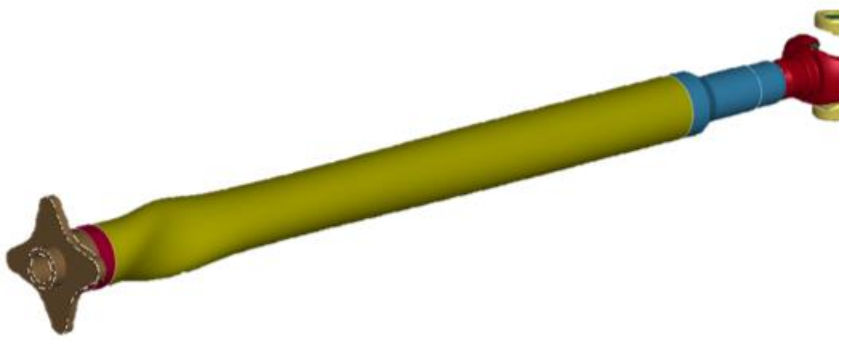

Figure 10 Detailed visualization of the torsional buckling mode

The torsional buckling mode starts at a torque value of 5080 Nm in the tube.

The experimental tests were repeated three times to ensure data validation and reliability of the results. Detailed analysis of the tests on Sample 1 revealed that as the torsional loads on the tube increased, torsional buckling of the tube occurred. This caused the tube to cease transmitting torque, at which point the test was terminated. The test results of Sample 1 and detailed images of the buckling mode are available at Figure 11

Figure 11 Buckling mode of the experimental test of Sample 1

The result graph of the experimental test performed for Sample 1 is presented Figure 12. The Ultimate Torsional Strength (UTS) value calculated according to the obtained graph was determined as 5182 Nm.

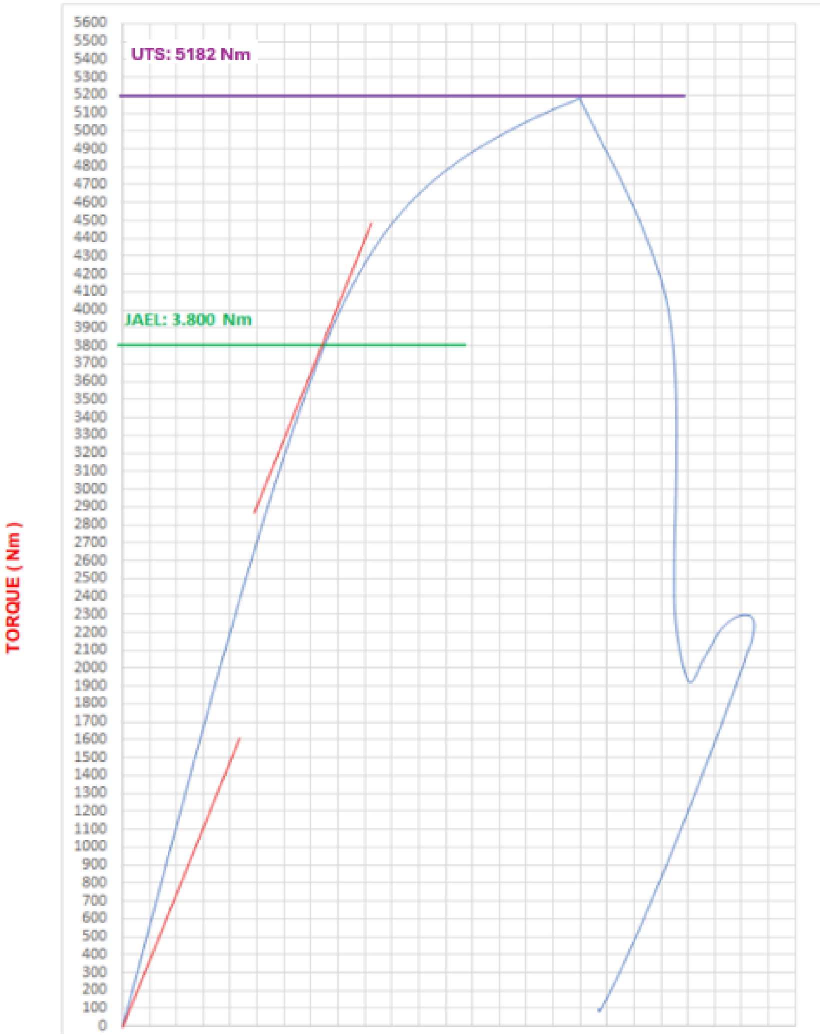

Figure 12 The reaction torque plot from the experimental test for Sample 1

When the experimental tests and FEA analysis of Sample 1 were examined in detail, a margin of error of only 1.97% was found between the results. This extremely low error rate demonstrates the high accuracy and reliability of the numerical analysis methodology. During the experimental tests, it is observed that the torque-selective buckling mode of Sample 1 occurs at 5182 Nm.

When the FEA analysis model results are analysed, the result of the sample 2 propeller shaft Figure 13 is shown below for a detailed visualisation of the buckling mode occurring in Sample 2 is shown in Figure 14.

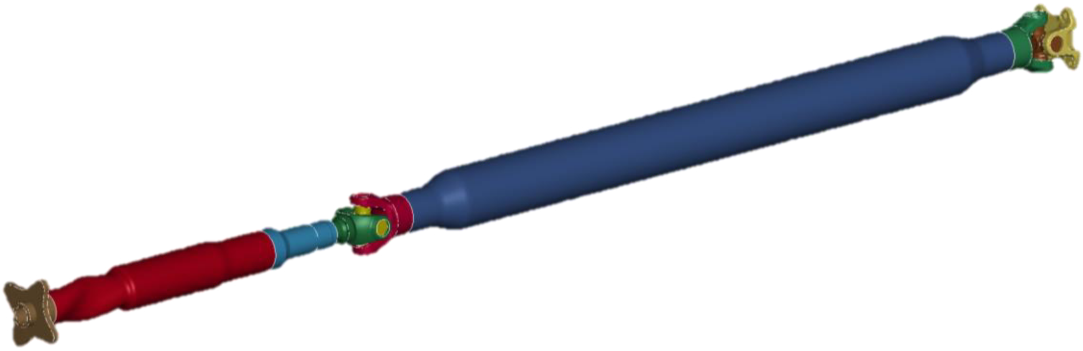

Figure 13 FEA analysis results of the Sample 2

Figure 14 Detailed visualization of the torsional buckling mode

The torsional buckling mode starts at a torque value of 4360 Nm in the tube.

The experimental tests were repeated three times to ensure data validation and reliability of the results. As for the test results of Sample 2, it was observed that buckling occurred especially in the Ø60-Ø80 swaging zone. This indicates that the swaging process has a significant effect on the structural behaviour of the tube and can affect the torsional capacity. The test results and buckling images of Sample 2 are available at Figure 15.

Figure 15 Buckling mode of the experimental test of Sample 2

The result graph of the experimental test performed for Sample 2 is presented Figure 16. The Ultimate Torsional Strength (UTS) value calculated according to the obtained graph was determined as 4770 Nm.

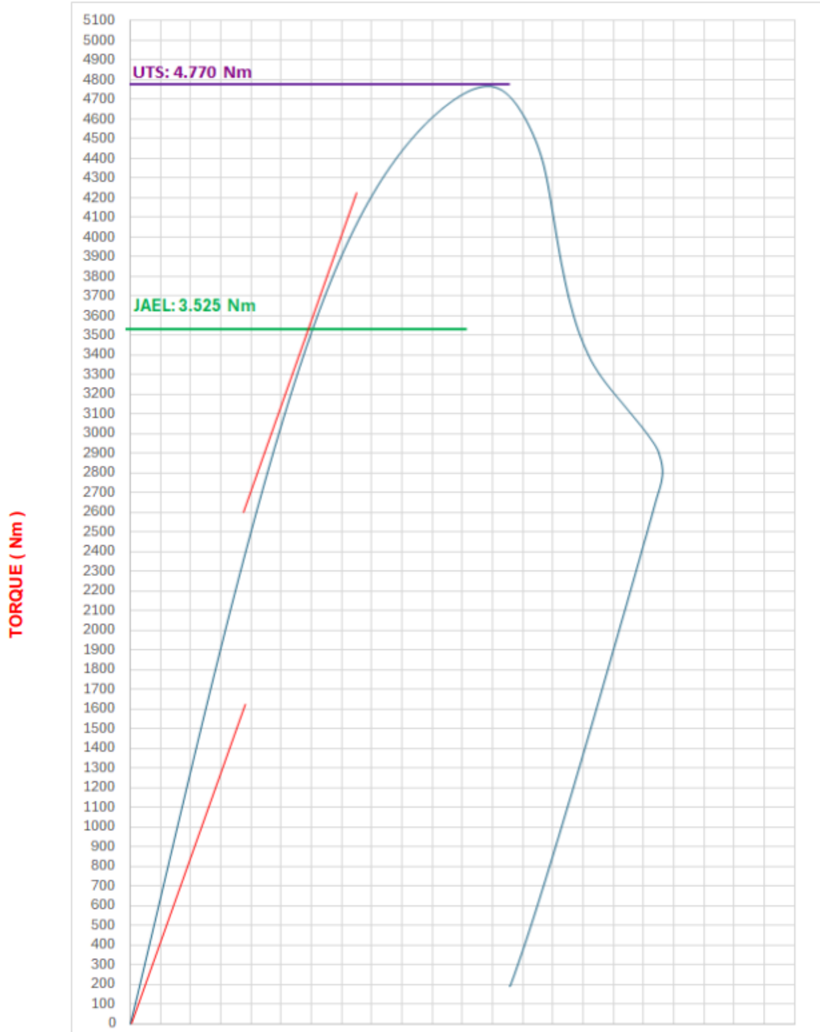

Figure 16 The reaction torque plot from the experimental test for Sample 2

Comparison of the test and FEA analysis results for Sample 2 reveals a margin of error of 8.6%. The probable reason for this higher error rate compared to Sample 1 is the pre-stress created in the tube by the tube swaging process. Tube swaging has the effect of increasing the torsional capacity of the tube. The experimental tests for Sample 2 showed that the tube was buckling at 4770 Nm. The compiled analysis and test results are shown in Table 4.

Table 4 Compiled results

	First Torsional Buckling Mode		
	Numerical Result	**Experimental Result**	**Margin of Error**
Sample 1	**5.080 Nm**	**5.182 Nm**	**1,97%**
Sample 2	**4.360 Nm**	**4.770 Nm**	**8,60%**

5. CONCLUSION

This study has successfully identified and verified through numerical analysis the torsional buckling modes of propeller shaft, which are often difficult to calculate due to their parts having complex operating dynamics. The research revealed that propeller shaft torsional buckling mode is occurred above functional torque limit of related propeller shaft.

The results of the analysis confirmed that tubes with a straight profile without swaging and tubes with a Ø60-Ø80 swaging profile exhibit different torsional buckling modes. These results show that the numerical analysis model is consistent with the experimental tests and that this type of structural analysis can be used as a reliable tool in engineering design.

The findings of the study show that the amount of torque that the tube profiles and tube diameters can carry has a determining effect on the torsional buckling behaviour of the propeller shaft. A margin of error of less than 10% was found between the test results and the finite element analysis (FEA) results, indicating that the finite element model successfully simulates the torsional buckling behaviour and provides high agreement with the experimental results.

For Sample 1, the margin of error between the experimental results and the FEA results was 1.97%, while for Sample 2 this difference was 8.6%. These results show that numerical analysis methods are reliable and can be used in the design of propeller shaft.

For future studies, it is recommended that the analysis parameters used in this research be applied to investigate the effects of variables such as material of the tubes, swaging profiles and thickness of the tubes on the torsional buckling mode. This approach will make a valuable contribution to further improve the design of propeller shaft and increase safety standards in the automotive industry.

REFERENCES

1. Ansys® Academic Research Mechanical, Release 19.2, Help System, Coupled Field Analysis Guide, ANSYS Inc.
2. Shokrieh M., Akbar, H., Larry, B., Shear buckling of a composite drive shaft under torsion, Composite Structures 64 (2004) 63–69
3. Işık, E. (2009). Topoloji optimizasyonu çatallı flanş uygulaması. Dokuz Eylül Üniversitesi, Fen Bilimleri Enstitüsü, Makine Mühendisliği Bölümü, Konstrüksiyon ve İmalat Anabilim Dalı, Yüksek Lisans Tezi. İzmir.
4. Nie, G.H. , Shi, R., Plastic and buckling behaviors of tubular beams under combined bending and torsion, ICF100322OR
5. Dr. Borrvall, T., A heuristic attempt to reduce transverse shear locking in fully integrated hexahedra with poor aspect ratio, 7th European LS-DYNA Conference
6. Nedelcu, M., Cucu, H., Buckling modes identification from FEA of thin-walled members using only GBT cross-sectional deformation modes, Thin-Walled Structures (2013)

A Research on The Effect of Class Numbers for An Algorithmical Based Solar Radiation Class Estimation

Kübra KAYSAL [1]

Fatih Onur HOCAOĞLU [2]

[1] Department of Electrical and Electronics Engineering, University of Afyon Kocatepe, Afyonkarahisar, Turkey

[2] Afyon Kocatepe University Solar and Wind Research and Application Center, Afyonkarahisar,Turkey

kkaysal@aku.edu.tr, fohocaoglu@gmail.com

Abstract

Solar energy is a common renewable energy source that varies depending on the amount of solar radiation and offers different production capacities at different times of the day. The change in the amount of solar radiation during the day causes fluctuations in the panel output power. Therefore, it is of great importance to examine the changes in solar radiation in detail in order to effectively manage the grid integration of solar electricity generation and optimize energy production. This study is a continuation of the previous research. In the previous study, solar radiation data was divided into four main cases. The prediction success of the Mycielski model was examined. In this study, the success of the algorithm was observed when the data was divided into different numbers of cases. The performance of the prediction of states is tested on a real-time dataset. As a result, it has been observed that the success of the algorithm decreases as the number of categories increases.

Keywords: Estimation; Solar Radiation; Mycielski algorithm.

1.INTRODUCTION

Factors such as increasing energy costs, depletion of fossil fuels, and increasing energy needs with population growth have made renewable energy sources popular. Renewable energy sources, which are clean, free and endless energy sources, also play an active role in reducing carbon emissions. Among renewable energy sources, solar energy has an important place. This energy source can meet the increasing energy demand while reducing carbon emissions. This energy, which has a great impact on the environment and meeting energy needs, must be used correctly [1]. Considering its geographical location, Türkiye is a country with high solar energy potential. According to the Turkish National Energy plan, in the scenario prepared by the Ministry of Energy and Natural Resources, it is planned to increase the solar energy installed capacity to 52.9 GW in the 2020-2025 period. For this purpose, the installed power of electricity based on solar energy was increased from 40 MW in 2014 to 8479 MW in 2022 [2].

The most commonly used systems to generate electricity from solar energy are solar panels. The most important quantity affecting the output power of the photovoltaic (PV) panel system is solar radiation. Solar radiation has a highly variable structure during the day. With this feature, it causes disruptive effects on the output power of PV systems. The solution to such problems can be achieved with effective analysis and accurate prediction models. Thus, interruptions that may occur due to insufficient production or storage problems due to overproduction will be prevented [3]. For this purpose, researchers have developed various models to estimate solar radiation.

In a study using regression-based methods, Jumin and colleagues developed an augmented decision tree regression (BDTR) model for solar radiation prediction. The developed model was compared with traditional regression algorithms. The success of the model was calculated to be higher than other models with a value of 0.90183 [4]. In another study, a weekly prediction study for photovoltaic panel energy was carried out with support vector regression (SVR). An attempt was made to determine the prediction success of the SVR model by using different functions. It was determined that the function with the most successful performance metrics is the radial kernel function [5]. There are also various studies using machine learning and deep learning methods in solar radiation estimation. Sorkun and colleagues used the long short-term memory (LSTM) model for short-term prediction of solar radiation. In the study, the success of univariate and multivariate LSTM models was observed. The multivariate LSTM model gave more successful results [6]. In another study, Ehteram and colleagues developed a hybrid LSTM model for solar radiation prediction. The success rate of the model in which Boruta-Random Forest feature selection was used for the best input scenario gave a high result with a rate of 0.998 [7]. There are also prediction models developed by finding algorithms with similar patterns for solar radiation prediction. In a study that made a significant contribution to the literature, Hocaoğlu and Serttaş proposed a new Mycielski-based model, assuming that solar radiation data were repeated in the past. It has been observed that the model gives successful results [8].

This study is a continuation of the previous research and the predictive performance of the Mycielski model was examined by dividing the data set into more detailed categories. For this purpose, hourly solar radiation data was converted into different numbers of states. The performance of the Mycielski model was measured in different numbers of cases of the data set, and the number of cases was determined for the best results. The article consists of four parts, and in the second part, details of the data set and method used are given. In the third section, the results and graphs of the model obtained in different categories are presented. Finally, discussion and conclusions are given in the fourth section.

2.MATERIAL AND METHOD

2.1 Data Set

The data set used in this study includes solar radiation data of a region measured hourly by the General Directorate of Meteorology between January 1, 2021 and December 31, 2021, and these data are presented graphically in Figure 1. Pre-processing of the data before it is presented to the prediction model is of great importance in increasing the success of the model. There are some data in the study that cannot be measured due to external factors. f the data is not available, missing data is determined by using the average of the data from the same time of the previous day and the next day [1].

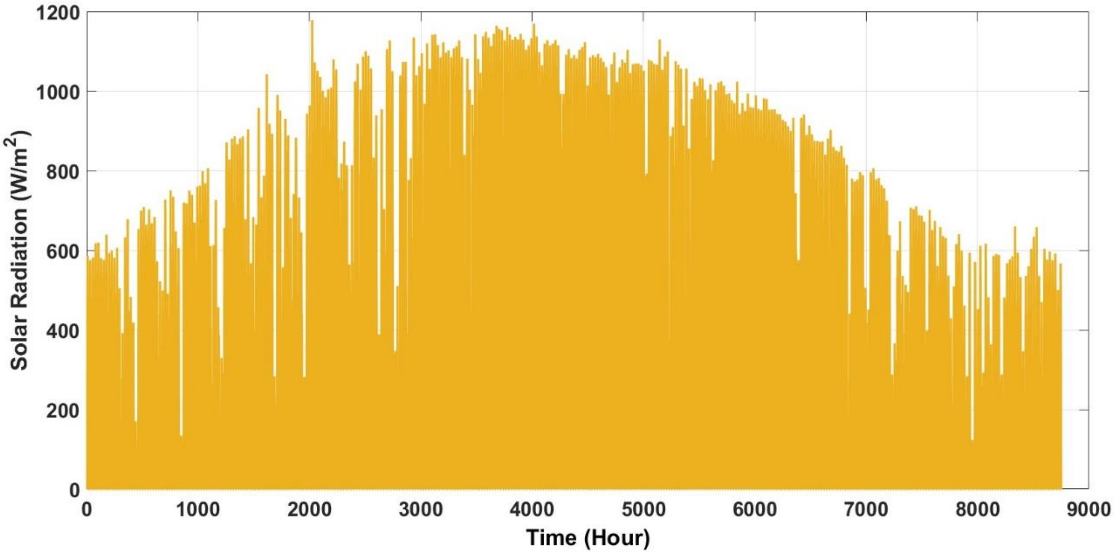

Figure 1. Hourly solar prediction values

To obtain information about the intervals, frequencies and trends where the data is concentrated and to observe the data distribution, a histogram graph was drawn and is given in Figure 2.

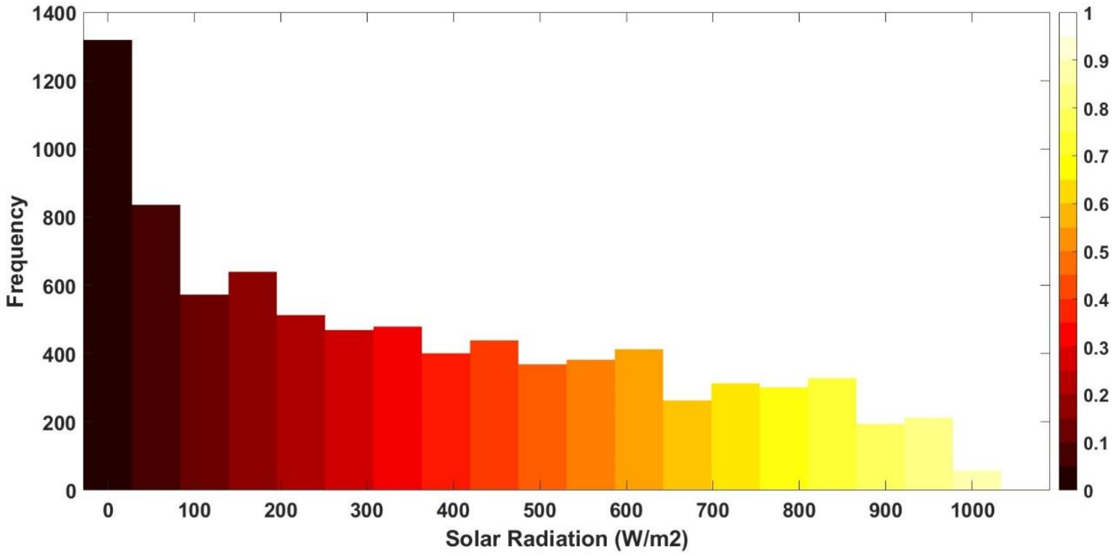

Figure 2. Hourly solar prediction values

In the histogram graph in Figure 2, drawn from the one-year solar radiation intensity data we have, it was observed that zero values have a high frequency. In order to improve analysis and processing efficiency, these zero values were removed from the data set to optimize the accuracy of the longest similarity sequence search algorithm. Next, the data set is divided into various numbers of cases. By dividing the data set into detailed cases, the success of the prediction performance of the Mycielski model was examined.

2.2. Mycielski Algorithm

Mycielski algorithm is a pattern recognition prediction model used to make deterministic predictions on discrete time series. This algorithm is based on predicting future values by analyzing similar data structures in the past. In this process, the longest historical subsequence is found in the data series. Based on this found subsequence, the value immediately after the sequence is used for prediction. The main purpose of the algorithm is to detect the longest match between the historical data series and the current data series. The approach of the algorithm is based on the assumption that by detecting similar series in the data set, the data set will exhibit similar behavior in the future. With this assumption, when the searched subsequence is found, the element following the subsequence is determined as the prediction value [1]. The algorithm starts the search process by analyzing the shortest historical data from the beginning of the data set and this process continues by adding prediction values, if any. The algorithm continues the search until a new data sequence that is not present in the past data is encountered or a longer sequence is obtained. The last sequence obtained in this process is considered the "most probable" signal used in estimating the next value [9].

The Mycielski methodology is used to find a historical equivalent of the last recorded data. The value after the found equivalent or the next data in the series is taken as the basis for the prediction. When multiple matches are found, the process is repeated by adding a new value to the data and the longest matching sequence is determined. The element after this sequence is used as a guess [8]. This algorithm can be expressed mathematically in Equation 1.

$$\hat{x}\,[n+1] = f_{n+1}(x[1], \dots, x[n]) \quad (1)$$

The $f(.)$ function expands the segments by adding an element to the left at each step, starting from the smallest data segment to find similarities in data sets. For example, if the data length is $x[n]$, segments are created first $(x[n-1], x[n])$, then $(x[n-2], x[n-1], x[n])$. This process is repeated step by step until the longest similar sequence is detected [10].

3.RESULTS

This study is a continuation of the previous study. In the previous study, the data set was divided into 4 different cases and the prediction performance of the Mycielski model was examined. In this study, the success of the algorithm was evaluated at different numbers of state values. In the study, the data set is divided into 5,6,7,8,10 and 20 cases. Each category is submitted to the Mycielski algorithm. To see the prediction success, the last ten strings of the data set were removed from the state universe during the state transition. For each case, the algorithm was run, starting from the last two sequences, until the longest similar sequence was found. The sequence after the longest similar sequence found was considered as the predictive value. This prediction was carried out in the same manner for the next ten hours for each case and compared with the actual values extracted from the data set. Algorithm success was calculated by Mean Square Error (MSE). As a result of the study, it was seen that as the number of cases increased, the success of the model in finding the longest similar sequence decreased. The longest number of similar sequences and MSE values found by the algorithm according to the number of cases are given in Table 1.

Table 1. The longest number of similar sequences and MSE values found by the algorithm according to the number of cases.

Number of Cases	*Number of Similar Sequences*	*MSE*
5 cases	23 similar series	**0.300**
6 cases	11 similar series	0.304
7 cases	22 similar series	0.307
8 cases	17 similar series	0.428
10 cases	6 similar series	0.515
20 cases	4 similar series	0.587

The most successful result for Table 1 was obtained when the data set was converted into 5 cases. The predicted values and actual values obtained from the model are given in Figure 3(a-b).

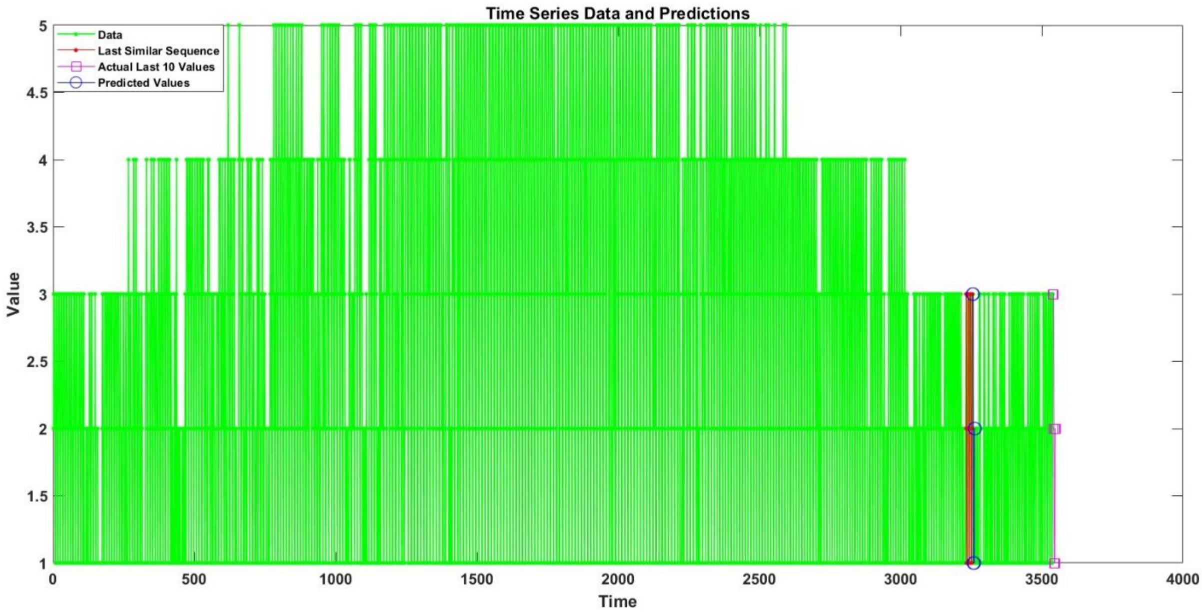

(a)

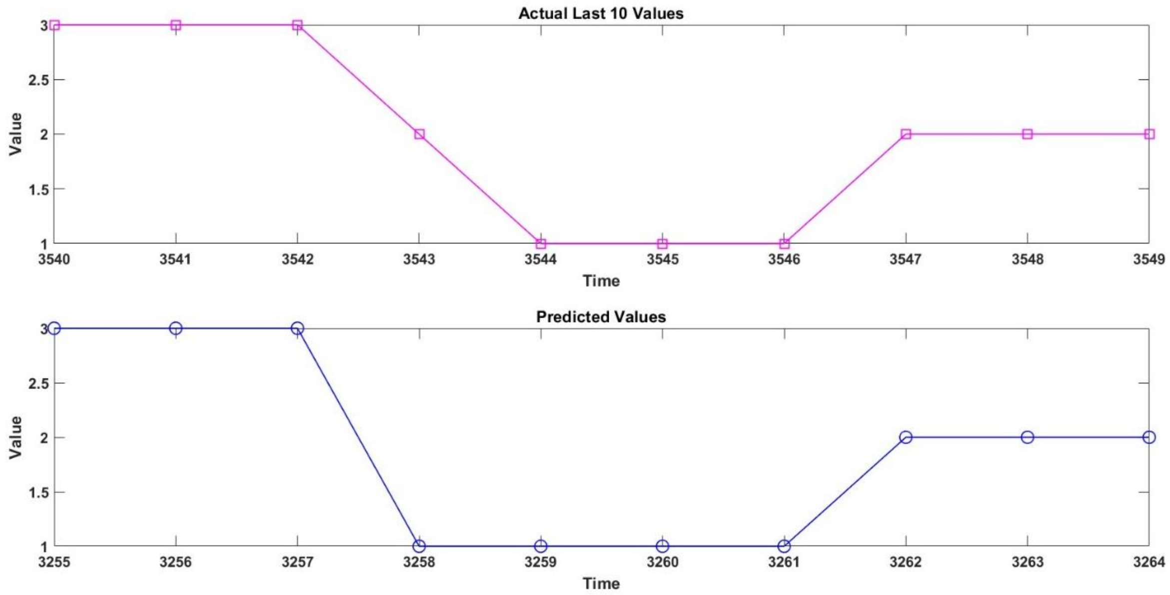

(b)

Figure 3. Last similar Sequence-PredictedValues (a) Magnified Original-Predicted Values (b)

4.CONCLUSIONS

Detailed analysis and accurate estimation of solar radiation is an important quantity for controlling the power output of photovoltaic panels. Accurately detecting patterns in solar radiation data is very effective in increasing the efficiency of panels. For this reason, this magnitude, which has a fluctuating structure during the day, needs to be estimated with an effective forecast model. In this study, the prediction success of the Mycielski algorithm for solar radiation data in different numbers of situations was measured. A detailed data analysis was conducted before the data was presented to the model. The data set is divided into 5,6,7,8,10 and 20 different cases. The MSE value of the model was calculated for each cases. It has been observed that success decreases as the number of situations increases in the model. The most successful result was measured for the data set divided into 5 cases.

The depletion of fossil resources has directed humanity towards renewable energy sources. Thus, electricity generation from solar energy, which is an unlimited, clean and free energy source, has become more popular day by day. Accurate and reliable forecast models are very important in using resources correctly and creating an effective road map for investors. For this purpose, it was observed that the pattern-based Mycielski model used in the study was successful in finding similarities in the data. However, it has been observed that the success rate decreases when the data set is divided into more complex situations. In future studies, it is planned to find solutions that will positively affect the performance of the model without removing zero values (evening hours when electricity is not produced) from the data set.

THANKS

This study was supported by the Scientific and Technological Research Council of Türkiye (TÜBİTAK) with project number 123E624. We would like to thank TÜBİTAK for its support to the project. We would also like to thank them for providing the data used in the study from the 5th Regional Directorate of Meteorology.

REFERENCES

1. Kaysal K., and Hocaoğlu F.O., "A Preliminary Study For Solar Radiation State Prediction," Presented At The 15. Uluslararası İstanbul Fen, Mühendislik ve Uygulamalı Bilimler Kongresi, İstanbul, 2023.
2. Güneş. https://enerji.gov.tr/eigm-raporlari, Erişim 30 Nisan 2024.
3. Saud, S., Jamil, B., Upadhyay, Y., and Irshad, K. "Performance improvement of empirical models for estimation of global solar radiation in India: A k-fold cross-validation approach. Sustainable Energy Technologies and Assessments," Vol:40, 100768, 2020.
4. Jumin, E., Basaruddin, F. B., Yusoff, Y. B. M., Latif, S. D., & Ahmed, A. N. "Solar radiation prediction using boosted decision tree regression model: A case study in Malaysia". Environmental Science and Pollution Research, 28, 26571-26583, 2021.
5. Akı, O., and Akal, T. T. "Destek Vektör Regresyon (SVR) Yöntemi Kullanılarak Haftalık Dönemde Fotovoltaik Panel Enerji Tahmini", V. International Agricultural, Biological & Life Science Conference (AGBIOL23), Turkiye / Edirne, 2023.
6. Sorkun, M. C., Incel, Ö. D., and Paoli, C. "Time series forecasting on multivariate solar radiation data using deep learning (LSTM)", Turkish Journal of Electrical Engineering and Computer Sciences, 28(1), 211-223, 2020.
7. Ehteram, M., Nia, M. A., Panahi, F., and Farrokhi, A. "Read-First LSTM model: A new variant of long short term memory neural network for predicting solar radiation data.", Energy Conversion and Management, 305, 118267, 2024.
8. Hocaoglu, F. O., and Serttas, F. "A novel hybrid (Mycielski-Markov) model for hourly solar radiation forecasting." Renewable Energy, 108, 635-643, 2017.
9. Hocaoğlu F.O. "Stochastic approach for daily solar radiation modeling.", Solar Energy,
10. Fidan M., Gerek O.N. "Mycielski Based 2d-Predictive Image Coding Algorithm.", Applied Mechanics and Materials. 850, 144-151, 2016.

Exponential inequalities involving Riemann-Liouville Fractional integral Fractional Integal Inequalities

[1]Funda Türk, [2]Samet Erden, [3]Burçin Gökkurt Özdemir

[1,2] Department of Mathematics, Faculty of Science, Bartn University, Bartın, Turkey,

[3] Department of Mathematics and Science Education, Faculty of Education, Bartın University, Bartn, Turkey

fundaturk44@gmail.com, erdensmt@gmail.com, gokkurtburcin@gmail.com,

Abstract

New inequalities related to Riemann-Liouville Fractional integrals for exponential functions are provided. Also, some special cases of these results are examined.

Keywords: Riemann-Liouville Fractional Integral, Ostrowski Inequality, Exponential Function.

1.INTRODUCTION

Ostrowski inequality [1] established by using functions whose first derivatives are bounded is stated in the following manner.

Theorem 1. Let $f:[a,b]\to R$ be a differentiable mapping on (a,b) whose derivative $f':(a,b)\to R$ is bounded on (a,b), *i.e.* $\|f'\|_\infty := \sup_{t\epsilon(a,b)} |f'(t)| < \infty$. Then, we have the inequality

$$\left|f(x)-\frac{1}{b-a}\int_a^b f(t)\,dt\right| \le \left[\frac{1}{4}+\frac{\left(x-\frac{a+b}{2}\right)^2}{(b-a)^2}\right](b-a)\|f'\|_\infty, \qquad (1)$$

for all $x\in[a,b]$. The constant $\frac{1}{4}$ is the best possible.

Inequality (1) has wide applications in numerical analysis and in the theory of some special means; estimating error bounds for some special means, some mid-point, trapezoid and Simpson rules and quadrature rules, etc. Hence inequality (1) has attracted considerable attention and interest from mathematicans and researchers. For example, some authors deduced new Ostrowski type inequalities for differentiable, twice differentiable or higher order differentiable functions in [2-7], and the references included there. Particularly, there are problems involving any-order derivative of a function besides the cases when first or second derivatives are required. Therefore, some mathematicians have studied on some integral inequalities for $n-$ times differentiable functions. For example, some researcher deduced new Ostrowski type results for higher order differentiable functions in [8-13], and the references included there.

Now, we recall the definition of Riemann Liouville factional integral, which has an important place in this study.

Definition: Let $f \in L_1[a,b]$. The Riemann-Liouville integrals $J_{a+}^{\alpha}f$ and $J_{b-}^{\alpha}f$ of order $\alpha > 0$ with $a \geq 0$ are defined by

$$J_{a+}^{\alpha}f(x) = \frac{1}{\Gamma(\alpha)}\int_a^x (x-t)^{\alpha-1}f(t)dt, \quad x > a$$

and

$$J_{b-}^{\alpha}f(x) = \frac{1}{\Gamma(\alpha)}\int_x^b (t-x)^{\alpha-1}f(t)dt, \quad x < b$$

respectively. Here, $\Gamma(\alpha)$ is the Gamma function and $J_{a+}^{0}f(x) = J_{b-}^{0}f(x) = f(x)$.

The fractional order differential and integral operators are non-local operators. This is one reason why fractional calculus theory provides an excellent instrument for description of memory and hereditary properties of various physical processes. Therefore, the application of fractional calculus theory has become a focus of international academic research. This calculus theory has also become popular among academics working on inequality. For example, Dragomir established some Ostrowski type inequalities including Riemann-Liouville fractional integrals for various classes of functions in [14-16]. Afterwards, some authors provided Ostrowski type fractional inequalities for double integrals in [17-18]. For recent studies about Ostrowski type inequalities involving Riemann-Liouville fractional integrals, the reader may look over [19-20], [8], and the references there in. Now, we give inequalities including Riemann-Liouville Fractional Integrals for functions whose higher-order derivatives are bounded. These identities are provided by Erden et al. in [21].

2.GENERAL PROPERTIES OF METHOD

Theorem 2. [21] $f : [a,b] \to R$ *be an* $n+1-$ times differantiable functions such that $n.th$ derivatives of f are absolutely continuous on $[a,b]$ with $a \geq 0$, for $n \in N^{+}$. *If* $f^{(n+1)} \in L_{\infty}$ $[a,b]$, i.e. $\left\|f^{(n+1)}\right\|_{\infty} := \sup_{t\epsilon(a,b)}\left|f^{(n+1)}(t)\right| < \infty$, then one has the inequalities

$$\begin{aligned}
&\left|J_{a+}^{\alpha}f(x) + (-1)^n J_{b-}^{\alpha}f(x) - \frac{(x-a)^{n+\alpha}+(b-x)^{n+\alpha}}{\Gamma(n+\alpha+1)}f^{(n)}(x)\right. \qquad (2)\\
&\left.-\sum_{k=0}^{n-1}\frac{(x-a)^{k+\alpha}f^{(k)}(a)+(-1)^{n+k}(b-x)^{k+\alpha}f^{(k)}(b)}{\Gamma(k+\alpha+1)}\right|\\
&\leq \frac{1}{(n+\alpha+1)\Gamma(n+\alpha)}\left\{(x-a)^{n+\alpha+1}\left\|f^{(n+1)}\right\|_{[a,x],\infty} + (b-x)^{n+\alpha+1}\left\|f^{(n+1)}\right\|_{[x,b],\infty}\right\}\\
&\leq \frac{1}{(n+\alpha+1)\Gamma(n+\alpha)}W\left(f^{(n+1)}\right)
\end{aligned}$$

for any $x \in (a,b)$ and $\alpha > 0$. Here, $W\left(f^{(n+1)}\right)$ is defined by

$$W\left(f^{(n+1)}\right) = \begin{cases} \left((x-a)^{n+\alpha+1} + (b-x)^{n+\alpha+1}\right)\left\|f^{(n+1)}\right\|_{[a,b],\infty} \\ \left(\left\|f^{(n+1)}\right\|_{[a,x],\infty}^{p} + \left\|f^{(n+1)}\right\|_{[x,b],\infty}^{p}\right)^{\frac{1}{p}}\left((x-a)^{(n+\alpha+1)q} + (b-x)^{(n+\alpha+1)q}\right)^{\frac{1}{q}} \\ \text{with } p,q > 1 \text{ and } \dfrac{1}{p} + \dfrac{1}{q} = 1 \\ \left(\left\|f^{(n+1)}\right\|_{[a,x],\infty} + \left\|f^{(n+1)}\right\|_{[x,b],\infty}\right)\left[\dfrac{1}{2}(b-a) + \left|x - \dfrac{a+b}{2}\right|\right]^{n+\alpha+1} \end{cases} \quad (3)$$

Theorem 3. [21] $f : [a,b] \to R$ be an $n+1-$ times differantiable functions such that $n.th$ derivatives of f are absolutely continuous *on* $[a,b]$ with $\alpha \geq 0$, for $n \in N$. *If* $f^{(n+1)} \in L_\infty$ $[a,b]$,

i.e. $\left\|f^{(n+1)}\right\|_\infty := \sup_{t\epsilon(a,b)}\left|f^{(n+1)}(t)\right| < \infty$, then we have the inequalities

$$\left|(-1)^n J_{x-}^{\alpha} f(a) + J_{x+}^{\alpha} f(b) - \sum_{k=0}^{n} \frac{(-1)^{n+k}(x-a)^{k+\alpha} + (b-x)^{k+\alpha}}{\Gamma(k+\alpha+1)} f^{(k)}(x)\right| \quad (4)$$

$$\leq \frac{1}{\Gamma(n+\alpha+2)}\left\{\left\|f^{(n+1)}\right\|_{[a,x],\infty}(x-a)^{n+\alpha+1} + \left\|f^{(n+1)}\right\|_{[x,b],\infty}(b-x)^{n+\alpha+1}\right\}$$
$$\leq \frac{1}{\Gamma(n+\alpha+2)} W\left(f^{(n+1)}\right)$$

for any $x \in (a,b)$ and $\alpha > 0$. Here, $W\left(f^{(n+1)}\right)$ is defined as in (3).

Theorem 4. [21] $f : [a,b] \to R$ be an $n+1-$ times differantiable functions such that $n.th$ derivatives of f are absolutely continuous on $[\mathrm{a},\mathrm{b}]$ with $\alpha \geq 0$, for $n \in N^+$. *If* $f^{(n+1)} \in L_\infty$ $[a,b]$, i.e. $\left\|f^{(n+1)}\right\|_\infty := \sup_{t\epsilon(a,b)}\left|f^{(n+1)}(t)\right| < \infty$, then the following inequalities hold*:*

$$\left|(-1)^n J_{b-}^{\alpha} f(a) + J_{a+}^{\alpha} f(b) - \frac{2(b-a)^{n+\alpha}}{\Gamma(n+\alpha+1)} f^{(n)}(x) - \sum_{k=0}^{n-1} \frac{(b-a)^{k+\alpha}\left[(-1)^{n+k} f^{(k)}(b) + f^{(k)}(a)\right]}{\Gamma(k+\alpha+1)}\right| \quad (5)$$

$$\leq \frac{(b-x)^{n+\alpha+1} + (x-a)^{n+\alpha+1} - (b-a)^{n+\alpha+1}}{\Gamma(n+\alpha+2)}\left(\left\|f^{(n+1)}\right\|_{[a,x],\infty} + \left\|f^{(n+1)}\right\|_{[x,b],\infty}\right)$$
$$+ \frac{(b-a)^{n+\alpha}}{\Gamma(n+\alpha+1)}\left((x-a)\left\|f^{(n+1)}\right\|_{[a,x],\infty} + (b-x)\left\|f^{(n+1)}\right\|_{[x,b],\infty}\right)$$
$$\leq \left\{2\frac{(b-x)^{n+\alpha+1} + (x-a)^{n+\alpha+1} -}{\Gamma(n+\alpha+2)} + \frac{n+\alpha-1}{\Gamma(n+\alpha+2)}(b-a)^{n+\alpha+1}\right\}\left\|f^{(n+1)}\right\|_{[a,b],\infty}$$

for any $x \in [a,b]$ *and* $\alpha > 0$.

In this work, natural applications of the above inequalities (2), (4) and (5) for exponential functions are observed. That is, the results of the application of $f(t) = e^t$ function to the inequalities are given. Some special cases of these exponential inequalities are also provided.

3.APPLICATIONS

In this section, it is observed how inequalities will come out when exponantial functions are considered. For convenience, we give the following notations $A_k(x)$, $B_k(x)$ and $C_n(x)$ that will be used throughout this section in order to simplify the details of presentations. $A_k(x)$, $B_k(x)$ and $C_n(x)$ are defined by

$$A_k(x) = \frac{(x-a)^{k+\alpha}e^a + (-1)^{n+k}(b-x)^{k+\alpha}e^b}{\Gamma(k+\alpha+1)},$$

$$B_k(x) = \frac{(-1)^{n+k}(x-a)^{k+\alpha} + (b-x)^{k+\alpha}}{\Gamma(k+\alpha+1)}$$

and

$$C_n(x) = \frac{(x-a)^{n+\alpha} + (b-x)^{n+\alpha}}{\Gamma(n+\alpha+1)}.$$

We first consider the exponential mapping $f(t) = e^t$ with $t \in R$, then one possesses

$$\left\|f^{(n+1)}\right\|_{[a,x],\infty} = e^x \ , \ \left\|f^{(n+1)}\right\|_{[x,b],\infty} = e^b \text{ and } \left\|f^{(n+1)}\right\|_{[a,b],\infty} = e^b \tag{6}$$

for $a \leq x \leq b$.

In this case, by the inequalities (2) and the equalities in (6), one has the inequalities

$$\left|[1+(-1)^{n-\alpha}]e^x - \frac{e^x}{\Gamma(\alpha)}[\Gamma(\alpha, x-a) + \Gamma(\alpha, x-b)] - C_n(x)e^x - \sum_{k=0}^{n-1} A_k(x)\right| \tag{7}$$

$$\leq \frac{1}{\Gamma(n+\alpha)(n+\alpha+1)}\{(x-a)^{n+\alpha+1}e^x + (b-x)^{n+\alpha+1}e^b\}$$
$$\leq \frac{1}{(n+\alpha+1)\Gamma(n+\alpha)}W(e)$$

for any $x \in (a,b)$ and $\alpha > 0$. Here, $\Gamma(\cdot,\cdot)$ is gamma function for two variable, and $W(e)$ is defined by

$$W(e)=\begin{cases} ((x-a)^{n+\alpha+1}+(b-x)^{n+\alpha+1})e^{b} \\ \left(e^{xp}+e^{bp}\right)^{\frac{1}{p}}\left((x-a)^{(n+\alpha+1)q}+(b-x)^{(n+\alpha+1)q}\right)^{\frac{1}{q}} \\ \text{with } p,q>1 \text{ and } \dfrac{1}{p}+\dfrac{1}{q}=1 \\ \left(e^{x}+e^{b}\right)\left[\dfrac{1}{2}(b-a)+\left|x-\dfrac{a+b}{2}\right|\right]^{n+\alpha+1} \end{cases}. \tag{8}$$

If we choose $x=\frac{a+b}{2}$ in (7), then we have

$$\left|[1+(-1)^{n-\alpha}]e^{\frac{a+b}{2}}-\frac{e^{x}}{\Gamma(\alpha)}\left[\Gamma\left(\alpha,\frac{b-a}{2}\right)+\Gamma\left(\alpha,\frac{a-b}{2}\right)\right]-\sum_{k=0}^{n-1}\frac{(b-a)^{k+\alpha}[e^{a}+(-1)^{n+k}e^{b}]}{2^{k+\alpha}\Gamma(k+\alpha+1)}\right.$$

$$\left.-\frac{(b-a)^{n+\alpha}}{2^{n+\alpha-1}\Gamma(n+\alpha+1)}e^{\frac{a+b}{2}}\right|$$

$$\leq\frac{(b-a)^{n+\alpha+1}\left(e^{\frac{a+b}{2}}+e^{b}\right)}{2^{n+\alpha+1}\Gamma(n+\alpha)(n+\alpha+1)}\leq\frac{(b-a)^{n+\alpha+1}}{2^{n+\alpha}\Gamma(n+\alpha)(n+\alpha+1)}e^{b}$$

which is midpoint type fractional integral inequalities for exponential functions.

Also, considering the inequalities (4) and the equalities in (6), then one possesses

$$\left|\frac{(-1)^{n-\alpha}e^{a}}{\Gamma(\alpha)}[\Gamma(\alpha)+\Gamma(\alpha,a-x)]+\frac{e^{b}}{\Gamma(\alpha)}[\Gamma(\alpha)+\Gamma(\alpha,b-x)]-\sum_{k=0}^{n}e^{x}B_{k}(x)\right| \tag{9}$$

$$\leq\frac{e^{x}(x-a)^{n+\alpha+1}+e^{b}(b-x)^{n+\alpha+1}}{\Gamma(n+\alpha+2)}$$

$$\leq\frac{1}{\Gamma(n+\alpha+2)}W(e)$$

for $a\leq x\leq b$ and $\alpha>0$. Here, $\Gamma(\cdot,\cdot)$ is gamma function for two variable, and $W(e)$ is defined as in (8).

If we choose $x=\frac{a+b}{2}$ in (9), then we have

$$\left|\frac{(-1)^{n-\alpha}e^{a}}{\Gamma(\alpha)}\left[\Gamma(\alpha)+\Gamma\left(\alpha,\frac{a-b}{2}\right)\right]+\frac{e^{b}}{\Gamma(\alpha)}\left[\Gamma(\alpha)+\Gamma\left(\alpha,\frac{b-a}{2}\right)\right]\right.$$

$$\left.-\sum_{k=0}^{n}\frac{(b-a)^{k+\alpha}[(-1)^{n+k}e^{b}+e^{a}]}{\Gamma(k+\alpha+1)}-\frac{2(b-a)^{n+\alpha}}{\Gamma(n+\alpha+1)}e^{\frac{a+b}{2}}\right|$$

$$\leq\frac{(n+\alpha-1)2^{n+\alpha-1}+1}{2^{n+\alpha}\Gamma(n+\alpha+2)}(b-a)^{n+\alpha+1}\left(e^{\frac{a+b}{2}}+e^{b}\right)$$

$$\leq\frac{(n+\alpha-1)2^{n+\alpha-1}+1}{2^{n+\alpha-1}\Gamma(n+\alpha+2)}(b-a)^{n+\alpha+1}e^{b}$$

which is midpoint type fractional integral inequalities for exponential functions.

Finally, if we deal with the inequalities (5), then we possess the inequalities

$$\left|\frac{(-1)^{n-\alpha}e^{a}}{\Gamma(\alpha)}[\Gamma(\alpha)+\Gamma(\alpha,a-b)]+\frac{e^{b}}{\Gamma(\alpha)}[\Gamma(\alpha)+\Gamma(\alpha,b-a)]\right. \tag{10}$$

$$\left.-\frac{2(b-a)^{n+\alpha}}{\Gamma(n+\alpha+1)}e^{x}-\sum_{k=0}^{n-1}\frac{(b-a)^{k+\alpha}[(-1)^{n+k}e^{b}+e^{a}]}{\Gamma(k+\alpha+1)}\right|$$

$$\leq\frac{(b-x)^{n+\alpha+1}+(x-a)^{n+\alpha+1}-(b-a)^{n+\alpha+1}}{\Gamma(n+\alpha+2)}\left(e^{x}+e^{b}\right)$$

$$+\frac{(b-a)^{n+\alpha}}{\Gamma(n+\alpha+1)}\left((x-a)e^{x}+(b-x)e^{b}\right)$$

$$\leq\left\{2\frac{(b-x)^{n+\alpha+1}+(x-a)^{n+\alpha+1}}{\Gamma(n+\alpha+2)}+\frac{n+\alpha-1}{\Gamma(n+\alpha+2)}(b-a)^{n+\alpha+1}\right\}e^{b}$$

for $a\leq x\leq b$ and $\alpha>0$. Here, $\Gamma(\cdot,\cdot)$ is gamma function for two variable.
If we choose $x=\frac{a+b}{2}$ in (10), then we have

$$\left|\frac{(-1)^{n-\alpha}e^{a}}{\Gamma(\alpha)}[\Gamma(\alpha)+\Gamma(\alpha,a-b)]+\frac{e^{b}}{\Gamma(\alpha)}[\Gamma(\alpha)+\Gamma(\alpha,b-a)]\right.$$

$$\left.-\sum_{k=0}^{n}\frac{(b-a)^{k+\alpha}[(-1)^{n+k}+1]}{2^{k+\alpha}\Gamma(k+\alpha+1)}e^{\frac{a+b}{2}}\right|$$

$$\leq\frac{(b-a)^{n+\alpha+1}}{2^{n+\alpha+1}\Gamma(n+\alpha+2)}\left\{e^{\frac{a+b}{2}}+e^{b}\right\}$$

$$\leq\frac{(b-a)^{n+\alpha+1}}{2^{n+\alpha}\Gamma(n+\alpha+2)}e^{b}.$$

REFERENCES

1. Ostrowski, A. M., Über die absolutabweichung einer differentiebaren funktion von ihrem integralmitelwert, Commentarii Mathematici Helvetici Vol:10, 226-227, 1937.
2. Cerone, P.;Dragomir, S.S., & Roumeliotis, J., An inequality of Ostrowski type for mappings whose second derivatives are bounded and applications, RGMIA Research Report Collection, Vol:1, No:1, 35-42, 1998.
3. Cerone, P.;Dragomir, S.S., & Roumeliotis, Some Ostrowski type inequalities for n-time differentiable mappings and applications, Demonstratio Math., Vol:32, No:4, 697-712.
4. Dragomir, S. S., Cerone, P., & Roumeliotis, J. A, New generalization of Ostrowski's integral inequality for mappings whose derivatives are bounded and applications in numerical integration and for special means. RGMIA Research Report Collection, Vol:2, No:1,105-111, 1999.

5. Dragomir, S. S. and Barnett, N.S. (1998). An Ostrowski type inequality for mappings whose second derivatives are bounded and applications. RGMIA Research Report Collection, Vol:1, No:2, 67-75, 1998.
6. Sarikaya, M. Z., On the Ostrowski type integral inequality. Acta Math. Univ. Comenianae, Vol:LXXIX, No:1, 129-134, 2010.
7. Sarikaya, M. Z. & Set, E., On new Ostrowski type Integral inequalities. Thai Journal of Mathematics, Vol:12, No:1, 145-154, 2014.
8. Wang M. & Zhao, X., Ostrowski type inequalities for higher-order derivatives. Journal of Inequalities and Applications, Article ID 162689, 1-8, 2009.
9. Sofo, A., Integral inequalities for n- times differentiable mappings, with multiple branches,on the L_p norm, Soochow Journal of Mathematics, Vol: 28, No:2, 179-221, 2002.
10. Budak, H.; Sarikaya, M. Z., & Erden, S., New weighted Ostrowski type inequalities for mappings whose nth derivatives are of bounded variation. International J. of Analysis and App., Vol:12, No:1, 71-79, 2016.
11. Dragomir, S. S., Approximating real functions which possess nth derivatives of bounded variation and applications. Computers and Mathematics with Applications, Vol:56, 2268—2278, 2008.
12. Kashif, A. R., Shoaib, M., & Latif, M. A., Improved version of perturbed Ostrowski type inequalities for n-times differentiable mappings with three-step kernel and its application. J. Nonlinear Sci. Appl, Vol:9, 3319-3332, 2016.
13. Qayyum, A., Shoaib, M., & Erden, S., Generalized fractional Ostrowski type inequality for higher order derivatives. New Trends in Mathematical Sciences (NTMSCI), Vol:4, No:2, 111-124, 2019.
14. Dragomir, S. S., Ostrowski type inequalities for generalized Riemann Liouville fractional integrals of bounded variation. Hölder and Lipschitzian functions. RGMIA Research Report Collection, Vol:20, 1-14, 2017.
15. Dragomir, S. S., Ostrowski Type inequalities for riemann-Liouville fractional integrals of absolutely continuous functions in terms of norms. RGMIA Research Report Collection, Vol:20, Article 49, 1-14, 2017.
16. Dragomir, S. S., Ostrowski Type inequalities for riemann-Liouville fractional integrals of absolutely continuous functions in terms of norms. RGMIA Research Report Collection, Vol:20, Article 50, 2017.
17. Erden, S., Budak, H., & Sarikaya, M. Z., Fractional Ostrowski type inequalities for functions of bounded variaton with two variables. Miskolc Mathematical Notes, Vol:21, No:1, 171-188, 2020.

18. Erden, S., Budak, H., Sarikaya, M. Z., Iftikhar, S., & Kumam, P., Fractional Ostrowski type inequalities for bounded functions. Journal of Inequalities and Applications, Vol:123, 1-11, 2020.

19. Aglić Aljinović, A., Montgomery identity and Ostrowski type inequalities for Riemann-Liouville fractional integral. Journal of Mathematics, Article ID 503195, 1-6, 2014.

20. Farid, G. , Some new Ostrowski type inequalities via fractional integrals. International Journal of Analysis and Applications, Vol:14, No:1, 64-68, 2017.

21. Erden, S., Gokkurt Ozdemir, B. and Alkan, S., Riemann-Liouville Fractional integral inequalities for bounded functions and Applications, Submitted, 2023.

SEVERAL INTEGRAL REPRESENTAIONS OF THE $p-k$ SRIVASTAVA'S TRIPLE HYPERGEOMETRIC FUNCTIONS

Zekiye Rana Lüsna[1] , Ali Olgun[2] , Oğuz Yağcı[3]

[1] Department of Mathematics, Kırıkkale University, Kırıkkale, Türkiye

[1]zekiyelusna@gmail.com, [2]aliolgun71@gmail.com, [3]oguzyagci@gmail.com

Abstract

This paper introduces newly ${}_pH_{A,k}$, ${}_pH_{B,k}$, and ${}_pH_{C,k}$ Srivastava's triple hypergeometric function using *p-k* Pochhammer symbol. We also present relationship between *p-k* Srivastava's triple hypergeometric functions and classical Srivastava's triple hypergeometric functions. Then, we obtain some properties of the *p-k* Srivastava's triple hypergeometric functions such as integral representations and recurrence formulas.

Keywords: Srivastava hypergeometric funtion, integral representations, derivative formula, recurrence relations.

1.INTRODUCTION

Throughout this paper, we use the notations

$$\mathbb{N}_0 = \{0,1,2,\dots\} \;\; and \;\; \mathbb{N} = \{1,2,3,\dots\}.$$

The classical gamma function can be defined [1,9,12] by

$$\Gamma(z) = \int_0^1 t^{z-1} \; exp(-t) \; dt \,, \;\; \Re(z) > 0.$$

For $\alpha \in \mathbb{C}$ and $n \in \mathbb{Z}/\ \mathbb{Z}^-$, the Pochhammer symbol $(\alpha)_n$ is defined by

$$(\alpha)_n = \alpha\,(\alpha+1)\,(\alpha+2)\dots(\alpha+n-1)$$

The Pochhammer symbol $(\alpha)_n$ is also known as the rising factorial, see [16,17,18,19,20] and closely related references therein.

For $x \in \mathbb{C};\ k, p \in \mathbb{R}^+ - \{0\}$ and $\mathbb{R}\ (x) > 0,\ n \in \mathbb{N}$, the *p-k* Gamma function was defined [14] as

$${}_p\Gamma_k\,(x) = \frac{1}{k} \lim_{n\to\infty} \frac{n!\, p^{n+1} (np)^{\frac{x}{k}}}{{}_p(x)_{n+1,k}} \tag{1.1}$$

or

$$ {}_p\Gamma_k\,(x) = \frac{1}{k}\lim_{n\to\infty}\frac{n!\,p^{n+1}(np)^{\frac{x}{k}-1}}{{}_p(x)_{n,k}}\,. \tag{1.2}$$

Lemma 1. The relation between *p-k* Gamma function, k- Gamma function and classical Gamma function is given by,

$$ {}_p\,\Gamma_k(x) = \left(\frac{p}{k}\right)^{\frac{x}{k}}\Gamma_k(x) \tag{1.3}$$

and

$$ {}_p\,\Gamma_k\,(x) = \frac{p^{\frac{x}{k}}}{k}\Gamma\left(\frac{x}{k}\right) \tag{1.4}$$

Also, for $x\in\mathbb{C}$; $k,p\in\mathbb{R}^{+}$-$\{0\}$ and $\mathbb{R}(x)>0$, $n\in\mathbb{N}$, Gehlot [14] presents the *p-k* Pochhammer symbol, ${}_p\,(x)_{\,n,k}$ is given by

$$ {}_p\,(x)_{\,n,k} = \left(\frac{xp}{k}\right)\left(\frac{xp}{k}+p\right)\left(\frac{xp}{k}+2p\right)\ldots\left(\frac{xp}{k}+(n-1)p\right). \tag{1.5}$$

Lemma 2. For $x\in\mathbb{C}$, $k\in\mathbb{Z}^{-}$; $n\in\mathbb{N}$;$k,p\in\mathbb{R}^{+}$ and $\mathbb{R}(x)>0$, then the relation between *p-k* Pochhammer symbol, *k*- Pochhammer symbol and classical Pochhammer symbol is given by [14],

$$ {}_p\,(x)_{\,n,k} = \left(\frac{p}{k}\right)^{n}(x)_{n,k}\ , \tag{1.6}$$

$$ {}_p\,(x)_{\,n,k} = p^{n}\left(\frac{x}{k}\right)_{n}\ . \tag{1.7}$$

Then, *p-k* Beta function ${}_pB_k(x,y)$ is given by

$$ {}_pB_k(x,y) = \frac{{}_p\Gamma_k\,(x)\ {}_p\Gamma_k\,(y)}{{}_p\Gamma_k\,(x+y)};\ \ \mathbb{R}(x)>0,\ \ \mathbb{R}(y)>0. \tag{1.8}$$

The main aim of this paper is to introduce ${}_pH_{A,k}$, ${}_pH_{B,k}$, and ${}_pH_{C,k}$ Srivastava's triple hypergeometric function by using Pochhammer symbol defined (1.5). A great number of extensions of Pochhammer symbol are available in the literature [21,22,23,24,25]. The paper is organized as follows: In Sec. (2), we introduce ${}_pH_{A,k}$, ${}_pH_{B,k}$, and ${}_pH_{C,k}$ Srivastava's triple hypergeometric function. In Sec. (3), integral representations for ${}_pH_{A,k}$, ${}_pH_{B,k}$, and ${}_pH_{C,k}$ are given. In Sec. (4), recurrence relations for ${}_pH_{A,k}$ is presented.

2. $p-k$ SRIVASTAVA HYPERGEOMETRİC FUNCTIONS

For $p,k\in\mathbb{R}^{+}$ is $r_1:=p|x|, r_2:=p|y|, r_3:=p|z|$; $\gamma,\delta_{\tau}\in\mathbb{C}$ for $\tau=1,2$, and $\nu_{\kappa}\in\mathbb{C}\setminus\mathbb{Z}_0$ for $\kappa=1,2,3$ we define

$$ {}_pH_{A,k}\,(\gamma,\delta_1,\delta_2\,;v_1,v_2\,;\;x,y,z)=\sum_{m,n,s=0}^{\infty}\frac{{}_p(\gamma)_{m+s,k}\;\;{}_p(\delta_1)_{m+n,k}\;\;\;{}_p(\delta_2)_{n+s,k}}{{}_p(v_1)_{m,k}\;\;\;{}_p(v_2)_{n+s,k}}\frac{x^m}{m!}\frac{y^n}{n!}\frac{z^s}{s!} $$

$(r_1 <1 ,\ r_2 <1 ,\ r_3 < (1-r_1)\,(1-r_2)\,)$, (2.1)

$$ {}_pH_{B,k}\,(\gamma,\delta_1,\delta_2\,;v_1,v_2,v_3\,;x,y,z)\;=\sum_{m,n,s=0}^{\infty}\frac{{}_p(\gamma)_{m+s,k}\;\;{}_p(\delta_1)_{m+n,k}\;\;\;{}_p(\delta_2)_{n+s,k}}{{}_p(v_1)_{m,k}\;\;\;{}_p(v_2)_{n,k}\;\;\;{}_p(v_3)_{s,k}}\frac{x^m}{m!}\frac{y^n}{n!}\frac{z^s}{s!} $$

$(r_1 + r_2 + r_3 + 2\sqrt{r_1\,r_2\,r_3} < 1)$ (2.2)

and

$$ {}_pH_{C,k}\,(\gamma,\delta_1,\delta_2;v\,;x,y,z)\;=\sum_{m,n,s=0}^{\infty}\frac{{}_p(\gamma)_{m+s,k}\;\;{}_p(\delta_1)_{m+n,k}\;\;\;{}_p(\delta_2)_{n+s,k}}{{}_p(v)_{m+n+s,k}}\frac{x^m}{m!}\frac{y^n}{n!}\frac{z^s}{s!} $$

$(r_1 <1 ,\ r_2 <1 ,\ r_3 < 1,\ r_1 + r_2 + r_3 - 2\sqrt{(1-r_1)\,(1-r_2)\,\,(1-r_3)} < 2)$. (2.3)

Now, taking advantage of the Pochhammer symbol relation (1.7) for the *p-k* Srivastava hypergeometric functions (2.1) - (2.3), we obtain following identities:

$${}_pH_{A,k}\,(\gamma,\delta_1,\delta_2\,;v_1,v_2\,;x,y,z)=H_A\,(\tfrac{\gamma}{k},\tfrac{\delta_1}{k},\tfrac{\delta_2}{k}\,;\tfrac{v_1}{k},\tfrac{v_2}{k}\,;px,py,pz)\,, \tag{2.4}$$

$${}_pH_{B,k}\,(\gamma,\delta_1,\delta_2\,;v_1,v_2,v_3\,;x,y,z)=H_B\,(\tfrac{\gamma}{k},\tfrac{\delta_1}{k},\tfrac{\delta_2}{k};\tfrac{v_1}{k},\tfrac{v_2}{k},\tfrac{v_3}{k};px,py,pz) \tag{2.5}$$

and

$${}_pH_{C,k}\,(\gamma,\delta_1,\delta_2\,;v\,;x,y,z)=H_C\,(\tfrac{\gamma}{k},\tfrac{\delta_1}{k},\tfrac{\delta_2}{k}\,;\tfrac{v}{k}\,;px,py,pz)\,. \tag{2.6}$$

Also, using of the Pochhammer symbol relation (1.6) for the *p-k* Srivastava hypergeometric functions (2.1) - (2.3), we have following identities

$${}_pH_{A,k}\,(\gamma,\delta_1,\delta_2\,;v_1,v_2\,;x,y,z)=H_{A,k}\,(\gamma,\delta_1,\delta_2\,;v_1,v_2\,;\tfrac{px}{k},\tfrac{py}{k},\tfrac{pz}{k})\,, \tag{2.7}$$

$${}_pH_{B,k}\,(\gamma,\delta_1,\delta_2\,;v_1,v_2,v_3\,;x,y,z)=H_{B,k}\,(\gamma,\delta_1,\delta_2\,;v_1,v_2,v_3\,;\tfrac{px}{k},\tfrac{py}{k},\tfrac{pz}{k}) \tag{2.8}$$

and

$${}_pH_{C,k}\,(\gamma,\delta_1,\delta_2\,;v\,;x,y,z)=H_{C,k}\,(\gamma,\delta_1,\delta_2\,;v\,;\tfrac{px}{k},\tfrac{py}{k},\tfrac{pz}{k})\,. \tag{2.9}$$

For, *p-k* Gauss hypergeometric function, where $k,\ p \in \mathbb{R}^+,\ \alpha,\ \beta,\ v \in \mathbb{C}$ and $v\neq 0$, we have the following equation:

$$ {}_pF_k(\,\alpha,\beta;\;v;\;x\,)=\sum_{n=0}^{\infty}\frac{{}_p(\alpha)_{n,k}\;{}_p(\beta)_{n,k}}{{}_p(v)_{n,k}}\frac{x^n}{n!} $$

$$\left(|x| < \frac{1}{p}\right). \tag{2.10}$$

Then, using the (1.5) in the equation (2.10), we have the following integral representation of the *p-k* Gauss hypergeometric function as follow:

$$ {}_pF_k(\alpha,\beta;\ v;\ x) = \frac{{}_p\Gamma_k(v)}{k\ {}_p\Gamma_k(\beta)\ {}_p\Gamma_k(v-\beta)} \tag{2.11}$$

$$\times \int_0^1 t^{\frac{\beta}{k}-1}\ (1-t)^{\frac{v-\beta}{k}-1}\ (1-pxt)^{-\frac{\alpha}{k}}\ dt\,,$$

Besides, taking consideration of the (1.4) in the *p-k* Gauss hypergeometric function (2.10) , we have

$$ {}_pF_k(\alpha,\beta;v;x) = F\left(\frac{\alpha}{k},\frac{\beta}{k};\frac{v}{k};px\right). \tag{2.12}$$

3. INTEGRAL REPRESENTATIONS FOR ${}_pH_{A,k}$, ${}_pH_{B,k}$, AND ${}_pH_{C,k}$

This section presents integral representations for ${}_pH_{A,k}$, ${}_pH_{B,k}$, and ${}_pH_{C,k}$ Srivastava's triple hypergeometric functions.

Theorem 1. ${}_pH_{A,k}$ $p-k$ Srivastava hypergeometric function has the following integral representations.

$$ {}_pH_{A,k}(\gamma,\delta_1,\delta_2;v_1\ v_2;x,y,z) = \frac{{}_p\Gamma_k(v_1)\ {}_p\Gamma_k(v_2)}{k^2\ {}_p\Gamma_k(\delta_1)\ {}_p\Gamma_k(\delta_2)\ {}_p\Gamma_k(v_1-\delta_1)\ {}_p\Gamma_k(v_2-\delta_2)}$$

$$\times \int_0^1\int_0^1 \xi^{\frac{\delta_1}{k}-1}\ \eta^{\frac{\delta_2}{k}-1}(1-\xi)^{\frac{v_1-\delta_1}{k}-1}\ (1-\eta)^{\frac{v_2-\delta_2}{k}-1}\ (1-py\eta)^{-\frac{\delta_1}{k}}$$

$$\times\ (1-px\xi-pz\eta)^{-\frac{\gamma}{k}}(1-pz\eta)^{-\frac{\delta_1}{k}}\left(1-\frac{p^2xy\xi\eta}{(1-py\eta)\ (1-px\xi-pz\eta)}\right)^{-\frac{\gamma}{k}} d\xi\ d\eta \tag{3.1}$$

$$(\mathbb{R}(v_1) > \mathbb{R}(\delta_1) > 0\,,\ \mathbb{R}(v_2) > \mathbb{R}(\delta_2) > 0)\,,$$

$$ {}_pH_{A,k}(\gamma,\delta_1,\delta_2;v_1,v_2;x,y,z) = \frac{{}_p\Gamma_k(v_2)}{k^2\ {}_p\Gamma_k(\delta_2)\ {}_p\Gamma_k(v_2-\delta_2)}$$

$$\times \int_0^1 \xi^{\frac{\delta_2}{k}-1}\ (1-\xi)^{\frac{v_2-\delta_2}{k}-1}\ (1-py\xi)^{-\frac{\delta_1}{k}}\ (1-pz\xi)^{-\frac{\gamma}{k}}$$

$$\times\ {}_pF_k\left(\gamma,\delta_1;v_1;\frac{x}{(1-py\xi)\ (1-pz\xi)}\right)d\xi \tag{3.2}$$

$$(\mathbb{R}(v_2) > \mathbb{R}(\delta_2) > 0)\,,$$

$$ {}_pH_{A,k}(\gamma,\delta_1,\delta_2;v_1,v_2;x,y,z) = \frac{{}_p\Gamma_k\,(v_2)\ (1+\lambda)^{\frac{\delta_2}{k}}}{k\ {}_p\Gamma_k\,(\delta_2)\ {}_p\Gamma_k\,(v_2-\delta_2)} $$

$$ \times \int_0^1 \xi^{\frac{\delta_2}{k}-1}\ (1-\xi)^{\frac{v_2-\delta_2}{k}-1}\ (1+\lambda\xi)^{\frac{\gamma+\delta_1-v_2}{k}}\ (1+\lambda\xi-(1+\lambda)py\xi)^{-\frac{\delta_1}{k}} $$

$$ \times\ {}_pF_k\left(\gamma,\delta_1;v_1;\frac{x(1+\lambda\xi)^2}{(1+\lambda\xi-(1+\lambda)py\xi)\ (1+\lambda\xi-(1+\lambda)pz\xi)}\right)d\xi \tag{3.3} $$

$$ (\mathbb{R}(v_2) > \mathbb{R}(\delta_2) > 0;\ \lambda > -1)\,, $$

$$ {}_pH_{A,k}(\gamma,\delta_1,\delta_2;v_1,\ v_2;x,y,z) = \frac{{}_p\Gamma_k\,(v_2)}{k\ {}_p\Gamma_k\,(\delta_2)\ {}_p\Gamma_k\,(v_2-\delta_2)} $$

$$ \times \int_0^1 \xi^{\frac{\delta_2}{k}-1}\ (1+\xi)^{\frac{\gamma+\delta_1-v_2}{k}}\ (1+\xi-py\xi)^{-\frac{\delta_1}{k}}\ (1+\xi-pz\xi)^{-\frac{\gamma}{k}} $$

$$ \times\ {}_pF_k\left(\gamma,\delta_1;v_1;\frac{x(1+\xi)^2}{(1+\xi-py\xi)\ (1+\xi-pz\xi)}\right)d\xi \tag{3.4} $$

$$ (\mathbb{R}(v_2) > \mathbb{R}(\delta_2) > 0)\,, $$

$$ {}_pH_{A,k}(\gamma,\delta_1,\delta_2;v_1,v_2;x,y,z) = \frac{{}_p\Gamma_k\,(v_2)}{k\ {}_p\Gamma_k\,(\delta_2)\ {}_p\Gamma_k\,(v_2-\delta_2)}\frac{(b-c)^{\frac{\delta_2}{k}}(a-c)^{\frac{v_2-\delta_2}{k}}}{(b-a)^{\frac{v_2-\gamma-\delta_1}{k}-1}} $$

$$ \times \int_a^b (b-\xi)^{\frac{v_2-\delta_2}{k}-1}\ (\xi-a)^{\frac{\delta_2}{k}-1}\ (\xi-c)^{\frac{\gamma+\delta_1-v_2}{k}}\ [(b-a)\,(\xi-c)-(b-c)\,(\xi-a)\,py]^{-\frac{\delta_1}{k}} $$

$$ \times [(b-a)\,(\xi-c)-(b-c)\,(\xi-a)\,pz]^{-\frac{\gamma}{k}}\,{}_pF_k(\gamma,\delta_1;v_1;x\sigma)d\xi $$

$$ (\mathbb{R}(v_2) > \mathbb{R}(\delta_2) > 0\,;c < a < b\,) \tag{3.5} $$

$$ \sigma := \frac{(b-a)^2\,(\xi-c)^2}{[(b-a)\,(\xi-c)-(b-c)\,(\xi-a)\,py]\,[(b-a)\,(\xi-c)-(b-c)\,(\xi-a)\,pz]}\,, $$

$$ {}_pH_{A,k}(\gamma,\delta_1,\delta_2;v_1,v_2;x,y,z) = \frac{{}_p\Gamma_k\,(v_2)}{k\,{}_p\Gamma_k\,(\delta_2)\,{}_p\Gamma_k\,(v_2-\delta_2)}\int_0^{\pi/2} (\sin^2\xi)^{\frac{\delta_2}{k}-\frac{1}{2}}\ (\cos^2\xi)^{\frac{v_2+\delta_2}{k}-\frac{1}{2}} $$

$$ \times (1-py\sin^2\xi)^{-\frac{\delta_2}{k}}(1-pz\sin^2\xi)^{-\frac{\gamma}{k}}\,{}_pF_k\left(\gamma,\delta_1;v_1;\frac{x}{(1-py\sin^2\xi)\ (1-pz\sin^2\xi)}\right)d\xi \tag{3.6} $$

$$ (\mathbb{R}(v_2) > \mathbb{R}(\delta_2) > 0)\,. $$

Here, ${}_pF_k$ is the *p-k* Gauss hypergeometric function (2.11) .

Proof. Using the (2.4) , and taking consideration of the integral representation of the classical Srivastava hypergeometric function H_A , we get

$$ {}_pH_{A,k}\ (\gamma,\ \delta_1,\ \delta_2\ ;\ v_1, v_2\ ;\ x, y, z) = H_A\ \left(\frac{\gamma}{k}, \frac{\delta_1}{k}, \frac{\delta_2}{k}\ ;\ \frac{v_1}{k}, \frac{v_2}{k}\ ;\ px, py, pz\right) $$

$$ = \frac{\Gamma\left(\frac{v_1}{k}\right)\ \Gamma\left(\frac{v_2}{k}\right)}{\Gamma\left(\frac{\delta_1}{k}\right)\Gamma\left(\frac{\delta_2}{k}\right)\Gamma\left(\frac{v_1-\delta_1}{k}\right)\Gamma\left(\frac{v_2-\delta_2}{k}\right)}\int_0^1\int_0^1 \xi^{\frac{\delta_1}{k}-1}\ \eta^{\frac{\delta_2}{k}-1}\ (1-\xi)^{\frac{v_1-\delta_1}{k}-1} $$

$$ \times (1-\eta)^{\frac{v_2-\delta_2}{k}-1}\ (1-py\eta)^{-\frac{\delta_1}{k}} $$

$$ \times\ (1-px\xi-pz\eta)^{-\frac{\gamma}{k}}(1-pz\eta)^{-\frac{\delta_1}{k}}\left(1-\frac{p^2xy\xi\eta}{(1-py\eta)\ (1-px\xi-pz\eta)}\right)^{-\frac{\gamma}{k}} d\xi\ d\eta $$

$$ = \frac{\frac{k}{p^{v_1/k}}\ {}_p\Gamma_k\ (v_1)\ \frac{k}{p^{v_2/k}}\ {}_p\Gamma_k\ (v_2)}{\frac{k}{p^{\delta_1/k}}\ {}_p\Gamma_k\ (\delta_1)\ \frac{k}{p^{\delta_2/k}}\ {}_p\Gamma_k\ (\delta_2)\ \frac{k}{p^{v_1-\delta_1/k}}\ {}_p\Gamma_k\ (v_1-\delta_1)\ \frac{k}{p^{v_2-\delta_2/k}}\ {}_p\Gamma_k\ (v_2-\delta_2)} $$

$$ \times\int_0^1\int_0^1 \xi^{\frac{\delta_1}{k}-1}\ \eta^{\frac{\delta_2}{k}-1}\ (1-\xi)^{\frac{v_1-\delta_1}{k}-1}\ \ (1-\eta)^{\frac{v_2-\delta_2}{k}-1}\ (1-py\eta)^{-\frac{\delta_1}{k}} $$

$$ \times\ (1-px\xi-pz\eta)^{-\frac{\gamma}{k}}(1-pz\eta)^{-\frac{\delta_1}{k}}\left(1-\frac{p^2xy\xi\eta}{(1-py\eta)\ (1-px\xi-pz\eta)}\right)^{-\frac{\gamma}{k}} d\xi\ d\eta $$

$$ = \frac{{}_p\Gamma_k\ (v_1)\ \ {}_p\Gamma_k\ (v_2)}{k^2\ \ {}_p\Gamma_k\ (\delta_1)\ {}_p\Gamma_k\ (\delta_2)\ {}_p\Gamma_k\ (v_1-\delta_1)\ \ {}_p\Gamma_k\ (v_2-\delta_2)} $$

$$ \times\int_0^1\int_0^1 \xi^{\frac{\delta_1}{k}-1}\ \eta^{\frac{\delta_2}{k}-1}\ (1-\xi)^{\frac{v_1-\delta_1}{k}-1}\ \ (1-\eta)^{\frac{v_2-\delta_2}{k}-1}\ (1-py\eta)^{-\frac{\delta_1}{k}} $$

$$ \times\ (1-px\xi-pz\eta)^{-\frac{\gamma}{k}}(1-pz\eta)^{-\frac{\delta_1}{k}}\left(1-\frac{p^2xy\xi\eta}{(1-py\eta)\ (1-px\xi-pz\eta)}\right)^{-\frac{\gamma}{k}} d\xi\ d\eta $$

Using same methodology, (3.2) – (3.6) can be yielded desired results.

Theorem 2. ${}_pH_{B,k}$ $p-k$ Srivastava hypergeometric function has the following integral representations.

$$ {}_pH_{B,k}\ (\gamma, \delta_1, \delta_2\ ; v_1, v_2, v_3\ ; x, y, z) = \frac{{}_p\Gamma_k\ (\gamma+\delta_1)}{k\ \ {}_p\Gamma_k\ (\gamma)\ \ {}_p\Gamma_k\ (\delta_1)}\int_0^1 \xi^{\frac{\gamma}{k}-1}\ \ (1-\xi)^{\frac{\delta_1}{k}-1} $$

$$ \times\ {}_pX_{4,k}\ (\gamma+\delta_1,\ \delta_2;\ v_1, v_2, v_3\ ; x\xi(1-\xi), y(1-\xi), z\xi)\ \ d\xi\ , \tag{3.7} $$

$$ (\min\{\mathbb{R}(\gamma), \mathbb{R}(\delta_1)\} > 0), $$

$$ {}_{p}H_{B,k}\,(\gamma,\delta_1,\delta_2\,;v_1,v_2,v_3\,;x,y,z)=\frac{{}_{p}\Gamma_k\,(\gamma+\delta_1)}{k\;{}_{p}\Gamma_k\,(\gamma)\;{}_{p}\Gamma_k\,(\delta_1)}\frac{(b-c)^{\frac{\gamma}{k}}\,(a-c)^{\frac{\delta_1}{k}}}{(b-a)^{\frac{\gamma+\delta_1-1}{k}}} $$

$$ \times\int_a^b (b-\xi)^{\frac{\delta_1}{k}-1}\;(\xi-a)^{\frac{\gamma}{k}-1}\;(\xi-c)^{\frac{-\gamma-\delta_1}{k}}\;{}_{p}X_{4,k}\,(\gamma+\delta_1,\;\delta_2;\;v_1,v_2,v_3\,;x\sigma_1,y\sigma_2,z\sigma_3)\;d\xi $$

$$ (\min\{\mathbb{R}(\gamma),\mathbb{R}(\delta_1)\}>0\,;\;c<a<b) \tag{3.8} $$

$$ \sigma_1:=\frac{(a-c)\,(b-c)\,(\xi-a)\,(b-\xi)}{(b-a)^2\,(\xi-c)^2},\sigma_2:=\frac{(a-c)\,(b-\xi)}{(b-a)\,(\xi-c)},\sigma_3:=\frac{(b-c)\,(\xi-a)}{(b-a)\,(\xi-c)}, $$

$$ {}_{p}H_{B,k}\,(\gamma,\delta_1,\delta_2\,;v_1,v_2,v_3\,;x,y,z)=\frac{2\,{}_{p}\Gamma_k\,(\gamma+\delta_1)}{k\;{}_{p}\Gamma_k\,(\gamma)\;{}_{p}\Gamma_k\,(\delta_1)}\int_0^{\pi/2}(sin^2\,\xi)^{\frac{\gamma}{k}-\frac{1}{2}}\;(cos^2\,\xi)^{\frac{\delta_1}{k}-\frac{1}{2}} $$

$$ \times\;{}_{p}X_{4,k}\,(\gamma+\delta_1,\;\delta_2;\;v_1,v_2,v_3\,;x\sigma_1,y\sigma_2,z\sigma_3)\;d\xi \tag{3.9} $$

$$ (\min\{\mathbb{R}(\gamma),\mathbb{R}(\delta_1)\}>0) $$

$$ \sigma_1:=sin^2\,\xi\;\;cos^2\,\xi\,,\sigma_2:=cos^2\,\xi\;\;,\sigma_3:=sin^2\,\xi\;, $$

$$ {}_{p}H_{B,k}\,(\gamma,\delta_1,\delta_2\,;v_1,v_2,v_3\,;x,y,z)=\frac{2\,{}_{p}\Gamma_k\,(\gamma+\delta_1)\;(1+\lambda)^{\frac{\gamma}{k}}}{k\;{}_{p}\Gamma_k\,(\gamma)\;{}_{p}\Gamma_k\,(\delta_1)}\int_0^{\pi/2}\frac{(sin^2\,\xi)^{\frac{\gamma}{k}-\frac{1}{2}}\;(cos^2\,\xi)^{\frac{\delta_1}{k}-\frac{1}{2}}}{(1+\lambda\,sin^2\,\xi)^{\gamma+\delta_1/k}} $$

$$ \times\;{}_{p}X_{4,k}\,(\gamma+\delta_1,\;\delta_2;\;v_1,v_2,v_3\,;x\sigma_1,y\sigma_2,z\sigma_3)\;d\xi \tag{3.10} $$

$$ (\min\{\mathbb{R}(\gamma),\mathbb{R}(\delta_1)\}>0;\;\lambda>-1) $$

$$ \sigma_1:=\frac{(1+\lambda)\,sin^2\,\xi\;\;cos^2\,\xi}{(1+\lambda\;sin^2\,\xi)^2},\sigma_2:=\frac{cos^2\,\xi}{1+\lambda\;sin^2\,\xi},\sigma_3:=\frac{(1+\lambda)\;sin^2\,\xi}{1+\lambda\;sin^2\,\xi}, $$

$$ {}_{p}H_{B,k}\,(\gamma,\delta_1,\delta_2\,;v_1,v_2,v_3\,;x,y,z)=\frac{2\,{}_{p}\Gamma_k\,(\gamma+\delta_1)\;\lambda^{\frac{\gamma}{k}}}{k\;{}_{p}\Gamma_k\,(\gamma)\;{}_{p}\Gamma_k\,(\delta_1)}\int_0^{\pi/2}\frac{(sin^2\,\xi)^{\frac{\gamma}{k}-\frac{1}{2}}\;(cos^2\,\xi)^{\frac{\delta_1}{k}-\frac{1}{2}}}{(cos^2\,\xi+\lambda\,sin^2\,\xi)^{\gamma+\delta_1/k}} $$

$$ \times\;{}_{p}X_{4,k}\,(\gamma+\delta_1,\;\delta_2;\;v_1,v_2,v_3\,;x\sigma_1,y\sigma_2,z\sigma_3)\;d\xi \tag{3.11} $$

$$ (\min\{\mathbb{R}(\gamma),\mathbb{R}(\delta_1)\}>0;\;\lambda>-1) $$

$$ \sigma_1:=\frac{\lambda\,sin^2\,\xi\;\;cos^2\,\xi}{(cos^2\,\xi+\lambda\;sin^2\,\xi)^2},\sigma_2:=\frac{cos^2\,\xi}{cos^2\,\xi+\lambda\;sin^2\,\xi},\sigma_3:=\frac{\lambda\;sin^2\,\xi}{cos^2\,\xi+\lambda\;sin^2\,\xi}\;. $$

Where, ${}_{p}X_{4,k}$ is the *p-k* generalization of the Exton hypergeometric function as follow:

$$ {}_{p}X_{4,k}\,(\alpha,\beta;v_1,v_2,v_3;x,y,z)\;=\sum_{m,n,s=0}^{\infty}\frac{{}_{p}(\alpha)_{2m+n+s,k}\;\;{}_{p}(\beta)_{n+s,k}}{{}_{p}(v_1)_{m,k}\;\;{}_{p}(v_2)_{n,k}\;\;{}_{p}(v_3)_{s,k}}\frac{x^m}{m!}\frac{y^n}{n!}\frac{z^s}{s!} $$

Proof. The proof of Theorem 2 is similar to the proof of Theorem 1. The details are omitted.

Theorem 3. ${}_pH_{C,k}$ $p-k$ Srivastava hypergeometric function has the following integral representations.

$$ {}_pH_{C,k}(\gamma,\delta_1,\delta_2;v;x,y,z)=\frac{{}_p\Gamma_k\,(v)}{k\ {}_p\Gamma_k\,(\gamma)\ {}_p\Gamma_k\,(\delta_1)\ {}_p\Gamma_k\,(v-\gamma-\delta_1)} $$

$$ \times\int_0^1\int_0^1 \xi^{\frac{\gamma}{k}-1}\ \eta^{\frac{\delta_1}{k}-1}\ \ (1-\xi)^{\frac{v-\gamma}{k}-1}\,(1-\eta)^{\frac{v-\gamma-\delta_1}{k}-1}\,(1-px\xi)^{\frac{\delta_2-\delta_1}{k}} $$

$$ \times\ (1-px\xi-py\eta-pz\xi+py\xi\eta+p^2xz\xi^2)^{-\frac{\delta_2}{k}}\,d\xi \tag{3.12} $$

$$ (\min\{\mathbb{R}(\gamma),\mathbb{R}(\delta_1),\mathbb{R}(v-\gamma-\delta_1)\}>0)\,, $$

$$ {}_pH_{C,k}(\gamma,\delta_1,\delta_2;v;x,y,z)=\frac{{}_p\Gamma_k\,(v)}{k\ {}_p\Gamma_k\,(\gamma)\ {}_p\Gamma_k\,(v-\gamma)} $$

$$ \times\int_0^1 \xi^{\frac{\gamma}{k}-1}\ \eta^{\frac{\delta_1}{k}-1}\ \ (1-\xi)^{\frac{v-\gamma}{k}-1}(1-\eta)^{\frac{v-\gamma-\delta_1}{k}-1} $$

$$ \times\,(1-px\xi)^{\frac{\delta_2-\delta_1}{k}}(1-px\xi-py\eta-pz\xi+py\xi\eta+p^2xz\xi^2)^{-\frac{\delta_2}{k}}\,d\xi \tag{3.13} $$

$$ (\mathbb{R}(v)>\mathbb{R}(\gamma)>0)\,, $$

$$ {}_pH_{C,k}(\gamma,\delta_1,\delta_2;v;x,y,z)=\frac{{}_p\Gamma_k\,(v)}{k^2\ \ {}_p\Gamma_k\,(\gamma)\ {}_p\Gamma_k\,(\delta_1)\ {}_p\Gamma_k\,(\delta_2)} $$

$$ \times\int_0^1\int_0^1 \xi^{\frac{\gamma}{k}-1}\ \eta^{\frac{\gamma+\delta_1}{k}-1}\ \ (1-\xi)^{\frac{\delta_1}{k}-1}\,(1-\eta)^{\frac{\delta_2}{k}-1}\,(1-px\xi)^{\frac{\delta_2-\delta_1}{k}} $$

$$ \times\ {}_pF_k\left(\frac{\gamma+\delta_1+\delta_2}{2},\frac{\gamma+\delta_1+\delta_2+1}{2};v;\ \Xi\,(\xi,\eta\,;\mathrm{x,y,z})\right)d\eta\,d\xi \tag{3.14} $$

$$ (\min\{\mathbb{R}(\gamma),\mathbb{R}(\delta_1),\mathbb{R}(\delta_2)\}>0) $$

$$ \Xi\,(\xi,\eta\,;\mathrm{x,y,z}):=4\eta\,[px\xi\,(1-\xi)\eta+py\,(1-\xi)\,(1-\eta)+pz\xi\,(1-\eta)]\,, $$

$$ {}_pH_{C,k}(\gamma,\delta_1,\delta_2;v;x,y,z)=\frac{{}_p\Gamma_k\,(v)\ \ (1+\lambda)^{\frac{\gamma}{k}}}{k\ {}_p\Gamma_k\,(\gamma)\ {}_p\Gamma_k\,(v-\gamma)}\int_0^1 \xi^{\frac{\gamma}{k}-1}\ \ (1-\xi)^{\frac{v-\gamma}{k}-1} $$

$$ \times\ \ (1+\lambda\xi)^{\frac{\delta_1+\delta_2-v}{k}}\ {}_pF_k\left(\delta_1,\delta_2;v-\gamma;\frac{y\ \ (1+\lambda\xi)\ \ (1-\xi)}{[1+\lambda\xi-(1+\lambda)px\xi]\ \ [1+\lambda\xi-(1+\lambda)pz\xi]}\right)d\xi \tag{3.15} $$

$$ (\mathbb{R}(v)>\mathbb{R}(\gamma)>0\,,\ \lambda>-1)\,, $$

$$ {}_pH_{C,k}(\gamma,\delta_1,\delta_2;v;x,y,z) = \frac{{}_p\Gamma_k(v)}{k\ {}_p\Gamma_k(\gamma)\ {}_p\Gamma_k(v-\gamma)} \frac{(b-c)^{\frac{\gamma}{k}}(a-c)^{\frac{v-\gamma}{k}}}{(b-a)^{\frac{v+\delta_1-\delta_2}{k}-1}} $$

$$ \times \int_a^b (b-\xi)^{\frac{v-\gamma}{k}-1}\ (\xi-a)^{\frac{\gamma}{k}-1}\ (\xi-c)^{\frac{\delta_1+\delta_2-v}{k}}\ [(b-a)(\xi-c)-(b-c)(\xi-a)x]^{-\frac{\delta_1}{k}} $$

$$ \times [(b-a)(\xi-c)-(b-c)(\xi-a)z]^{-\frac{\delta_2}{k}}\ {}_pF_k(\delta_1,\delta_2;v-\gamma;y\sigma)\,d\xi \tag{3.16} $$

$$ (\min\{\mathbb{R}(\gamma),\mathbb{R}(\delta_1)\}>0\,;\ c<a<b) $$

$$ \sigma := \frac{(b-a)(a-c)(\xi-c)(b-\xi)}{[(b-a)(\xi-c)-(b-c)(\xi-a)px]\,[(b-a)(\xi-c)-(b-c)(\xi-a)pz]}, $$

$$ {}_pH_{C,k}(\gamma,\delta_1,\delta_2;v;x,y,z) = \frac{{}_p\Gamma_k(v)\ (1+\lambda)^{\frac{\gamma}{k}}}{k\ {}_p\Gamma_k(\gamma)\ {}_p\Gamma_k(v-\gamma)} \int_0^\infty \xi^{\frac{\gamma}{k}-1}\ (1+\xi)^{\frac{\delta1+\delta2-v}{k}} $$

$$ \times\ (1+\xi-x\xi)^{-\frac{\delta_1}{k}}(1+\xi-z\xi)^{-\frac{\delta_2}{k}}\ {}_pF_k(\delta_1,\delta_2;v-\gamma;y\sigma)\,d\xi \tag{3.17} $$

$$ (\mathbb{R}(v)>\mathbb{R}(\gamma)>0) $$

$$ \sigma := \frac{1+\xi}{(1+\xi-px\xi)(1+\xi-pz\xi)}, $$

$$ {}_pH_{C,k}(\gamma,\delta_1,\delta_2;v;x,y,z) = \frac{2\ {}_p\Gamma_k(v)}{k\ {}_p\Gamma_k(\gamma)\ {}_p\Gamma_k(v-\gamma)} \int_0^{\pi/2} (sin^2\xi)^{\frac{\gamma}{k}-\frac{1}{2}}\ (cos^2\xi)^{\frac{v-\gamma}{k}-\frac{1}{2}} $$

$$ \times\ (1-px\sin^2\xi)^{-\frac{\delta_1}{k}}(1-pz\sin^2\xi)^{-\frac{\delta_2}{k}}\ {}_pF_k(\delta_1,\delta_2;v-\gamma;y\sigma)\,d\xi \tag{3.18} $$

$$ (\mathbb{R}(v)>\mathbb{R}(\gamma)>0) $$

$$ \sigma := \frac{cos^2\xi}{(1-px\,sin^2\xi)(1+\xi-pz\,sin^2\xi)}. $$

Here, ${}_pF_k$ is the $p-k$ Gauss hypergeometric function (2.11).

Proof. The proof of Theorem 3 is similar to the proof of Theorem 1. The details are omitted.

4.RECURRENCE RELATİONS FOR ${}_pH_{A,k}$

Theorem 4. Some iteration formulas of ${}_pH_{A,k}$ Srivastava hypergeometric functions [3 − 5, 15] are as follows.

$$ {}_pH_{A,k}\ [\gamma+kn,\ \delta_1,\ \delta_2\,;\ v_1,v_2\,;\ x,y,z] = {}_pH_{A,k}[\gamma,\ \delta_1,\ \delta_2\,;\ v_1,v_2\,;\ x,y,z] \tag{4.1} $$

$$+\frac{\delta_1}{v_1}px\sum_{m=1}^{n} {}_pH_{A,k}\ [\gamma+km,\ \delta_1+k,\ \delta_2\ ;\ v_1+k, v_2\ ;\ x,y,z]$$

$$+\frac{\delta_2}{v_2}pz\sum_{m=1}^{n} {}_pH_{A,k}\ [\gamma+km,\ \delta_1,\ \delta_2+k\ ;\ v_1, v_2\ +k;\ x,y,z]\,,$$

$${}_pH_{A,k}\ [\gamma-kn,\ \delta_1,\ \delta_2\ ;\ v_1, v_2\ ;\ x,y,z] = {}_pH_{A,k}[\ \gamma,\ \delta_1,\ \delta_2\ ;\ v_1, v_2\ ;\ x,y,z] \tag{4.2}$$

$$-\frac{\delta_1}{v_1}px\sum_{m=0}^{n-1} {}_pH_{A,k}\ [\gamma-km,\ \delta_1+k,\ \delta_2\ ;\ v_1+k, v_2\ ;\ x,y,z]$$

$$-\frac{\delta_2}{v_2}pz\sum_{m=0}^{n-1} {}_pH_{A,k}\ [\gamma-km,\ \delta_1,\ \delta_2+k\ ;\ v_1, v_2\ +k;\ x,y,z]\,,$$

$${}_pH_{A,k}\ [\gamma,\ \delta_1+kn,\ \delta_2\ ;\ v_1, v_2\ ;\ x,y,z] = {}_pH_{A,k}[\ \gamma,\ \delta_1,\ \delta_2\ ;\ v_1, v_2\ ;\ x,y,z] \tag{4.3}$$

$$+\frac{\gamma}{v_1}px\sum_{m=1}^{n} {}_pH_{A,k}\ [\gamma+k,\ \delta_1+km,\ \delta_2\ ;\ v_1+k, v_2\ ;\ x,y,z]$$

$$+\frac{\delta_2}{v_2}py\sum_{m=1}^{n} {}_pH_{A,k}\ [\gamma,\ \delta_1+km,\ \delta_2+k\ ;\ v_1, v_2\ +k;\ x,y,z]\,,$$

$${}_pH_{A,k}\ [\gamma,\ \delta_1-kn,\ \delta_2\ ;\ v_1, v_2\ ;\ x,y,z] = {}_pH_{A,k}[\ \gamma,\ \delta_1,\ \delta_2\ ;\ v_1, v_2\ ;\ x,y,z] \tag{4.4}$$

$$-\frac{\gamma}{v_1}px\sum_{m=0}^{n-1} {}_pH_{A,k}\ [\gamma+k,\ \delta_1-km,\ \delta_2\ ;\ v_1+k, v_2\ ;\ x,y,z]$$

$$-\frac{\delta_2}{v_2}py\sum_{m=0}^{n-1} {}_pH_{A,k}\ [\gamma,\ \delta_1-km,\ \delta_2+k\ ;\ v_1, v_2\ +k;\ x,y,z]\,,$$

Proof.

$$H_A\ [\gamma+n,\ \delta_1,\ \delta_2\ ;\ v_1, v_2\ ;\ x,y,z] = H_A[\ \gamma,\ \delta_1,\ \delta_2\ ;\ v_1, v_2\ ;\ x,y,z]$$

$$+\frac{\delta_1}{v_1}x\sum_{m=1}^{n} {}_pH_{A,k}\ [\gamma+m,\ \delta_1+1,\ \delta_2\ ;\ v_1+1, v_2\ ;\ x,y,z]$$

$$+\frac{\delta_2}{v_2}z\sum_{m=1}^{n} {}_pH_{A,k}\ [\gamma+m,\ \delta_1,\ \delta_2+1\ ;\ v_1, v_2\ +1;\ x,y,z]$$

If $\gamma=\gamma+kn$ is used in the equation and the necessary adjustments are made,

$${}_pH_{A,k}\ [\gamma+kn,\ \delta_1,\ \delta_2\ ;\ v_1, v_2\ ;\ x,y,z]$$

$$= H_A\ \left[\frac{\gamma}{k}+n, \frac{\delta_1}{k}, \frac{\delta_2}{k}\ ;\ \frac{v_1}{k}, \frac{v_2}{k};\ px, py, pz\right]$$

$$= H_A\left[\frac{\gamma}{k}, \frac{\delta_1}{k}, \frac{\delta_2}{k}\ ;\ \frac{v_1}{k}, \frac{v_2}{k};\ px, py, pz\right]$$

$$+\frac{\frac{\delta_1}{k}}{\frac{v_1}{k}} px \sum_{m=1}^{n} H_A\left[\frac{\gamma}{k}+m, \frac{\delta_1}{k}+1, \frac{\delta_2}{k}\ ;\ \frac{v_1}{k}+1, \frac{v_2}{k};\ px, py, pz\right]$$

$$+\frac{\frac{\delta_2}{k}}{\frac{v_2}{k}} pz \sum_{m=1}^{n} H_A\left[\frac{\gamma}{k}+m, \frac{\delta_1}{k}, \frac{\delta_2}{k}+1\ ;\ \frac{v_1}{k}, \frac{v_2}{k}+1;\ px, py, pz\right]$$

$$= {}_pH_{A,k}[\gamma, \delta_1, \delta_2\ ;\ v_1, v_2\ ;\ x, y, z]$$

$$+\frac{\delta_1}{v_1} px \sum_{m=1}^{n} {}_pH_{A,k}\ [\gamma+km, \delta_1+k, \delta_2\ ;\ v_1+k, v_2\ ;\ x, y, z]$$

$$+\frac{\delta_2}{v_2} pz \sum_{m=1}^{n} {}_pH_{A,k}\ [\gamma+km, \delta_1, \delta_2+k\ ;\ v_1, v_2+k;\ x, y, z]$$

is obtained, which completes the (4.1) proof. Likewise, (4.2)-(4.4) proof of other recursion formulas can be shown in a similar way.

REFERENCES

1. Altın, A., 2021, Uygulamalı Matematik, Gazi Kitabevi, Ankara.
2. Lauricella, G., 1893, Sulle funzioni iper-geometriche a piu variabili. Rend. Cire. Mat. Palermo. 7,111-158.
3. Hasanov A., Srivastava H.M. and Turaev M., 2006, Decomposition formulas for some triple hypergeometric functions, J. Math. Anal. Appl. , 324, 955-969.
4. Srivastava, H. M., 1964, Hypergeometric functions of three variables, Ganita, 15,97-108.
5. Srivastava, H. M., 1967, Some integrals representing triple hypergeometric functions, Rendiconti del Circolo Matematico di Palermo, 16, 99-115.
6. Srivastava, H. M., Karlsson, P. W., 1985, Multiple Gaussian Hypergeometric Series, Halsted Press (Ellis Horwood Limited, Chicherster), John Wiley and Sons, New York, Chichester, Brisbane and Toronto.
7. Srivastava, H. M., Manocha, H. L., 1984, A Treatise on Generating Functions, Halsted Press (Ellis Horwood Limited, Chicherster), John Wiley and Sons, New York, Chichester, Brisbane and Toronto.
8. Diaz, R., Pariguan, E., 2007, On hypergeometric functions and Pochhammer k-symbol, Divulg. Mat., 15, 179--192.
9. Mubeen, S., Rehman, A., 2014, A note on k-Gamma function and Pochhammer k-symbol, Journal of Informatics and Mathematical Sciences, 6(2), 93-107.
10. Kıymaz, İ. O., Çetinkaya, A., Agarwal, P., 2017, A study on the k-generalizations of some known functions and fractional operators, Journal of Inequalities and Special Functions, 8(4), 31-41.
11. Mubeen, S., 2012, k-analogue of Kummer's first formula, J. Inequalities Spec. Funct., 3(3), 41-44.
12. Mubeen, S., Habibullah , G. M., 2012, An integral representation of some k-hypergeometric functions, Int. Math. Forum, 7(4), 203-207.
13. Mubeen, S., Iqbal, S., Rahman, G., 2015, Contiguous function relations and an integral representation for Appell k-series F1,k, International Journal of Mathematical Research, 4(2), 53-63.
14. Gehlot, K. S., 2017, Two parameter gamma function and its properties. arXiv preprint arXiv:1701.01052.

15. Choi, J., Hasanov, A., Srivastava, H. M., Turaev, M., 2011, Integral representations for Srivastava's triple hypergeometric functions, Taiwanese J. Math., 15(6), 2751-2762.
16. F. Qi and B.-N. Guo, Relations among Bell polynomials, central factorial numbers, and central Bell polynomials, Math. Sci. Appl. E-Notes 7(2), 191-194, 2019.
17. F. Qi, D.-W. Niu, D. Lim and B.-N. Guo, Closed formulas and identities for the Bell polynomials and falling factorials, Contrib. Discrete Math. 14(2), 1-11, 2019.
18. F. Qi, D.-W. Niu, D. Lim and Y.-H. Yao, Special values of the Bell polynomials of the second kind for some sequences and functions, Journal of Mathematical Analysis and Applications 491(2), 2020.
19. F. Qi, X.-T. Shi and F.-F. Liu, Several identities involving the falling and rising factorials and the Cauchy, Lah, and Stirling numbers, Acta Univ. Sapientiae Math. 8(2), 282-297, 2016.
20. F. Qi, G.-S. Wu and B.-N. Guo, An alternative proof of a closed formula for central factorial numbers of the second kind, Turkish J. Anal. Number Theory 7(2), 56-58, 2019
21. R. Şahin and O. Yağcı, A New Generalization of Pochhammer Symbol and Its Applications, Applied Mathematics and Nonlinear Sciences 5(1), 255-266, 2020.
22. R. Şahin, O. Yağcı, Fractional Calculus of the Extended Hypergeometric Function, Applied Mathematics and Nonlinear Sciences 5(1), 369-384, 2020.
23. H.M. Srivastava, A. Çetinkaya and İ.O. Kıymaz, A certain generalized Pochhammer symbol and its applications to hypergeometric functions, Appl. Math. Comput. 226, 484-491, 2014.
24. Srivastava, G. Rahman and K.S. Nisar, Some Extensions of the Pochhammer Symbol and the Associated Hypergeometric Functions, Iranian Journal of Science and Technology, Transactions A: Science 43(5), 2601-2606, 2019.
25. M. Safdar, G. Rahman, Z. Ullah, A. Ghaffar and K.S. Nisar, A New Extension of the Pochhammer Symbol and Its Application to Hypergeometric Functions, International Journal of Applied and Computational Mathematics 5(6), 151, 2019. PanWang, BoTian, Kun Sun, Feng-Hua Qi, Thetitle of Paper, Applied Mathematics and Computation, Vol:2, No:1, 233–242, 2015.

ESTIMATIONS OF INTEGRAL MAJORIZATION INEQUALITY FOR DIFFERENTIABLE CONVEX FUNCTIONS AND APPLICATIONS

Artion Kashuri[1] **, Rozana Liko**[2]

[1]Department of Mathematical Engineering, Polytechnic University of Tirana, Tirana 1001, Albania

[2]Department of Mathematics, Faculty of Technical and Natural Sciences, University Ismail Qemali, 9400 Vlora, Albania

a.kashuri@fimif.edu.al, rozana.liko@univlora.edu.al

Abstract

This study aims to estimate integral majorization inequalities by taking third-differentiable convex functions. By using Hölder, Power-mean and Jensen inequalities, we derive some new relations involving integral majorization. Additionally, our study explores various applications in information theory, including estimations for the Csiszár and Kullback–Leibler divergences, Shannon entropy, and Jeffrey's distance.

Keywords: Convex function; Majorization inequality; Hölder's inequality; Power-mean inequality; Jensen's inequality; Information theory.

1. INTRODUCTION

Inequalities play a fundamental role in mathematics and its many applications, such as probability, statistics, optimization, mathematics finance, physics, and other applied sciences. Convex functions are very important in the study of mathematical inequality and in solving optimization theory problems. Many well-known inequalities are direct consequences of these functions. Convex functions and their generalizations have various applications in pure and applied science, see [1-10]. Owing to these applications, it is currently the most attractive research area. The class of convex functions is well known in the literature and is typically defined as follows:

Definition 1.1. Let J be an interval in $\mathbb{R}$. A function $f : J \to \mathbb{R}$, is said to be convex on J, if the following inequality holds true

$$f(t\xi_1 + (1-t)\xi_2) \leq tf(\xi_1) + (1-t)f(\xi_2). \qquad (1.1)$$

This concept is closely related to many known inequalities, such as Jensen inequality, Hölder inequality, Hermite−Hadamard inequality, etc. A statement of Jensen's inequality is given below.

Theorem 1.1. Let $\phi: [\nu_1, \nu_2] \rightarrow R$ be a convex function. Assume that $p, q: [\mu_1, \mu_2] \rightarrow [\nu_1, \nu_2]$ be integrable function, q a nonnegative function with $q^* := \int_{\mu_1}^{\mu_2} q(t)dt \neq 0$, and $\phi \circ p$ is an integrable function, then

$$\phi\left(\frac{1}{q^*}\int_{\mu_1}^{\mu_2} p(t)q(t)dt\right) \leq \frac{1}{q^*}\int_{\mu_1}^{\mu_2} q(t)\phi\big(p(t)\big)dt. \tag{1.2}$$

If the function ϕ is concave, then the inequality is in the opposite direction. Jensen inequality is the source of Hölder inequality and Hermite-Hadamard inequality as well. Hölder inequality is given as follows.

Theorem 1.2. Let $p, q: [\mu_1, \mu_2] \longrightarrow [\nu_1, \nu_2]$ be two integrable functions and $r > 1$, $\frac{1}{r} + \frac{1}{s} = 1$, then

$$\int_{\mu_1}^{\mu_2} |p(x)q(x)|dx \leq \left(\int_{\mu_1}^{\mu_2} |p(x)|^r \, dx\right)^{\frac{1}{r}} \left(\int_{\mu_1}^{\mu_2} |q(x)|^s \, dx\right)^{\frac{1}{s}}. \tag{1.3}$$

The theory of majorization is a versatile and potent tool that can be utilized to solve a diverse array of mathematical problems [11-17]. To provide the most comprehensive definition of majorization, we will now proceed.

Definition 1.2. [10] Let $p, q: [\mu_1, \mu_2] \longrightarrow \mathbb{R}$ are integrable real value functions. The function $q(x)$ majorize $p(x)$, $q(x) \succ p(x)$, for $x \in [\mu_1, \mu_2]$, if

$$\int_{\mu_1}^{\tau} p(x)dx \leq \int_{\mu_1}^{\tau} q(x)dx, \quad \text{for } \tau \in [\mu_1, \mu_2],$$

and

$$\int_{\mu_1}^{\mu_2} p(x)dx = \int_{\mu_1}^{\mu_2} q(x)dx.$$

Theorem 1.3. [10] Let $p, q: [\mu_1, \mu_2] \longrightarrow [\nu_1, \nu_2]$ be decreasing functions such that $q(\boldsymbol{\tau}) \succ p(\boldsymbol{\tau})$, for $\boldsymbol{\tau} \in [\mu_1, \mu_2]$, and Φ is a convex function on $[\nu_1, \nu_2]$, then

$$\int_{\mu_1}^{\mu_2} \Phi(p(x))dx \leq \int_{\mu_1}^{\mu_2} \Phi\big(q(x)\big)dx.$$

Theorem 1.4. [18] Let ω, p, q be positive functions on $[\mu_1, \mu_2]$. Suppose Φ is a convex function on $[0, +\infty)$, and that

$$\int_{\mu_1}^{\boldsymbol{\tau}} \omega(x)p(x)dx \leq \int_{\mu_1}^{\boldsymbol{\tau}} \omega(x)q(x)dx, \quad \text{for } \tau \in [\mu_1, \mu_2],$$

and

$$\int_{\mu_1}^{\mu_2} \omega(x)p(x)dx = \int_{\mu_1}^{\mu_2} \omega(x)q(x)dx.$$

i. If $p(x)$ is a decreasing function on $[\mu_1, \mu_2]$, then
$$\int_{\mu_1}^{\mu_2} \omega(x)\Phi(p(x))dx \leq \int_{\mu_1}^{\mu_2} \omega(x)\Phi\big(q(x)\big)dx.$$

ii. If $q(x)$ is an increasing function on $[\mu_1, \mu_2]$, then

$$\int_{\mu_1}^{\mu_2} \omega(x)\Phi\big(q(x)\big)dx \leq \int_{\mu_1}^{\mu_2} \omega(x)\Phi\big(p(x)\big)dx.$$

Our remaining paper is organised as follows: In Section 2, we present a crucial lemma, which provides estimates for the majorization difference by applying well-known Hölder, Power-mean, and Jensen type inequalities. In Section 3, we deduce some applications in information theory for suitable choices of functions from our main results. In Section 4, the conclusions and recommendations for further studies are given.

2. MAIN RESULTS

The goal of this section is to find estimates for majorization differences by considering third-differentiable functions and applying the notion of convexity, and some known inequalities.

We start by giving a following lemma.

Lemma 2.1. Let $\phi: [\nu_1, \nu_2] \longrightarrow \mathbb{R}$ be a third differentiable function, such that ϕ''' is integrable, and $p, q: [\mu_1, \mu_2] \longrightarrow [\nu_1, \nu_2]$, $\omega: [\mu_1, \mu_2] \longrightarrow [\,0, +\infty)$ are integrable functions, then

$$\begin{aligned}
&\int_{\mu_1}^{\mu_2} \omega(x)\, \phi(q(x))dx - \int_{\mu_1}^{\mu_2} \omega(x)\phi\big(p(x)\big)dx \\
&\qquad = \frac{1}{2}\int_{\mu_1}^{\mu_2} \omega(x)[q(x)-p(x)]^3 \int_0^1 t^2\phi'''\big(tq(x)+(1-t)p(x)\big)dtdx \\
&\qquad -\frac{1}{2}\int_{\mu_1}^{\mu_2} \omega(x)[q(x)-p(x)]^2\phi''\big(q(x)\big)\,dx \\
&\qquad +\int_{\mu_1}^{\mu_2} \omega(x)[q(x)-p(x)]\phi'\big(q(x)\big)\,dx.
\end{aligned}$$

Proof. Assume that $p(x) \neq q(x)$ for all $x \in [\mu_1, \mu_2]$. Utilizing twice integration by parts, we have

$$\begin{aligned}
&\int_0^1 t^2\phi'''\big(tq(x)+(1-t)p(x)\big)dt \\
&\qquad = \frac{1}{q(x)-p(x)}\phi''\big(q(x)\big) - \frac{2}{[q(x)-p(x)]^2}\phi'\big(q(x)\big) \\
&\qquad + \frac{2}{[q(x)-p(x)]^3}\phi\big(q(x)-p(x)\big).
\end{aligned}$$

So,

$$\int_{\mu_1}^{\mu_2} \omega(x)[q(x)-p(x)]^3 \int_0^1 t^2\phi'''\left(tq(x)+(1-t)p(x)\right)dtdx$$
$$= \int_{\mu_1}^{\mu_2} \omega(x)[q(x)-p(x)]^3 \left[\frac{1}{q(x)-p(x)}\phi''\big(q(x)\big) - \frac{2}{[q(x)-p(x)]^2}\phi'\big(q(x)\big)\right.$$
$$\left. + \frac{3}{[q(x)-p(x)]^3}\phi(q(x)-p(x))\right]dx$$
$$= \int_{\mu_1}^{\mu_2} \omega(x)[q(x)-p(x)]^2\phi''\big(q(x)\big)\,dx$$
$$-2\int_{\mu_1}^{\mu_2} \omega(x)[q(x)-p(x)]\phi'\big(q(x)\big)\,dx + 2\int_{\mu_1}^{\mu_2} \omega(x)\left[\phi\big(q(x)\big)-\phi\big(p(x)\big)\right]dx.$$

The proof of Lemma 2.1 is completed. ■

Theorem 2.1. Let $\phi: [\nu_1, \nu_2] \longrightarrow \mathbb{R}$ be a third differentiable function, such that ϕ''' is integrable and $|\phi'''|^r$ is convex, for $r > 1$. Assume that $p, q: [\mu_1, \mu_2] \longrightarrow [\nu_1, \nu_2]$, $\omega: [\mu_1, \mu_2] \longrightarrow [0, +\infty)$ are integrable functions. Then

$$\int_{\mu_1}^{\mu_2} \omega(x)\,\phi(q(x))dx - \int_{\mu_1}^{\mu_2} \omega(x)\phi\big(p(x)\big)dx$$
$$\leq \frac{1}{2}\int_{\mu_1}^{\mu_2} \omega(x)[q(x)-p(x)]^3 \left(\frac{(2r+1)\left|\phi'''\big(q(x)\big)\right|^r + |\phi'''(p(x))|^r}{(2r+1)(2r+2)}\right)^{1/r} dx$$
$$-\frac{1}{2}\int_{\mu_1}^{\mu_2} \omega(x)[q(x)-p(x)]^2\phi''\big(q(x)\big)\,dx$$
$$+\int_{\mu_1}^{\mu_2} \omega(x)[q(x)-p(x)]\phi'\big(q(x)\big)\,dx.$$

Proof. Since $\phi(x) \leq |\phi(x)|$, for all $x \in [\mu_1, \mu_2]$, then from Lemma 2.1, we have

$$\int_{\mu_1}^{\mu_2} \omega(x)\,\phi(q(x))dx - \int_{\mu_1}^{\mu_2} \omega(x)\phi\big(p(x)\big)dx$$
$$\leq \frac{1}{2}\int_{\mu_1}^{\mu_2} \omega(x)[q(x)-p(x)]^3 \int_0^1 t^2\left|\phi'''\left(tq(x)+(1-t)p(x)\right)\right|dtdx$$
$$-\frac{1}{2}\int_{\mu_1}^{\mu_2} \omega(x)[q(x)-p(x)]^2\phi''\big(q(x)\big)\,dx$$
$$+\int_{\mu_1}^{\mu_2} \omega(x)[q(x)-p(x)]\phi'\big(q(x)\big)\,dx.$$

By using Hölder's inequality, we get

$$\int_{\mu_1}^{\mu_2}\omega(x)\,\phi(q(x))dx-\int_{\mu_1}^{\mu_2}\omega(x)\phi\big(p(x)\big)dx$$
$$\leq\frac{1}{2}\int_{\mu_1}^{\mu_2}\omega(x)[q(x)-p(x)]^3\left(\int_0^1 t^{2r}\left|\phi'''\left(tq(x)+(1-t)p(x)\right)\right|^r dt\right)^{\frac{1}{r}}dx$$
$$-\frac{1}{2}\int_{\mu_1}^{\mu_2}\omega(x)[q(x)-p(x)]^2\phi''\big(q(x)\big)\,dx$$
$$+\int_{\mu_1}^{\mu_2}\omega(x)[q(x)-p(x)]\phi'\big(q(x)\big)\,dx.$$

Applying the convexity of the function $|\phi'''|^r$, we obtain

$$\int_{\mu_1}^{\mu_2}\omega(x)\,\phi(q(x))dx-\int_{\mu_1}^{\mu_2}\omega(x)\phi\big(p(x)\big)dx$$
$$\leq\frac{1}{2}\int_{\mu_1}^{\mu_2}\omega(x)[q(x)-p(x)]^3$$
$$\cdot\left(\int_0^1 t^{2r}\left(t\left|\phi'''\big(q(x)\big)\right|^r+(1-t)|\phi'''(p(x))|^r\right)dt\right)^{\frac{1}{r}}dx$$
$$-\frac{1}{2}\int_{\mu_1}^{\mu_2}\omega(x)[q(x)-p(x)]^2\phi''\big(q(x)\big)\,dx$$
$$+\int_{\mu_1}^{\mu_2}\omega(x)[q(x)-p(x)]\phi'\big(q(x)\big)\,dx.$$

Hence,

$$\int_{\mu_1}^{\mu_2}\omega(x)\,\phi(q(x))dx-\int_{\mu_1}^{\mu_2}\omega(x)\phi\big(p(x)\big)dx$$
$$\leq\frac{1}{2}\int_{\mu_1}^{\mu_2}\omega(x)[q(x)-p(x)]^3\cdot\left(\frac{(2r+1)\left|\phi'''\big(q(x)\big)\right|^r+\left|\phi'''\big(p(x)\big)\right|^r}{(2r+1)(2r+2)}\right)^{\frac{1}{r}}dx$$
$$-\frac{1}{2}\int_{\mu_1}^{\mu_2}\omega(x)[q(x)-p(x)]^2\phi''\big(q(x)\big)\,dx$$
$$+\int_{\mu_1}^{\mu_2}\omega(x)[q(x)-p(x)]\phi'\big(q(x)\big)\,dx,$$

which completes the proof of Theorem 2.1. ■

Corollary 2.1. Let $\phi:[\nu_1,\nu_2]\longrightarrow\mathbb{R}$ be a third differentiable function, such that ϕ''' is integrable and $|\phi'''|^r$ is convex, for $r>1$. Assume that $p,q:[\mu_1,\mu_2]\longrightarrow[\nu_1,\nu_2]$, $\omega:[\mu_1,\mu_2]\longrightarrow[\,0,+\infty)$ are integrable functions and $\omega^*:=\int_{\mu_1}^{\mu_2}\omega(x)dx>0$, $\bar{p}:=\frac{1}{\omega^*}\int_{\mu_1}^{\mu_2}\omega(x)p(x)dx$. Then

$$\begin{aligned}\phi(\bar{p}) &- \frac{1}{\omega^*}\int_{\mu_1}^{\mu_2}\omega(x)\phi\big(p(x)\big)dx \\ &\le \frac{1}{2}\bar{p}^2\phi''(\bar{p}) - \frac{1}{2\omega^*}\phi''(\bar{p})\int_{\mu_1}^{\mu_2}\omega(x)p^2(x)dx \\ &+ \frac{1}{2\omega^*}\int_{\mu_1}^{\mu_2}\omega(x)[\bar{p}-p(x)]^3\left(\frac{(2r+1)|\phi'''(\bar{p})|^r + \left|\phi'''\big(p(x)\big)\right|^r}{(2r+1)(2r+2)}\right)^{\frac{1}{r}} dx.\end{aligned}$$

Proof. Taking $q = \bar{p}$ in Theorem 2.1, we obtain the required result.

Theorem 2.2. Let $\phi: [\nu_1, \nu_2] \longrightarrow \mathbb{R}$ be a third differentiable function, such that ϕ''' is integrable and $|\phi'''|^r$ is convex, for $r > 1$. Asume that $p, q: [\mu_1, \mu_2] \longrightarrow [\nu_1, \nu_2]$, $\omega: [\mu_1, \mu_2] \longrightarrow [0, +\infty)$ are integrable functions and $\frac{1}{s} + \frac{1}{r} = 1$. Then

$$\begin{aligned}\int_{\mu_1}^{\mu_2}&\omega(x)\,\phi(q(x))dx - \int_{\mu_1}^{\mu_2}\omega(x)\phi\big(p(x)\big)dx \\ &\le \frac{1}{2}\left(\frac{1}{2s+1}\right)^{\frac{1}{s}}\int_{\mu_1}^{\mu_2}\omega(x)[q(x)-p(x)]^3\left(\frac{\left|\phi'''\big(q(x)\big)\right|^r + \left|\phi'''\big(p(x)\big)\right|^r}{2}\right)^{\frac{1}{r}} dx \\ &-\frac{1}{2}\int_{\mu_1}^{\mu_2}\omega(x)[q(x)-p(x)]^2\phi''\big(q(x)\big)\,dx \\ &+\int_{\mu_1}^{\mu_2}\omega(x)[q(x)-p(x)]\phi'\big(q(x)\big)\,dx.\end{aligned}$$

Proof. From the fact that $\phi(x) \le |\phi(x)|$ and Hölder's inequality, we get

$$\begin{aligned}\int_{\mu_1}^{\mu_2}&\omega(x)\,\phi(q(x))dx - \int_{\mu_1}^{\mu_2}\omega(x)\phi\big(p(x)\big)dx \\ &\le \frac{1}{2}\int_{\mu_1}^{\mu_2}\omega(x)[q(x)-p(x)]^3 \\ &\cdot\left(\int_0^1 t^{2s}\,dt\right)^{1/s}\left(\int_0^1\left|\phi'''\,\big(tq(x)+(1-t)p(x)\big)\right|^r dt\right)^{\frac{1}{r}} dx \\ &-\frac{1}{2}\int_{\mu_1}^{\mu_2}\omega(x)[q(x)-p(x)]^2\phi''\big(q(x)\big)\,dx \\ &+\int_{\mu_1}^{\mu_2}\omega(x)[q(x)-p(x)]\phi'\big(q(x)\big)\,dx.\end{aligned}$$

Applying the convexity of the function $|\phi'''|^r$, we obtain

$$\int_{\mu_1}^{\mu_2} \omega(x)\, \phi(q(x))dx - \int_{\mu_1}^{\mu_2} \omega(x)\phi\big(p(x)\big)dx$$

$$\leq \frac{1}{2}\int_{\mu_1}^{\mu_2} \omega(x)[q(x)-p(x)]^3$$

$$\cdot \left(\frac{1}{2s+1}\right)^{\frac{1}{s}} \left(\int_0^1 \left[t\left|\phi'''\big(q(x)\big)\right|^r + (1-t)\left|\phi'''\big(p(x)\big)\right|^r\right]dt\right)^{\frac{1}{r}} dx$$

$$-\frac{1}{2}\int_{\mu_1}^{\mu_2} \omega(x)[q(x)-p(x)]^2\phi''\big(q(x)\big)\,dx$$

$$+\int_{\mu_1}^{\mu_2} \omega(x)[q(x)-p(x)]\phi'\big(q(x)\big)\,dx$$

$$= \frac{1}{2}\left(\frac{1}{2s+1}\right)^{\frac{1}{s}} \int_{\mu_1}^{\mu_2} \omega(x)[q(x)-p(x)]^3 \cdot \left(\frac{\left|\phi'''\big(q(x)\big)\right|^r}{2} + \frac{\left|\phi'''\big(p(x)\big)\right|^r}{2}\right)^{\frac{1}{r}} dx$$

$$-\frac{1}{2}\int_{\mu_1}^{\mu_2} \omega(x)[q(x)-p(x)]^2\phi''\big(q(x)\big)\,dx$$

$$+\int_{\mu_1}^{\mu_2} \omega(x)[q(x)-p(x)]\phi'\big(q(x)\big)\,dx.$$

So,

$$\int_{\mu_1}^{\mu_2} \omega(x)\, \phi(q(x))dx - \int_{\mu_1}^{\mu_2} \omega(x)\phi\big(p(x)\big)dx$$

$$\leq \frac{1}{2}\left(\frac{1}{2s+1}\right)^{\frac{1}{s}} \int_{\mu_1}^{\mu_2} \omega(x)[q(x)-p(x)]^3 \left(\frac{\left|\phi'''\big(q(x)\big)\right|^r + \left|\phi'''\big(p(x)\big)\right|^r}{2}\right)^{\frac{1}{r}} dx$$

$$-\frac{1}{2}\int_{\mu_1}^{\mu_2} \omega(x)[q(x)-p(x)]^2\phi''\big(q(x)\big)\,dx$$

$$+\int_{\mu_1}^{\mu_2} \omega(x)[q(x)-p(x)]\phi'\big(q(x)\big)\,dx,$$

which completes the proof of Theorem 2.2. ■

Corollary 2.2. Assume that the conditions of Theorem 2.2 are fulfilled. Then

$$\phi(\bar{p}) - \frac{1}{\omega^*}\int_{\mu_1}^{\mu_2} \omega(x)\phi\big(p(x)\big)dx$$

$$\leq \frac{1}{2}\bar{p}^2\phi''(\bar{p}) - \frac{1}{2\omega^*}\phi''(\bar{p})\int_{\mu_1}^{\mu_2} \omega(x)p^2(x)dx$$

$$+\frac{1}{2\omega^*}\left(\frac{1}{2s+1}\right)^{\frac{1}{s}} \int_{\mu_1}^{\mu_2} \omega(x)[\bar{p}-p(x)]^3 \left(\frac{|\phi'''(\bar{p})|^r + \left|\phi'''\big(p(x)\big)\right|^r}{2}\right)^{\frac{1}{r}} dx.$$

Proof. Choosing $q = \bar{p}$ in Theorem 2.2, we obtain the required result.

Theorem 2.3. Let $\phi:[\nu_1,\nu_2]\longrightarrow\mathbb{R}$ be a third differentiable function, such that ϕ''' is integrable and $|\phi'''|$ is concave function. Asume that $p,q:[\mu_1,\mu_2]\longrightarrow[\nu_1,\nu_2]$, $\omega:[\mu_1,\mu_2]\longrightarrow[0,+\infty)$ are integrable functions. Then

$$\begin{aligned}\int_{\mu_1}^{\mu_2}\omega(x)\,\phi(q(x))dx-\int_{\mu_1}^{\mu_2}\omega(x)\phi\big(p(x)\big)dx \\ \leq\frac{1}{6}\int_{\mu_1}^{\mu_2}\omega(x)[q(x)-p(x)]^3\left|\phi'''\left(\frac{3q(x)+p(x)}{4}\right)\right|dx \\ -\frac{1}{2}\int_{\mu_1}^{\mu_2}\omega(x)[q(x)-p(x)]^2\phi''\big(q(x)\big)\,dx \\ +\int_{\mu_1}^{\mu_2}\omega(x)[q(x)-p(x)]\phi'\big(q(x)\big)\,dx.\end{aligned}$$

Proof. From Lemma 2.1 and the property of modulus, we have

$$\begin{aligned}\int_{\mu_1}^{\mu_2}\omega(x)\phi\big(q(x)\big)dx-\int_{\mu_1}^{\mu_2}\omega(x)\phi\big(p(x)\big)dx \\ \leq\frac{1}{2}\int_{\mu_1}^{\mu_2}\omega(x)[q(x)-p(x)]^3\int_0^1\left|t^2\phi'''\big(tq(x)+(1-t)p(x)\big)\right|dtdx \\ -\frac{1}{2}\int_{\mu_1}^{\mu_2}\omega(x)[q(x)-p(x)]^2\phi''\big(q(x)\big)\,dx \\ +\int_{\mu_1}^{\mu_2}\omega(x)[q(x)-p(x)]\phi'\big(q(x)\big)\,dx.\end{aligned}$$

Utilizing the Jensen's inequality, we obtain

$$\begin{aligned}\int_{\mu_1}^{\mu_2}\omega(x)\phi\big(q(x)\big)dx-\int_{\mu_1}^{\mu_2}\omega(x)\phi\big(p(x)\big)dx \\ \leq\frac{1}{2}\int_{\mu_1}^{\mu_2}\omega(x)[q(x)-p(x)]^3 \\ \cdot\left(\int_0^1 t^2dt\right)\left|\phi'''\left(\frac{\int_0^1 t^2[tq(x)+(1-t)p(x)]dt}{\int_0^1 t^2dt}\right)\right|dx \\ -\frac{1}{2}\int_{\mu_1}^{\mu_2}\omega(x)[q(x)-p(x)]^2\phi''\big(q(x)\big)\,dx \\ +\int_{\mu_1}^{\mu_2}\omega(x)[q(x)-p(x)]\phi'\big(q(x)\big)\,dx.\end{aligned}$$

Computing the above integral, we get the desired result. ■

Corollary 2.3. Let $\phi:[\nu_1,\nu_2]\longrightarrow\mathbb{R}$ be a third differentiable function, such that ϕ''' is integrable and $|\phi'''|$ is concave. Asume that $p,q:[\mu_1,\mu_2]\longrightarrow[\nu_1,\nu_2]$, $\omega:[\mu_1,\mu_2]\longrightarrow[0,+\infty)$ are integrable functions and $\omega^*:=\int_{\mu_1}^{\mu_2}\omega(x)dx>0$, $\bar{p}:=\frac{1}{\omega^*}\int_{\mu_1}^{\mu_2}\omega(x)p(x)dx$. Then

$$\phi(\bar{p})-\frac{1}{\omega^*}\int_{\mu_1}^{\mu_2}\omega(x)\phi\big(p(x)\big)dx$$
$$\leq\frac{1}{6\omega^*}\int_{\mu_1}^{\mu_2}\omega(x)[\bar{p}-p(x)]^3\left|\phi'''\left(\frac{3\bar{p}+p(x)}{4}\right)\right|dx+\frac{1}{2}\bar{p}^2\phi''(\bar{p})$$
$$-\frac{1}{2\omega^*}\phi''(\bar{p})\int_{\mu_1}^{\mu_2}\omega(x)p^2(x)dx.$$

Proof. Taking $q=\bar{p}$ in Theorem 2.3, we obtain the required result.

Theorem 2.4. Let $\phi:[\nu_1,\nu_2]\longrightarrow\mathbb{R}$ be a third differentiable function, such that ϕ''' is integrable and $|\phi'''|^r$ is convex, for $r>1$. Assume that $p,q:[\mu_1,\mu_2]\longrightarrow[\nu_1,\nu_2]$, $\omega:[\mu_1,\mu_2]\longrightarrow[\,0,+\infty)$ are integrable functions. Then

$$\int_{\mu_1}^{\mu_2}\omega(x)\,\phi(q(x))dx-\int_{\mu_1}^{\mu_2}\omega(x)\phi\big(p(x)\big)dx$$
$$\leq\frac{1}{6}\left(\frac{3}{4}\right)^{1/r}\int_{\mu_1}^{\mu_2}\omega(x)[q(x)-p(x)]^3\left(\frac{3\left|\phi'''\big(q(x)\big)\right|^r+\left|\phi'''\big(p(x)\big)\right|^r}{3}\right)^{\frac{1}{r}}dx$$
$$-\frac{1}{2}\int_{\mu_1}^{\mu_2}\omega(x)[q(x)-p(x)]^2\phi''\big(q(x)\big)\,dx$$
$$+\int_{\mu_1}^{\mu_2}\omega(x)[q(x)-p(x)]\phi'\big(q(x)\big)\,dx.$$

Proof. By utilizing Power-mean inequality, we obtain

$$\int_{\mu_1}^{\mu_2}\omega(x)\,\phi(q(x))dx-\int_{\mu_1}^{\mu_2}\omega(x)\phi\big(p(x)\big)dx$$
$$\leq\frac{1}{2}\int_{\mu_1}^{\mu_2}\omega(x)[q(x)-p(x)]^3$$
$$\cdot\left(\int_0^1 t^2\,dt\right)^{1-\frac{1}{r}}\left(\int_0^1 t^2\left|\phi'''\,\big(tq(x)+(1-t)p(x)\big)\right|^r dt\right)^{\frac{1}{r}}dx$$
$$-\frac{1}{2}\int_{\mu_1}^{\mu_2}\omega(x)[q(x)-p(x)]^2\phi''\big(q(x)\big)\,dx$$
$$+\int_{\mu_1}^{\mu_2}\omega(x)[q(x)-p(x)]\phi'\big(q(x)\big)\,dx.$$

By the convexity of the function $|\phi'''|^r$, we have

$$
\begin{aligned}
&\int_{\mu_1}^{\mu_2}\omega(x)\,\phi(q(x))dx-\int_{\mu_1}^{\mu_2}\omega(x)\phi\big(p(x)\big)dx\\
&\qquad\le\frac{1}{2}\left(\frac{1}{3}\right)^{1-\frac{1}{r}}\int_{\mu_1}^{\mu_2}\omega(x)[q(x)-p(x)]^3\\
&\qquad\cdot\left(\int_0^1 t^2\left[t\left|\phi'''\left(q(x)\right)\right|^r+(1-t)\left|\phi'''\left(p(x)\right)\right|^r\right]dt\right)^{\frac{1}{r}}dx\\
&\qquad-\frac{1}{2}\int_{\mu_1}^{\mu_2}\omega(x)[q(x)-p(x)]^2\phi''\big(q(x)\big)\,dx\\
&\qquad+\int_{\mu_1}^{\mu_2}\omega(x)[q(x)-p(x)]\phi'\big(q(x)\big)\,dx\\
&\qquad=\frac{1}{2}\left(\frac{3}{4}\right)^{\frac{1}{r}}\int_{\mu_1}^{\mu_2}\omega(x)[q(x)-p(x)]^3\cdot\left(\frac{3\left|\phi'''\left(q(x)\right)\right|^r+\left|\phi'''\left(p(x)\right)\right|^r}{3}\right)^{\frac{1}{r}}dx\\
&\qquad-\frac{1}{2}\int_{\mu_1}^{\mu_2}\omega(x)[q(x)-p(x)]^2\phi''\big(q(x)\big)\,dx\\
&\qquad+\int_{\mu_1}^{\mu_2}\omega(x)[q(x)-p(x)]\phi'\big(q(x)\big)\,dx.
\end{aligned}
$$

Hence, the proof of Theorem 2.4 is completed. ■

Corollary 2.4. Assume that the conditions of Theorem 2.4 are fulfilled. Then

$$
\begin{aligned}
&\phi(\bar{p})-\frac{1}{\omega^*}\int_{\mu_1}^{\mu_2}\omega(x)\phi\big(p(x)\big)dx\\
&\qquad\le\frac{1}{6\omega^*}\left(\frac{3}{4}\right)^{\frac{1}{r}}\int_{\mu_1}^{\mu_2}\omega(x)[\bar{p}-p(x)]^3\left(\frac{3|\phi'''(\bar{p})|^r+\left|\phi'''\big(p(x)\big)\right|^r}{3}\right)^{\frac{1}{r}}dx\\
&\qquad+\frac{1}{2}\bar{p}^2\phi''(\bar{p})-\frac{1}{2\omega^*}\phi''(\bar{p})\int_{\mu_1}^{\mu_2}\omega(x)p^2(x)dx.
\end{aligned}
$$

Proof. Choosing $q=\bar{p}$ in Theorem 2.4, we get the required result.

3. APPLICATIONS

In this section, we will provide some applications of our main results in information theory. More precisely, estimations for Csiszár and Kullback–Leibler divergences, and Shannon entropy.

Definition 3.1. Let $\Phi:(0,+\infty)\longrightarrow\mathbb{R}$ be a convex function and $p,q:[\mu_1,\mu_2]\longrightarrow(0,+\infty)$ are two integrable functions. Then the Csiszár divergence is defined by

$$
C_\Phi(p,q):=\int_{\mu_1}^{\mu_2}p(x)\Phi\left(\frac{q(x)}{p(x)}\right)dx.
$$

Definition 3.2. Let $p,q:[\mu_1,\mu_2]\longrightarrow(0,+\infty)$ be two probability distributions. Then the Kullback–Leibler divergence is given by

$$\mathrm{KL}(p,q) := \int_{\mu_1}^{\mu_2} p(x)\log\left(\frac{q(x)}{p(x)}\right) dx.$$

Definition 3.3. Let $p : [\mu_1, \mu_2\ ] \longrightarrow (0, +\infty)$ be a positive probability distribution. Then the Shannon entropy is defined by

$$\mathcal{SE}(p) := -\int_{\mu_1}^{\mu_2} p(x)\log\big(p(x)\big)\, dx.$$

Definition 3.4. Let $p, q : [\mu_1, \mu_2\ ] \longrightarrow (0, +\infty)$ be two probability distributions. Then the Jeffrey's distance is given by

$$D_J(p,q) := \int_{\mu_1}^{\mu_2} [p(x) - q(x)]\log\left(\frac{p(x)}{q(x)}\right) dx.$$

Proposition 3.1. Let $\phi : [\nu_1, \nu_2] \longrightarrow \mathbb{R}$ be a third differentiable function, such that ϕ''' is integrable and $|\phi'''|^r$ is convex, for $r > 1$. Assume that $p, q: [\mu_1, \mu_2] \longrightarrow (0, +\infty)$, $\omega: [\mu_1, \mu_2] \longrightarrow (0, +\infty)$ are integrable functions, and $\frac{p(x)}{\omega(x)}, \frac{q(x)}{\omega(x)} \in [\nu_1, \nu_2]$, for $x \in [\mu_1, \mu_2]$. Then

$$\begin{aligned}
&C_\Phi(\omega, q) - C_\Phi(\omega, p) \\
&\quad\le \frac{1}{2}\int_{\mu_1}^{\mu_2} \frac{[q(x) - p(x)]^3}{\omega^2(x)}\left(\frac{(2r+1)\left|\phi'''\left(\frac{q(x)}{\omega(x)}\right)\right|^r + \left|\phi'''\left(\frac{p(x)}{\omega(x)}\right)\right|^r}{(2r+1)(2r+2)}\right)^{\frac{1}{r}} dx \\
&\quad\quad - \frac{1}{2}\int_{\mu_1}^{\mu_2} \frac{[q(x) - p(x)]^2}{\omega(x)}\phi''\left(\frac{q(x)}{\omega(x)}\right) dx + \int_{\mu_1}^{\mu_2} [q(x) - p(x)]\phi'\left(\frac{q(x)}{\omega(x)}\right) dx.
\end{aligned}$$

Proof. By taking $p(x) = \frac{p(x)}{\omega(x)}$ and $q(x) = \frac{q(x)}{\omega(x)}$ and utilizing Theorem 2.1, we get the desired result.

Proposition 3.2. Assume that $\phi: [\nu_1, \nu_2] \longrightarrow \mathbb{R}$ be a third differentiable function, such that ϕ''' is integrable and $|\phi'''|^r$ is convex, for $r > 1$; $q, \omega: [\mu_1, \mu_2] \longrightarrow (0, +\infty)$, are integrable functions with $\int_{\mu_1}^{\mu_2} q(x)dx = \int_{\mu_1}^{\mu_2} \omega(x)dx = 1$, for $x \in [\mu_1, \mu_2]$. Then

$$\begin{aligned}
&\mathcal{SE}(p) - \mathrm{KL}(\omega, q) \\
&\le \int_{\mu_1}^{\mu_2} \frac{[q(x) - 1]^3}{\omega^2(x)}\left(\frac{(2r+1)\left(\frac{\omega(x)}{q(x)}\right)^{3r} + \big(\omega(x)\big)^{3r}}{(2r+1)(2r+2)}\right)^{\frac{1}{r}} dx \\
&- \frac{1}{2}\int_{\mu_1}^{\mu_2} \frac{[q(x) - 1]^2}{\omega(x)}\left(\frac{\omega(x)}{q(x)}\right)^2 dx - \int_{\mu_1}^{\mu_2} [q(x) - 1]\frac{\omega(x)}{q(x)} dx.
\end{aligned}$$

Proof. Applying Proposition 3.1 for $\phi(x) = -\log(x)$ and $p(x) = 1$, we obtain the desired result.

Proposition 3.3. Let $\omega, p, q : [\mu_1, \mu_2] \longrightarrow (0, +\infty)$ be integrable functions with $\int_{\mu_1}^{\mu_2} q(x)dx = \int_{\mu_1}^{\mu_2} \omega(x)dx = \int_{\mu_1}^{\mu_2} p(x)dx = 1$. Then

$$\begin{aligned}
&KL(\omega, q) - KL(\omega, p) \\
&\leq \int_{\mu_1}^{\mu_2} \frac{[q(x) - p(x)]^3}{\omega^2(x)} \left(\frac{(2r+1)\left(\frac{\omega(x)}{q(x)}\right)^{3r} + \left(\frac{\omega(x)}{p(x)}\right)^{3r}}{(2r+1)(2r+2)} \right)^{\frac{1}{r}} dx \\
&- \frac{1}{2}\int_{\mu_1}^{\mu_2} \frac{[q(x) - p(x)]^2}{\omega(x)} \left(\frac{\omega(x)}{q(x)}\right)^2 dx - \int_{\mu_1}^{\mu_2} [q(x) - p(x)] \frac{\omega(x)}{q(x)} dx.
\end{aligned}$$

Proof. Applying Proposition 3.1 for $\phi(x) = -\log(x)$, we get the desired result.

Proposition 3.4. Let $\omega, p, q : [\mu_1, \mu_2] \longrightarrow (0, +\infty)$ be integrable functions with $\int_{\mu_1}^{\mu_2} q(x)dx = \int_{\mu_1}^{\mu_2} \omega(x)dx = \int_{\mu_1}^{\mu_2} p(x)dx = 1$. Then

$$\begin{aligned}
&D_J(q, \omega) - D_J(p, \omega) \\
&\leq \frac{1}{2}\int_{\mu_1}^{\mu_2} \frac{[q(x) - p(x)]^3}{\omega^2(x)} \left(\frac{(2r+1)\left(\frac{q}{\omega} + 2\right)^r \left(\frac{\omega(x)}{q(x)}\right)^{3r} + \left(\frac{p}{\omega} + 2\right)^r \left(\frac{\omega(x)}{p(x)}\right)^{3r}}{(2r+1)(2r+2)} \right)^{\frac{1}{r}} dx \\
&- \frac{1}{2}\int_{\mu_1}^{\mu_2} \frac{[q(x) - p(x)]^2}{\omega(x)} \left(\frac{q}{\omega} + 1\right) \left(\frac{\omega(x)}{q(x)}\right)^2 dx \\
&- \int_{\mu_1}^{\mu_2} [q(x) - p(x)] \left\{ \log\left(\frac{q(x)}{\omega(x)}\right) + 1 - \frac{\omega(x)}{q(x)} \right\} dx.
\end{aligned}$$

Proof. Applying Proposition 3.1 for $\phi(x) = (x-1)\log(x)$ and replace $q(x) := \frac{q(x)}{\omega(x)}, p(x) := \frac{p(x)}{\omega(x)}$, respectively, we obtain the desired result.

4. CONCLUSIONS

The main goal in this paper was the estimations of the integral majorization using the class of third-differentiable convex functions pertaining to Hölder, Power-mean and Jensen type inequalities. We offer some applications of information theory in order to demonstrate the validity of our main results. We believe that our idea and technique can help interested researchers working in this field to study other different classes of convexity and find new interesting results.

REFERENCES

1. Gholamreza Zabandan, A new refinement of the Hermite-Hadamard inequality for convex functions, Journal of Inequalities in Pure and Applied Mathematics, Vol:10, No:2, 7 pp., 2009.
2. S. Mohammdi Aslani, Mohsen Rostamian Delavar, S. Mansour Vaezpour, Inequalities of Fejér type related to generalized convex functions with applications, International Journal of Analysis and Applications, Vol:16, No:1, 38-49, 2018.
3. Opeyemi Omotoyinbo, A. Mogbodemu, Some new Hermite-Hadamard integral inequalities for convex functions, International Journal of Science and Innovation Technology, Vol:1, No:1, 1-12, 2014.
4. Artion Kashuri, Rozana Liko, Some new Hermite-Hadamard type inequalities and their applications, Studia Scientarum Mathematicarum Hungarica, Vol:56, 103-142, 2019.
5. Serap Özcan, İmdat İşcan, Some new Hermite–Hadamard type inequalities for s-convex functions and their applications., Journal of inequalities and applications, Vol:2019, 1-11, 2019.
6. Silvestru Sever Dragomir, Josip Pecarič, Lars-Erik Persson, Some inequalities of Hadamard type, Soochow Journal of Mathematics, Vol:21, No:3, 335–341, 2001.
7. Mahir Kadakal, Imdat İşcan, Huriye Kadakal, Kerim Bekar, On improvements of some integral inequalities, Honam Mathematical Journal, Vol:43, No:3, 441–452, 2021.
8. A. McD. Mercer, A variant of Jensen's inequality, Journal of Inequalities in Pure and Applied Mathematics, Vol:4, No:4, 73, 2003.
9. Josip Pečarić, A companion inequality to Jensen–Steffensen's inequality, Journal of Approximation Theory, Vol:44, 289–291, 1985.
10. Josip Pečarić, Frank Proschan, Yung Liang Tong, Convex Functions, Partial Orderings and Statistcal Applications, Academic Press, 1992.
11. Albert W. Marshall, Ingram Olkin, Barry C. Arnold, Inequalities: Theory of majorization and its applications, 2nd ed., Springer Series in Statistics, Springer, 2011.
12. Shan-He Wu, Muhammad Adil Khan, Abdul Basir, Reza Saadati, Some majorization integral inequalities for functions defined on rectangles, Journal of Inequalities and Applications, Vol:2018, No:1, 1-13, 2018.
13. Shan- He Wu, Huan-Nan Shi, A relation of weak majorization and its applications to certain inequalities for means., Mathematica Slovaca, Vol:61, No:4, 561–570, 2009.
14. Muhammad Adil Khan, Shan- He Wu, Hidayat Ullah, Yu-Ming Chu, Discrete majorization type inequalities for convex functions on rectangles, Journal of Inequalities and Applications , Vol:2019, No:1, 1-18, 2019.
15. Silvestru Sever Dragomir, Some majorization type discrete inequalities for convex functions, Mathematical Inequalities and Applications, Vol:7, 207–216, 2004.
16. Shan-He Wu, Muhammad Adil Khan, Hidayat Ullah Haleemzai, Refinements of majorization inequality involving convex functions via Taylor's theorem with mean value form of the remainder, Mathematics, Vol:7, No:8, 663, 2019.
17. Abdul Basir, Muhammad Adil Khan, Hidayat Ullah, Yahya Almalki, Chanisara Metpattarahiran, Thanin Sitthiwirattham, Improvements of integral majorization inequality with applications to divergences, Axioms, Vol:13, No:1, 21, 2024.

18. Naveed Latif, Josif Pečarić, Ivan Perić, On Majorization, Favard and Berwald's Inequalities, Annals of Functional Analysis, Vol:2**,** No:1, 31-50, 2011.

EXPLORING MACHINE LEARNING TECHNIQUES FOR GENDER VOICE RECOGNITION USING LIMITED SPEECH DATA

Gözde Karataş Baydoğmuş[1], Şahsene Altınkaya[2], Nahide Zeynep Cicekli[3]

[1]Department of Computer Engineering, Marmara University, Istanbul, Türkiye

gkaratas@marmara.edu.tr,

[2]Department of Mathematics, Istanbul Beykent University, Istanbul, Türkiye

sahsenealtinkaya@beykent.edu.tr

[3]Nobel Ilac, Istanbul, Turkey

nzeynepcicekli@gmail.com

Abstract

Voice recognition has gained popularity, leading to extensive research in the artificial intelligence field, primarily utilizing machine learning algorithms. However, determining effective voice recognition algorithms for small datasets remains really hard challenge. This study focuses on the significance of machine learning algorithms in gender voice recognition. The study examines the impact of machine learning algorithms on a dataset of number of 3168 data and 21 features. Machine learning algorithms used in this study are Decision Tree, XGBoost, LightGBM, AdaBoost, Gradient Boosting, and $k-$Nearest Neighbor. These learning algorithms, especially boosting methods known for their success, are chosen for this study. Experimental results show that machine learning algorithms achieve successful performance rates particularly the Gradient Boosting algorithm. At the end, the study reaches 98.26% accuracy rate while deep learning approaches in existing literature achieves an accuracy rate of 97%. As a result of the study, it is seen that a high performance rate is achieved by using machine learning algorithms in small-sized datasets.

Keywords: Voice recognition, Gender, Machine learning, Sound processing.

1.INTRODUCTION

Gender voice recognition is a significant field of research that aims to develop automated systems capable of identifying the gender of a speaker based on their voice characteristics. This technology finds applications in various domains, such as speech recognition systems, voice assistants, forensic analysis, and social robotics. Traditionally, gender recognition has been performed manually by human listeners, but with the advancements in machine learning algorithms, automated methods have gained popularity due to their efficiency and accuracy.

Nowadays, the landscape of gender voice recognition has undergone a transformative shift with the emergence of machine learning algorithms. These algorithms have revolutionized the field by empowering computers to process extensive datasets and identify distinctive features that differentiate between male and female voices. These algorithms can be broadly classified into two categories: traditional machine learning algorithms and deep learning algorithms. Traditional approaches, such as support vector machines (SVM) and logistic regression, have gained widespread usage in gender classification tasks. These methods rely on manually engineered features derived from voice signals, such as pitch, formants, and spectral characteristics, to train their models. Conversely, deep learning algorithms, such as convolutional neural networks (CNNs) and recurrent neural networks (RNNs), have exhibited exceptional performance in automatically extracting features, acquiring hierarchical representations, and capturing intricate patterns within voice data. In this study, it is aimed to examine the performance of new but successful algorithms instead of frequently used algorithms in the literature. In this sense, 6 machine learning algorithms, namely XGBoost, LightGBM, AdaBoost, Gradient Boosting, Decision Tree and $K-$Nearest Neighbor, form the basis of the study. These algorithms are examined with the selected Gender Recognition by Voice dataset and the results are evaluated. Since the study focuses on examining the performance of boosting algorithms, not all machine learning algorithms are included in the study.

The research in gender voice recognition using machine learning algorithms has witnessed significant advancements in terms of accuracy and robustness. Numerous studies have explored different datasets, feature extraction techniques, and classification models to improve gender classification performance. Moreover, researchers have also investigated the impact of various factors, such as language, accent, age, and emotional state, on gender voice recognition. By incorporating diverse datasets and advanced machine learning algorithms, researchers strive to develop more sophisticated and reliable gender recognition systems that can adapt to real-world scenarios and achieve high accuracy rates.

Alnuaim and his colleagues employed Mozilla's "Common Voice" repository, an openly available assemblage of vocal samples accompanied by data on the speaker's gender [4]. Through the process of refining pre-existing ImageNet models using audio spectrograms, they attained favorable results on the MOZILLA dataset and satisfactory outcomes on the SVD and RAVDESS datasets. The research noted that the pretrained models maintained their prior knowledge, particularly in the initial layers, whereas the intermediate layers underwent substantial modifications to suit the audio classification objective.

In 2016, researchers discussed the utilization of acoustic properties of voices and speech for voice gender detection [5]. An MLP model was employed to classify voice samples based on the provided dataset parameters. It is suggested that incorporating a larger dataset of voice samples can help reduce incorrect classifications resulting from variations in intonation. Furthermore, a webpage was created to facilitate the development of the model by allowing users to upload male and female voice samples as examples.

Gupta and their team created a computer program that utilizes sound-based cues to determine gender in speech [6]. Instead of relying solely on one characteristic, the research took into account twenty acoustic variables and employs three distinct models. While fuzzy logic-based techniques were investigated, they proved to be less precise when compared to neural network-based systems. To improve efficiency and minimize errors, a stacked model was utilized, leveraging the outcomes of each individual model to train new models. This approach resulted in a 96.74% accuracy rate when using stacked Random Forest and stacked Neural Network models, with no notable changes observed when applying stacked SVM.

Zvarevashe and Olugbara introduced the RF-RFE technique for selecting features in gender voice recognition [7]. The experiments demonstrated that RF-RFE enhances the accuracy of gender voice recognition, albeit with a marginal improvement when compared to the GBMs, FFNN, and ELMs algorithms. However, it is suggested that with larger datasets, the increment in accuracy could be more significant. The GBM algorithm showed surprisingly high recognition accuracy, making it a viable option for gender voice recognition, while FFNN and ELMs also achieved relatively high accuracy. However, GBMs and FFNN exhibited slower computational performance compared to ELMs, requiring more processing power.

In a study conducted in 2019, the primary objective was to examine the identification of gender in Javanese speech. The research employed techniques to reduce noise and focused on 10 individuals (comprising 5 males and 5 females) for analysis. The MFFC approach was utilized to extract features from 150 distinct gender-related sounds [8]. Classification methods, namely Logistic Regression, Support Vector Machines (SVM), and Deep Learning, were applied, resulting in varying levels of accuracy, classification error, and AUC. Notably, the Deep Learning approach outperformed the other methods, achieving a remarkable accuracy rate of 97.78% in gender speech recognition.

In 2021, a group of researchers conducted a study comprised of three key elements: audio preprocessing, feature extraction, and machine learning classification [9]. The audio preprocessing stage aimed to diminish background noise and highlight human voices, as the audio recordings were not captured in controlled environments. The study employed MFCC coefficients for analysis purposes. Two datasets and seven machine learning algorithms were utilized. The findings revealed that the integration of machine learning classifiers in the classification procedure enhanced accuracy, with RF classifiers achieving a 97.9% accuracy rate.

The following parts of the study are as follows; information about the proposed model and dataset is given in Section 2. In Section 3, the experimental results are mentioned. And in Section 4, the results of the study and future studies are mentioned.

2.GENERAL PROPERTIES OF METHOD

In this section, the selected dataset, the examined machine learning algorithms and the proposed model are presented.

2.1.Dataset

For this research, the Gender Recognition by Voice dataset sourced from Kaggle was employed [10]. This dataset was curated by discerning the gender of voices through the analysis of their acoustic characteristics and speech patterns. It encompasses a combined total of 3168 voice records, categorized as either male or female. The audio samples underwent processing within the frequency range of 0Hz to 280Hz, which corresponds to the typical range of human vocalizations.

TABLE 1: Features in the dataset

"meanfreq","sd","median","Q25","Q75","IQR","skew","kurt","sp.ent","sfm", "mode","centroid","meanfun","minfun","maxfun","meandom","mindom", "maxdom","dfrange","modindx","label"

It consists of 22 features in total. 21 of these properties are general properties of the data, and one of them is the Label column. The properties of the dataset are given in Table 1.

TABLE 2: Label's in the dataset

Label	Numerical Representation	Number of Data
Male	0	1584
Female	1	1584

2.2.Machine Learning Algorithms

Decision Tree algorithm is a versatile and interpretable method for classification and regression tasks [11]. It creates a tree-like structure where each node represents a feature or attribute and each leaf node represents a class label or numerical value. By traversing the tree using decision rules, predictions are made based on input features. Decision trees handle both numerical and categorical features, can handle missing values, and automatically select relevant features. Pruning and ensembling techniques can improve their performance. Overall, Decision Trees offer a flexible and intuitive approach to problem-solving in machine learning.

XGBoost is an advanced machine learning algorithm that has gained significant popularity due to its exceptional performance in various data science competitions [12]. It stands for Extreme Gradient Boosting and is based on the gradient boosting framework. XGBoost uses a combination of weak prediction models, typically decision trees, and sequentially improves them by minimizing a specific loss function. It employs a gradient descent optimization technique to efficiently learn and update model parameters. XGBoost also incorporates regularization methods to prevent overfitting and enhance generalization. This algorithm supports both classification and regression tasks and has robust handling capabilities for missing values and categorical features. It also provides a range of hyperparameters that allow fine-tuning to achieve optimal model performance. XGBoost's speed, scalability, and high accuracy make it a powerful tool in machine learning applications.

LightGBM is a popular gradient boosting framework that offers high performance and efficiency in machine learning tasks. It stands for Light Gradient Boosting Machine and is designed to handle large-scale datasets efficiently [13]. LightGBM uses a technique called Gradient-based One-Side Sampling (GOSS) to select and prioritize the most informative data instances during the boosting process, which significantly reduces memory consumption and improves training speed. It also employs a histogram-based approach to binning numerical features, enabling faster computation and better accuracy. LightGBM supports both classification and regression tasks, and it incorporates regularization techniques like L1 and L2 to prevent overfitting. Additionally, it provides a wide range of hyperparameters that can be tuned to optimize model performance. With its speed, memory efficiency, and accuracy, LightGBM is a valuable algorithm in machine learning applications, particularly when dealing with large and complex datasets.

AdaBoost, short for Adaptive Boosting, is a popular ensemble learning algorithm in machine learning [14]. It combines multiple weak classifiers to create a strong classifier. The algorithm works by assigning weights to each training example, with more emphasis on the misclassified examples in each iteration. In subse- quent iterations, the weak classifiers focus on correctly classifying the previously misclassified examples. By iteratively adjusting the weights and combining the weak classifiers, AdaBoost gradually improves its performance. The final prediction is made by taking a weighted vote from all the weak classifiers. AdaBoost is particularly effective in handling complex classification problems and has shown good generalization capabilities. It can be used with various base classifiers, such as decision trees or linear models. AdaBoost is known for its ability to achieve high accuracy and has been widely used in practical applications.

Gradient Boosting is a powerful machine learning algorithm that combines weak prediction models to create a strong predictive model [14]. It operates in an iterative manner, where each weak model is trained to correct the mistakes made by the previous models. The algorithm focuses on minimizing a specified loss function by employing gradient descent optimization. At each iteration, the algorithm calculates the gradient of the loss function and updates the model accordingly. Gradient Boosting is capable of handling both regression and classification tasks and can accommodate various loss functions. It is known for its ability to capture complex patterns in data and produce accurate predictions. By carefully selecting hyperparameters and preventing overfitting, Gradient Boosting can yield impressive results across a wide range of applications.

K-Nearest Neighbor (KNN) algorithm is a simple yet effective supervised learning method used for classification and regression tasks [15]. It operates on the principle of similarity, where the prediction for a new data point is determined by the "k" nearest neighbors in the training set. The value of "k" represents the number of neighbors considered for the prediction. In the classification task, the majority class label among the neighbors is assigned to the new data point. For regression, the average of the target values of the neighbors is used as the prediction. KNN does not make any assumptions about the underlying data distribution and can handle both numerical and categorical features. However, it is sensitive to the choice of distance metric and requires sufficient training data. KNN is known for its simplicity and interpretability, making it a popular choice in various machine learning applications.

2.3.Proposed Model

The study investigates the effects of six machine learning algorithms on gender voice recognition. Specifically, the performances of boosting algorithms are evaluated, and their performance in voice recognition is observed. Accuracy rate, precision, recall, and F1-score values are measured as performance metrics. The formulas used for these evaluations are given in Equation 1 to Equation 4;

$$Accuracy = \frac{TP + TN}{TP + TN + FP + FN}, \tag{1}$$

$$Precision = \sum_{i=1}^{L} \frac{TP_i}{TP_i + FP_i}, \tag{2}$$

$$Recall = \sum_{i=1}^{L} \frac{TP_i}{TP_i + FN_i}, \tag{3}$$

$$F1\,Score = \frac{(\beta^2 + 1)Precision \times Recall}{\beta^2 Precision \times Recall}, \tag{4}$$

where TN is true negative, TP is true positive, FN is false negative, FP is false positive, L is number of classes, and β is a balancing factor.

The flow chart of the study is given in Figure 1.

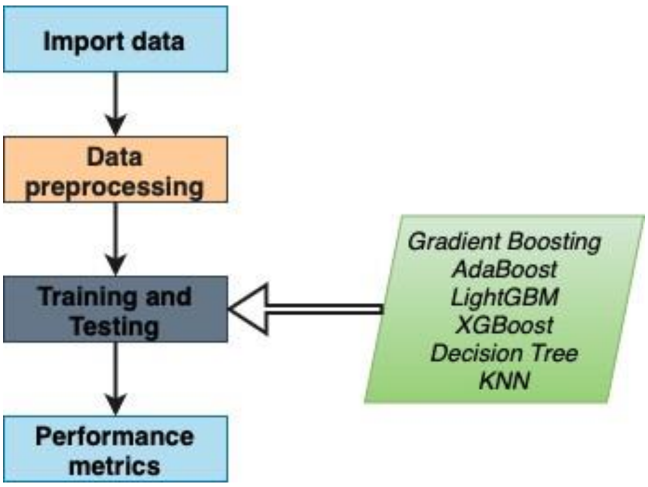

Fig. 1: Flaw chart of the study

When examining Figure 1, the first step involves dividing the dataset into training and testing sets. Following preliminary research in the literature, 80% of the dataset is allocated for training, while the remaining 20% is designated for testing purposes. Subsequently, each algorithm is individually trained using the dataset, and the previously mentioned performance evaluations are conducted. An important consideration in this process is determining the parameters of the algorithms. To ensure comparability with the literature, default parameters are used for all algorithms. For the KNN algorithm, a value of 2 is selected for the k parameter due to the binary classification.

TABLE 3: Precision and recall results

Algorithm	Precision (%)	Recall (%)
Gradient Boosting	98	98
XGBoost	98	98
AdaBoost	98	98
LightGBM	98	98
Decision Tree	97	97
KNN	91	71

3. EXPERIMENTAL RESULTS

For the study, a computer equipped with an 11th Gen Intel(R) Core(TM) i5-1145G7 CPU @ 2.60GHz, 2.61GHz, and 6GB RAM is utilized. Information, including the precision and recall values of the algorithms employed in the study, can be found in Table 3.

When examining Table 3, it can be observed that boosting algorithms outperform standard machine learning algorithms, yielding significantly better results. Moreover, the precision values of the boosting algorithms excees 98%.

Figure 2 shows the accuracy rate results of the selected algorithms.

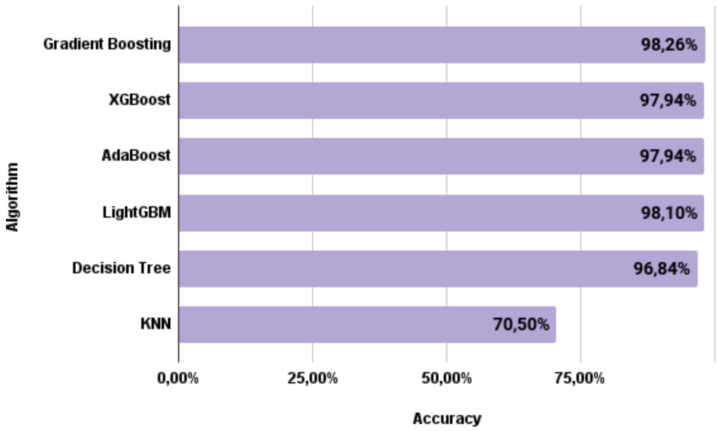

Fig. 2: Algorithms accuracy rates

When examining Figure 2, it becomes evident that all machine learning algorithms perform well in gender voice recognition. However, since the focus of the study is on examining boosting algorithms, they are specifically evaluated, and it is observed that the Gradient Boosting algorithm exhibited exceptional prediction capabilities.

Figure 3 displays the F1-score values of the selected machine learning algorithms. Once again, upon examining the graph, it is evident that the boosting algorithms demonstrate remarkable success.

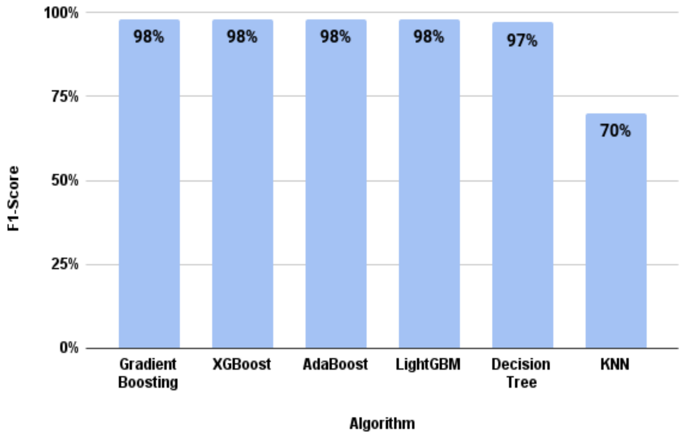

Fig. 3: Algorithms F1-scores

4.CONCLUSIONS

Voice recognition processes have gained significant popularity in recent years, capturing the attention of researchers. Particularly, with the advancement of artificial intelligence algorithms, extensive research has been conducted in this field. A literature and market search reveals that the majority of voice recognition studies utilize artificial neural networks and deep learning algorithms. While these algorithms yield better results with big data, determining effective voice recognition algorithms on small datasets has become a focal point of this study.

This study examines the significance of boosting machine learning algorithms in gender voice recognition. The impact of machine learning algorithms is observed on a dataset comprising 3168 data and 21 features. Given the notable success achieved by boosting algorithms in recent years, their potential for successful results in gender voice recognition is explored, making them the preferred choice in this study. Upon analyzing the overall results, it is found that machine learning algorithms deliver successful outcomes. While the literature-based studies utilizing deep learning achieves an accuracy rate of 97% [6], [8], [9], this study attains a accuracy rate of 98.26% using the Gradient Boosting algorithm. These findings demonstrate the successful utilization of boosting algorithms in gender voice recognition.

Future research endeavors will primarily focus on disease detection through sound analysis. Studies will be conducted to estimate the type of disease a patient has based on coughing, sneezing, speaking, breathing, and other related sounds.

REFERENCES

[1] Tandel, N. H., Prajapati, H. B., Dabhi, V. K. (2020). Voice recognition and voice comparison using machine learning techniques: A survey. In 2020 6th International Conference on Advanced Computing and Communication Systems (ICACCS) (pp. 459-465). IEEE.

[2] Nassif, A. B., Shahin, I., Attili, I., Azzeh, M., Shaalan, K. (2019). Speech recognition using deep neural networks: A systematic review. IEEE access, 7, 19143-19165.

[3] Padmanabhan, J., Johnson Premkumar, M. J. (2015). Machine learning in automatic speech recognition: A survey. IETE Technical Review, 32(4), 240-251.

[4] Alnuaim, A. A., Zakariah, M., Shashidhar, C., Hatamleh, W. A., Tarazi, H., Shukla, P. K., Ratna, R. (2022). Speaker gender recognition based on deep neural networks and ResNet50. Wireless Communications and Mobile Computing, 2022, 1-13.

[5] Buyukyilmaz, M., Cibikdiken, A. O. (2016). Voice gender recognition using deep learning. In 2016 International Conference on Modeling, Simulation and Optimization Technologies and Applications (MSOTA2016) (pp. 409-411). Atlantis Press.

[6] Gupta, P., Goel, S., Purwar, A. (2018). A stacked technique for gender recognition through voice. In 2018 Eleventh International Conference on Contemporary Computing (IC3) (pp. 1-3). IEEE.

[7] Zvarevashe, K., Olugbara, O. O. (2018). Gender voice recognition using random forest recursive feature elimination with gradient boosting machines. In 2018 International conference on advances in big data, computing and data communication systems (icABCD) (pp. 1-6). IEEE.

[8] Nugroho, K., Noersasongko, E., Santoso, H. A. (2019). Javanese gender speech recognition using deep learning and singular value decomposition. In 2019 International Seminar on Application for Technology of Information and Communication (iSemantic) (pp. 251- 254). IEEE.

[9] Ali, A. T., Abdullah, H. S., Fadhil, M. N. (2021). Voice recognition sys- tem using machine learning techniques. Materials Today: Proceedings, 1-7.

[10] "Gender Recognition by Voice", https://www.kaggle.com/datasets

[11] De Ville, B. (2013). Decision trees. Wiley Interdisciplinary Reviews: Computational Statistics, 5(6), 448-455.

[12] Dong, W., Huang, Y., Lehane, B., Ma, G. (2020). XGBoost algorithm- based prediction of concrete electrical resistivity for structural health monitoring. Automation in Construction, 114, 103155.

[13] Ke, Guolin, et al. Lightgbm: A highly efficient gradient boosting decision tree, Advances in neural information processing systems 30 (2017).

[14] Schapire, Robert E. Explaining adaboost, Empirical Inference: Festschrift in Honor of Vladimir N. Vapnik (2013): 37-52.

[15] Peterson, Leif E. K-nearest neighbour. Scholarpedia 4.2 (2009): 1883.

ON ρ-STATISTICAL CONVERGENCE DEFINED BY MODULAR SEQUENCE SPACES OF ORDER α

Gülcan Atıcı Turan [1]

[1] Vocational School of Tunceli, Munzur University, Tunceli, Turkey

gatici23@hotmail.com,

Abstract

In this paper, we introduce Wijsman ρ-statistical convergence of order α and Wijsman strongly ρ-convergence of order α and define $\left[W_\rho^\alpha, \mathcal{M}, v, p\right]$ by using a sequence of Orlicz functions. Also, some inclusion theorems are presented.

Keywords: Wijsman convergence; statistical convergence; Orlicz function.

1.INTRODUCTION

Zygmund [1] was the person behind the introduction of the idea of statistical convergence. The concept of statistical convergence was formally given by Fast [2] and Steinhaus [3]. This concept was studied by Schoenberg [4] as a non-matrix summability method. Also, the concept of statistical convergence has been extended by several authors.

A real or complex number sequence $x = (x_k)$ is said to be statistically convergent to ℓ if for every $\epsilon > 0$

$$\lim_{n\to\infty} \frac{1}{n} |\{k \le n: |x_{\mathrm{k}} - \ell| \ge \epsilon\}| = 0.$$

Let (X, σ) be a metric space. The distance $d(x, \mathrm{A})$ from a point x to a non-empty subset A of (X, σ) is defined to be

$$\mathrm{d}(\mathrm{X}, \sigma) = \inf_{y\in A} \sigma(x, y).$$

If $sup_k d(x, \mathrm{A_k}) < \infty$ (for each $x\epsilon X$), then we say that the sequence $\{\mathrm{A_k}\}$ is bounded.

Nuray and Rhoades [5] were given the concepts of Wijsman statistical convergence for the sequence and the concept were generalized by Ulusu et al. ([6],[7]).

Let (X, σ) be a metric space and $\alpha\epsilon(0,1]$. For any non-empty closed subsets $\mathrm{A}, \mathrm{A_k} \subset \mathrm{X}$, we say that the sequence $\{\mathrm{A_k}\}$ is Wijsman ρ-statistical convergent to A of order α (or WS_ρ^α-convergent to A) if for each $\epsilon > 0$ and $x\epsilon X$,

$$\lim_{n\to\infty} \frac{1}{\rho_n^\alpha} |\{k \le n: |d(x, \mathrm{A_k}) - d(x, \mathrm{A})| \ge \epsilon\}| = 0,$$

1

where $\rho = (\rho_n)$ is a non-decreasing sequence of positive real numbers tending to ∞ such that

$$\limsup_n \frac{\rho_n}{n} < \infty, \quad \Delta\rho_n = O(1) \quad \text{and} \quad \Delta\rho_n = \rho_{n+1} - \rho_n$$

for each positive integer n. In this case, we write $\mathrm{A_k} \to A(WS_\rho^\alpha)$. The set of all Wijsman ρ-statistical convergent sequences to A of order α will be denoted by WS_ρ^α [8].

Let (X, σ) be a metric space and $\alpha \epsilon (0,1]$. For any non-empty closed subsets $\mathrm{A}, \mathrm{A_k} \subset \mathrm{X}$, we say that the sequence $\{\mathrm{A_k}\}$ is said to be Wijsman strongly ρ-summable of order α to A, if for each $\epsilon > 0$ and $x \epsilon X$,

$$\lim_{n\to\infty} \frac{1}{\rho_n^\alpha} \sum_{k=1}^{n} |d(x, \mathrm{A_k}) - d(x, \mathrm{A})| = 0.$$

The set of all Wijsman strongly ρ-summable sequences of order α to A will be denoted by W_ρ^α. In this case we write $\mathrm{A_k} \to A(W_\rho^\alpha)$ [8].

In the following definition, theorems and results, the sequence $\rho = (\rho_n)$ will be used as above.

2.MAIN RESULTS

An Orlicz function is a function $M: [0, \infty) \to [0, \infty)$ which is continuous, non-decreasing and convex with $M(0) = 0$, $M(x) > 0$ for $x > 0$ and $M(x) \to \infty$ as $x \to \infty$.

It is well known that if M is a convex function and $M(0) = 0$, then $M(\lambda x) \leq \lambda M(x)$ for all λ with $0 \leq \lambda \leq 1$.

Lindenstrauss and Tzafriri [9] used the idea of Orlicz function to define what is called an Orlicz sequence space

$$\ell_M = \left\{ x \in w: \sum_{k=1}^{\infty} M\left(\frac{|x_k|}{\rho}\right) < \infty, \text{for some } \rho > 0 \right\}$$

which is a Banach space with the norm

$$\|x\| = inf \left\{ \rho > 0: \sum_{k=1}^{\infty} M\left(\frac{|x_k|}{\rho}\right) \leq 1 \right\}.$$

Definition 1. Let $\mathcal{M} = (M_k)$ be a sequence of Orlicz functions and (X, σ) be a metric space. Let $p = (p_k)$ be a sequence of strictly positive real numbers, $v = (v_k)$ be a sequence of positive real numbers, $\alpha \in (0,1]$, $\rho = (\rho_n)$ be a sequence and for $\lambda > 0$. Then we define the following sequence space:

$$\left(W_\rho^\alpha, \mathcal{M}, p, v\right) = \left\{ \{A_k\} \in X : \frac{1}{\rho_n^\alpha} \sum_{k=1}^{n} v_k \left[M_k \left(\frac{|d(x, A_k) - d(x, A)|}{\lambda} \right) \right]^{p_k} \to 0, \right.$$

$$\left. \text{for some } A \text{ and for } x \in X \right\}.$$

If $p_k = 1$ for all $k \in \mathbb{N}$ then we shall write $\left(W_\rho^\alpha, \mathcal{M}, p, v\right) = \left(W_\rho^\alpha, \mathcal{M}, v\right)$. If $M_k(x) = x$ for all $k \in \mathbb{N}$ then we shall write $\left(W_\rho^\alpha, \mathcal{M}, p, v\right) = \left(W_\rho^\alpha, p, v\right)$. If $M_k(x) = x$, $v_k = 1$ and $p_k = 1$ for all $k \in \mathbb{N}$ then we shall write $\left(W_\rho^\alpha, \mathcal{M}, p, v\right) = W_\rho^\alpha$.

In the following theorems, assume that the sequence $p = (p_k)$ is bounded and $0 < h = inf_k p_k \leq p_k \leq sup_k p_k = H < \infty$.

Theorem 2. Let $\mathcal{M} = (M_k)$ be a sequence of Orlicz functions, $0 < \alpha \leq \beta \leq 1$ and $\rho = (\rho_n)$ be a sequence, then $\left(W_\rho^\alpha, \mathcal{M}, p, v\right) \subset WS_\rho^\beta$.

Proof. Let $\{A_k\} \in \left(W_\rho^\alpha, \mathcal{M}, p, v\right)$. Let $\epsilon > 0$ be given. As $\rho_n^\alpha \leq \rho_n^\beta$ for each n we can write

$$\frac{1}{\rho_n^\alpha} \sum_{k=1}^{n} v_k \left[M_k \left(\frac{|d(x, A_k) - d(x, A)|}{\lambda} \right) \right]^{p_k} =$$

$$\frac{1}{\rho_n^\alpha} \sum_{\substack{k=1 \\ |d(x,A_k)-d(x,A)| \geq \epsilon}}^{n} v_k \left[M_k \left(\frac{|d(x, A_k) - d(x, A)|}{\lambda} \right) \right]^{p_k}$$

$$+ \frac{1}{\rho_n^\alpha} \sum_{\substack{k=1 \\ |d(x,A_k)-d(x,A)| < \epsilon}}^{n} v_k \left[M_k \left(\frac{|d(x, A_k) - d(x, A)|}{\lambda} \right) \right]^{p_k}$$

$$\geq \frac{1}{\rho_n^\beta} \sum_{\substack{k=1 \\ |d(x,A_k)-d(x,A)| \geq \epsilon}}^{n} v_k \left[M_k \left(\frac{|d(x, A_k) - d(x, A)|}{\lambda} \right) \right]^{p_k}$$

$$+ \frac{1}{\rho_n^\beta} \sum_{\substack{k=1 \\ |d(x,A_k)-d(x,A)| < \epsilon}}^{n} v_k \left[M_k \left(\frac{|d(x, A_k) - d(x, A)|}{\lambda} \right) \right]^{p_k}$$

$$\geq \frac{1}{\rho_n^\beta} \sum_{\substack{k=1 \\ |d(x,A_k)-d(x,A)| \geq \epsilon}}^{n} v_k \left[M_k \left(\frac{\epsilon}{\lambda} \right) \right]^{p_k} \geq \frac{1}{\rho_n^\beta} \sum_{\substack{k=1 \\ |d(x,A_k)-d(x,A)| \geq \epsilon}}^{n} min([M_k(\epsilon_1)]^h, [M_k(\epsilon_1)]^H)$$

$$\geq \frac{1}{\rho_n^\beta} |\{k \leq n : |d(x, A_k) - d(x, A)| \geq \epsilon\}| min([M_k(\epsilon_1)]^h, [M_k(\epsilon_1)]^H)$$

where $\epsilon_1 = \frac{\epsilon}{\lambda}$. From the above inequality we have $\{A_k\} \in WS_\rho^\alpha$.

Corollary 3.

(i) Let $\mathcal{M} = (M_k)$ be a sequence of Orlicz functions, $0 < \alpha \leq 1$ and $\rho = (\rho_n)$ be a sequence, then $\left(W_\rho^\alpha, \mathcal{M}, p, v\right) \subset WS_\rho^\alpha$.

(ii) Let $\mathcal{M} = (M_k)$ be a sequence of Orlicz functions, $0 < \alpha \leq \beta \leq 1$ and $\rho = (\rho_n)$ be a sequence, then $\left(W_\rho^\alpha, \mathcal{M}, v\right) \subseteq WS_\rho^\beta$.

Theorem 4. Let $\mathcal{M} = (M_k)$ be a sequence of Orlicz functions, $0 < \alpha \leq \beta \leq 1$ and $\rho = (\rho_n)$ be a sequence, then $\left(W_\rho^\alpha, \mathcal{M}, v\right) \subseteq \left(W_\rho^\beta, \mathcal{M}, v\right)$.

Theorem 5. Let $\mathcal{M} = (M_k)$ be a sequence of Orlicz functions, $0 < \alpha \leq \beta \leq 1$ and $\rho = (\rho_n)$ and $\tau = (\tau_n)$ be two sequences such that $\rho_n \leq \tau_n$ for all $n \in \mathbb{N}$. If $\lim_{n\to\infty} \frac{\rho_n^\alpha}{\tau_n^\beta} = t > 0$, then $\left(W_\tau^\beta, \mathcal{M}, v\right) \subseteq \left(W_\rho^\alpha, \mathcal{M}, v\right)$.

Corollary 6. Let $\mathcal{M} = (M_k)$ be a sequence of Orlicz functions, $\rho = (\rho_n)$ and $\tau = (\tau_n)$ be two sequences such that $\rho_n \leq \tau_n$ for all $n \in \mathbb{N}$. If $\lim_{n\to\infty} \frac{\rho_n^\alpha}{\tau_n^\beta} = t > 0$ holds, then $(W_\tau^\alpha, \mathcal{M}, v) \subseteq \left(W_\rho^\alpha, \mathcal{M}, v\right)$ for $0 < \alpha \leq 1$.

Theorem 7. Let $\mathcal{M} = (M_k)$ be a sequence of Orlicz functions, $0 < \alpha \leq \beta \leq 1$ and $\rho = (\rho_n)$ and $\tau = (\tau_n)$ be two sequences such that $\rho_n \leq \tau_n$ for all $n \in \mathbb{N}$. If $\lim_{n\to\infty} \frac{\rho_n^\alpha}{\tau_n^\beta} = 1$, then $\left(W_\tau^\beta, \mathcal{M}, v\right) \subseteq WS_\rho^\alpha$.

Theorem 8. Let $\mathcal{M} = (M_k)$ be a sequence of Orlicz functions and $inf_k p_k > 0$, the limit of any sequence $\{A_k\} \in \left(W_\rho^\alpha, \mathcal{M}, p, v\right)$ is unique.

Proof. Let $lim_k p_k = s > 0$. Suppose that $A_k \to A_1\left(\left(W_\rho^\alpha, \mathcal{M}, p, v\right)\right)$ and $A_k \to A_2\left(\left(W_\rho^\alpha, \mathcal{M}, p, v\right)\right)$. Then there exists $\lambda_1 > 0$ and $\lambda_2 > 0$ such that

$$\lim_{n\to\infty} \frac{1}{\rho_n^\alpha} \sum_{k=1}^{n} v_k \left[M_k\left(\frac{|d(x, A_k) - d(x, A_1)|}{\lambda_1}\right)\right]^{p_k} = 0,$$

and

$$\lim_{n\to\infty} \frac{1}{\rho_n^\alpha} \sum_{k=1}^{n} v_k \left[M_k\left(\frac{|d(x, A_k) - d(x, A_2)|}{\lambda_2}\right)\right]^{p_k} = 0.$$

Define $\lambda = max\{2\lambda_1, 2\lambda_2\}$. Since M_k are nondecreasing and convex, we have

$$\frac{1}{\rho_n^\alpha}\sum_{k=1}^{n} v_k\left[M_k\left(\frac{|d(x,A_1)-d(x,A_2)|}{\lambda}\right)\right]^{p_k}$$

$$=\frac{D}{\rho_n^\alpha}\sum_{k=1}^{n}\frac{1}{2^{p_k}}v_k\left[M_k\left(\frac{|d(x,A_k)-d(x,A_1)|}{\lambda_1}\right)\right]^{p_k}$$
$$+\frac{D}{\rho_n^\alpha}\sum_{k=1}^{n}\frac{1}{2^{p_k}}v_k\left[M_k\left(\frac{|d(x,A_k)-d(x,A_2)|}{\lambda_2}\right)\right]^{p_k}\to 0$$

as $n\to\infty$, where $sup_k p_k = H$ and $D = max(1, 2^{H-1})$. Therefore we get

$$\lim_{n\to\infty}\frac{1}{\rho_n^\alpha}\sum_{k=1}^{n} v_k\left[M_k\left(\frac{|d(x,A_1)-d(x,A_2)|}{\lambda}\right)\right]^{p_k}=0.$$

As $lim_k p_k = s$, we have

$$\left[M_k\left(\frac{|d(x,A_1)-d(x,A_2)|}{\lambda}\right)\right]^{p_k}=\left[M_k\left(\frac{|d(x,A_1)-d(x,A_2)|}{\lambda}\right)\right]^{s}$$

and so $A_1 = A_2$. This proves that the limit is unique.

REFERENCES

1. Antoni Zygmund, Trigonometric Series, 2nd edition, Cambridge University Press, London, 1979.
2. Henry Fast, Sur la convergence statistique, Colloquium Mathematicae, Vol:2, 241–244, 1951.
3. Hugo Steinhaus, Sur La Convergence Ordinaire Et La Convergence Asymptotique, Colloq. Math., Vol:2, 73–74, 1951.
4. Isaac Jacob Schoenberg, The Integrability of Certain Functions and Related Summability Methods, Amer. Math. Monthly, Vol:66, No:5, 361–375, 1959.
5. Fatih Nuray and Billy Eugene Rhoades, Statistical convergence of sequences of sets, Fasc. Math., Vol: 49, 87–99, 2012.
6. Uğur Ulusu and Erdinç Dündar, I-Lacunary Statistical Convergence of Sequences of Sets, Filomat, Vol:28, No:8, 1567–1574, 2014.
7. Uğur Ulusu and Fatih Nuray, Lacunary statistical convergence of sequence of sets, Prog. Appl. Math., Vol:4, No:2, 99–109, 2012.
8. Nazlım Deniz Aral, Hacer Şengül Kandemir, Mikail Et, On P-Statistical Convergence of Order a of Sequences of Sets, Miskolc Mathematical Notes, Vol:24, No:2, 569-578, 2023.
9. Joram Lindenstrauss and Lior Tzafriri, On Orlicz sequence spaces, Israel Journal of Mathematics, Vol:10, 379–390, 1971.
10. Karl Lindberg, On Subspaces of Orlicz Sequence Spaces, Studia Math., Vol:45, No:2, 119–146, 1973.

PERSONALITY ANALYSIS USING ARTIFICIAL INTELLIGENCE ACCORDING TO THE EYE DESCRIPTIONS IN MARIFETNÂME

Semra Çelebi[1], İbrahim Türkoğlu[2]

[1,2] Firat University, Faculty of Technology, Software Engineering Department, Elazig, Turkey

[1]scelebi@firat.edu.tr,

[2]iturkoglu@firat.edu.tr

Abstract

Body language, facial structure and general appearance can give many clues about a person's character at first impression. Therefore, people often form their prejudices about a person by basing their first impressions on these clues. The relationship between certain physical characteristics and character and intelligence has been remarkable historically as well as in modern science. In Old Turkish Literature, there are works aimed at character analysis from human physical characteristics. One of these works is Marifetnâme, written by the famous scientist and clergyman İbrahim Hakkı of Erzurum in 1756. In the section of Marifetnâme called "mirror of bodies", a connection is established between the human body and facial structures and the spiritual aspect. In this study, this connection written by İbrahim Hakkı was transformed into practice with today's technologies and artificial intelligence was used to carry out the character analysis of İbrahim Hakkı. For the decision process, training was performed with three different deep learning-based CNN models (AlexNet, ResNet and YOLOv8) and the results were compared. The proposed application process is based on three steps: In the first step, from each image in the dataset, first the face regions and then the areas where the eyes are located are cropped with a facial landmark detection algorithm. In the second step, an artificial intelligence model was determined to predict the eye structure in each frame. The third step aims to detect in real time the character trait associated with the eye structure determined using this model in Marifetnâme. As a result of this study, character analysis matched with 98% accuracy according to the developed artificial intelligence-based application process.

Keywords: İbrahim Hakkı; Marifetnâme; Artificial intelligence; Character analysis; Personality.

1.INTRODUCTION

Marifetnâme (Hakkı, 1756), written by the famous scientist and Sufi İbrahim Hakkı in 1756, is an important work of Islamic history. This work, which aroused great interest at the time it was written and is still the subject of current research today, has an encyclopedic structure as it contains comprehensive information in many different fields such as astronomy, anatomy, psychology, geography, mathematics, and philosophy. In the work, the section devoted to the science of anatomy, called "the mirror of bodies" by İbrahim Hakkı, presents detailed information and perspectives about the body (Okumuş, 2008). In Ulusoy's simplification (Ulusoy, 1980), in the seventeenth chapter of the third volume of Marifetnâme, information is given on the wisdom of the shapes and forms of body organs. The fourth article in this section, titled "Describes the shapes and forms of the head and neck and their related habits and natures", is the part related to our study. In this section, it is claimed that the body reflects the inner world of the person and that information about the human habit, character and morality can be obtained based on the body structure. The approaches here are noteworthy because of their similarity to the approaches to defining humans based on physiological foundations, which are prominent in the history of modern psychology (Sevinç, 2012).

Artificial intelligence is a discipline that aims to ensure that computer systems have a decision mechanism similar to human intelligence. By using large data sets and various algorithms and deep learning techniques, systems that can perform complex tasks and have learning and decision-making abilities can be developed. Facial recognition is a popular application of this technology. By analyzing visual data with advanced artificial intelligence architectures, facial expressions and other physical features can be interpreted. This widespread use has enabled the effective use of artificial intelligence in psychological evaluations such as character analysis. In this way, the data obtained from the individual's facial features can be analyzed in detail by artificial intelligence algorithms to obtain comprehensive information about their character properties. With its strong analytical capabilities in this field, artificial intelligence offers a new perspective on character analysis.

The main purpose of this study is to combine character analyzes derived from physiological characteristics in Marifetnâme with artificial intelligence-based methods. In Marifetnâme, personality traits are evaluated by examining the physiological structure of prominent parts of the face such as eyes, eyebrows, forehead, nose and mouth. Based on the important information obtained here, certain character traits are classified by analyzing the person's eye structure. This study discusses the creation of a model that categorizes these specific classes with the highest accuracy using multiple CNN (Convolutional Neural Network) architectures. It also focuses on how to integrate the model so that character properties can be instantly detected using user data obtained from the front camera.

In the second part, personality theories and commonly used models for analyzing personality traits through eye structure are discussed. The third section covers all the details of the study, from methodology to model training. Eye structure and personality matches in Marifetnâme, details of the data set used, use of Haar Cascade Classifier and facial landmark detection algorithm, and model training are among the topics discussed in this section. In the last section, a general evaluation was made about the application and the results obtained and information was given about the future work plan.

2. PERSONALITY ANALYSIS FROM THE EYES

As a highly social species, humans engage in complex interactions to support functioning in all aspects of their lives. Social communication between individuals depends on a type of signal exchange and the ability of individuals to make sense of these signals. Although speech is the most basic of these signals, there are many more signals such as facial expression, body posture, and gaze (Frith and Frith, 2008). One of the richest and most powerful tools in social communication is the face, which contains clues about individuals' gender, race, age, emotionality and even personal characteristics (Jack and Schyns, 2015). The richness of clues encoded in the human face has encouraged the scientific world to examine facial features in depth for personality analysis. Different indicators are used to describe people's personality types. The Myers-Briggs Indicator of Personality (MBTI) identifies a personality in four two-pole psychological dimensions and associates the person assessed with his preferences in each dimension: introverted (I) - outward (E), perceiving (S) - intuitive (N), thinking (T) - feeling (F) and judging (J) – understanding (P) (Harrington and Loffredo, 2010). The MBTI model proposes sixteen different personalities that contain combinations of different preferences. Five Factor Model (FFM) is a personality model that considers personality according to five basic dimensions. It includes the factors of openness (imagination, creativity, adventurism), extraversion (enterprising, talkativeness), adaptability (confidence, altruism), emotional balance (anxiety, depression, hostility) and sense of duty (self-discipline, order) (Yin et al., 2021). The Hans Eysenck model argues that genetic factors and environmental interactions affect personality variations (Eysenck, 2016). In this model, three basic dimensions are taken into account: extraversion, emotional stability and psychoticism. The most common method used to determine a person's personality in models such as MBTI, FFM, Hans Eysenck model is to ask people survey questions and decide on their potential personality by adapting their answers to the model (Bahri et al., 2023).

The organ structure and shape on the face contains information about individuals' personalities, in addition to information such as their emotional states, reactions, age and gender. Facial expression detection is used in many areas such as personality detection for the educational process of individuals (Bahri et al., 2023), diagnosis of neuropsychiatric disorders (Hamm et al., 2011), and pain assessment in patients (Rojo et al., 2015). Facial Action Coding System (FACS) is one of the most effective methods used in facial emotion analysis. Hidden emotions are determined by using micro-expressions formed as a result of emotions in the facial muscles (Gavrilescu, 2015). Each facial expression based on anatomical differences is considered as an action unit (AU). In each action unit, the position and movement of a certain part of the face such as eyebrows, eyes, lips, nose are classified according to their intensity and location (Yin et al., 2017), creating 44 action units and each of them is named with a different numerical code. 30 of these action units are related to the contraction of specific facial muscles, 12 of which are defined for the upper face and 18 for the lower face (Tian et al., 2001). Some of the eye identifications made with FACS are shown in Figure 1.

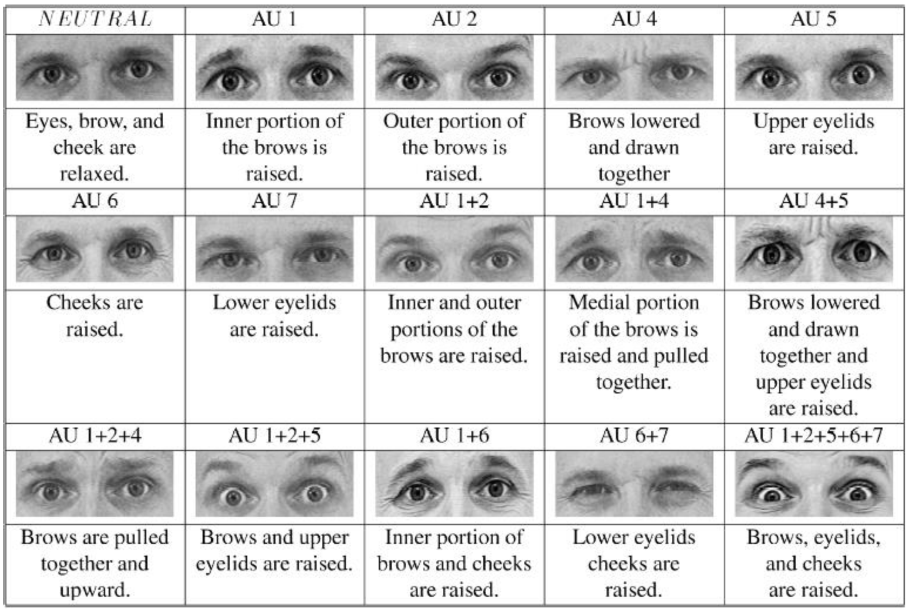

Figure 1. Some Eyes Combinations from Facial Action System (Tian et al., 2001)

Another method that can provide information about a person based on the eyes is eye tracking technology. By monitoring a person's eye movements, information such as what the person focuses on and for how long, his emotional state, and his reactions to visual stimuli are obtained. Eye tracking technology can be used to detect eye fatigue in the work environment (Li et al., 2024), to obtain aesthetic appreciation information for products (İlhan and Togay, 2023), to analyze consumers' risk preference (Zhen et al., 2024), to identify abnormal eye movements in patients with depression. It is used in many research fields such as (Gao et al., 2023). OpenFace, an open source software package, is a tool with important functions such as detecting facial expressions, estimating head pose, identifying facial action units, and eye gaze classification (Aydın, 2022). Emotient FACET and Affectiva AFFDEX are widely used systems to predict emotional reactions such as sadness, fear, joy, disgust and contempt from facial expressions in any scenario (Vogel et al., 2023).

3.APPLICATIONS

In this study, it is aimed to perform real-time personality analysis based on the eye structure of the given individuals in the input images. For this purpose, three different models were created by training with different architectures that perform the same classification. The goal was to identify the architecture that achieved the highest efficiency. AlexNet, ResNet, and YOLO architectures were used and compared to determine the model that achieved the most accurate results.

Images in the dataset was trimmed using Haar Cascade Classifier and landmark detection. After training using various architectures, the model that achieved the most efficient results was made ready to be used on real-time data. Real-time input images were also cropped using Haar Cascade Classifier and landmark detection and given as input to the trained model. The class detected by the model was associated with a personality trait, taking into account the limitations in Marifetnâme. The steps of our experimental methodology are shown in Figure 2.

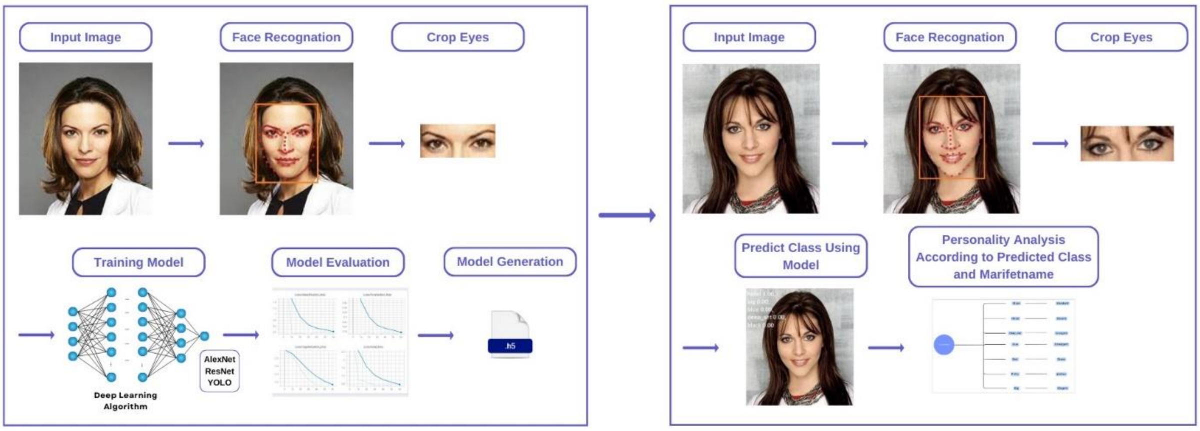

Figure 2. Flowchart of the Application

3.1. Evaluation of Eye Structure in Marifetnâme

The famous Turkish thinker and Sufi, İbrahim Hakkı of Erzurum, who lived in the 18th century, acquired comprehensive information by benefiting from the works of Islamic thinkers who lived before him, and wrote many books by blending this information with the knowledge and discoveries of his age. Marifetnâme, which he wrote in 1756, is İbrahim Hakkı's most important works. Work; It has an encyclopedic structure in that it includes many sciences such as astronomy, anatomy, psychology, geography, mathematics and philosophy. The original work is in two volumes and consists of a total of five chapters: an introduction, three main chapters and a conclusion. The work, originally in Turkish, had various editions made in Egypt, Kazan, Istanbul and Ankara and was translated into Arabic, Persian and French (Yılmaz, 2013).

In this study, information and perspectives about the eye in the anatomy section, which is called the "mirror of bodies" by İbrahim Hakkı in Marifetnâme and also contains information about physiognomy, are discussed. İbrahim Hakkı argues that the human head and neck region has various characteristics and that each feature contains information about human morality and character. By benefiting from the views of philosophers, he explains the subject as "The clothing of the head and neck limbs" discussed in verse under the title (Okumuş, 2008). The evaluations made about the eye structure are as follows; Having a hollow eye is evidence of being arrogant. Those with black eyes are obedient, those with red eyes are brave. The one with blue eyes is intelligent, the one with hazel eyes is decent and well-mannered. Big eyes are elegant and delicate, lumpy eyes are jealous. In this study, personality traits are analyzed from this perspective of İbrahim Hakkı.

3.2. Image Acquisition

In this study, VGGFace2, a dataset consisting of a total of 3.3 million different images belonging to more than 9000 different people, is used (Cao et al., 2018). There are an average of 370 photos for each person. It was created by downloading images of individuals selected from different ethnicities, different age groups and different professions from Google image search. The images have different resolutions and are different images. The data set is divided into 3.1 million training data and 200 thousand test data. In this study, a total of 4150 images were selected from the VGGFace2 dataset, including seven different eye structures (black, blue, hazel, large, lumpy, red and hollow) analyzed in Marifetnâme. This data is divided into 80% training data, 10% validation data and 10% test data to be used in neural networks.

3.3. Pre-Processing

3.3.1. Haar Cascade Classifier

Haar Cascade algorithm is a machine learning-based object detection algorithm proposed by Paul Viola and Michael Jones in their 2001 article (Viola and Jones, 2001). It is noteworthy that the algorithm can distinguish faces and body parts in an image (Yaddanapudi et al., 2023). The algorithm is trained with many positive (face-containing) and negative (face-free) images and then features are extracted using Haar Features in Figure 3.

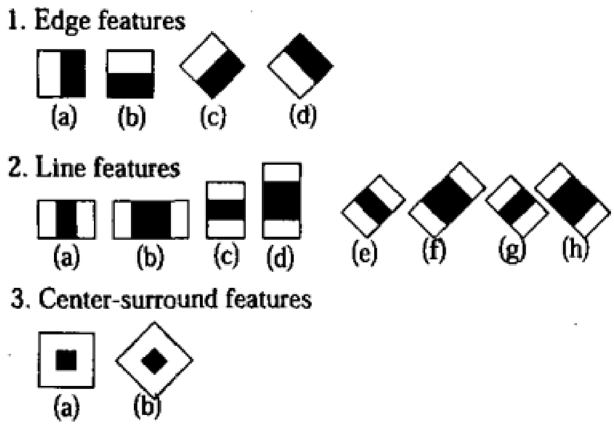

Figure 3. Haar object detector Features (Lienhart and Maydt, 2002)

Each feature is calculated by taking the average of the pixels in the white rectangle and the difference between the average of the pixels in the black rectangle. As a result, Haar pixel values are calculated using equation (1).

$$Pixel\ Value = \frac{Sum\ of\ the\ dark\ pixels}{Number\ of\ the\ dark\ pixels} - \frac{Sum\ of\ the\ light\ pixels}{Number\ of\ the\ light\ pixels} \quad (1)$$

If the difference is above a specified value, Haar features are considered to be present. The equation needs to be applied for each feature calculation, making it difficult to find features for large images. For this purpose, the integral images technique is used, which reduces the calculations for one pixel to a process involving four pixels. A machine learning algorithm called AdaBoost is used to determine the best features to use when training classifiers. The cascade classifier is a decision tree consisting of a combination of classifiers added one after the other, making inferences about whether the object is found or not (Meddeb et al., 2023). In this study, using Haar Cascade Classifier, the parts containing faces were detected from images in the data set and cropped as shown in Figure 4.

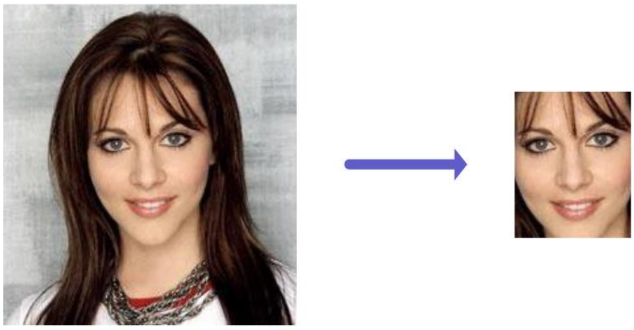

Figure 4. Face Detection with Haar Cascade Classifier

3.3.2. Facial Landmark Detection

Parsing facial features and specific parts of the face is a specific facial analysis subproblem. Predefined sets of points that define the shape of the face and are generally aligned around the chin, mouth, nose, and eyes are called facial landmarks. Localization of facial landmarks is a fundamental step and landmark for many facial analysis methods (Wu and Ji, 2019). The landmark point cluster defines facial features as shown in Figure 5. In this study, from the face images cropped with Haar Cascade Classifier, the parts where the eyes are located were cropped using facial landmarks, as shown in Figure 5.

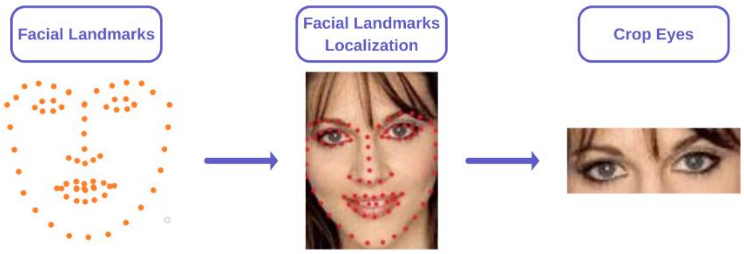

Figure 5. Cropping Eyes from Images with Face Landmark Detection

3.4. Training

AlexNet, ResNet and YOLO are widely used deep learning architectures. In order to determine which architecture would give better results, the data set was used with these architectures and the results were compared. The training process was carried out over the cloud using Google Colab. Training for all architectures was run for 50 epochs with a batch size of 32. Accuracy and loss values of the trained models are shown in Table 1.

Mimari	**Doğruluk**	**Kayıp**
AlexNet	0.97	0.05
ResNet	0.76	0.01
YOLO	0.98	0.01

Table 1. Accuracy and Loss of Trained Models

When models based on different architectures are compared, it is seen that the highest performance value is provided by the YOLOv8 architecture. The training and testing accuracy graph for the model based on the YOLOv8 architecture is shown in Figure 6. When the graph is examined, it is seen that the accuracy values reach high values over time and the verification accuracy increases. This shows that the model is learning from the training data. In addition, the validation accuracy is higher than the training accuracy, indicating that the model has high generalization ability and does not overfit.

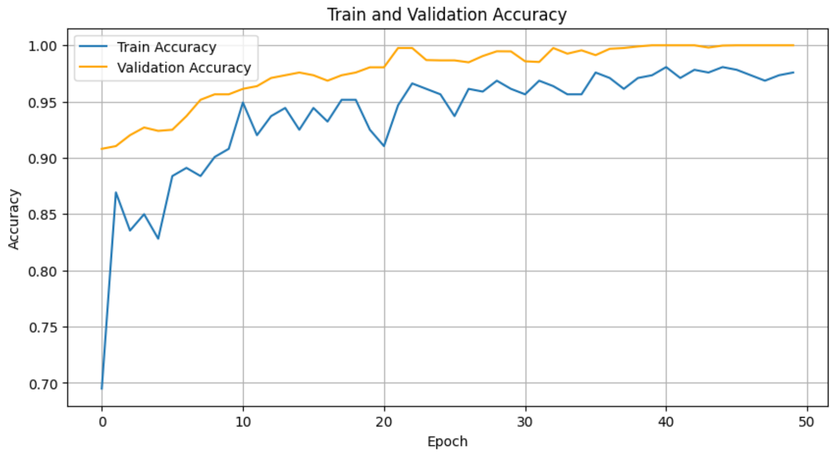

Figure 6. The YOLOv8 Eye Detection Accuracy Curve during Train and Validation Process

The training and validation loss graph for the model based on YOLO architecture is shown in Figure 7. When the graph is examined, it can be seen that both training and validation loss are decreasing. This shows that the model is learning and its performance is improving over time. The fact that the verification loss decreases over time indicates a successful training process.

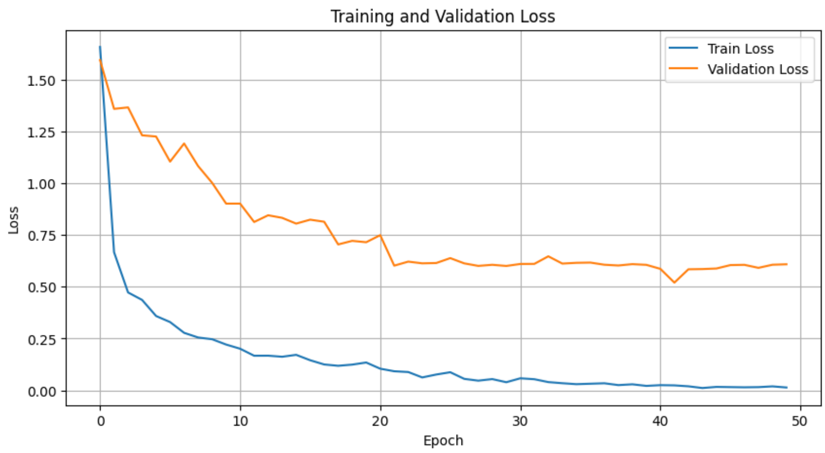

Figure 7. The YOLOv8 Eye Detection Loss Curve during Train and Validation Process

The detection ability of the trained model was evaluated using test data and the complexity matrix in Figure 8 was obtained. The complexity matrix shows that predictions based on test data yield successful results without overfitting.

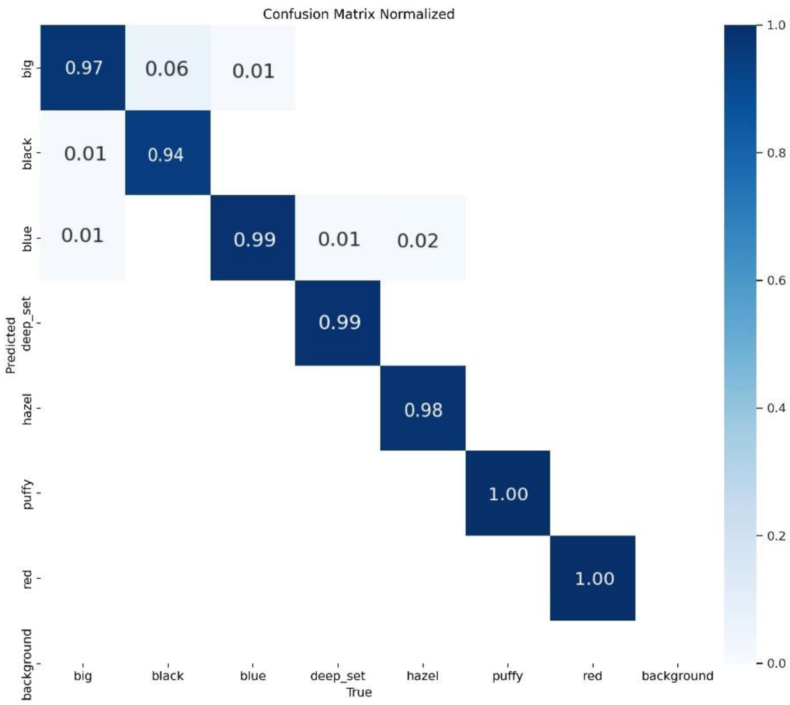

Figure 8. Confusion Matrix of YOLOv8 Eye Estimation

4.CONCLUSIONS

The aim of this study is to determine the personality characteristics of individuals through real-time data. In this direction, a new data set was created by using the data taken from the VGGFace2 data set and cropping the face regions with the Haar Cascade Classifier method and the eye regions with the facial markings coding algorithm. The physiological personality approach in Marifetnâme was used as a personality model. Considering this approach, training was performed using three different CNN architectures (AlexNet, ResNet and YOLO) on the categorized data and the results were compared. The goal here was to find the best CNN architecture to use. It has been observed that the YOLOv8 model gives better results than AlexNet and ResNet and reaches 98% accuracy. Due to the high detection quality, it was decided to use the YOLOv8 eye features specific model in the application. Similarly, from real-time data, eye regions were cropped using the Haar Cascade Classifier and Facial marks coding system and personality analysis was performed using the YOLOv8 eye features specific model. In future studies, it is aimed to create artificial intelligence models for other personality traits in Marifetnâme and to create a decision tree that allows these models to be evaluated together.

ACKNOWLEDGEMENT

This study was supported by Scientific Research Projects Unit of Firat University (FUBAP) under the Grant Number ADEP.22.06. The authors thank to FUBAP for their supports.

REFERENCES

1. Hakkı, İ., 1756. Marifetnâme.
2. Okumuş, E., 2008. Marifetnâme'de Beden. Dinbilimleri Akademik Araştırma Dergisi, 8(4), pp. 9-44.
3. Ulusoy, İ. T., 1980. Marifetnâme (Simplification).
4. Sevinç, K., 2012. Marifetnâme'de Kişilik Tipolojisi ve Bunun Rasyonelliği. Bütün Yönleriyle İbrahim Hakkı Hazretleri Sempozyumu, pp. 483-497, Erzurum.
5. Frith, C.D., Frith, U., 2008. Social cognition in humans, Current Biology, 18(17), pp. 729-732, doi: 10.1016/j.cub.2007.05.068.
6. Jack, R. E., Schyns, P.G., 2015. The Human Face as a Dynamic Tool for Social Communication, Current Biology, 25(14), pp. 621-634, doi: 10.1016/j.cub.2015.05.052.
7. Harrington, R., Loffredo, D. A., 2010. MBTI personality type and other factors that relate to preference for online versus face-to-face instruction, The Internet and Higher Education, 13(1–2), pp. 89-95, doi: 10.1016/j.iheduc.2009.11.006.
8. Yin, K., Lee, P., Sheldon, O. J, Li, C., Zhao, J., 2021. Personality profiles based on the FFM: A systematic review with a person-centered approach, Personality and Individual Differences, Vol. 180, doi: 10.1016/j.paid.2021.110996.
9. Eysenck, M. W., 2016. Hans Eysenck: A research evaluation, Personality and Individual Differences, Vol. 103, pp. 209-219, doi: 10.1016/j.paid.2016.04.039
10. Bahri, N. E., Itahriouan, Z., Abtoy, A., Belhaouari, S. B., (2023). Using convolutional neural networks to detect learner's personality based on the Five Factor Model, Computers and Education: Artificial Intelligence, doi: 10.1016/j.caeai.2023.100163.
11. Hamm, J., Kohler, C. G., Gur, R. C., Verma, R., 2011, Automated Facial Action Coding System for dynamic analysis of facial expressions in neuropsychiatric disorders, Journal of Neuroscience Methods, 200 (2), pp. 237-256, doi: 10.1016/j.jneumeth.2011.06.023.
12. Rojo, R., Prados-Frutos, J. C., López-Valverde, A, 2015. Evaluación del dolor mediante el Sistema de Codificación de la Acción Facial. Revisión sistemática, Medicina Clínica, 145 (8), pp. 350-355, doi: 10.1016/j.medcle.2014.08.002.
13. M. Gavrilescu, 2015. Study on determining the Big-Five personality traits of an individual based on facial expressions, 2015 E-Health and Bioengineering Conference (EHB), Iasi, Romania, pp. 1-6, doi: 10.1109/EHB.2015.7391604.

14. Yin, D. B. M., Omar, S., Talip, B. A., Muklas, A., Norain, N. A. M, Othman, A. T., 2017. Fusion of face recognition and facial expression detection for authentication: a proposed model, 11th International Conference on Ubiquitous Information Management and Communication (IMCOM '17). New York, NY, USA, 21 (1–8), doi: 10.1145/3022227.3022247.
15. Tian, Y., -I, Kanade, T., Cohn, J. F., 2001. Recognizing action units for facial expression analysis, IEEE Transactions on Pattern Analysis and Machine Intelligence, 23 (2), pp. 97-115, doi: 10.1109/34.908962.
16. Li, J., Zhu, J., Guan, C., 2024. Assessing illumination fatigue in tunnel workers through eye-tracking technology: A laboratory study, Advanced Engineering Informatics, Vol. 59, doi: 10.1016/j.aei.2023.102335.
17. Ilhan, A. E., Togay, A., 2023. Pursuit of methodology for data input related to taste in design: Using eye tracking technology, Displays, Vol. 76, doi: 10.1016/j.displa.2022.102335.
18. Zhen, S., Xia, X., Huang, L., Cao, Y., Fu, H., Ren, Y., 2024. Does risk preference matter to consumers' willingness to pay for functional food: Evidence from lab experiments using the eye-tracking technology, Food Quality and Preference, Vol. 119, doi: 10.1016/j.foodqual.2024.105197.
19. Gao, M., Xin, R., Wang, O., Gao, D., Wang, J., Yu, Y., 2023. Abnormal eye movement features in patients with depression: Preliminary findings based on eye tracking technology, General Hospital Psychiatry, Vol. 84, pp. 25-30, doi: 10.1016/j.genhosppsych.2023.04.010.
20. Aydın, A. İ., 2022. Çocuklarda Ameliyat Sonrası Ağrının Bilgisayar Destekli Yüz İfadesi Analiziyle Değerlendirilmesi, pp. 22-23, (Doctoral dissertation), Istanbul University.
21. Vogel, C., Ahmad, K., 2023. Agreement and disagreement between major emotion recognition systems, Knowledge-Based Systems, Vol. 276, doi: 10.1016/j.knosys.2023.110759.
22. Yılmaz, D., 2013. Marifetnâme (Simplification), pp. 29-30.
23. Okumuş, E., 2008. "Marifetnâme'de Beden", Dinbilimleri Akademik Araştırma Dergisi 8/4, pp. 9-4.
24. Cao, Q., Shen, L., Xie, W., Parkhi, O.M. and Zisserman, A., 2018. Vggface2: A dataset for recognising faces across pose and age, Automatic Face & Gesture Recognition (FG 2018), 13th IEEE International Conference on, IEEE, pp.67–74.

25. Viola, P., Jones, M., 2001. Rapid object detection using a boosted cascade of simple features, Proceedings of the 2001 IEEE Computer Society Conference on Computer Vision and Pattern Recognition. CVPR 2001, Kauai, HI, USA, pp. I-I, doi: 10.1109/CVPR.2001.990517.
26. Yaddanapudi, S. D., Makala, B. P., Yarlagadda, A., Sapram, C. T., Parsa, S. T., Nallamadugu,, S., 2023. Collection of plastic bottles by reverse vending machine using object detection technique, Materials Today: Proceedings, Vol. 80, Part 3, pp. 1995-1999, doi: 10.1016/j.matpr.2021.06.037.
27. Lienhart, R., Maydt, J., 2002. An extended set of Haar-like features for rapid object detection, Proceedings. International Conference on Image Processing, Rochester, NY, USA, pp. I-I, doi: 10.1109/ICIP.2002.1038171.
28. Meddeb, H., Abdellaoui, Z., Houaidi, F., 2023. Development of surveillance robot based on face recognition using Raspberry-PI and IOT, Microprocessors and Microsystems, Vol. 96, doi: 10.1016/j.micpro.2022.104728.
29. Wu, Y., Ji, Q., 2019. Facial Landmark Detection: A Literature Survey. Int J Comput Vis 127, pp. 115–142, doi: 10.1007/s11263-018-1097-z.

SOME NEW RESULTS OF THE NONLINEAR CONFORMABLE MODEL ARISING IN PLASMA PHYSICS

Md. Nur Alam[1], Onur Alp İlhan[2, a], Md. Shahid Hasan[3], Uzzal Saha[4] and F. Berna Benli[2, b]

[1,3,4]Department of Mathematics, Pabna University of Science and Technology, Pabna, 6600, Bangladesh.
[2]Faculty of Education, Erciyes University, 38039 Melikgazi, Kayseri, Turkey
E-mail address: [1] nuralam.pstu23@gmail.com, [2, a] oailhan@erciyes.edu.tr, [3]shahid.math43@gmail.com, [4]uzzalsaha671@gmail.com and [2, b] akpinarb@erciyes.edu.tr

Abstract

The nonlinear conformable model that arises in plasma physics is the 3D conformable Zakharov-Kuznetsov equation (CZKE) with power law nonlinearity (PLNL). The current study applies a modification of the (G'/G)-expansion (MG'/GE) approach to this model and obtains certain closed-form precise wave solutions. By going backwards into the 3D CZKE with PLNL, the obtained results are confirmed, and they are noted as being particularly advantageous over a number of current methods. For the other nonlinear conformable models in physics, mathematics, and engineering, the aforementioned approach could also be used to obtain closed-form wave solutions $(CFWSs)$.

Key Word: Conformable derivative The variation of (G'/G)-expansion method the 3D CZKE with power law nonlinearity.

PACS Nos: 05.45.Yv; 02.70.Wz; 02.60.Lj; 04.20.Jb; 03.40.Kf.

1 Introduction

Conformable wave models $(CWDs)$ are mathematical tools utilized to represent a broad range of phenomena seen in several fields of applied science and materials science, such as physics, quantum mechanics, biology, fluid mechanics, electricity, chemistry, plasma physics, and others. The practical implementation of complex nonlinear physical elements in various devices significantly impacts the outcomes of conformable wave dynamics. This has implications for enhancing understanding in this field. In previous studies, various scientific and mathematical schemes have been employed to obtain CFWSs for nonlinear CWDs. These techniques include the sub-equation method proposed by [1], the extensive sinh-Gordon extension scheme studied by [2, 3], the sine-Gordon expansion method investigated by [4, 5], the Jacobi elliptic equation method explored by [6, 7], the first integral method analyzed by [8], the Bernoulli sub-model task scheme examined by [9, 10], the extended spectral method proposed by [11], the functional variable method studied by [12, 13], the modified simple equation method investigated by [14, 15], the generalized Kudryashov method explored by [16, 17], the modified Khater method analyzed by [18, 19], the auxiliary equation method proposed by [20], and the $\exp(-\phi(\varpi))$-expansion method investigated by [21, 22]. Additionally, a novel generalized method has been introduced. The (G'/GE) approach [23, 24, 25], the $(G\text{â€™}/G)$-advanced extension scheme [26], the new advanced direct algebraic approach [27, 28], the fractional sub-equation scheme [29], the trial equation way [30, 31], and other related methods [32, 33, 34] have been proposed in the literature.

The point of this investigation is to utilize the Â MG'/GE approach to determine precise $CFWSs$ for the 3D CZKE with PLNL [35, 36, 37, 38] in the form

$$\frac{\partial^\gamma u}{\partial t^\gamma} + \alpha u^\nu \frac{\partial u}{\partial x} + \beta \frac{\partial}{\partial x}\left(\frac{\partial^2 u}{\partial x^2} + \frac{\partial^2 u}{\partial y^2} + \frac{\partial^2 u}{\partial z^2}\right) = 0, \alpha \neq 0, \beta \neq 0 \text{and} \nu \geq 1. \tag{1}$$

Where ν represents the PLNL parameter Â and $\frac{\partial^\gamma}{\partial t^\gamma}$ is the γ-th order derivative operator in the conformable derivative (CV) sense described in the next sector. The Eq. (1) typically appears the behavior of weakly nonlinear ion-acoustic waves in a plasma comprising cold ions and hot isothermal electrons in the attendance of a uniform magnetic field.Â Eq. (1) involves significant interesting equations, for examples

(i) The 3D CMKdV-ZK equation [39] is given by Equation (1):

$$\frac{\partial^\gamma u}{\partial t^\gamma} + \alpha u^2 \frac{\partial u}{\partial x} + \beta \frac{\partial}{\partial x}\left(\frac{\partial^2 u}{\partial x^2} + \frac{\partial^2 u}{\partial y^2} + \frac{\partial^2 u}{\partial z^2}\right) = 0. \tag{2}$$

(ii) The 3D CZK equation [40]Â is represented by the following equation:

$$\frac{\partial^\gamma u}{\partial t^\gamma} + \alpha u \frac{\partial u}{\partial x} + \beta \frac{\partial}{\partial x}\left(\frac{\partial^2 u}{\partial x^2} + \frac{\partial^2 u}{\partial y^2} + \frac{\partial^2 u}{\partial z^2}\right) = 0.\text{Â} \tag{3}$$

The article is structured in the following manner: Section 2 presents an introduction to the definition and several aspects of CVs. Section 2 provides a comprehensive explanation of the core concept and procedural processes involved in the MG'/GE approach. The solutions of Equation (1) are derived using the method described in Section 4. Section 5 presents a visual representation of numerical simulations. The final section of the paper presents several findings.

2 Conformable derivative

In this context, we present the theory of conformable calculus as discussed in the works of [41, 42].

We consider $\rho: (0, \infty) \to \mathbb{R}$, then CV of ρ of order γ:

$${}_tD^\gamma \rho(t) = lim_{\varepsilon \to 0} \frac{\rho(t+\varepsilon t^{1-\gamma}) - \rho(t)}{\varepsilon}, \quad t > 0, \quad 0 < \gamma \leq 1. \tag{4}$$

The Conformable derivative possesses in the following properties.

We will analyze the conditions $0 < \gamma \leq 1$ and ρ, ρ being γ-differentiable at a certain point t.

- ${}_tD^\gamma(a\rho + b\rho) = a({}_tD^\gamma v) + b({}_tD^\gamma \rho)$.
- ${}_tD^\gamma(t^\mu) = \mu t^{\mu-\gamma}$.
- ${}_tD^\gamma(\rho + \rho) = \rho({}_tD^\gamma \rho) + \rho({}_tD^\gamma \rho)$.
- ${}_tD^\gamma(\frac{\rho}{\rho}) = \frac{u({}_tD^\gamma \rho)-\rho({}_tD^\gamma \rho)}{\rho^2}$.
- ${}_tD^\gamma \rho(\rho o \rho)(t) = t^{1-\gamma}\rho'(t)\rho'(\rho(t))$.

3 The methodology

First, we investigate the nonlinear conformable partial differential equation:

$$E(\Upsilon, \frac{\partial^\gamma \Upsilon}{\partial t^\gamma}, \frac{\partial \Upsilon}{\partial x}, \frac{\partial \Upsilon}{\partial y}, \frac{\partial \Upsilon}{\partial z}, \frac{\partial^{2\gamma} \Upsilon}{\partial t^{2\gamma}}, \frac{\partial^2 \Upsilon}{\partial x^2}) = 0, \qquad t \geq 0, \quad 0 < \gamma \leq 1, \tag{5}$$

where E is a function of $\Upsilon(x, y, z, t)$. Let

$$\Upsilon = \Upsilon(\varpi) = \Upsilon(x, y, z, t), \qquad \varpi = x + y + z - c\frac{t^\gamma}{\gamma},$$

where c stands for wave speed. Then the Eq. (5) becomes:

$$F(\Upsilon, \frac{\partial \Upsilon}{\partial \varpi}, \frac{\partial^2 \Upsilon}{\partial \varpi^2}, \dots) = 0. \tag{6}$$

Step 1: Calculate the value of N using the balance procedure as described in Equation (6).

Step 2: Considering the solution of Eq. (6):

$$\Upsilon(\varpi) = \sum_{i=0}^{M} a_i L^i + \sum_{i=1}^{M} b_i L^{i-1} H, \tag{7}$$

where $L = \frac{G\prime}{G}$, $H = \frac{N\prime}{N}$ and $G = G(\varpi)$ and $N = N(\varpi)$ represents

$$G'(\varpi) = -G(\varpi)N(\varpi), \tag{8}$$

$$N'(\varpi) = 1 - N(\varpi)^2. \tag{9}$$

The above equations give:

$$G(\varpi) = \pm sech(\varpi), N(\varpi) = tanh(\varpi), \tag{10}$$

$$G(\varpi) = \pm csch(\varpi), N(\varpi) = coth(\varpi). \tag{11}$$

Step 3: A polynomial expression that includes the variables L or N can be derived by inserting equation (7) into equation (6). The procedure of equating the coefficients of the equivalent power of L or N to zero results in a system of algebraic equations. Subsequently, the aforementioned equations can be resolved by employing the software MAPLE in order to obtain the respective values of a_i and b_i.

4 Implementation of the nonlinear conformable model arising in plasma physics

In this section, we will employ the proposed method discussed in Section 2 to solve Equation (1). Let

$$u = U(\varpi) \qquad \varpi = x + y + z - \lambda\frac{t^\gamma}{\gamma}, \tag{12}$$

By substituting the connection (12) and its derivatives into equation (1), we may obtain the following expression:

$$-\lambda\frac{\partial U}{\partial\varpi}+\alpha U^{\nu}\frac{\partial U}{\partial\varpi}+b\frac{\partial}{\partial\varpi}(\frac{\partial^2 U}{\partial\varpi^2}+\frac{\partial^2 U}{\partial\varpi^2}+\frac{\partial^2 U}{\partial\varpi^2})=0. \tag{13}$$

By doing the process of integration on the aforementioned equation, we obtain:

$$-\lambda U+\frac{\alpha}{\nu+1}U^{\nu+1}+3\beta\frac{\partial^2 U}{\partial\varpi^2}=0. \tag{14}$$

By using the algebraic transformation $U=v^{\frac{1}{\nu}}$, Equation (14) can be rewritten as:

$$3bn(\nu+1)v\frac{\partial^2 v}{\partial\varpi^2}+3b(\nu^2-1)(\frac{\partial v}{\partial\varpi})^2-\nu^2(1+\nu)Vv^2+\alpha\nu^2v^3=0, n\neq 0,\pm 1 \tag{15}$$

Through the balance rule on the Eq. (15), yields $M=2$. Accordingly, Eq. (15) diminishes to

$$v(\varpi)=a_0-a_1N+a_2N^2-b_1N+\frac{b_1}{N}-b_2+b_2N^2 \tag{16}$$

where a_0, a_1, a_2, b_1 and b_2 are constants. Inserting Eq. (16) into Eq. (15) and then evaluating each coefficients of L or N to zeros, we get:

Case I:

$$\lambda=-\frac{3(3\nu+1)\beta}{\nu^2},\quad a_0=\frac{\alpha\nu b_2+6\beta\nu+6\beta}{\alpha\nu},\quad a_1=0,\quad a_2=-\frac{\alpha\nu b_2+18\beta\nu+18\beta}{\alpha\nu},\quad b_1=0.$$

Case II:

$$\lambda=\frac{3(5\nu-1)\beta}{\nu^2},\quad a_0=\frac{\alpha\nu b_2+18\beta\nu+18\beta}{\alpha\nu},\quad a_1=0,\quad a_2=-\frac{\alpha\nu b_2+18\beta\nu+18\beta}{\alpha\nu},\quad b_1=0.$$

Taking case *I* into account, the solutions of Eq. (1) can be obtained as

$$u_1(x,y,z,t)=(\frac{-12\beta(\nu+1)}{\alpha\nu}+\frac{18\beta(\nu+1)}{\alpha\nu}sech^2(x+y+z+\frac{3\beta(2\nu+1)}{\nu^2}\frac{t^{\gamma}}{\gamma}))^{\frac{1}{\nu}}, \tag{17}$$

$$u_2(x,y,z,t)=(\frac{-12\beta(\nu+1)}{\alpha\nu}-\frac{18\beta(\nu+1)}{\alpha\nu}csch^2(x+y+z+\frac{3\beta(2\nu+1)}{\nu^2}\frac{t^{\gamma}}{\gamma}))^{\frac{1}{\nu}}. \tag{18}$$

Taking case *II* into account, the solutions of Eq. (1) can be obtained as

$$u_3(x,y,z,t)=(\frac{18\beta(\nu+1)}{\alpha\nu}sech^2(x+y+z+\frac{3\beta(2\nu+1)}{\nu^2}\frac{t^{\gamma}}{\gamma}))^{\frac{1}{\nu}}, \tag{19}$$

$$u_4(x,y,z,t)=(-\frac{18\beta(\nu+1)}{\alpha\nu}csch^2(x+y+z+\frac{3\beta(2\nu+1)}{\nu^2}\frac{t^{\gamma}}{\gamma}))^{\frac{1}{\nu}}. \tag{20}$$

5 Graphical Representation

In this part, all of our obtained closed-form exact wave solutions are represented in the following figures 1-4. These figures describe the Real $3D$, complex $3D$, real contour and complex contour shapes of $u_i(x,y,z,t)$ $(i=1,2,3,4)$. Figures 1-4 show solutions given by Eq. (1) with the parameters $\gamma=0.35$, $a=0.1$, $\beta=0.2$, $n=2$, $b_2=0.5$ and $t=0.01$ for contour shapes.

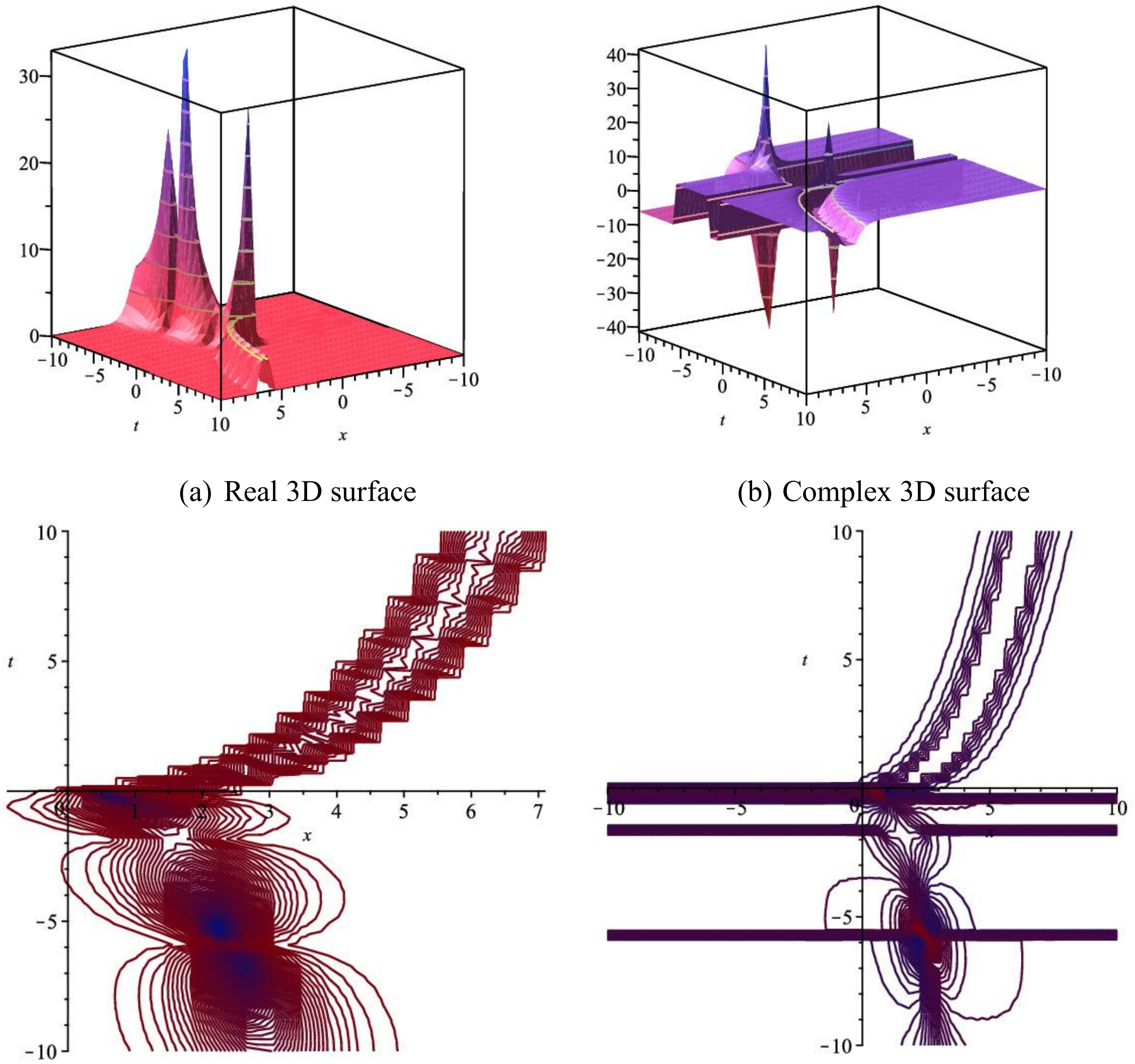

(a) Real 3D surface (b) Complex 3D surface

(c) Real contour shape (d) Comlex contour shape

Figure 1: Surface illustration of the result of the Eq. (17) under the parameters α = 0.1, β = 0.2, γ = 0.35, ν = 2, b2 = 0.5 and t = 0.01 for contour shapes.

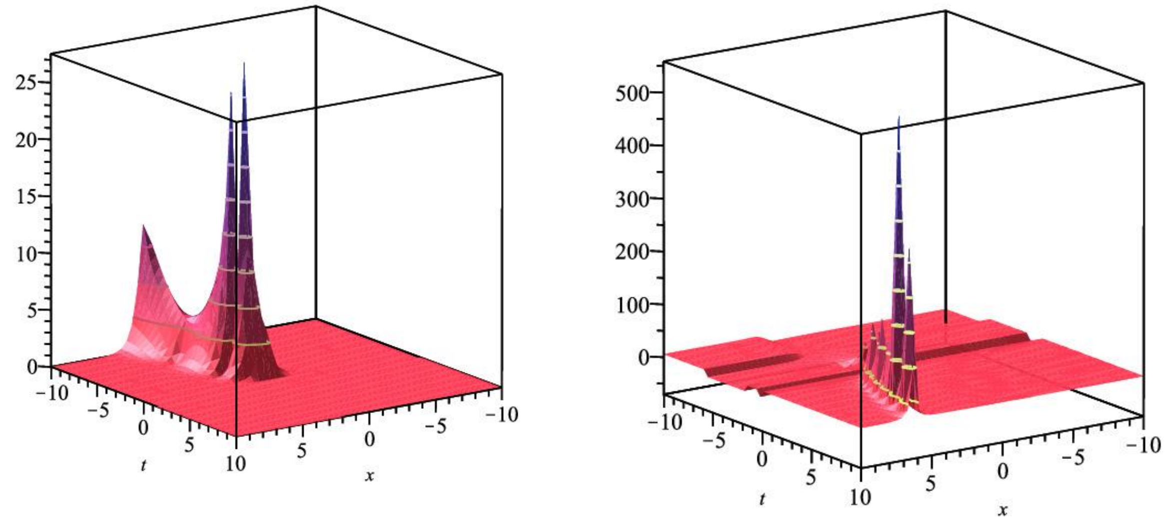

(a) Real 3D surface (b) Complex 3D surface

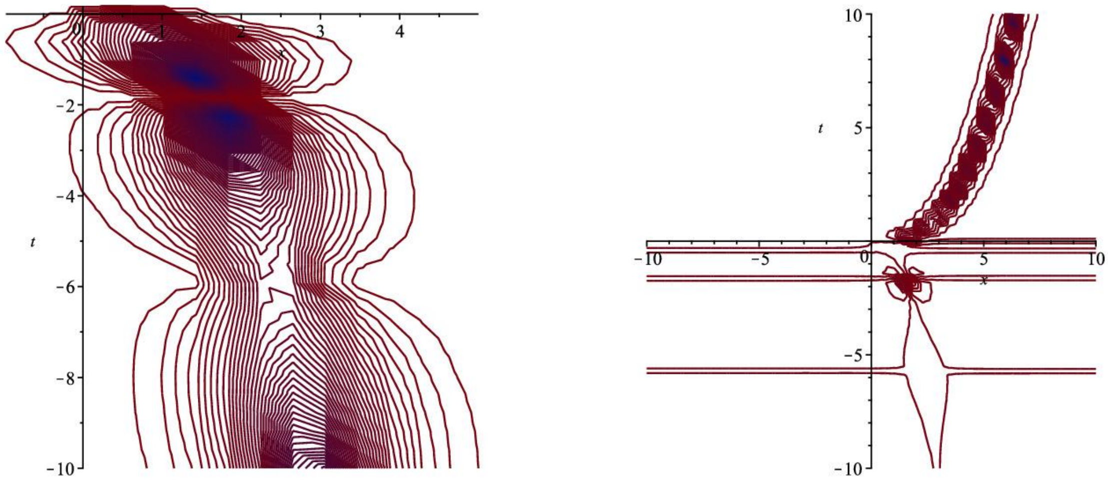

(c) Real contour shape (d) Comlex contour shape

Figure 2: Surface illustration of the result of the Eq. (18) under the parameters $\alpha = 0.1$, $\beta = 0.2$, $\gamma = 0.35$, $\nu = 2$, $b2 = 0.5$ and $t = 0.01$ for contour shapes.

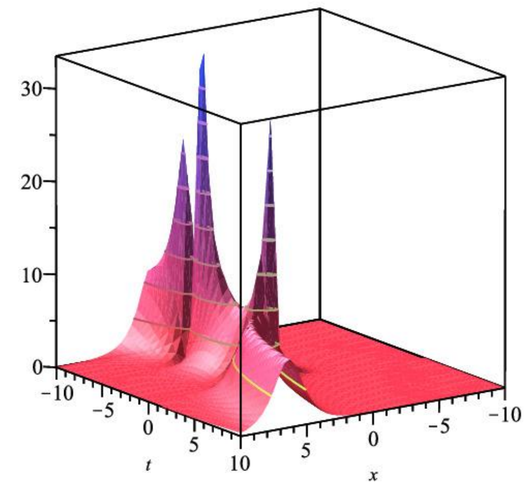

(a) Real 3D surface

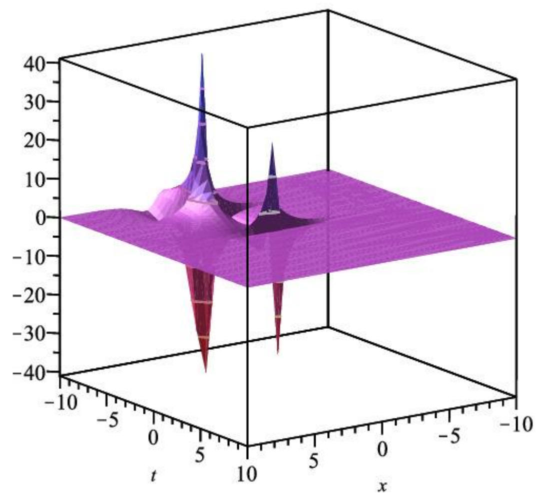

(b) Complex 3D surface

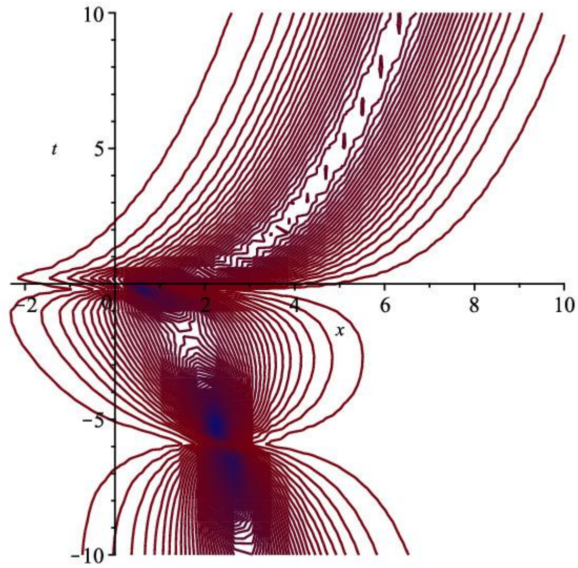

(c) Real contour shape

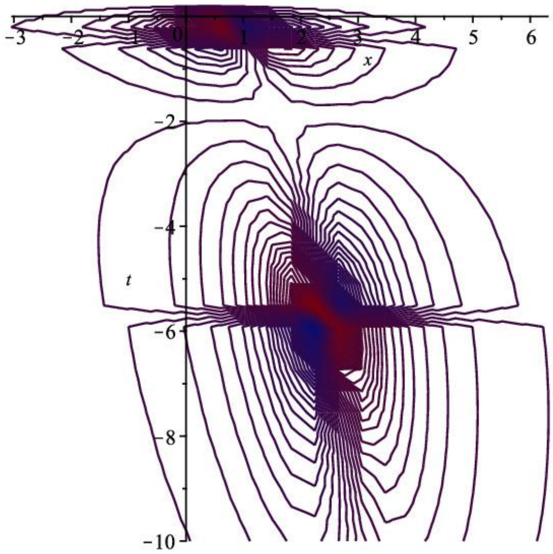

(d) Complex contour shape

Figure 3: Surface illustration of the result of the Eq. (19) under the parameters α = 0.1, β = 0.2, γ = 0.35, ν = 2, b2 = 0.5 and t = 0.01 for contour shapes.

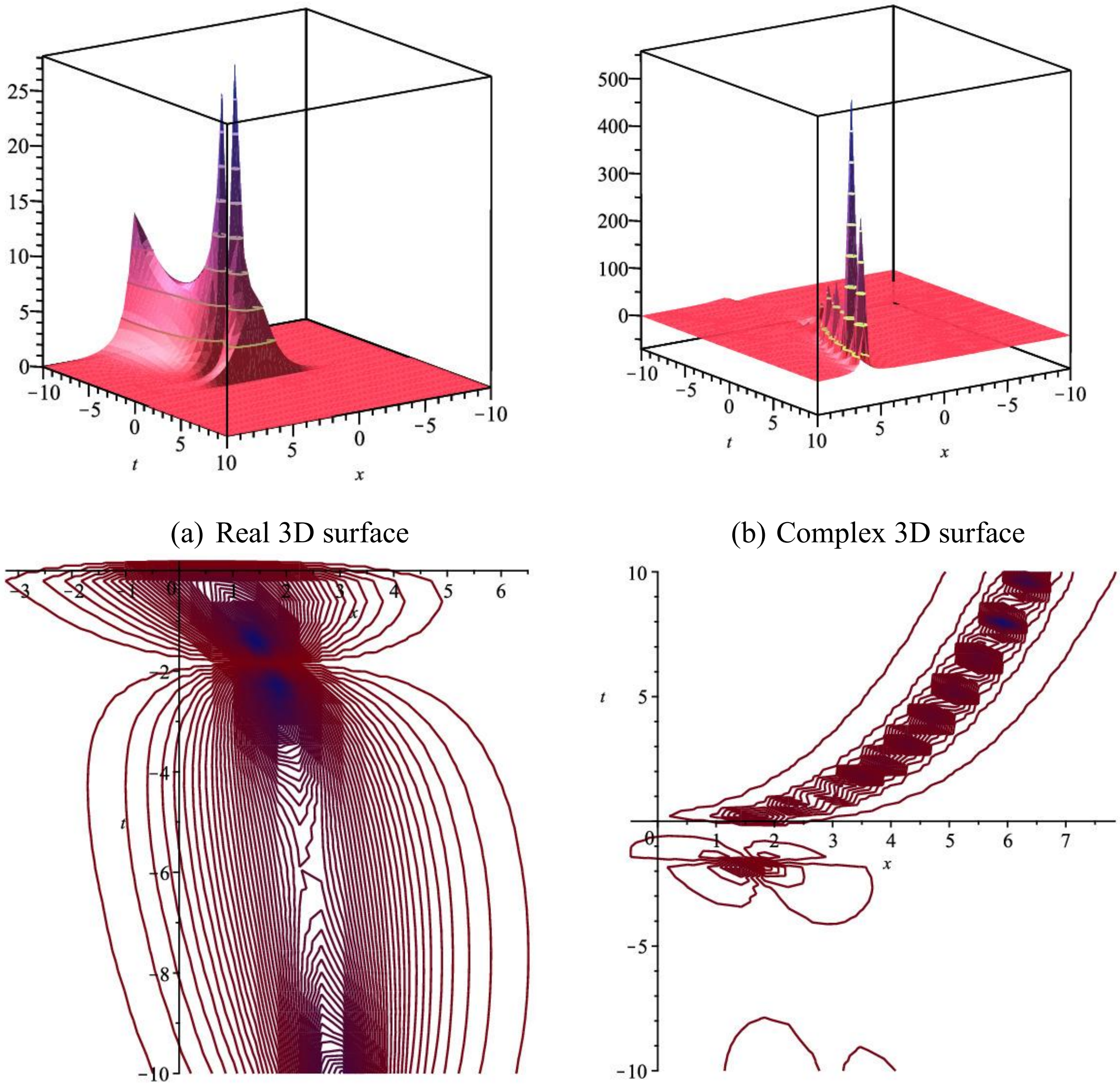

(a) Real 3D surface (b) Complex 3D surface

(c) Real contour shape (d) Complex 3D surface

Figure 4: Surface illustration of the result of the Eq. (20) under the parameters a = 0.1, $\beta = 0.2$, $\gamma = 0.35$, n = 2, b2 = 0.5 and t = 0.01 for contour shapes.

6 Conclusion

This study successfully demonstrates the efficacy of the proposed approach in obtaining CFWSs expressed in terms of hyperbolic tasks for the 3D CZKE with PLNL. Precise CFWSs are employed in diverse domains of non-linear dynamics, such as physics, nonlinear optics, fluid mechanics, plasma physics, biology, quantum mechanics, electricity, chemistry, among others. Based on the obtained results, it can be inferred that the explored methodology has notable efficacy and confidence in generating diverse novel outputs for different nonlinear conformable models. Hence, the investigation of closed-form solutions for an additional nonlinear conformable model using the proposed methodology warrants further scholarly exploration.

Data Availability

No data were used for the research described in the article.

Conflicts of Interest

The authors declare that they have no conflicts of interest.

References

[1] H. Y. Martineza, J. F. G. Aguilarb, D. Baleanu, Beta-derivative and sub-equation method applied to the optical solitons in medium with parabolic law nonlinearity and higher order dispersion, Optik 155 (2018) 357–365.

[2] L. Alzaleq, D. Al-zaleq, S. Alkhushayni, Traveling Waves for the Generalized Sinh-Gordon Equation with Variable Coefficients, Mathematics 10 (2022), 822.

[3] H. M. Baskonus, T. A. Sulaiman, H. Bulut, T. Aktürk, Investigations of dark, bright, combined dark-bright optical and other soliton solutions in the complex cubic nonlinear schrödinger equation with δ-potential, Superlattices and Microstructures 115 (2018) 19–29.

[4] N. Kheaomaingam, S. Phibanchon, S. Chimchinda, Sine-Gordon expansion method for the kink soliton to Oskolkov equation, Journal of Physics: Conference Series 2431 (2023) 012097.

[5] H. Bulut, T. A. Sulaiman, H. M. Baskonus, New solitary and optical wave structures to the kortewegâ€“de vries equation with dual-power law nonlinearity, Opt. Quant. Electron 48 (2016) 1â€“14.

[6] B. Zheng, Q. Feng, The jacobi elliptic equation method for solving fractional partial differential equations, Abstract and Applied Analysis 2014 (2014) 9.

[7] V. S. Kumar, H. Rezazadeh, M. Eslami, F. Izadi, M. Osman, Jacobi elliptic function expansion method for solving kdv equation with conformable derivative and dual-power law nonlinearity, International Journal of Applied and Computational Mathematics 5 (5) (2019) 127.

[8] B. Lu, The first integral method for some time fractional differential equations, J Math Anal Appl 395 (2012) 684–693.

[9] G. Yel, T. A. Sulaiman, H. Baskonus, On the complex solutions to the (3+ 1)-dimensional conformable fractional modified kdv–zakharov–kuznetsov equation, Modern Physics Letters B (2020) 2050069.

[10] M. S. Shehata, H. Rezazadeh, E. H. Zahran, E. Tala-Tebue, A. Bekir, New optical soliton solutions of the perturbed fokas-lenells equation, Communications in Theoretical Physics 71 (11) (2019) 1275.

[11] H. Khalil, R. A. Khan, Extended spectral method for fractional order three-dimensional heat conduction problem, Progr. Fract. Differ. Appl 1 (2015) 165–185.

[12] W. Liu, K. Chen, The functional variable method for finding exact solutions of some nonlinear timefractional differential equations, Pramana J Phys 81 (2013) 3.

[13] Y. Cenesiz, O. Tasbozan, A. Kurt, Functional variable method for conformable fractional modified kdv-zkequation and maccari system, Tbilisi Math J. 10 (2017) 117–125.

[14] N. Raza, A. Javid, Optical dark and singular solitons to the biswas–milovic equation in nonlinear optics with spatio-temporal dispersion, Optik 158 (2018) 1049–1057.

[15] A. Javid, N. Raza, Singular and dark optical solitons to the well posed lakshmanan–porsezian–daniel model, Optik 171 (2018) 120–129.

[16] L. Qian, R. A. Attia, Y. Qiu, D. Lu, M. M. Khater, The shock peakon wave solutions of the general degasperis–procesi equation, International Journal of Modern Physics B (2019) 1950351.

[17] D. Lu, A. R. Seadawy, M. M. Khater, Structure of solitary wave solutions of the nonlinear complex fractional generalized zakharov dynamical system, Advances in Difference Equations 2018 (1) (2018) 266.

[18] D. Lu, M. Osman, M. Khater, R. Attia, D. Baleanu, Analytical and numerical simulations for the kinetics of phase separation in iron (fe–cr–x (x= mo, cu)) based on ternary alloys, Physica A: Statistical Mechanics and its Applications 537 (2020) 122634.

[19] M. Khater, J. Alzaidi, R. A. Attia, D. Lu, et al., Analytical and numerical solutions for the current and voltage model on an electrical transmission line with time and distance, Physica Scripta.

[20] M. K. A. Akbulut, A. Bekir, Auxiliary equation method for fractional differential equations with modified riemann-liouville derivative, Int. J. Nonlin. Sci. Num. 17 (2016) 413–420.

[21] M. N. Alam, F. Belgacem, Microtubules nonlinear models dynamics investigations through the $exp(-\phi(\xi))$-expansion method implementation, Mathematics 4 (2016) 6.

[22] M. N. Alam, C. Tunc, An analytical method for solving exact solutions of the nonlinear bogoyavlenskii equation and the nonlinear diffusive predator-prey system, Alexandria Eng. J. 55 (2016) 1855–1865.

[23] M. N. Alam, Y. Stepanyants, New generalized (G'/G)-expansion method in investigating the traveling wave solutions to the typical breaking soliton and the benjamin-bona-mahony equations, Internat. J. Math. Comput. 27 (2016) 69–82.

[24] M. N. Alam, Exact solutions to the foam drainage equation by using the new generalized (G'/G)-expansion method, Resul. In Phys. 5 (2015) 168–177.

[25] M. N. Alam, M. Akbar, M. Hoque, Exact traveling wave solutions of the $(3+1)$-dimensional mkdv-zk equation and the $(1+1)$-dimensional compound kdvb equation using new approach of the generalized (G'/G)-expansion method, Pramana J. Phys. 83 (2014) 317–329.

[26] W. Gao, H. F. Ismael, A. M. Husien, H. Bulut, H. M. Baskonus, Optical soliton solutions of the cubic-quartic nonlinear schrödinger and resonant nonlinear schrödinger equation with the parabolic law, Applied Sciences 10 (1) (2020) 219.

[27] Q. Zhou, H. Rezazadeh, A. Korkmaz, M. Eslami, M. Mirzazadeh, M. Rezazadeh, New optical solitary waves for unstable schrödinger equation in nonlinear medium, Optica Applicata 49 (1).

[28] A. Souleymanou, A. Korkmaz, H. Rezazadeh, S. P. T. Mukam, A. Bekir, Soliton solutions in different classes for the kaup–newell model equation, Modern Physics Letters B (2019) 2050038.

[29] S. Zhang, H. Q. Zhang, Fractional sub-equation method and its applications to nonlinear fractional pdes, Phys. Lett. A 375 (2011) 1069.

[30] N. Raza, M. Abdullah, A. R. Butt, I. Ghulam, M. Sial, New exact periodic elliptic wave solutions for extended quantum zakharovâ€“kuznetsov equation, Optical and Quantum Electronics 50 (2018) 177.

[31] N. Raza, M. R. Aslam, S. Sial, New optical solitons of tzitzeca type evolution equations using extended trial approach, Optical and Quantum Electronics 50 (3) (2018) 141.

[32] M. N. Alam, An analytical technique to obtain traveling wave solutions to nonlinear models of fractional order, Partial Differential Equations in Applied Mathematics, 8 (2023) 100533.

[33] M. N. Alam, Soliton solutions to the electric signals in telegraph lines on the basis of the tunnel diode, Partial Differential Equations in Applied Mathematics, 7 (2023) 100491.

[34] M. Kaplan, R. T. Alqahtani, Exploration of New Solitons for the Fractional Perturbed Radhakrishnanâ€“Kunduâ€“Lakshmanan Model, Mathematics 11 (2023) 2562.

[35] A. Wazwaz, Exact solutions with solitons and periodic structures for the zakharov-kuznetsov equation and its modified form, Communications in Nonlinear Science and Numerical Simulation 10 (2005) 597–606.

[36] M.S.Osman, H. Rezazadeh, M. Eslami, Traveling wave solutions for (3+1)-dimensional conformable fractional zakharov-kuznetsov equation with power law nonlinearity, Nonlinear Engineering 8 (2019) 559–567.

[37] B. T. Matebese, A. R. Adem, C. M. Khalique, A. Biswas, Solutions of zakharov-kuznetsov equation with power law nonlinearity in $(1+3)$-dimensions, Physics of Wave Phenomena 19 (2011) 148–154.

[38] D. Z. Zhou, C. Yong, L. Y. Huai, Symmetry reduction and exact solutions of the $(3+1)$-dimensional zakharov-kuznetsov equation, Chinese Physics B 19 (2010) 090205.

[39] K. Al-Ghafri, H. Rezazadeh, Solitons and other solutions of (3+ 1)-dimensional space–time fractional modified kdv–zakharov–kuznetsov equation, Applied Mathematics and Nonlinear Sciences 4 (2) (2019) 289–304.

[40] A. Korkmaz, Exact solutions to (3+ 1) conformable time fractional jimbo–miwa, zakharov–kuznetsov and modified zakharov–kuznetsov equations, Communications in Theoretical Physics 67 (5) (2017) 479.

[41] R. Khalil, M. AlHorani, A. Yousef, M. Sababheh, A new definition of fractional derivative, Journal of Computational and Applied Mathematics 264 (2014) 65–70.

[42] T. Abdeljawad, On conformable fractional calculus, Journal of computational and Applied Mathematics 279 (2015) 57–66.

GENERALIZED FRACTIONAL THE VERTICAL MOTION OF A FALLING BODY PROBLEM

Erdal BAS[1], **Ali SELCUK**[1]

[1] Department of Mathematics, University of Firat, Elazig, Turkey

erdalmat@yahoo.com,ali_selcuk@hotmail.com

Abstract

In this study, the vertical motion of the falling body problem is considered by the newly given *M*-derivative and generalized fractional derivative. Analytical solutions to the modeling problem are obtained and supported by various graphs including different values comparatively with *M*-derivative and generalized fractional derivatives. The Laplace transform is used as the method of choice [1-4].

Keywords: *M*-derivative; Generalized fractional derivative; Mathematical Model; Laplace transform.

1. INTRODUCTION

Fractional analysis is a mathematical field that has been the focus of interest of many mathematicians from the past to the present, expressing that the orders of derivative and integral operators can be derivatives of arbitrary numbers. Fractional analysis is as old as classical analysis. The first definition of the derivative is the *nth* order derivative of $\frac{d^n y}{dx^n} = \mathcal{D}^\alpha y$ for $n \in N^+$ in 1695 by Leibniz, and L'Hospital's letter to Leibniz asking whether the order of the derivative should be fractional can be shown as the origin of fractional analysis. After Leibniz defined the fractional order derivative, the use of derivative and integral became widespread. In parallel with this widespread use, there was a need for further development of the derivative and integral.

The non-integer order derivative, or fractional derivative as it is commonly used, is as important and old as the integer order derivative, yet for many years it was not used by the scientific community. Today, the fractional derivative includes a large number of important definitions, each of which is unique and applied in its way [7-9]. Since 1974, after the first international conference on the fractional derivative, it has been recognized and consolidated with numerous applications in fields as diverse as mathematics, physics, biology, and engineering. Famous mathematicians such as Lagrange, Abel, Euler, Liouville, Liouville, Riemann and more recently Caputo and Mainardi have contributed to this recognition and popularisation. In this direction, various types of fractional derivatives were introduced by Riemann-Liouville, Caputo, Hadamard, Caputo-Hadamard, and Riesz [10]. Most of these derivatives are represented by the Riemann-Liouville fractional integral structure.

In 2017, Jarad, Ugurlu, Abdeljawad, and Baleanu introduced a new fractional derivative called the Liouville-Caputo fractional compatible derivative [11]. In the same year, Sousa and Oliveira found an *M*-derivative involving the Mittag-Leffler function with a parameter satisfying the properties of the integer order calculus [3]. The fractional computation methods used in the past are compared with the results obtained in different types of real-life problems [12-20].

In 2020, Fahd Jarad and Thabet Abdeljawad calculated generalized fractional differential equations of many orders using the generalized Laplace transform [4]. The results obtained by comparing the results obtained previously for classical differential equations with fractional Riemann-Liouville and Caputo derivatives by the classical Laplace transform with the results obtained for generalized fractional derivatives solved by the generalized Laplace transform are compared with the previous results. In this context, it is suggested that generalized fractional differential equations solved by generalized Laplace transform can be used as a more effective tool for solving dynamical systems depending on generalized fractional operators with singular kernels. Moreover, this method opens the possibility of developing a new integral transformation that can be easily applied to solve dynamical systems with nonsingular fractional operators [4].

In this paper, the vertical motion of falling body problems used in different disciplines from the past to the present are solved using the classical derivative, *M*-derivative, and generalized fractional derivative. Before solving these problems, some important theorems about auxiliary operators, including some other types of fractional operators, that successfully reflect the properties of standard fractional calculus, are discussed. In this context, we will obtain the solution of the vertical motion of the falling body problem using the Laplace transform of the *M*-derivative and the generalized Laplace transform of the generalized fractional derivative. The obtained analytical results will be shown on the graph and compared with the results of the methods previously applied to these problems [4-6].

The vertical motion of falling body problem is widely used in physics, engineering, and aviation. With this problem, the amount and distance of the fall of an object released from any height or thrown with a certain speed are calculated according to gravity, air friction, and time variables. The historical beginning of this problem in science has reached the present day with Newton's three laws of motion. The vertical motion of a falling body problem in a resistive medium is defined classically as,

$$m\frac{dv(t)}{dt} = -mg - mkv(t)$$

$$v(0) = v_0.$$

Where $v(t)(m/s)$ is velocity, $t(s)$ is time, $g(m/s^2)$ is gravitational acceleration, $m(kg)$ is mass, and $k(s^{-1})$ is air resistance [1,5].

2.GENERAL PROPERTIES OF METHOD

2.1.*M*-DERIVATIVE

Let $f:[0,\infty)\to\mathbb{R}$ and $t>0$. For $0<\alpha<1$ we define the *M*-derivative of order α of function f [3],

$$\mathcal{D}_{\mathrm{M}}^{\alpha,\beta}=\lim_{\varepsilon\to 0}\frac{f(tE_{\beta}(\varepsilon t^{-\alpha}))-f(t)}{\varepsilon}.$$

2.2. LAPLACE TRANSFORM OF *M*-DERIVATIVE

Let $f:[a,\infty)\to\mathbb{R}$, $a\in\mathbb{R}$, $\beta>0$ and $0<\alpha\leq 1$. Then the Laplace transform by means of truncated *M*-derivative is defined below [3],

$$\mathcal{L}_{\alpha,\beta}^{a}\{\mathrm{f(t)}\}=F_{\alpha,\beta}^{a}\{s\}=\Gamma(\beta+1)\int_0^{\infty}e^{-s\frac{\Gamma(\beta+1)(t-a)^{\alpha}}{\alpha}}f(t)(t-a)^{\alpha-1}dt.$$

Through the *M*-derivative, we can express the Laplace transforms of some functions as follows [3]:

1. $\mathcal{L}_{\alpha,\beta}^{a}\{\mathrm{t}\}(s)=\dfrac{\Gamma\left(1+\frac{1}{\alpha}\right)\left(\frac{\alpha}{\Gamma(\beta+1)}\right)^{\frac{1}{\alpha}}}{s^{\frac{1+\alpha}{\alpha}}}$

2. $\mathcal{L}_{\alpha,\beta}^{a}\left\{e^{c\Gamma(\beta+1)\frac{t^{\alpha}}{\alpha}}\right\}(s)=\dfrac{1}{s-c}$

3. $\mathcal{L}_{\alpha,\beta}^{a}\{t^{k}\}(s)=\dfrac{\Gamma\left(1+\frac{k}{\alpha}\right)\left(\frac{\alpha}{\Gamma(\beta+1)}\right)^{\frac{k}{\alpha}}}{s^{\frac{k+\alpha}{\alpha}}}$

4. $\mathcal{L}_{\alpha,\beta}^{a}\left\{\Gamma(\beta+1)\dfrac{t^{\alpha}}{\alpha}e^{c\Gamma(\beta+1)\frac{t^{\alpha}}{\alpha}}\right\}(s)=\dfrac{1}{(s-c)^{2}}$

5. $\mathcal{L}_{\alpha,\beta}^{a}\left\{\sin(b\Gamma(\beta+1)\dfrac{t^{\alpha}}{\alpha})\right\}(s)=\dfrac{b}{b^{2}+s^{2}}$

6. $\mathcal{L}_{\alpha,\beta}^{a}\left\{\cos(b\Gamma(\beta+1)\dfrac{t^{\alpha}}{\alpha})\right\}(s)=\dfrac{s}{b^{2}+s^{2}}$

7. $\mathcal{L}_{\alpha,\beta}^{a}\left\{e^{-c\Gamma(\beta+1)\frac{t^{\alpha}}{\alpha}}\sin(b\Gamma(\beta+1)\dfrac{t^{\alpha}}{\alpha})\right\}(s)=\dfrac{b}{(s+c)^{2}+b^{2}}$

2.3. GENERALIZED FRACTIONAL DERIVATIVE

Let $g(t),(a,b)$ be a strictly increasing function with continuous derivative g' in the interval $g(t),(a,b)$. For $\Re(\alpha)>0$, the left Riemann-Liouville fractional integral of f with respect to the function g of order α ,

$$({}_aI_g^\alpha f)(t)=\frac{1}{\Gamma(\alpha)}\int_a^t (g(t)-g(u))^{\alpha-1} f(u)g'(u)du \tag{2.1}$$

is defined in the form clearly, when, $g(t)=t$ 2.1 is the classical Riemann-Liouville fractional integral and when $g(t)=lnt$ 2.1 is the Hadamarad fractional integral [4]. Therefore, 2.1 can be treated as a generalized Riemann-Liouville fractional integral. For $\Re(\alpha)>0$, the left Riemann-Liouville fractional derivative of a function f of order α with respect to g is defined as

$$({}_aD_g^\alpha f)(t)=\frac{(\frac{1}{g'(t)}\frac{d}{dt})^n}{\Gamma(n-\alpha)}\int_a^t (g(t)-g(u))^{n-\alpha-1} f(u)g'(u)du. \tag{2.2}$$

Where $n=[\Re(\alpha)]+1, g^{(i)}\neq 0, i=2,...n.$ It is clear that when $g(t)=t$, 2.2 is the classical Riemann-Liouville fractional derivative and when $g(t)=lnt$, 2.2 is the Hadamard fractional derivative [4].

2.4. GENERALIZED LAPLACE TRANSFORM OF GENERALIZED FRACTIONAL DERIVATIVE

Let $\alpha>0$ for any $b>0$ and let $f\in AC_g^n[a,b]$. For $g\in C^n[a,b]$ and $g'(t)>0$, let ${}_aI_g^{n-k-\alpha} f, k=0,1,\ldots,n-1$ be the function f of exponential order $g(t)$,

$$\mathcal{L}_g\{({}_aD_g^\alpha f)(t)\}(s)=s^\alpha\mathcal{L}_g\{f(t)\}-\sum_{k=0}^{n-1} s^{n-k-1}\left({}_aI_g^{n-k-\alpha} f\right)(a^+)$$

equality is defined as Laplace transform of the generalized fractional derivative [4].

2.5. GENERALIZED LAPLACE TRANSFORM OF GENERALIZED FRACTIONAL DERIVATIVE

Let $\Re(\alpha)>0$ and $|\frac{\lambda}{s^\alpha}|<1$. Some generalized Laplace transforms of the Mittag Leffler functions are given below [4].

1. $\mathcal{L}_g\left\{E_\alpha\left(\lambda(g(t)-g(a))^\alpha\right)\right\}=\dfrac{s^{\alpha-1}}{s^\alpha-\lambda}$
2. $\mathcal{L}_g\left\{(g(t)-g(a))^{\beta-1}E_{\alpha,\beta}\left(\lambda(g(t)-g(a))^\alpha\right)\right\}=\dfrac{s^{\alpha-\beta}}{s^\alpha-\lambda}$

3.APPLICATIONS

3.1. THE VERTICAL MOTION OF FALLING BODY PROBLEM WITH *M*-DERIVATIVE

If the vertical motion problem of a falling body is written using the *M*-derivative operator instead of the classical derivative and using initial conditions,

$$m\,{}_aD_M^{\alpha,\beta}v(t) = -mg - mkv(t),\ \alpha > 0,\ 0 < \beta \le 1$$

$$v(0) = v_0$$

equation is obtained. Where $v(t)$ is the velocity, t is time, g is the gravitational acceleration, m is the mass and k is the air resistance. If the Laplace transform of the *M*-derivative is applied to equation,

$$L_{\alpha,\beta}^{a}\{{}_aD_M^{\alpha,\beta}v(t)\} = -\mathcal{L}_{\alpha,\beta}^{a}\{g\} - \mathcal{L}_{\alpha,\beta}^{a}\{kv(t)\} \tag{3.1}$$

results are obtained. When the obtained results are substituted in equation 3.1,

$$sv_{\alpha},_{\beta}(s) - v_0 = -\frac{g}{s} - kv_{\alpha},_{\beta}(s) \tag{3.2}$$

is obtained. When $v_{\alpha,\beta}(s)$ is left alone in equation3.2 as follows,

$$v_{\alpha},_{\beta}(s) = \frac{v_0}{(s+k)} - \frac{g}{sk} + \frac{g}{k(s+k)} \tag{3.3}$$

equation is obtained. If the inverse Laplace transform of the *M*-derivative is applied to both sides of the equation 3.3,

$$\mathcal{L}_{\alpha,\beta}^{-1}\{v_{\alpha,\beta}(s)\} = v_0\mathcal{L}_{\alpha,\beta}^{-1}\left\{\frac{1}{s+k}\right\} - g\mathcal{L}_{\alpha,\beta}^{-1}\left\{\frac{1}{s+k}\right\} + \frac{g}{k}\mathcal{L}_{\alpha,\beta}^{-1}\left\{\frac{1}{s+k}\right\}$$

equation is found. From property 2 of the Laplace transform of the *M*-derivative,

$$v(t) = (v_0 + \frac{g}{k})e^{\frac{-k\Gamma(\beta+1)t^{\alpha}}{\alpha}} - \frac{g}{k}$$

solution is obtained. With this solution, the velocity function is obtained. Since it is known that height is $velocity \times time$,

$$H(t) = h + t(v_0 + \frac{g}{k})e^{\frac{-k\Gamma(\beta+1)t^{\alpha}}{\alpha}} - \frac{gt}{k}$$

the height function is obtained.

3.2. THE VERTICAL MOTION OF FALLING BODY PROBLEM WITH GENERALIZED FRACTIOANAL DERIVATIVE

The vertical motion problem of a falling body using the generalized fractional derivative operator and initial conditions,

$$m\,{}_aD_{\mathrm{g}}^{\alpha}v(t) = -mg - mkv(t),\ t > a,\ 0 < \alpha \le 1,\ k \in \mathrm{R},$$

$$v(0) = {}_0I_{\mathrm{g}}^{1-\alpha}(0^+) = v_0$$

is expressed as. Where $v(t)$ is the velocity, t is time, g is the gravitational acceleration, m is the mass and k is the air resistance. If the generalized Laplace transform is applied to equation,

$$\mathcal{L}_{\mathrm{g}}^{\alpha}\{{}_aD_{\mathrm{g}}^{\alpha}(t)\} = -\mathcal{L}_{\mathrm{g}}^{\alpha}\{g\} - \mathcal{L}_{\mathrm{g}}^{\alpha}\{kv(t)\} \tag{3.4}$$

results are obtained. When the obtained results are substituted in equation 3.4,

$$s^{\alpha} v_{g}(s) - {}_{0}I_{g}^{1-\alpha}(0^{+}) = -\frac{g}{s} - k v_{g}(s) \tag{3.5}$$

is obtained. If $v_{g}(s)$ is left alone in equation 3.5,

$$v_{g}(s) = \frac{v_0}{(s^{\alpha}+k)} - \frac{g}{s(s^{\alpha}+k)}$$

equality is found. If the generalized inverse Laplace transform is applied to both sides of this equation;

$$\mathcal{L}_{g}^{-1}\{v_{g}(\mathrm{s})\} = \mathcal{L}_{g}^{-1}\{\frac{v_0}{\mathrm{s}^{\alpha}+\mathrm{k}}\} - \mathcal{L}_{g}^{-1}\{\frac{\mathrm{g}}{\mathrm{s}(\mathrm{s}^{\alpha}+\mathrm{k})}\}$$

equation is obtained. From property 2 of the generalized Laplace transform of the Mittag Leffler function,

$$v_{g}(\mathrm{t}) = (v_0 + \frac{g}{k})(g(t)-g(a))^{\alpha-1} E_{\alpha,\alpha}(-k(g(t)-g(a))^{\alpha}) - \frac{g}{k} \tag{3.6}$$

equation is obtained. It is known that the generalized fractional derivative for $g(t)=t$ is the classical Riemann Lioville. If $g(t)=t$ is taken in equation 3.6,

$$v(\mathrm{t}) = t^{\alpha-1} E_{\alpha,\alpha}(-kt^{\alpha})\left(v_0 + \frac{g}{k}\right) - \frac{g}{k}$$

solution is obtained. With this solution, the velocity function is obtained. Since it is known that height is $velocity \times time$,

$$H(\mathrm{t}) = h + t^{\alpha} E_{\alpha,\alpha}(-kt^{\alpha})\left(v_0 + \frac{g}{k}\right) - \frac{gt}{k}$$

the height function is obtained. The vertical falling body problem is solved with *M*-derivative and generalized fractional derivatives, $h = 31.400m$, $v_0 = 5m/s$, $g = 9m/s^2$ and the results obtained at different derivative orders are shown on graphs and compared to other solutions [1-3].

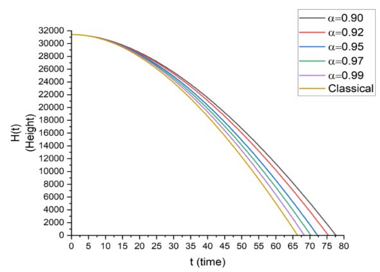

Figure 1: $\beta = 0.90$ and for values of α in the range 0.90 – 0.99, The vertical motion of falling body problem Analysis with *M*-Derivative.

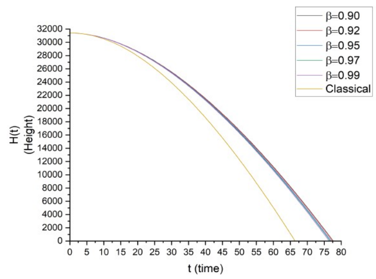

Figure 2: $\alpha = 0.90$ and for values of β in the range 0.90 – 0.99, The vertical motion of falling body problem Analysis with *M*-Derivative.

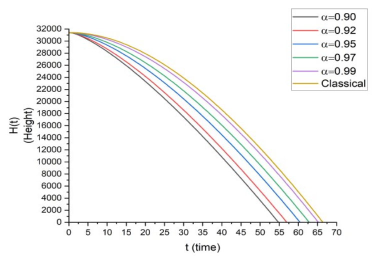

Figure 3: For values of α in the range 0.90 – 0.99, The vertical motion of falling body problem Analysis with generalized fractional derivative.

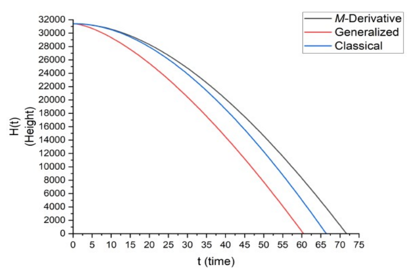

Figure 4: Comparison of the results obtained by *M*-derivative, generalized fractional derivative and classical derivative for $\alpha = 0.95$ and $\beta = 0.95$ values.

4.CONCLUSIONS

It is possible to use some general expressions by interpreting the results obtained from the solutions with classical derivative, *M*-derivative, and generalized fractional derivatives on the graph. In this direction, it has been observed that there are differences in the direction, intensity, rate of change, etc. of the graphs according to the values of α and β in the solutions made in fractional derivative orders. It is predicted that different results can be obtained by using any of the orders in the range of $0-1$ according to the application area in which the problems to which we apply fractional order derivative will be used. When the fractional derivative orders were chosen close to 1 while solving the vertical motion of a falling body problem, the curves moved similarly to the curve in the classical solution.

REFERENCES

1. Ozarslan, R. Ercan, A., Bas, E. (2019). Novel fractional models compatible with real world problems. Fractal and Fractional, 3(2), 15.
2. Acay, B., Bas, E., Abdeljawad, T. (2020). Non-local fractional calculus from different viewpoint generated by truncated *M*-derivative. Journal of Computational and Applied Mathematics, 366, 112410.
3. J.V.D.C. Sousa, E.C. de Oliveira, A new truncated *M*-fractional derivative type unifying some fractional derivative types with classical properties, 2017, arXiv preprint arXiv:1704.08187.
4. Jarad, F., Abdeljawad, T. (2020). Generalized fractional derivatives and Laplace transform. Discrete and Continuous Dynamical Systems -S, 2020,13(3): 709-722.
5. Murray R. Spiegel - Applied Differential Equations-Prentice-Hall, Inc: 62-67 (1967).
6. Schaum’s outline of theory and problems of Laplace transforms. McGraw-Hill Book Co, New York, [©1965].
7. G. W. Leibniz, Letter from Hanover, Germany to G.F.A L'Hospital, September 30, 1695, Leibniz Mathematische Schriften. Olms-Verlag, Hildesheim, Germany, 301, 302, (First published in 1849).
8. G. W. Leibniz, Letter from Hanover, Germany to Johann Bernoulli, December 28, 1695, Leibniz Mathematische Schriften. Olms-Verlag, Hildesheim, Germany, 1962, 226, (First published in 1849).
9. G. W. Leibniz, Letter from Hanover, Germany to John Wallis, May 30, 1697, Leibniz Mathematische Schriften. Olms-Verlag, Hildesheim, Germany, 1962, 25, (First published in 1849).

10. E. Capelas de Oliveira and J. A. Tenreiro Machado, A Review of Definitions for Fractional Derivatives and Integral. Math. Probl. Eng., 2014, (238459), (2014).

11. Jarad, F.; Uğurlu, E.; Abdeljawad, T.; Baleanu, D. On a new class of fractional operators. Adv. Differ. Equ. 2017, 2017, 247.

12. Vanterler, Jose & Capelas de Oliveira, Edmundo. (2017). A new truncated *M*-fractional derivative unifying some fractional derivatives with classical properties. International Journal of Analysis and Applications. 16.

13. Podlubny, I. Fractional Differential Equations; Academic Press: San Diego, CA, USA, 1999.

14. Bas, E.; Ozarslan, R. Real world applications of fractional models by Atangana–Baleanu fractional derivative. Chaos Solitons Fractals 2018, 116, 121–125.

15. Bas, E.; Acay, B.; Ozarslan, R. Fractional models with singular and non-singular kernels for energy efficient buildings. Chaos 2019, 29, 023110.

16. Bas, E.; Ozarslan, R.; Baleanu, D.; Ercan, A. Comparative simulations for solutions of fractional Sturm–Liouville problems with non-singular operators. Adv. Differ. Equ. 2018, 2018, 350.

17. Bas, E. The Inverse Nodal problem for the fractional diffusion equation. Acta Sci. Technol. 2015, 37, 2.

18. Atangana, A.; Baleanu, D. New fractional derivatives with non-local and nonsingular kernel: Theory andapplication to heat transfer model. Therm. Sci. 2016, 20, 763–769.

19. Atangana, A.; Baleanu, D.; Alsaedi, A. Analysis of time-fractional Hunter–Saxton equation: A model ofneumatic liquid crystal. Open Phys. 2016, 14, 145–149.

20. R.; Bastos, N.R.; Monteiro, M.T.T. Modeling some real phenomena by fractional differential equations. Math. Methods Appl. Sci. 2016, 39, 4846–4855.

Investigation of extended type a NLS equation using the extended direct algebraic method

Ahmed Abuhatim[1] and Ebru Cavlak Aslan[1]

[1] Department of Mathematics, University of Firat, Elazig, Turkey

Abstract:

In this study, the soliton solutions of the extended type nonlinear Schrödinger equation are investigated using an extended direct algebraic method. The solutions are found in the form of hyperbolic, trigonometric, and rational functions. Various types of well-known optical solitons, including dark, bright and combo optical soliton have been extracted here.

Keywords: Extended direct algebraic method; the extended type NLSE; Optical soliton; Soliton.

Introduction

The present paper deals with an extended nonlinear Schrödinger (ENLS) equation, expressed in the following dimensionless form:

$$\varphi_t + 3\alpha|\varphi|^2\varphi_x - i\rho\varphi_{xx} + \sigma\varphi_{xxx} - i\delta|\varphi|^2\varphi = 0, \tag{1}$$

where $\varphi(x,t)$ is the unknown complex field, subscripts denote partial derivatives, and α, ρ, σ and δ are real constants. Equation (1) has important applications in distinct physical and mathematical contexts.

1.General properties of proposed method

First of all, the considered nonlinear partial differential equations (NLPDEs)

$$P(u, u_t, u_x, u_{tt}, u_{xx}, \cdots) = 0 \tag{1.1}$$

may be reduced into nonlinear ordinary differential equation by using the wave transformation

$$u(x,t) = U(\varepsilon), \quad \varepsilon = x - vt. \tag{1.2}$$

as

$$G(U, U', U'', \cdots) = 0 \tag{1.3}$$

where v ≠ 0 and $U' = \frac{dU}{d\varepsilon}$. Now, Suppose that the solution of Eq. (1.3) can be consid- ered as following

$$U(\varepsilon) = \sum_{i=0}^{N} \chi_i \varphi^i(\varepsilon), \qquad \chi_N \neq 0 \tag{1.4}$$

Where χ_i, $(0 \leq \mathrm{i} \leq \mathrm{n})$ are constant coefficients to be determined later and $\varphi(\varepsilon)$ satisfies the ODE in theform of

$$\varphi'(\varepsilon) = \ln(A)[\alpha + \beta\varphi(\rho) + \gamma\varphi^2(\rho)], \quad A \neq 0, 1 \tag{1.5}$$

where α, β *and* γ are real constants and respect to parameters seen in the auxiliary equation there are many solutions listed below:

1- When $\beta^2 - 4\alpha\gamma < 0$ and $\gamma \neq 0$,

$$\varphi_1(\varepsilon) = -\frac{\beta}{2\gamma} + \frac{\sqrt{-(\beta^2 - 4\alpha\gamma)}}{2\gamma} tan_A\left(\frac{\sqrt{-(\beta^2 - 4\alpha\gamma)}}{2}\varepsilon\right) \tag{1.6}$$

$$\varphi_2(\varepsilon) = -\frac{\beta}{2\gamma} - \frac{\sqrt{-(\beta^2 - 4\alpha\gamma)}}{2\gamma} cot_A\left(\frac{\sqrt{-(\beta^2 - 4\alpha\gamma)}}{2}\varepsilon\right) \tag{1.7}$$

$$\varphi_3(\varepsilon) = -\frac{\beta}{2\gamma} + \frac{\sqrt{-(\beta^2 - 4\alpha\gamma)}}{2\gamma} \times \left[tan_A\left(\sqrt{-(\beta^2 - 4\alpha\gamma)}\varepsilon\right) \pm \sqrt{pq}sec_A\left(\sqrt{-(\beta^2 - 4\alpha\gamma)}\varepsilon\right)\right] \tag{1.8}$$

$$\varphi_4(\varepsilon) = -\frac{\beta}{2\gamma} + \frac{\sqrt{-(\beta^2 - 4\alpha\gamma)}}{2\gamma} \times \left[cot_A\left(\sqrt{-(\beta^2 - 4\alpha\gamma)}\varepsilon\right) \pm \sqrt{pq}sec_A\left(\sqrt{-(\beta^2 - 4\alpha\gamma)}\varepsilon\right)\right] \tag{1.9}$$

$$\varphi_5(\varepsilon) = -\frac{\beta}{2\gamma} + \frac{\sqrt{-(\beta^2 - 4\alpha\gamma)}}{4\gamma} \times \left[tan_A\left(\frac{\sqrt{-(\beta^2 - 4\alpha\gamma)}\varepsilon}{4}\right) - cot_A\left(\frac{\sqrt{-(\beta^2 - 4\alpha\gamma)}\varepsilon}{4}\right)\right] \tag{1.10}$$

2-When $\beta^2 - 4\alpha\gamma > 0$ and $\gamma \neq 0$

$$\varphi_6(\varepsilon) = -\frac{\beta}{2\gamma} - \frac{\sqrt{\beta^2 - 4\alpha\gamma}}{2\gamma} tanh_A\left(\frac{\sqrt{\beta^2 - 4\alpha\gamma}}{2}\varepsilon\right) \tag{1.11}$$

$$\varphi_7(\varepsilon) = -\frac{\beta}{2\gamma} - \frac{\sqrt{\beta^2 - 4\alpha\gamma}}{2\gamma} coth_A\left(\frac{\sqrt{\beta^2 - 4\alpha\gamma}}{2}\varepsilon\right) \tag{1.12}$$

$$\varphi_8(\varepsilon) = -\frac{\beta}{2\gamma} + \frac{\sqrt{\beta^2 - 4\alpha\gamma}}{2\gamma}\left[tanh_A\left(\sqrt{\beta^2 - 4\alpha\gamma}\varepsilon\right) \pm i\sqrt{pq}sech_A\left(\sqrt{\beta^2 - 4\alpha\gamma}\varepsilon\right)\right] \tag{1.13}$$

$$\varphi_9(\varepsilon) = -\frac{\beta}{2\gamma} + \frac{\sqrt{\beta^2 - 4\alpha\gamma}}{2\gamma}\left[coth_A\left(\sqrt{\beta^2 - 4\alpha\gamma}\varepsilon\right) \pm \sqrt{pq}csch_A\left(\sqrt{\beta^2 - 4\alpha\gamma}\varepsilon\right)\right] \tag{1.14}$$

$$\varphi_{10}(\varepsilon) = -\frac{\beta}{2\gamma} - \frac{\sqrt{\beta^2 - 4\alpha\gamma}}{4\gamma}\left[tanh_A\left(\frac{\sqrt{\beta^2 - 4\alpha\gamma}\varepsilon}{4}\right) \pm coth_A\left(\frac{\sqrt{\beta^2 - 4\alpha\gamma}\varepsilon}{4}\right)\right] \tag{1.15}$$

3-When $\alpha\gamma > 0$ *and* $\beta = 0$

$$\varphi_{11}(\varepsilon) = \sqrt{\frac{\alpha}{\gamma}}tan_A(\sqrt{\alpha\gamma}\varepsilon) \tag{1.16}$$

$$\varphi_{12}(\varepsilon) = -\sqrt{\frac{\alpha}{\gamma}}cot_A(\sqrt{\alpha\gamma}\varepsilon) \tag{1.17}$$

$$\varphi_{13}(\varepsilon) = \sqrt{\frac{\alpha}{\gamma}}\left[tan_A(2\sqrt{\alpha\gamma}\varepsilon) \pm \sqrt{pq}sec_A(2\sqrt{\alpha\gamma}\varepsilon)\right] \tag{1.18}$$

$$\varphi_{14}(\varepsilon) = \sqrt{\frac{\alpha}{\gamma}}\left[cot_A(2\sqrt{\alpha\gamma}\varepsilon) \pm \sqrt{pq}csc_A(2\sqrt{\alpha\gamma}\varepsilon)\right] \tag{1.19}$$

$$\varphi_{15}(\varepsilon) = \frac{1}{2}\sqrt{\frac{\alpha}{\gamma}}\left[tan_A\left(\frac{\sqrt{\alpha\gamma}}{2}\varepsilon\right) - cot_A\left(\frac{\sqrt{\alpha\gamma}}{2}\varepsilon\right)\right] \tag{1.20}$$

4-When $\alpha\gamma < 0$ *and* $\beta = 0$

$$\varphi_{16}(\varepsilon) = -\sqrt{-\frac{\alpha}{\gamma}}tan_A(\sqrt{-\alpha\gamma}\varepsilon) \tag{1.21}$$

$$\varphi_{17}(\varepsilon) = -\sqrt{-\frac{\alpha}{\gamma}}cot_A(\sqrt{-\alpha\gamma}\varepsilon) \tag{1.22}$$

$$\varphi_{18}(\varepsilon) = \sqrt{-\frac{\alpha}{\gamma}}\left[-tan_A(2\sqrt{-\alpha\gamma}\varepsilon) \pm \sqrt{pq}sec_A(2\sqrt{-\alpha\gamma}\varepsilon)\right] \tag{1.23}$$

$$\varphi_{19}(\varepsilon) = \sqrt{-\frac{\alpha}{\gamma}}\left[-cot_A(2\sqrt{-\alpha\gamma}\varepsilon) \pm \sqrt{pq}csc_A(2\sqrt{-\alpha\gamma}\varepsilon)\right] \tag{1.24}$$

$$\varphi_{20}(\varepsilon) = -\frac{1}{2}\sqrt{-\frac{\alpha}{\gamma}}\left[tan_A\left(\frac{\sqrt{-\alpha\gamma}}{2}\varepsilon\right) - cot_A\left(\frac{\sqrt{-\alpha\gamma}}{2}\varepsilon\right)\right] \tag{1.25}$$

5-When $\beta = 0$ *and* $\gamma = \alpha$,

$$\varphi_{21}(\varepsilon) = tan_A(\alpha\varepsilon) \tag{1.26}$$

$$\varphi_{22}(\varepsilon) = -cot_A(\alpha\varepsilon) \tag{1.27}$$

$$\varphi_{23}(\varepsilon) = tan_A(2\alpha\varepsilon) \pm \sqrt{pq}sec_A(2\alpha\varepsilon) \tag{1.28}$$

$$\varphi_{24}(\varepsilon) = -cot_A(2\alpha\varepsilon) \pm \sqrt{pq}csc_A(2\alpha\varepsilon) \tag{1.29}$$

$$\varphi_{25}(\varepsilon) = \frac{1}{2}\left[tan_A\left(\frac{\alpha}{2}\varepsilon\right) - cot_A\left(\frac{\alpha}{2}\varepsilon\right)\right] \tag{1.30}$$

6-When $\beta = 0\ and\ \gamma = -\alpha,$

$$\varphi_{26}(\varepsilon) = -tan_A(\alpha\varepsilon) \tag{1.31}$$

$$\varphi_{27}(\varepsilon) = -cot_A(\alpha\varepsilon) \tag{1.32}$$

$$\varphi_{28}(\varepsilon) = -tan_A(2\alpha\varepsilon) \pm \sqrt{pq}sec_A(2\alpha\varepsilon) \tag{1.33}$$

$$\varphi_{29}(\varepsilon) = -cot_A(2\alpha\varepsilon) \pm \sqrt{pq}csc_A(2\alpha\varepsilon) \tag{1.34}$$

$$\varphi_{30}(\varepsilon) = -\frac{1}{2}\left[tan_A\left(\frac{\alpha}{2}\varepsilon\right) - cot_A\left(\frac{\alpha}{2}\varepsilon\right)\right] \tag{1.35}$$

7-When $\beta^2 = 4\alpha\gamma$

$$\varphi_{31}(\varepsilon) = -\frac{2\alpha(\beta\varepsilon\ln(A) + 2)}{\beta^2\varepsilon\ln(A)} \tag{1.36}$$

8-When $\beta = k, \alpha = mk(m \neq 0) and\ \gamma = 0$

$$\varphi_{32}(\varepsilon) = A^{k\varepsilon} - m \tag{1.37}$$

9-When $\beta = \gamma = 0$

$$\varphi_{33}(\varepsilon) = \alpha\varepsilon\ln(A) \tag{1.38}$$

10-When $\beta = \alpha = 0$

$$\varphi_{34}(\varepsilon) = -\frac{1}{\gamma\varepsilon\ln(A)} \tag{1.39}$$

11-When $\alpha = 0\ and\ \beta \neq 0$

$$\varphi_{35}(\varepsilon) = -\frac{p\beta}{\gamma[cosh_A(\beta\varepsilon) - sinh_A(\beta\varepsilon) + p]} \tag{1.40}$$

$$\varphi_{36}(\varepsilon) = -\frac{\beta[cosh_A(\beta\varepsilon) + sinh_A(\beta\varepsilon)]}{\gamma[cosh_A(\beta\varepsilon) + sinh_A(\beta\varepsilon) + q]} \quad (1.41)$$

12-When $\beta = k, \gamma = mk(m \neq 0) and\ \alpha = 0$

$$\varphi_{37}(\varepsilon) = \frac{pA^{k\varepsilon}}{p - mqA^{k\varepsilon}} \quad (1.42)$$

Where

$$\begin{gathered} tanh_A(\varepsilon) = \frac{pA^{\varepsilon} - qA^{-\varepsilon}}{pA^{\varepsilon} + qA^{-\varepsilon}}, \quad coth_A(\varepsilon) = \frac{pA^{\varepsilon} + qA^{-\varepsilon}}{pA^{\varepsilon} - qA^{-\varepsilon}} \\ sinh_A(\varepsilon) = \frac{pA^{\varepsilon} - qA^{-\varepsilon}}{2}, \quad cosh_A(\varepsilon) = \frac{pA^{\varepsilon} + qA^{-\varepsilon}}{2} \\ tan_A(\varepsilon) = -i\left(\frac{pA^{i\varepsilon} - qA^{-i\varepsilon}}{pA^{i\varepsilon} + qA^{-i\varepsilon}}\right), \quad cot_A(\varepsilon) = i\left(\frac{pA^{i\varepsilon} + qA^{-i\varepsilon}}{pA^{i\varepsilon} - qA^{-i\varepsilon}}\right) \end{gathered} \quad (1.43)$$

where p, q > 0 are arbitrary constants. Determining positive integer N, can be found with the help of balance principle being the highest order derivativewith the highest order nonlinear term in Eq. (1.2). Substituting Eq. (1.4)along with its required derivatives into Eq. (1.2) and compare the coefficients of powers of $\varphi(\varepsilon)$ in resultant equation for obtaining the set of algebraic equations. By solving the over determined system of nonlinear algebraic equa- tions by use of symbolic computation programs, we can get these unknowns $\chi_1, \chi_2, \cdots, \chi_N$. Therefore, we have many new analytical solitons to the Eq. (1.1)

2.Application of method to the extended NLS

$$\varphi_t + 3a_1|\varphi|^2\varphi_x - ia_2\varphi_{xx} + a_3\varphi_{xxx} - ia_4|\varphi|^2\varphi = 0, \quad (2.1)$$

in the equation

$$\varphi(x,t) = \vartheta(\delta)e^{i\mu(x,t)}, \delta = x - vt, \mu(x,t) = -kx + \omega t + \theta \quad (2.2)$$

If the transformation is done, the real and complex parts of equation (2.1) respectively are:

$$(-v - 2ka_2 - 3k^2a_3)\vartheta' + 3a_1\vartheta^2\vartheta' + (a_2 + 3ka_3)\vartheta'' = 0 \quad (2.3)$$

$$(\omega + k^2a_2 + k^3a_3)\vartheta + (-3ka_1 - a_4)\vartheta^3 + a_3\vartheta''' = 0 \quad (2.4)$$

The equation is in this form after solving.
The balancing term N is found to be 1/2 in the equation.

$$\vartheta(\delta) = z(\delta)^{\frac{1}{2}} \quad (2.5)$$

If the transformation is applied

$$\frac{1}{2}(-v - 2ka_2 - 3k^2a_3)z^{\frac{-1}{2}}z' + \frac{3}{2}a_1z^{\frac{1}{2}}z' + (a_2 + 3ka_3)\left(-\frac{1}{4}z^{\frac{-3}{2}}z'^2 + \frac{1}{2}z''z^{-\frac{1}{2}}\right) = 0 \quad (2.6)$$

If we multiply both sides of equation (2.6) by $z^{3/2}$:

$$\frac{1}{2}(-v-2ka_2-3k^2a_3)zz'+\frac{3}{2}a_1z^2z'-\frac{(a_2+3ka_3)}{4}z'^2+\frac{(a_2+3ka_3)}{2}z''z=0 \tag{2.7}$$

Ordinary differential equations in the form have been obtained. Here, the balancing term M=1 is found for equation (2.7) from the terms z^2z' *and* $z''z$.

From equation (1.4)

$$z(\delta)=\chi_0+\chi_1\emptyset(\delta) \tag{2.8}$$

The equation is in this form after solving.

Equation (2.8) is used in (2.7), and the resulting equation is rearranged according to $\emptyset(\delta)$.

$$-\frac{1}{4}\alpha^2a_2\chi_1^2ln^2(A)+\frac{1}{2}\alpha a_2\beta\chi_0\chi_1ln^2(A)+\frac{3}{2}\alpha a_2\chi_0^2\chi_1\ln(A)-\frac{1}{2}\alpha a_3k^2\chi_0\chi_1\ln(A)$$
$$-\frac{1}{4}\alpha^2a_3k\chi_1^2ln^2(A)+\frac{3}{2}\alpha a_3\beta k\chi_0\chi_1ln^2(A)-\alpha a_3k\chi_0\chi_1\ln(A)-\frac{1}{2}\alpha v\chi_0\chi_1\ln(A)=0 \tag{2.9}$$

$$\alpha a_2\gamma\chi_0\chi_1ln^2(A)+3\alpha a_1\chi_0\chi_1^2\ln(A)+\frac{1}{2}a_2\beta^2\chi_0\chi_1ln^2(A)+\frac{3}{2}a_1\beta\chi_0^2\chi_1\ln(A)-\frac{1}{2}\alpha a_3k^2\chi_1^2\ln(A)-$$
$$\frac{3}{2}a_3\beta k^2\chi_0\chi_1\ln(A)+3\alpha a_2\gamma k\chi_0\chi_1log^2(A)-\alpha a_2k\chi_1^2\ln(A)+\frac{3}{2}a_3\beta^2k\chi_0\chi_1ln^2(A)-$$
$$a_2\beta\chi_0\chi_1\ln(A)-\frac{1}{2}\alpha v\chi_1^2\ln(A)-\frac{1}{2}\beta v\chi_0\chi_1\ln(A)=0 \tag{2.10}$$

$$\frac{1}{2}\alpha a_2\gamma\chi_1^2ln^2(A)+\frac{3}{2}\alpha a_1\chi_1^3\ln(A)+\frac{1}{4}a_2\beta^2\chi_1^2ln^2(A)+\frac{3}{2}a_2\beta\gamma\chi_0\chi_1ln^2(A)+3a_1\beta\chi_0\chi_1^2\ln(A)+$$
$$\frac{3}{2}a_1\gamma\chi_0^2\chi_1\ln(A)-\frac{3}{2}a_3\beta k^2\chi_1^2\ln(A)-\frac{3}{2}a_3\gamma k^2\chi_0\chi_1\ln(A)+\frac{3}{2}\alpha a_3\gamma k\chi_1^2ln^2(A)+$$
$$\frac{3}{4}a_3\beta^2k\chi_1^2ln^2(A)+\frac{9}{2}a_3k\beta\gamma\chi_0\chi_1ln^2(A)-a_2\beta k\chi_1^2\ln(A)-a_2\gamma k\chi_0\chi_1\ln(A)-\frac{1}{2}\beta v\chi_1^2\ln(A)-$$
$$\frac{1}{2}\gamma v\chi_0\chi_1\ln(A)=0 \tag{2.11}$$

$$a_2\beta\gamma\chi_1^2ln^2(A)+\frac{3}{2}a_1\beta\chi_1^3\ln(A)+a_2\gamma^2\chi_0\chi_1\ln^2(A)+3a_1\gamma\chi_0\chi_1^2\ln(A)-\frac{3}{2}a_3\gamma k^2\chi_1^2\ln(A)+$$
$$3a_3k\beta\gamma\chi_1^2\ln^2(A)+3a_3\gamma^2k\chi_0\chi_1\ln^2(A)-a_2\gamma k\chi_1^2\ln(A)-\frac{1}{2}\gamma v\chi_1^2\ln(A)=0 \tag{2.12}$$

$$\frac{3}{4}a_2\gamma^2\chi_1^2ln^2(A)+\frac{3}{2}a_1\gamma\chi_1^3\ln(A)+\frac{9}{4}a_3\gamma^2k\chi_1^2ln^2(A)=0 \tag{2.13}$$

An algebraic system of equations is obtained. When this system is solved using Mathematica program,

$$k=\frac{-2v-a_2\beta\ln(A)}{4a_2},\ a_3=0,\ \chi_0=\frac{v+2ka_2-a_2\beta}{3a_1},\ \chi_1=\frac{\gamma\chi_0}{\beta},\ \alpha=0,\ \beta(\beta+\gamma)\neq 0,\ a_1\neq 0,\ \ \gamma\ln(A)\neq 0 \tag{2.14}$$

terms are found.

Case 1:When $\beta^2-4\alpha\gamma<0$ *and* $\gamma\neq 0$

$$\varphi_{1,1}(x,t)=\left(-\frac{a_2}{4a_1}(\beta+\sqrt{-\beta^2}tan\left(\frac{1}{2}\sqrt{-\beta^2}(x-vt)\right))\right)^{\frac{1}{2}}e^{i(\theta-kx+t\omega)} \tag{2.15}$$

$$\varphi_{1,2}(x,t)=\left(-\frac{a_2}{4a_1}(\beta-\sqrt{-\beta^2}cot\left(\frac{1}{2}\sqrt{-\beta^2}(x-vt)\right))\right)^{\frac{1}{2}}e^{i(\theta-kx+t\omega)} \tag{2.16}$$

$$\varphi_{1,3}(x,t) = \Big(-\frac{a_2}{4a_1}(\beta + \sqrt{-\beta^2}tan\left(\sqrt{-\beta^2}(x-vt)\right)$$
$$\pm\sqrt{-\beta^2}\sqrt{pq}sec\left(\sqrt{-\beta^2}(x-vt)\right))\Big)^{1/2} e^{i(\theta-kx+t\omega)} \quad (2.17)$$

$$\varphi_{1,4}(x,t) = \Big(-\frac{a_2}{4a_1}(\beta - \sqrt{-\beta^2}cot\left(\sqrt{-\beta^2}(x-vt)\right)$$
$$\pm\sqrt{-\beta^2}\sqrt{pq}csc\left(\sqrt{-\beta^2}(x-vt)\right))\Big)^{1/2} e^{i(\theta-kx+t\omega)} \quad (2.18)$$

Trigonometric function solutions are found in this form.

Case 2:When $\beta^2 - 4\alpha\gamma > 0$ and $\gamma \neq 0$

$$\varphi_{2,1}(x,t) = \sqrt{-\frac{a_2\left(\beta - \sqrt{-\beta^2}tanh\left(\frac{\sqrt{\beta^2}(x-vt)}{2}\right)\right)}{4a_1}} e^{i(\theta-kx+t\omega)} \quad (2.19)$$

$$\varphi_{2,2}(x,t) = \sqrt{-\frac{a_2\left(\beta - \sqrt{-\beta^2}coth\left(\frac{\sqrt{\beta^2}(x-vt)}{2}\right)\right)}{4a_1}} e^{i(\theta-kx+t\omega)} \quad (2.20)$$

$$\varphi_{2,3}(x,t) = \sqrt{-\frac{a_2\left(\beta + i\sqrt{\beta^2}\sqrt{pq}\,\mathrm{sech}\left(\sqrt{\beta^2}(x-vt)\right) - \sqrt{\beta^2}\tanh\left(\sqrt{\beta^2}(x-vt)\right)\right)}{4a_1}} e^{i(\theta-kx+t\omega)} \quad (2.21)$$

$$\varphi_{2,4}(x,t) = \sqrt{-\frac{a_2\left(\beta + \sqrt{\beta^2}\sqrt{pq}\,\mathrm{csch}\left(\sqrt{\beta^2}(x-vt)\right) - \sqrt{\beta^2}\coth\left(\sqrt{\beta^2}(x-vt)\right)\right)}{4a_1}} e^{i(\theta-kx+t\omega)} \quad (2.22)$$

In this way, analytical solutions are found. This leads to the discovery of dark optical soliton, dark-bright optical soliton, and singular soliton solutions.

Case 3:When $\beta = \alpha = 0$

$$\varphi_{3,1}(x,t) = \sqrt{-\frac{a_2\left(\beta - \frac{1}{x-vt}\right)}{2a_1}} e^{i(\theta-kx+t\omega)} \quad (2.23)$$

Are found.

Case 4:When $\alpha = 0$ and $\beta \neq 0$

$$\varphi_{4,1}(x,t) = \sqrt{-\frac{a_2\left(\beta - \frac{\beta p}{p - sinh(\beta r) + \cosh(\beta r)}\right)}{2a_1}} e^{i(\theta-kx+t\omega)} \quad (2.24)$$

$$\varphi_{4,2}(x,t) = \sqrt{-\frac{a_2 \beta p}{2a_1(q + sinh(\beta r) + \cosh(\beta r))}} e^{i(\theta - kx + t\omega)} \tag{2.25}$$

The solutions are found in the form of hyperbolic functions.

Conclusion.

The paper explores different types of soliton solutions for the extended nonlinear Schrödinger equation using various mathematical methods. The study reveals the existence of dark optical solitons, dark-bright optical solitons, and singular solitons through the application of trigonometric, hyperbolic, and rational functions. The balance principle and extended direct algebraic method are utilized to derive new analytical soliton solutions, leading to the discovery of diverse optical soliton types in the mathematical model.

References

Kurt, A. a. (2020). Applying the new extended direct algebraic method to solve the equation of obliquely interacting waves in shallow waters. *Journal of Ocean University of China, 19*, 772--780.

Rabie, W. B. (2024). Abundant solitons for highly dispersive nonlinear Schrödinger equation with sextic-power law refractive index using modified extended direct algebraic method. *Alexandria Engineering Journal*, 680--689.

Ren, Y. a. (2006). New generalized hyperbolic functions and auto-Backlund transformation to find new exact solutions of the (2+ 1)-dimensional NNV equation. *Physics Letters A*, 438--448.

Rezazadeh, H. (2018). New solitons solutions of the complex Ginzburg-Landau equation with Kerr law nonlinearity. *Optik*, 218--227.

Yepez-Martinez, H. a. (2019). The extended modified method applied to optical solitons solutions in birefringent fibers with weak nonlocal nonlinearity and four wave mixing. *Chinese Journal of Physics*, 137--150.

Zhou, Q. a. (2019). ew optical solitary waves for unstable Schrödinger equation in nonlinear medium. *Optica Applicata*, 135--150.

CONVERSION OF INTEGRAL AND DIFFERENTIAL EQUATIONS TO EACH OTHER

Cemil İNAN[1]

Department of Numerical Methods, University of Mardin Artuklu, Mardin, Turkey

Abstract

In this paper, the conversion of differential equations and integral equations to each other was examined. Differential and integral equations are important topics used in problem solving in applied mathematics and mathematical physics. The ability to transform integral equations and differential equations into each other in problem solving makes it easier to solve problems

Keywords: Differential and İntegral equations, applied mathematics and mathematical physics

1.INTRODUCTION

Equations containing unknown functions under the integral sign are called INTEGRAL EQUATIONS. It is one of the most important types of equations into which many problems especially in applied mathematics and mathematical physics are transformed. While classifying integral equations, the equation is considered from different angles and therefore integral equations emerge under different names. An integral equation for functions of one variable is the most general

$$\Psi(x).\ \Phi(x)-\lambda\int_a^b K(x,y)\Phi dy = f(x)$$

We can give it in its form. Here a and b are constant numbers, λ is a parameter, Ψ (x), f(x) and K(x,y) are functions, and Φ(x) is the unknown function, the domain $a \leq x \leq b$, $a \leq y < b$. Known functions with . The function K(x,y) is called the kernel of the integral equation. (Lovitt-1950)

$$\int_b^x K(x,y)\Phi dy = f(x)$$

If one of the integral limits is a variable such as x, as in the equation, this equation is called "VOLTERRA" Integral Equation,

$$\int_a^b K(x,y)\Phi(y)dy = f(x)$$

As in the equation, both integral limits can be fixed, or equations where one is constant while the other is infinite, or both limits are infinite, are called "FREDHOLM" Integral Equations.

Equations containing an unknown function and some of its derivatives are called differential equations.

$$\frac{dy}{dx} = 2x + 6 \qquad (1)$$

1.Department of Numerical Methods, University of Mardin Artuklu, Mardin, Turkey

2.This study; It was prepared by scanning the literature from the author's graduate thesis seminar at Fırat University, Department of Mathematics, as stated in the sources.

$$5\frac{d^2}{dx^2} + sinx\frac{dy}{dx} - 4xy = 0 \qquad (2)$$

are some differential equations written according to the unknown function?

If an unknown function in a differential equation depends on one and only one independent variable, such equations are called ordinary differential equations.

If the unknown function in a differential equation depends on two or more independent variables, such equations are called partial differential equations.

$$x\frac{d^6y}{dx^6} + 2x^2(\frac{dy}{dx})^2 = Inx \qquad (3)$$

$$ә\frac{ә^2y}{ә\,x^2} + \ 7\frac{ә^2y}{ә\,t^2} = 0 \qquad (4)$$

While the equations up to are ordinary differential equations because they contain only the independent variable, equation (4) is a partial differential equation because it includes both x and t independent variables.

2. GENERAL PROPERTIES OF METHOD

The Concept of Conversion: A differential equation with variable or constant coefficients given with initial conditions can be transformed into a Volterra type integral equation, and an integral equation can also be converted into a differential equation. Therefore, an integral equation can also be considered as a boundary value problem of the differential equation provided for the initial conditions.

1. **Converting a differential equation to an integral equation**

$$\frac{d^ny}{dx^n} + a_1(x)\frac{d^{n-1}y}{dx^{n-1}} + a_2(x)\frac{d^{n-2}y}{dx^{n-2}} + \ldots\ldots + a_{n-1}(x)\frac{dy}{dx} + \ a_n\,(x)y \ = f(x) \qquad (1.1)$$

Let's consider the linear differential equation. Here (i= 1,2,..........,n), the starting point for the ai (x) functions is the smooth point. Also, there are n numbers,

$$y(0) = c_0\,,\ \ y^{\iota}(0) = c_1\ \ ,\ \ \ldots\ldots\ldots\ldots,y^{(n-1)}\,(0) = \ c_{n-1} \qquad (1.2)$$

Let′s assume that the initial conditions are given.

$$\frac{d^ny}{dx^n} = u(x) \qquad (1.3)$$

Let's apply the conversion. This expression

$$\frac{d^ny}{dx^n} = \frac{d}{dx}\left(\frac{d^{n-1}\,y}{dx^{n-1}}\right) = \ u(x)$$

$$\int_0^x d\ \left(\frac{d^{n-1}\,y}{dx^{n-1}}\right) = \int_0^x u(x)dx$$

1.Department of Numerical Methods, University of Mardin Artuklu, Mardin, Turkey

2.This study; It was prepared by scanning the literature from the author's graduate thesis seminar at Fırat University, Department of Mathematics, as stated in the sources.

$$\frac{d^{n-1}y}{dx^{n-1}} = \int_0^x u(x)dx + C_{n-1}$$

Acting similarly, by calculating as follows, the derivative order is reduced by one order.

$$\int_0^x d\left(\frac{d^{n-2}y}{dx^{n-2}}\right) = \int_0^x \left[\!\left[\int_0^x u(x)dx + C_{n-1}\right]\!\right] dx + C_{n-2}$$

$$\left(\frac{d^{n-2}y}{dx^{n-2}}\right) = \int_0^x \int_0^x u(x)dx\,dx + C_{n-1}\int_0^x dx + C_{n-2}$$

$$\left(\frac{d^{n-2}y}{dx^{n-2}}\right) = \int_0^x \int_0^x u(x)dx\,dx + C_{n-1} + C_{n-2}$$

And if we continue thus,

$$\left(\frac{d^{n-3}y}{dx^{n-3}}\right) = \int_0^x \int_0^x \int_0^x u(x)dxdxdx + \frac{1}{2!}C_{n-1}x^2 + C_{n-2}x + C_{n-3}$$

....

....

$$\frac{dy}{dx} = \int_0^x \dots (n-1) \dots \int_0^x u(x)dxdxdx \dots dx + \frac{1}{(n-1)!}C_{n-1}x^{n-2} + \frac{1}{(n-3)!}C_{n-2}x^{n-3} + \dots + C_1$$

And by integrating once more,

$$y = \int_0^x \dots (n) \dots \int_0^x u(x)dx.dx \dots .dx + \frac{1}{(n-1)!}C_{n-1}x^{n-1} + \frac{1}{(n-2)!}C_{n-2}x^{n-2} + \dots + C_1x + C_0$$

It is found.

$$\int \dots (n) \dots \int \square \,(\textit{Write the equation here.})$$

As can be seen here, you will often have to perform operations with multiple (n-fold) integrals. To show this,

$$u(x) + a_1(x)\int_0^x u(x)dx + C_{n-1}a_1(x) + a_2(x)\int_0^x\int_0^x u(x)dx\,dx + C_{n-1}a_2(x) + C_{n-2}a_2(x) +$$

$$a_3(x)\int_0^x\int_0^x\int_0^x u(x)dxdxdx + \frac{1}{2!}C_{n-1}x^2 a_3(x) + C_{n-2}x\,a_3(x) + C_{n-3}a_3(x) + \dots\dots$$

$$+ a_{n-1}(x)\int_0^x \dots (n-1) \dots \int_0^x u(x)dx \dots .dx + \frac{1}{(n-2)!}C_{n-1}x^{n-2}a_{n-1}(x) + \frac{1}{(n-3)!}$$

1.Department of Numerical Methods, University of Mardin Artuklu, Mardin, Turkey

2.This study; It was prepared by scanning the literature from the author's graduate thesis seminar at Fırat University, Department of Mathematics, as stated in the sources.

$$C_{n-2}\, x^{n-3}\, a_{n-1}(x) + \cdots + C_1\ a_{n-1}(x) + a_n(x) \int_0^x \ldots (n) \ldots \int_0^x u(x)dx \ldots\ldots dx + \frac{1}{(n-1)!}$$

$$C_{n-1}\, x^{n-1}\, a_n(x) + \frac{1}{(n-2)!} C_{n-2}\, x^{n-2}\, a_n(x) + \cdots . + C_1 x\ \ a_n(x) + C_0\, a_n(x) = f(x)$$

Also this expression

$$u(x) + a_1(x) \int_0^x u(x)dx + a_2(x) \int_0^x \int_0^x u(x)dx\, dx + a_3(x) \int_0^x \int_0^x \int_0^x u(x)dxdxdx + \cdots +$$

$$a_n(x) \int_0^x \ldots (n) \ldots \int_0^x u(x)dx \ldots\ldots dx = f(x) - C_{n-1}\, a_1(x) - C_{n-1} a_2(x) - \cdots - \int_0^x + \frac{1}{(n-1)!}$$

$$C_{n-1}\, x^{n-1}\, a_n(x) - \ldots - C_{n-2} a_2(x) - C_{n-2}\, x\, a_3(x) - \ldots - \frac{1}{(n-2)!} C_{n-2}\, x^{n-2}\, a_n(x) - \ldots -$$

$$C_1\ a_{n-1}(x) - C_1\ a_{n-1}(x) - C_0\, a_n(x)$$

If it is arranged as follows, the right side of the equation is a function of x and let's denote it with F(x). Here,

$$u(x) + x a_2(x) + \frac{x^2}{2!} a_3(x) + \cdots + \frac{x^{n-1}}{(n-1)!} a_n(x) = f_{n-1}(x)$$

$$a_2(x) + x\, a_3(x) + \ldots + \frac{x^{n-2}}{(n-2)!} a_n(x) = f_{n-2}(x)$$

....

....

$$a_{n-1}(x) + x\, a_n(x) = f_1(x)$$

$$a_n(x) = f_0(x)$$

If it is denoted with

$$F(x) = f(x) - \{C_{n-1}\, f_{n-1}(x) + C_{n-2}(x) f_{n-2}(x) + \ldots\ldots + C_1\, f_1(x) + C_0\, f_0(x))$$

It appears to be the case. The left side of the equation is,

$$\int_0^x \ldots (n) \ldots \int_0^x u(t)dt \ldots dt = \int_0^x \frac{(x-t)^{n-1}}{(n-1)!} u(t)dt \qquad (1.4)$$

It can be expressed as a single integral with the help of the relation. According to this

$$u(x) + a_1(x) \int_0^x u(x)dx + a_2(x) \int_0^x (x-t)u(t) + \cdots . + a_n(x) \int_0^x \frac{(x-t)^{n-1}}{(n-1)!} u(t)dt = F(x)$$

1.Department of Numerical Methods, University of Mardin Artuklu, Mardin, Turkey

2.This study; It was prepared by scanning the literature from the author's graduate thesis seminar at Fırat University, Department of Mathematics, as stated in the sources.

It can be expressed as follows. This is done by taking advantage of definite integral properties.,

$$\mathbf{u(x)} + \int_0^x \left[\mathbf{a_1(x)} + \mathbf{a_2(x)}\,(\boldsymbol{x}-\boldsymbol{t}) + \boldsymbol{a_3(x)}\,\frac{\boldsymbol{x}-\boldsymbol{t})^2}{\mathbf{2!}} + \cdots + \mathbf{a_n(x)}\frac{\mathbf{(x-t)^{n-1}}}{\mathbf{(n-1)!}}\right]\boldsymbol{u(t)dt} = \boldsymbol{F(x)}$$

It can be written as . If the expression in square brackets is considered as a function K (x, t),

$$\boldsymbol{K(x\,,t)} = \mathbf{a_1(x)} + \mathbf{a_2(x)}\,(\boldsymbol{x}-\boldsymbol{t}) + \boldsymbol{a_3(x)}\,\frac{\boldsymbol{x}-\boldsymbol{t})^2}{\mathbf{2!}} + \cdots + \mathbf{a_n(x)}\frac{\mathbf{(x-t)^{n-1}}}{\mathbf{(n-1)!}}$$

It happens. This is the core function and if we write it instead,

$$\mathbf{u(x)} + \int_0^x K(x\,,t)\mathbf{u(t)}\boldsymbol{dt} \;=\; \boldsymbol{F(x)}$$

ın form, II. A typical Volterra equation is arrived at. Thus, the differential equation given by (1.1) turns into an integral equation.

2.Converting Integral Equation to Differential Equation

ıt is also possible to convert an integral equation to a differential equation. For this, it is sufficient to apply the LEIBNITZ relation. This relation performs the differentiation under the integral.

The Leibnitz formula,

$$\frac{dy}{dx}\int_{A(x)}^{B(x)}\frac{\partial F(x,t)}{\partial x}\boldsymbol{dt} + \boldsymbol{F\{x, B(x)\}}\,\frac{dB}{dx} - \boldsymbol{F\{x, A(x)\}}\frac{dA}{dx}$$

If A(x) and B(x) are constants,, $\frac{dA}{dx} = \mathbf{0}$, $\frac{dB}{dx} = \mathbf{0}$ ***Since the formula will be***

$$\frac{dy}{dx}\int_A^B \boldsymbol{\partial F(x,t\,dt} = \int_A^B \frac{\partial F(x,t)}{\partial x}\boldsymbol{dt}$$

used as.

3.APPLICATIONS

1. $$\frac{d^2\,y}{dx^2} + \boldsymbol{p(x)}\frac{dy}{dx} + \boldsymbol{q(x)y} = \boldsymbol{f(x)} \qquad (1.5)$$

Differential equation,

$$\mathbf{y(0)=}\,\boldsymbol{C_0} \quad , \quad \boldsymbol{y^{\iota}}\,\mathbf{(0)} = \boldsymbol{C_1}$$

Let's convert it into an integral equation with initial conditions.

1.Department of Numerical Methods, University of Mardin Artuklu, Mardin, Turkey

2.This study; It was prepared by scanning the literature from the author's graduate thesis seminar at Fırat University, Department of Mathematics, as stated in the sources.

Solution:

$$\frac{\mathbf{d^2\,y}}{\mathbf{dx^2}} = \mathbf{u(x)}$$

let's choose

$$\frac{\mathbf{d^2\,y}}{\mathbf{dx^2}} = \frac{d}{dx}\left(\frac{dy}{dx}\right) = \frac{dy^{\iota}}{dx} \quad ve \quad \frac{dy^{\iota}}{dx} = \mathbf{u(x)}$$

By

$$\int_0^x dy^{\iota} = \int_0^x \mathbf{u(x)}\, dx$$

$$|y^{\iota}|\binom{x}{0} = \int_0^x \mathbf{u(x)} dx \quad \rightarrow y^{\iota}(x) - y^{\iota}(0) = \int_0^x \mathbf{u(x)}\, dx$$

$$y^{\iota}(x) - C_1 = \int_0^x \mathbf{u(x)}\, dx \rightarrow y^{\iota}(x) = \frac{dy}{dx} = \int_0^x \mathbf{u(x)}\, dx + C_1$$

From here too

$$\int_0^x dy = \int_0^x \int_0^x \mathbf{u(x)}\, dxdx + C_1 \int_0^x dx$$

$$|y^{\iota}|\binom{x}{0} = \int_0^x \int_0^x \mathbf{u(x)}\, dxdx + C_1\, |x|\binom{x}{0}$$

$$\mathbf{y(x)} - y(0) = \int_0^x \int_0^x \mathbf{u(x)}\, dxdx + C_1(x-0)$$

$$\mathbf{y(x)} = \int_0^x \int_0^x \mathbf{u(x)}\, dxdx + C_1 x + C_0$$

It is available. On the other hand, according to equation (1.5),

$$\int_0^x \int_0^x \mathbf{u(t)}\, dtdt = \int_0^x (\mathbf{x-t})\, u(t) dt$$

Since they can be written, these can be substituted in equation (1 .5) to give

$$\mathbf{u(x)} + p(x)\left[\int_0^x \mathbf{u(x)}\, dx + C_1\right] + q(x)\left[\int_0^x \int_0^x \mathbf{u(x)}\, dxdx + C_1 x + C_0\right] = f(x)$$

$$\mathbf{u(x)} + p(x) \int_0^x u(t)dt + C_1\, p(x) + q(x) \int_0^x (x-t)\, u(t)dt + (C_1 x + C_0) q(x) = f(x)$$

It is found. this expression

$$\mathbf{u(x)} + \int_0^x [p(x) + (x-t) q(x)]\, u(t)dt = f(x) - [C_1\, p(x) + C_0 q(x) + C_1\, x\, q(x)]$$

If it is arranged as follows, (1.5) the differential equation

$$\mathbf{u(x)} + \int_0^x K(x,t) u(t) dt = F(x)$$

1.Department of Numerical Methods, University of Mardin Artuklu, Mardin, Turkey

2.This study; It was prepared by scanning the literature from the author's graduate thesis seminar at Fırat University, Department of Mathematics, as stated in the sources.

The transformation into a Volterra integral equation is completed in the form

2. Where A and B are constant coefficients,

$$\frac{d^2 y}{dx^2} + A\,\frac{dy}{dx} + By = f(x) \qquad \textbf{(1.6)}$$

Differential equation,

$$f(x) = 0 \quad ;, \quad f(x) \neq 0$$

Let's try to find integral equations suitable for the possible situations.

$$\text{y(0)}= C_0 \quad , \quad y^{\iota}\,(0) = C_1$$

Let's assume that the initial conditions are given.

Solution:

$$\frac{\mathrm{d}^2\,\mathrm{y}}{\mathrm{dx}^2} = \mathbf{u}(\mathbf{x})$$

let's integrate

$$\frac{dy}{dx} = \int_0^x \mathbf{u}(\mathbf{t})\,dt + C_1 \quad \rightarrow y = \int_0^x (x-t)u(t)dt + C_1 x + C_0$$

They will be expressed as . Let's substitute these into equation (1.6).

$$\mathbf{u}(\mathbf{x}) + A\int_0^x u(t)dt + AC_1 + B\int_0^x (\mathrm{x}-\mathrm{t})\,u(t)dt + BC_2\ x + BC_0 = f(x)$$

$$\mathbf{u}(\mathbf{x}) + \int_0^x [A + B(x-t)u(t)dt] = f(x) - [BC_1 x + AC_1 + BC_0\,]$$

$$-\{\mathbf{u}(\mathbf{x}) + BC_1 x + AC_1 + BC_0\} = \int_0^x \{A + B(x-t)\}\ U(t)dt$$

It is arranged as follows and the first side of the equation is

$$\emptyset(x) = -\{\mathbf{u}(\mathbf{x}) + BC_1 x + AC_1 + BC_0\}$$

If considered as a function like, the integral equation

$$\emptyset(x) = \int_0^x \{A + B(x-t)\}\ U(t)dt$$

It takes the form, which is the Volterra equation of Kind I.

Conclusion: If a linear, second-order differential equation with constant coefficients has a second side, II. It is understood that if the genus is second neutral, it will turn into a Genterra I integral equation. However, in both cases, the kernel function f K(x, t) remains unchanged since it is independent of f(x).,

1.Department of Numerical Methods, University of Mardin Artuklu, Mardin, Turkey

2.This study; It was prepared by scanning the literature from the author's graduate thesis seminar at Fırat University, Department of Mathematics, as stated in the sources.

$$K(x,t) = A + B(x-t)$$

It will be found in the form

3.

Given the initial conditions y= 0, y'=1 for x= 0, (1.7)

$$\frac{d^2 y}{dx^2} + y = \boldsymbol{Cosx}$$

Converting a differential equation to an integral equation.

Solution :

$$\frac{d^2 y}{dx^2} = u(x) \rightarrow \int_0^x dy^{\iota} = \int_0^x u(x)dx$$

$$|y^{\iota}(x)|\binom{x}{0} = \int_0^x u(x)dx \rightarrow y^{\iota}(x) - y^{\iota}(0) = \int_0^x u(x)dx$$

$$y^{\iota}(x) - 1 = \int_0^x u(x)dx \rightarrow y^{\iota} = \frac{dy}{dx} = 1 + \int_0^x u(x)dx$$

If it's integrals again

$$\int_0^x dy = \int_0^x [1 + \int_0^x u(x)dx]dx \rightarrow |y(x)|\binom{x}{0} = \int_0^x dx + \int_0^x \int_0^x u(x)dx$$

$$y(x) - y(o) = |x|\binom{x}{0} + \int_0^x (x-t)u(t)dt \rightarrow x + \int_0^x (x-t)u(t)dt = Cosx$$

It is possible. If these are written into equation (1.7),

$$u(x) + x + \int_0^x (x-t)u(t)dt = Cosx$$

Or

$$u(x) = Cosx - x + \int_0^x (x-t)u(t)dt$$

Type II Volterra integral equation is obtained.

4.

$$u(x) - \int_0^x u(t)\, tg\ t\, dt = Sinx \qquad (1.8)$$

The integral equation is given. Since it is known that the initial condition is u(x)=0 for x=0, let's try to convert this integral equation into a differential equation.

Solution:

If the derivative of both sides of the given integral equation is taken,

1.Department of Numerical Methods, University of Mardin Artuklu, Mardin, Turkey

2.This study; It was prepared by scanning the literature from the author's graduate thesis seminar at Fırat University, Department of Mathematics, as stated in the sources.

$$\frac{du(x)}{dx} - \frac{d}{dx}\int_0^x u(t).\,tg\,tdt = \frac{d(sinx)}{dx}$$

$$u^{\iota}(x) - \frac{d}{dx}\int_0^x u(t).\,tg\,tdt = cosx$$

And, according to the Leibnitz formula,

$$\frac{d}{dx}\int_0^x u(t).\,tg\,tdt = \int_0^x 0\,.\,dt + u(x)tg\,x.1 = u(x).\,tg(x)$$

It is found Thus (1.8) of the integral equation

$$u^{\iota}(x) - u(x).\,tg(x) = Cosx$$

It can be seen that it turns into a first order linear differential equation.

5.

$$u(x) = x + \lambda\int_0^x x\,u(t)dt \qquad (1.9)$$

Converting integral equation to differential equation.

Solutıon

If the derivative of both sides is taken,

$$\frac{du(x)}{dx} = \frac{d}{dx} + \lambda\frac{d}{dx}\int_0^x xu(t)dt \qquad (1.10)$$

$$u^{\iota}(x) = 1 + \lambda\frac{d}{dx}\int_0^x xu(t)dt$$

and by applying the Leibnitz formula

$$\frac{d}{dx}\int_0^x xu(t)dt = \int_0^x u(t)dt + x.\,u(x)$$

With

$$u^{\iota}(x) = 1 + \lambda\left[\int_0^x u(t)dt + x.\,u(x)\right]$$

If we differentiate again,

$$\frac{du^{\iota}(x)}{dx} = \frac{d}{dx}(1) + \lambda\frac{d}{dx}\int_0^x u(t)dt + \lambda\frac{d}{dx}\{x.\,u(x)\}$$

$$u^{II}(x) = 0 + \lambda\,u(x) + \lambda\{u(x) + x.\,u^{\iota}(x)\}$$

By arranging this, the differential equation in accordance with equation (1.10) is obtained.

$$u^{II}(x) - \lambda\,u(x) - 2\,\lambda u(x) = 0$$

1.Department of Numerical Methods, University of Mardin Artuklu, Mardin, Turkey

2.This study; It was prepared by scanning the literature from the author's graduate thesis seminar at Fırat University, Department of Mathematics, as stated in the sources.

4.CONCLUSIONS

Creating mathematical models for the problems encountered in the fields studied is important in the theoretical development of almost every field of science. In some branches of science, solving a problem requires establishing a mathematical relation (or mathematical model) that bears the characteristics of the problem. Such a relation usually appears as an equation containing an unknown function and its derivatives, or as a transformed integral equation. In this respect, when difficulties are encountered in solving two equations, it becomes easier to solve them by converting them into each other. It is thought that revisiting these issues will contribute to the literature.

References

1. Aksoy Y., (1998) *İntegral denklemler* Yıldız Teknik Üniversitesi pp1-24
2. Çatalbaş M. N., (1994) *Pizzetti expansion in terms of a singular elliptic operator and some applications*. J. Of Pure& Applied; Math Sci. Vol.39. no:1-2, pp.41-57
3. Çatalbaş M. N., (1991) *Maximum principles for solution of some fourth order singular elliptic equations* Twenty Second Annual Iranian Mathematics Conference Proceedings p.86-90 March 13-16, Ferdowsi University of Mashhad
4. Çatalbaş M. N., & Akın. Ö. (1999 *On maximum principle for a class of forth- under semilinerar singular elliptic equation* J. Of Science Research Foundation science and Engineering. Vol. 2 No:2 p:20-30
5. Esi. A & Çatalbaş M. N (1999) *On solutıons of J. Of Inst. Of math& comp. Sci(Math.Ser.) vol.12 no:2 p:85-93*
6. Mikhlin, S. G.(1957*) İntegral Equations* London pp:23-57
7. Temizer, Ö. F (1997*) integral Denklemler* İnönü Üniversitesi Malatya pp.1-29/63-87
8. Tricomi, F. G (1957) İntegral *Equations pp.32-46 Newyork*
9. Pişkin, E. (2017) *Teori ve Çözümlü Problemlerle Diferansiyel Denklemler* , Seçkin Yayınları ANKara

1.Department of Numerical Methods, University of Mardin Artuklu, Mardin, Turkey

2.This study; It was prepared by scanning the literature from the author's graduate thesis seminar at Fırat University, Department of Mathematics, as stated in the sources.

Ostrowski type inequalities via fractional integrals and related results

Funda Türk[1] **, Samet Erden**[2]

[1,2]Department of Mathematics, University of Bartın, Turkey

fundaturk44@gmail.com, serden@bartin.edu.tr

Abstract

In this work, we introduced the Ostrowski inequality based on M-fractional integrals. we initially established an identity concerning this inequality to prove the Ostrowski inequality based on M-fractional integrals. We derive some results for the Ostrowski inequality utilizing this identity, different convex of classes of functions, and well-known inequalities.

Keywords: Ostrowski; Convex function; Fractional inequality.

1.INTRODUCTION

In 1938, Ostrowski expressed inequality, which has an important place in mathematics, as follows:

Supposing that $\psi : [a,b] \rightarrow R$ is a differentiable function on (a,b) such that the derivative $\psi' : (a,b) \rightarrow R$ is bounded on (a,b), i.e., $\|\psi'\|_\infty = \sup_{\tau \in (a,b)} |\psi'(\tau)| < \infty$. Then, we have

$$\left|\psi(x) - \frac{1}{b-a}\int_a^b \psi(\tau)d\tau\right| \leq \left[\frac{1}{4} + \frac{\left(? - \frac{a+b}{2}\right)^2}{(b-a)^2}\right](b-a)\|\psi'\|_\infty$$

for all $x \in [a,b]$. The constant $\frac{1}{4}$ is the best possible.

Using the Ostrowski inequality, we can estimate the deviation of a smooth function's values from its mean value. Numerous variants of Ostrowski-type inequalities have been examined over time for various classes of functions, including functions of bounded variation, bounded functions, and convex functions. Given that convexity theory is a highly effective and powerful tool for addressing various problems across different branches of pure and applied mathematics, many studies have focused on Ostrowski inequality for convex functions. For example, Alomari et al. established several Ostrowski-type inequalities for s-convex functions [1]. Additionally, previous research has investigated Ostrowski-type inequalities for other forms of convexity [2-5]. Notably, Set was the first to obtain the Riemann--Liouville fractional version of Ostrowski inequality for s-convex functions [6]. Furthermore, many researchers have concentrated on developing Ostrowski-type inequalities for specific fractional integral operators. Muhammed Adil Khan et al. established several Ostrowski-type inequalities for conformable fractional integrals [7]. This study aims to establish some Ostrowski-type inequalities for *M*-fractional integrals. This paper presents many Ostrowski-type inequalities using *M*-fractional integrals, proves an identity related to the Ostrowski inequality for M-fractional integrals, and gives applications in bivariate means theory. Novel and attractive are the concepts and findings presented.

Supposing that $f \; : [0, \infty) \to R$ and $t > 0$. For $0 < \alpha < 1$, we define the M —derivative of order α of function f, denoted $D_M^{\alpha,\beta} f(t)$, by

$$D_M^{\alpha,\beta} f(t) := \lim_{\varepsilon \to 0} \frac{f(tE_\beta(\varepsilon t^{-\alpha})) - f(t)}{\varepsilon},$$

where $E_\beta(x) = \sum_{k=0}^{\infty} \frac{x^k}{\Gamma(\beta k+1)}$, $\beta > 0$, is the Mittag-Leffler function with one parameter. Note that if f is α-differentiable in some interval $(0, a)$, $a > 0$, and $lim_{t\to 0^+} D_M^{\alpha,\beta} f(t)$ exists, then we have

$$D_M^{\alpha,\beta} f(0) = \lim_{t \to 0^+} D_M^{\alpha,\beta} f(t).$$

2.GENERAL PROPERTIES OF METHOD

Lemma 1. *Let* $g \; : \; [a_1, a_2] \to R$ *be an* M *— fractional differentiable function on* (a_1, a_2) *with* $0 \le a_1 < a_2$, $\alpha \in (0,1]$ *and* $\beta > 0$. *If* $D_M^{\alpha,\beta}(g) \in L_\alpha^1([a_1, a_2])$, *then we have the identity*

$$\frac{1}{\Gamma(\beta+1)} g(x) - \frac{\alpha}{(a_2^\alpha - a_1^\alpha)(\Gamma(\beta+1))^2} \int_{a_1}^{a_2} g(s) d_\alpha s$$
$$= \frac{x - a_1}{(a_2^\alpha - a_1^\alpha)} \int_0^1 \left[((1-t)a_1 + tx)^{2\alpha-1} - a_1^\alpha ((1-t)a_1 + tx)^{\alpha-1} \right]$$
$$\times D_M^{\alpha,\beta}(g)((1-t)a_1 + tx) \frac{t^{1-\alpha}}{\Gamma(\beta+1)} d_\alpha t$$
$$+ \frac{a_2 - x}{(a_2^\alpha - a_1^\alpha)} \int_0^1 \left[((1-t)a_2 + tx)^{2\alpha-1} - a_2^\alpha ((1-t)a_2 + tx)^{\alpha-1} \right]$$
$$\times D_M^{\alpha,\beta}(g)((1-t)a_2 + tx) \frac{t^{1-\alpha}}{\Gamma(\beta+1)} d_\alpha t. \tag{1}$$

Proof. Considering the right side of the equality (1), because $d_\alpha t = \frac{\Gamma(\beta+1)}{t^{1-\alpha}}$, it follows that

$$\frac{x - a_1}{(a_2^\alpha - a_1^\alpha)} \int_0^1 \left[((1-t)a_1 + tx)^{2\alpha-1} - a_1^\alpha ((1-t)a_1 + tx)^{\alpha-1} \right]$$
$$\times D_M^{\alpha,\beta}(g)((1-t)a_1 + tx) \frac{t^{1-\alpha}}{\Gamma(\beta+1)} d_\alpha t$$
$$+ \frac{a_2 - x}{(a_2^\alpha - a_1^\alpha)} \int_0^1 \left[((1-t)a_2 + tx)^{2\alpha-1} - a_2^\alpha ((1-t)a_2 + tx)^{\alpha-1} \right]$$
$$\times D_M^{\alpha,\beta}(g)((1-t)a_2 + tx) \frac{t^{1-\alpha}}{\Gamma(\beta+1)} d_\alpha t$$
$$= \frac{x - a_1}{(a_2^\alpha - a_1^\alpha)} \int_0^1 \left[((1-t)a_1 + tx)^{2\alpha-1} - a_1^\alpha ((1-t)a_1 + tx)^{\alpha-1} \right] D_M^{\alpha,\beta}(g)((1-t)a_1 + tx) dt$$

$$+\frac{a_2-x}{(a_2^\alpha-a_1^\alpha)}\int_0^1\left[\left((1-t)a_2+tx\right)^{2\alpha-1}-a_2^\alpha\left((1-t)a_2+tx\right)^{\alpha-1}\right]D_M^{\alpha,\beta}(g)\left((1-t)a_2+tx\right)dt.$$

Because of the realtion between M-fractional derivative and clasical derivative, one has

$$\int_0^1\left[\left((1-t)a_1+tx\right)^{2\alpha-1}-a_1^\alpha\left((1-t)a_1+tx\right)^{\alpha-1}\right]D_M^{\alpha,\beta}(g)\left((1-t)a_1+tx\right)dt$$
$$=\frac{1}{\Gamma(\beta+1)}\int_0^1\left[\left((1-t)a_1+tx\right)^{\alpha}-a_1^\alpha\right]g'\left((1-t)a_1+tx\right)dt$$

and

$$\int_0^1\left[\left((1-t)a_2+tx\right)^{2\alpha-1}-a_2^\alpha\left((1-t)a_2+tx\right)^{\alpha-1}\right]D_M^{\alpha,\beta}(g)\left((1-t)a_2+tx\right)dt.$$
$$=\frac{1}{\Gamma(\beta+1)}\int_0^1\left[\left((1-t)a_2+tx\right)^{\alpha}-a_2^\alpha\right]g'\left((1-t)a_2+tx\right)dt.$$

Using the change of the variable $(1-t)a_1+tx=u$ and $dt=\frac{du}{x-a_1}$ after applying integration by parts for M-fractional integrals

$$\frac{1}{\Gamma(\beta+1)}\int_0^1\left[\left((1-t)a_1+tx\right)^{\alpha}-a_1^\alpha\right]g'\left((1-t)a_1+tx\right)dt$$
$$=\frac{1}{\Gamma(\beta+1)}\left[\left((1-t)a_1+tx\right)^{\alpha}-a_1^\alpha\right]\frac{g\left((1-t)a_1+tx\right)}{(x-a_1)}\Bigg|_0^1$$
$$-\frac{1}{\Gamma(\beta+1)}\int_0^1\alpha\left((1-t)a_1+tx\right)^{\alpha-1}g\left((1-t)a_1+tx\right)dt$$
$$=\frac{1}{\Gamma(\beta+1)}\left(\frac{x^\alpha-a_1^\alpha}{x-a_1}g(x)-\frac{\alpha}{(x-a_1)\Gamma(\beta+1)}\int_{a_1}^x g(s)d_\alpha s\right),$$

and using the change of the variable $(1-t)a_2+tx=v$ and $dt=\frac{dv}{x-a_2}$ after applying integration by parts for M-fractional integrals

$$\frac{1}{\Gamma(\beta+1)}\int_0^1\left[\left((1-t)a_2+tx\right)^{\alpha}-a_2^\alpha\right]g'\left((1-t)a_2+tx\right)dt$$
$$=\frac{1}{\Gamma(\beta+1)}\left[\left((1-t)a_2+tx\right)^{\alpha}-a_2^\alpha\right]\frac{g\left((1-t)a_2+tx\right)}{x-a_2}\Bigg|_0^1$$
$$-\frac{1}{\Gamma(\beta+1)}\int_0^1\alpha\left((1-t)a_2+tx\right)^{\alpha-1}g\left((1-t)a_2+tx\right)dt$$
$$=\frac{1}{\Gamma(\beta+1)}\left(\frac{a_2^\alpha-x^\alpha}{a_2-x}g(x)-\frac{\alpha}{(a_2-x)\Gamma(\beta+1)}\int_x^{a_2} g(s)d_\alpha s\right)$$

Then we have the equality

$$\frac{x-a_1}{(a_2^\alpha-a_1^\alpha)}\int_0^1\left[\left((1-t)a_1+tx\right)^{2\alpha-1}-a_1^\alpha\left((1-t)a_1+tx\right)^{\alpha-1}\right]D_M^{\alpha,\beta}(g)\left((1-t)a_1+tx\right)dt$$

$$+\frac{a_2-x}{(a_2^\alpha-a_1^\alpha)}\int_0^1\left[\left((1-t)a_2+tx\right)^{2\alpha-1}-a_2^\alpha\left((1-t)a_2+tx\right)^{\alpha-1}\right]D_M^{\alpha,\beta}(g)\left((1-t)a_2+tx\right)dt$$
$$=\frac{x-a_1}{(a_2^\alpha-a_1^\alpha)}\frac{1}{\Gamma(\beta+1)}\left(\frac{x^\alpha-a_1^\alpha}{x-a_1}g(x)-\frac{\alpha}{(x-a_1)\Gamma(\beta+1)}\int_{a_1}^{x}g(s)d_\alpha s\right)$$
$$+\frac{a_2-x}{(a_2^\alpha-a_1^\alpha)}\frac{1}{\Gamma(\beta+1)}\left(\frac{a_2^\alpha-x^\alpha}{a_2-x}g(x)-\frac{\alpha}{(a_2-x)\Gamma(\beta+1)}\int_{x}^{a_2}g(s)d_\alpha s\right)$$
$$=\frac{1}{\Gamma(\beta+1)}g(x)-\frac{\alpha}{(a_2^\alpha-a_1^\alpha)\left(\Gamma(\beta+1)\right)^2}\int_{a_1}^{a_2}g(s)d_\alpha s$$

Theorem 2. *Let* $g\ :\ [a_1,a_2]\to R$ *be an* $M-$*fractional differentiable function on* (a_1,a_2) *with* $0\le a_1<a_2$, $\alpha\in(0,1]$, $\beta>0$, *and* $D_M^{\alpha,\beta}(g)\in L_\alpha^1([a_1,a_2])$. *If* $|g'(x)|$ *is convex on* $[a_1,a_2]$, *then one has the inequality*

$$\left|\frac{1}{\Gamma(\beta+1)}g(x)-\frac{\alpha}{(a_2^\alpha-a_1^\alpha)\left(\Gamma(\beta+1)\right)^2}\int_{a_1}^{a_2}g(s)d_\alpha s\right|$$
$$\le\frac{x-a_1}{(a_2^\alpha-a_1^\alpha)\Gamma(\beta+1)}\Delta_1+\frac{a_2-x}{(a_2^\alpha-a_1^\alpha)\Gamma(\beta+1)}\Delta_2 \tag{2}$$

where

$$\Delta_1=\frac{1}{6}a_1^{\alpha-1}x|g'(a_1)|+\frac{1}{12}x^{\alpha-1}a_1|g'(a_1)|+\frac{1}{12}x|g'(a_1)|-\frac{1}{4}a_1^\alpha|g'(a_1)|$$
$$+\frac{1}{12}a_1|g'(x)|+\frac{1}{12}x^{\alpha-1}a_1|g'(x)|+\frac{1}{4}x|g'(x)|-\frac{1}{2}a_1^\alpha x|g'(x)|,$$
$$\Delta_2=\frac{1}{6}a_2^\alpha|g'(a_2)|-\frac{1}{6}x^\alpha|g'(a_2)|+\frac{1}{3}a_2^\alpha|g'(x)|-\frac{1}{3}x^\alpha|g'(x)|.$$

proof: *Let* $y>0,\theta_1,\theta_2$ and $|g'|$ be convex function then $\theta_1=y^{\alpha-1}$ $\theta_2(y)=-y^\alpha$. *it follows from Lemma 1 that*

$$\left|\frac{1}{\Gamma(\beta+1)}g(x)-\frac{\alpha}{(a_2^\alpha-a_1^\alpha)\left(\Gamma(\beta+1)\right)^2}\int_{a_1}^{a_2}g(s)d_\alpha s\right|$$
$$\le\frac{x-a_1}{(a_2^\alpha-a_1^\alpha)\Gamma(\beta+1)}\int_0^1\left[\left((1-t)a_1+tx\right)^\alpha-a_1^\alpha\right]\left|g'\left((1-t)a_1+tx\right)\right|dt$$
$$+\frac{a_2-x}{(a_2^\alpha-a_1^\alpha)\Gamma(\beta+1)}\int_0^1[(a_2^\alpha-(1-t)a_2+tx)^\alpha]\left|g'\left((1-t)a_2+tx\right)\right|dt$$
$$\le\frac{x-a_1}{(a_2^\alpha-a_1^\alpha)\Gamma(\beta+1)}\int_0^1\left[\left((1-t)a_1+tx\right)^{\alpha-1}\left((1-t)a_1+tx\right)-a_1^\alpha\right]\left|g'\left((1-t)a_1+tx\right)\right|dt$$
$$+\frac{a_2-x}{(a_2^\alpha-a_1^\alpha)\Gamma(\beta+1)}\int_0^1[(a_2^\alpha-(1-t)a_2^\alpha+tx^\alpha)]\left|g'\left((1-t)a_2+tx\right)\right|dt$$

$$\le\frac{x-a_1}{(a_2^\alpha-a_1^\alpha)\Gamma(\beta+1)}\int_0^1\left[\left((1-t)a_1^{\alpha-1}+tx^{\alpha-1}\right)\left((1-t)a_1+tx\right)-a_1^\alpha\right]\left|g'\left((1-t)a_1+tx\right)\right|dt$$
$$+\frac{a_2-x}{(a_2^\alpha-a_1^\alpha)\Gamma(\beta+1)}\int_0^1[(a_2^\alpha-(1-t)a_2^\alpha+tx^\alpha)]\left|g'\left((1-t)a_2+tx\right)\right|dt$$

$$\leq \frac{x-a_1}{(a_2^\alpha - a_1^\alpha)\Gamma(\beta+1)} \int_0^1 \left[\left((1-t)a_1^{\alpha-1} + tx^{\alpha-1}\right)\left((1-t)a_1 + tx\right) - a_1^\alpha\right]$$

$$\times [(1-t)|g'(a_1)| + t|g'(x)|]\mathrm{d}t$$

$$+\frac{a_2-x}{(a_2^\alpha - a_1^\alpha)\Gamma(\beta+1)} \int_0^1 [(a_2^\alpha - (1-t)a_2^\alpha + tx^\alpha)][(1-t)|g'(a_2)| + t|g'(x)|]dt$$

$$= \frac{x-a_1}{(a_2^\alpha - a_1^\alpha)\Gamma(\beta+1)} \Delta_1 + \frac{a_2-x}{(a_2^\alpha - a_1^\alpha)\Gamma(\beta+1)} \Delta_2$$

If we calculate the integrals

$$\Delta_1 = \int_0^1 \left[\left((1-t)a_1^{\alpha-1} + tx^{\alpha-1}\right)\left((1-t)a_1 + tx\right) - a_1^\alpha\right][(1-t)|g'(a_1)| + t|g'(x)|]dt$$

$$= |g'(a_1)| \int_0^1 \left[\left((1-t)a_1^{\alpha-1} + tx^{\alpha-1}\right)\left((1-t)a_1 + tx\right) - a_1^\alpha\right](1-t)dt$$

$$+|g'(x)| \int_0^1 \left[\left((1-t)a_1^{\alpha-1} + tx^{\alpha-1}\right)\left((1-t)a_1 + tx\right) - a_1^\alpha\right]tdt$$

and

$$\Delta_2 = \int_0^1 [(a_2^\alpha - (1-t)a_2^\alpha + tx^\alpha)][(1-t)|g'(a_2)| + t|g'(x)|]dt$$

$$= |g'(a_2)| \int_0^1 [(a_2^\alpha - (1-t)a_2^\alpha + tx^\alpha)](1-t)dt$$

$$+|g'(x)| \int_0^1 [(a_2^\alpha - (1-t)a_2^\alpha + tx^\alpha)]tdt,$$

then we reach the requaired inequaity (2).

Corollary 3. *Let* $x = (a_1 + a_2)/2$ *. Then theorem 2 leads to*

$$\left|\frac{1}{\Gamma(\beta+1)} g\left(\frac{a_1+a_2}{2}\right) - \frac{\alpha}{(a_2^\alpha - a_1^\alpha)\left(\Gamma(\beta+1)\right)^2} \int_{a_1}^{a_2} g(s) d_\alpha s\right|$$

$$\leq \frac{a_2-a_1}{2(a_2^\alpha - a_1^\alpha)\Gamma(\beta+1)} \left[\left(\frac{2a_1^{\alpha-1}a_2 - 10a_1^\alpha + a_1 + a_2}{24}\right)|g'(a_1)| -\right.$$

$$+\frac{a_1}{12}\left(\frac{a_1+a_2}{2}\right)^{\alpha-1} |g'(a_1)| + \left(\frac{5a_1 + 3a_2 - 12a_1^\alpha}{24}\right)\left|g'\left(\frac{a_1+a_2}{2}\right)\right|$$

$$+\frac{a_1}{12}\left(\frac{a_1+a_2}{2}\right)^{\alpha-1} \left|g'\left(\frac{a_1+a_2}{2}\right)\right| + \frac{1}{6}a_2^\alpha|g'(a_2)| - \frac{1}{6}\left(\frac{a_1+a_2}{2}\right)^\alpha |g'(a_2)|$$

$$\left.+\frac{a_2^\alpha}{3}\left|g'\left(\frac{a_1+a_2}{2}\right)\right| - \frac{1}{3}\left(\frac{a_1+a_2}{2}\right)^\alpha \left|g'\left(\frac{a_1+a_2}{2}\right)\right|\right].$$

Remark 4. *If* $\alpha = \beta = 1$, then corollary 3 becomes

$$\left|\frac{1}{\Gamma(\beta+1)} g\left(\frac{a_1+a_2}{2}\right) - \frac{\alpha}{(a_2^\alpha - a_1^\alpha)\left(\Gamma(\beta+1)\right)^2} \int_{a_1}^{a_2} g(s) d_\alpha s\right|$$

$$\le \frac{a_2-a_1}{24\Gamma(\beta+1)}\left(\frac{a_1+a_2}{2}\right)^{\alpha-1}\left(|g'(a_1)|+4\left|g'\left(\frac{a_1+a_2}{2}\right)\right|+|g'(a_2)|\right)$$
$$\le \frac{a_2-a_1}{8\Gamma(\beta+1)}(|g'(a_1)|+|g'(a_2)|)$$

where the second inequality is obtained by using the convexity of $|g'|$.

Theorem 5. *Let* $q>1$, $K>0$, $g : [a_1,a_2]\to R$ *be an* $M-$*fractional differentiable function on* (a_1,a_2) *with* $0\le a_1<a_2$, $\alpha\in(0,1]$, $\beta>0$, *and* $D_M^{\alpha,\beta}(g)\in L_\alpha^1([a_1,a_2])$. *If* $|g'(x)|$ *is convex on* $[a_1,a_2]$,. *then the inequality*

$$\left|\frac{1}{\Gamma(\beta+1)}g\left(\frac{a_1+a_2}{2}\right)-\frac{\alpha}{(a_2^\alpha-a_1^\alpha)\big(\Gamma(\beta+1)\big)^2}\int_{a_1}^{a_2}g(s)d_\alpha s\right|$$
$$\le K\frac{x-a_1}{(a_2^\alpha-a_1^\alpha)\Gamma(\beta+1)}\big(A_1(\alpha)\big)^{1-1/q}\big(A_2(\alpha)+A_3(\alpha)\big)^{1/q}$$
$$+K\frac{a_2-x}{(a_2^\alpha-a_1^\alpha)\Gamma(\beta+1)}\big(B_1(\alpha)\big)^{1-1/q}\big(B_2(\alpha)+B_3(\alpha)\big)^{1/q}$$

from $|g'|^q$ is convex on $[a_1,a_2]$ and $|g'(x)|^q\le K$, that

$$A_1(\alpha)=\frac{x^{\alpha+1}-a_1^{\alpha+1}}{(\alpha+1)(x-a_1)}-a_1^\alpha,\ B_1(\alpha)=a_2^\alpha-\frac{x^{\alpha+1}-a_2^{\alpha+1}}{(\alpha+1)(a_2-x)}$$
$$A_2(\alpha)=-\frac{a_1^{\alpha+1}}{(\alpha+1)(x-a_1)}\frac{(\alpha+2)(x-a_1)+a_1}{(\alpha+2)(x-a_1)}+\frac{x^{\alpha+2}}{(\alpha+1)(x-a_1)^2(\alpha+2)}-\frac{a_1^\alpha}{2},$$
$$B_2(\alpha)=\frac{a_2^\alpha}{2}+\frac{a_2^{\alpha+1}}{(\alpha+1)(a_2-x)}\frac{(\alpha+2)(a_2-x)+a_2}{(\alpha+2)(a_2-x)}-\frac{x^{\alpha+2}}{(\alpha+1)(a_2-x)^2(\alpha+2)}$$
$$A_3(\alpha)=\frac{x^{\alpha+1}}{(\alpha+1)(x-a_1)}\frac{(\alpha+2)(x-a_1)-x}{(\alpha+2)(x-a_1)}+\frac{a_1^{\alpha+2}}{(\alpha+1)(x-a_1)^2(\alpha+2)}-\frac{a_1^\alpha}{2},$$
$$B_3(\alpha)=\frac{a_2^\alpha}{2}-\frac{x^{\alpha+1}}{(\alpha+1)(a_2-x)}\frac{(\alpha+2)(a_2-x)-x}{(\alpha+2)(a_2-x)}-\frac{a_2^{\alpha+2}}{(\alpha+1)(a_2-x)^2(\alpha+2)}.$$

Proof: power-mean inequality and the convexity of $|g'|^q$ together with and from lemma 1, the identities

$$\int_0^1\left(\big((1-t)a_1+tx\big)^\alpha-a_1^\alpha\right)dt=\frac{x^{\alpha+1}-a_1^{\alpha+1}}{(\alpha+1)(x-a_1)}-a_1$$

and

$$\int_0^1\left(a_2^\alpha-\big((1-t)a_2+tx\big)^\alpha\right)dt=a_2^\alpha-\frac{x^{\alpha+1}-a_2^{\alpha+1}}{(\alpha+1)(a_2-x)}$$

we clearly see that

$$\left|\frac{1}{\Gamma(\beta+1)}g(x)-\frac{\alpha}{(a_2^\alpha-a_1^\alpha)\big(\Gamma(\beta+1)\big)^2}\int_{a_1}^{a_2}g(s)d_\alpha s\right|$$
$$\le\frac{x-a_1}{(a_2^\alpha-a_1^\alpha)\Gamma(\beta+1)}\int_0^1\left[\big((1-t)a_1+tx\big)^\alpha-a_1^\alpha\right]\left|g'\big((1-t)a_1+tx\big)\right|dt$$

$$+\frac{a_2-x}{(a_2^\alpha-a_1^\alpha)\Gamma(\beta+1)}\int_0^1\left(a_2^\alpha-\left((1-t)a_2+tx\right)^\alpha\right)\left|g'\left((1-t)a_2+tx\right)\right|dt \tag{3}$$

$$\int_0^1\left[\left((1-t)a_1+tx\right)^\alpha-a_1^\alpha\right]\left|g'\left((1-t)a_1+tx\right)\right|dt$$
$$\leq\left(\int_0^1\left(\left((1-t)a_1+tx\right)^\alpha-a_1^\alpha\right)dt\right)^{1-1/q}$$
$$\times\left(\int_0^1\left(\left((1-t)a_1+tx\right)^\alpha-a_1^\alpha\right)\left|g'\left((1-t)a_1+tx\right)\right|^q dt\right)^{1/q} \tag{4}$$

and

$$\int_0^1\left(a_2^\alpha-\left((1-t)a_2+tx\right)^\alpha\right)\left|g'\left((1-t)a_2+tx\right)\right|dt$$
$$\leq\left(\int_0^1\left(a_2^\alpha-\left((1-t)a_2+tx\right)^\alpha\right)dt\right)^{1-1/q}$$
$$\times\left(\int_0^1\left(a_2^\alpha-\left((1-t)a_2+tx\right)^\alpha\right)\left|g'\left((1-t)a_2+tx\right)\right|^q dt\right)^{1/q}, \tag{5}$$

from this integrals

$$\int_0^1\left(\left((1-t)a_1+tx\right)^\alpha-a_1^\alpha\right)\left|g'\left((1-t)a_1+tx\right)\right|^q dt$$
$$\leq\int_0^1\left(\left((1-t)a_1+tx\right)^\alpha-a_1^\alpha\right)[(1-t)|g'(a_1)|^q+t|g'(x)|^q]dt$$
$$=|g'(a_1)|^q\int_0^1\left(\left((1-t)a_1+tx\right)^\alpha-a_1^\alpha\right)(1-t)dt$$
$$+|g'(x)|^q\int_0^1\left(\left((1-t)a_1+tx\right)^\alpha-a_1^\alpha\right)t\,dt$$
$$=|g'(a_1)|^q\left(-\frac{a_1^{\alpha+1}}{(\alpha+1)(x-a_1)}\frac{(\alpha+2)(x-a_1)+a_1}{(\alpha+2)(x-a_1)}+\frac{x^{\alpha+2}}{(\alpha+1)(x-a_1)^2(\alpha+2)}-\frac{a_1^\alpha}{2}\right)$$
$$+|g'(x)|^q\left(\frac{x^{\alpha+1}}{(\alpha+1)(x-a_1)}\frac{(\alpha+2)(x-a_1)-x}{(\alpha+2)(x-a_1)}+\frac{a_1^{\alpha+2}}{(\alpha+1)(x-a_1)^2(\alpha+2)}-\frac{a_1^\alpha}{2}\right)$$
$$\leq K^q\left(-\frac{a_1^{\alpha+1}}{(\alpha+1)(x-a_1)}\frac{(\alpha+2)(x-a_1)+a_1}{(\alpha+2)(x-a_1)}+\frac{x^{\alpha+2}}{(\alpha+1)(x-a_1)^2(\alpha+2)}-\frac{a_1^\alpha}{2}\right)$$
$$+K^q\left(\frac{x^{\alpha+1}}{(\alpha+1)(x-a_1)}\frac{(\alpha+2)(x-a_1)-x}{(\alpha+2)(x-a_1)}+\frac{a_1^{\alpha+2}}{(\alpha+1)(x-a_1)^2(\alpha+2)}-\frac{a_1^\alpha}{2}\right) \tag{6}$$

and

$$\int_0^1\left(a_2^\alpha-\left((1-t)a_2+tx\right)^\alpha\right)\left|g'\left((1-t)a_2+tx\right)\right|^q dt$$
$$\leq\int_0^1\left(a_2^\alpha-\left((1-t)a_2+tx\right)^\alpha\right)[(1-t)|g'(a_2)|^q+t|g'(x)|^q]dt$$
$$=|g'(a_2)|^q\int_0^1\left(a_2^\alpha-\left((1-t)a_2+tx\right)^\alpha\right)(1-t)dt$$

$$+|g'(x)|^q \int_0^1 \left(a_2^\alpha - \left((1-t)a_2 + tx\right)^\alpha\right) t dt$$

$$= |g'(a_2)|^q \left(\frac{a_2^\alpha}{2} + \frac{a_2^{\alpha+1}}{(\alpha+1)(a_2-x)} \frac{(\alpha+2)(a_2-x)+a_2}{(\alpha+2)(a_2-x)} - \frac{x^{\alpha+2}}{(\alpha+1)(a_2-x)^2(\alpha+2)}\right)$$

$$+|g'(x)|^q \left(\frac{a_2^\alpha}{2} - \frac{x^{\alpha+1}}{(\alpha+1)(a_2-x)} \frac{(\alpha+2)(a_2-x)-x}{(\alpha+2)(a_2-x)} - \frac{a_2^{\alpha+2}}{(\alpha+1)(a_2-x)^2(\alpha+2)}\right)$$

$$\leq K^q \left(\frac{a_2^\alpha}{2} + \frac{a_2^{\alpha+1}}{(\alpha+1)(a_2-x)} \frac{(\alpha+2)(a_2-x)+a_2}{(\alpha+2)(a_2-x)} - \frac{x^{\alpha+2}}{(\alpha+1)(a_2-x)^2(\alpha+2)}\right)$$

$$+K^q \left(\frac{a_2^\alpha}{2} - \frac{x^{\alpha+1}}{(\alpha+1)(a_2-x)} \frac{(\alpha+2)(a_2-x)-x}{(\alpha+2)(a_2-x)} - \frac{a_2^{\alpha+2}}{(\alpha+1)(a_2-x)^2(\alpha+2)}\right). \tag{7}$$

Thus, Theorem 5 follows easily from (3)-(7).

Remark 6. *Let* $\alpha = 1$. Then Theorem 5 becomes

$$\left|\frac{1}{\Gamma(\beta+1)} g(x) - \frac{\alpha}{(a_2^\alpha - a_1^\alpha)\left(\Gamma(\beta+1)\right)^2} \int_{a_1}^{a_2} g(s) d_\alpha s\right|$$

$$\leq K \frac{x-a_1}{(a_2-a_1)\Gamma(\beta+1)} \left(A_1(1)\right)^{1-1/q} [A_2(1) + A_3(1)]^{1/q}$$

$$+ \frac{a_2-x}{(a_2-a_1)\Gamma(\beta+1)} \left(B_1(1)\right)^{1-1/q} [B_2(1) + B_3(1)]^{1/q}$$

where

$$A_1(1) = \frac{x-a_1}{2}, \quad B_1(1) = \frac{a_2-x}{2},$$

$$A_2(1) = \frac{3a_1^2 x + 6a_1^2 + x^3 - 3a_1 x^2 - 3a_1^3}{6(x-a_1)^2},$$

$$B_2(1) = \frac{7a_2^3 x + 3a_2 x^2 - 9a_2^2 x - x^3}{6(a_2-x)^2},$$

$$A_3(1) = \frac{2x^3 - 2a_1^3 - 6a_1 x^2 + 6a_1^2 x}{6(x-a_1)^2},$$

$$B_3(1) = \frac{2a_2^3 x - 6a_2 x + 2x^3}{6(a_2-x)^2}.$$

Theorem 7. *Let* $q > 1, K > 0$, $g : [a_1, a_2] \to R$ be an $M-$fractional differentiable function with $0 \leq a_1 < a_2$, $\alpha \in (0,1]$, $\beta > 0$, *and* $D_M^{\alpha,\beta}(g) \in L_\alpha^1([a_1, a_2])$. Then

$$\left|\frac{1}{\Gamma(\beta+1)} g(x) - \frac{\alpha}{(a_2^\alpha - a_1^\alpha)\left(\Gamma(\beta+1)\right)^2} \int_{a_1}^{a_2} g(s) d_\alpha s\right|$$

$$\leq K \frac{x-a_1}{(a_2^\alpha - a_1^\alpha)\Gamma(\beta+1)} \left(A_1(\alpha)\right)^{1-1/q} \left(\frac{-8a_1^\alpha + 2a_1^{\alpha-1}x + 2x^{\alpha-1}a_1 + 4x^\alpha}{12}\right)^{1/q}$$

$$+K \frac{a_2-x}{(a_2^\alpha - a_1^\alpha)\Gamma(\beta+1)} \left(B_1(\alpha)\right)^{1-1/q} \left(\frac{a_2^\alpha - x^\alpha}{2}\right)^{1/q}$$

from $|g'|^q$ is convex on $[a_1, a_2]$ and $|g'(x)|^q \leq K,$ where

$$A_1(\alpha) = \frac{2a_1^\alpha + a_1^{\alpha-1}x + x^{\alpha-1}a_1 + 2x^\alpha - 6a_1^\alpha}{6}, \quad B_1(\alpha) = \frac{a_2^\alpha - x^\alpha}{2}.$$

Proof. We obtain from the proof of Theorem 2 that

$$\left|\frac{1}{\Gamma(\beta+1)} g(x) - \frac{\alpha}{(a_2^\alpha - a_1^\alpha)\big(\Gamma(\beta+1)\big)^2} \int_{a_1}^{a_2} g(s) d_\alpha s\right|$$
$$\leq \frac{x - a_1}{(a_2^\alpha - a_1^\alpha)\Gamma(\beta+1)} \int_0^1 \left[\left((1-t)a_1^{\alpha-1} + tx^{\alpha-1}\right)\left((1-t)a_1 + tx\right) - a_1^\alpha\right] \left|g'\left((1-t)a_1 + tx\right)\right| dt$$
$$+ \frac{a_2 - x}{(a_2^\alpha - a_1^\alpha)\Gamma(\beta+1)} \int_0^1 [(a_2^\alpha - (1-t)a_2^\alpha + tx^\alpha)] \left|g'\left((1-t)a_2 + tx\right)\right| dt \tag{8}$$

from the identities together with the power-mean inequality and convexity of $|g'|^q$

$$\int_0^1 \left[\left((1-t)a_1^{\alpha-1} + tx^{\alpha-1}\right)\left((1-t)a_1 + tx\right) - a_1^\alpha\right] dt = \frac{2a_1^\alpha + a_1^{\alpha-1}x + x^{\alpha-1}a_1 + 2x^\alpha - 6a_1^\alpha}{6}$$

and

$$\int_0^1 [(a_2^\alpha - (1-t)a_2^\alpha + tx^\alpha)] dt = \frac{a_2^\alpha - x^\alpha}{2}$$

we get

$$\int_0^1 \left[\left((1-t)a_1^{\alpha-1} + tx^{\alpha-1}\right)\left((1-t)a_1 + tx\right) - a_1^\alpha\right] \left|g'\left((1-t)a_1 + tx\right)\right| dt$$
$$\leq \left(\int_0^1 \left(\left((1-t)a_1^{\alpha-1} + tx^{\alpha-1}\right)\left((1-t)a_1 + tx\right) - a_1^\alpha\right) dt\right)^{1-1/q}$$
$$\times \left(\int_0^1 \left(\left((1-t)a_1^{\alpha-1} + tx^{\alpha-1}\right)\left((1-t)a_1 + tx\right) - a_1^\alpha\right) \left|g'\left((1-t)a_1 + tx\right)\right|^q dt\right)^{1/q} \tag{9}$$

and

$$\int_0^1 \left(a_2^\alpha - \left((1-t)a_2^\alpha + tx^\alpha\right)\right) \left|g'\left((1-t)a_2 + tx\right)\right| dt$$
$$\leq \left(\int_0^1 \left(a_2^\alpha - \left((1-t)a_2^\alpha + tx^\alpha\right)\right) dt\right)^{1-1/q}$$
$$\times \left(\int_0^1 \left(a_2^\alpha - \left((1-t)a_2^\alpha + tx^\alpha\right)\right) \left|g'\left((1-t)a_2 + tx\right)\right|^q dt\right)^{1/q} \tag{10}$$

We obtain

$$\int_0^1 \left(\left((1-t)a_1^{\alpha-1} + tx^{\alpha-1}\right)\left((1-t)a_1 + tx\right) - a_1^\alpha\right) \left|g'\left((1-t)a_1 + tx\right)\right|^q dt$$
$$\leq \int_0^1 \left(\left((1-t)a_1^{\alpha-1} + tx^{\alpha-1}\right)\left((1-t)a_1 + tx\right) - a_1^\alpha\right) [(1-t)|g'(a_1)|^q + t|g'(x)|^q] dt$$

$$= |g'(a_1)|^q \int_0^1 \left(\left((1-t)a_1^{\alpha-1} + tx^{\alpha-1}\right)\left((1-t)a_1 + tx\right) - a_1^\alpha\right)(1-t)dt$$
$$+|g'(x)|^q \int_0^1 \left(\left((1-t)a_1^{\alpha-1} + tx^{\alpha-1}\right)\left((1-t)a_1 + tx\right) - a_1^\alpha\right)tdt$$
$$= |g'(a_1)|^q \left(\frac{1}{4}a_1^\alpha + \frac{1}{12}a_1^{\alpha-1}x + \frac{1}{12}x^{\alpha-1}a_1 + \frac{1}{12}x^\alpha - \frac{1}{2}a_1^\alpha\right)$$
$$+|g'(x)|^q \left(\frac{1}{12}a_1^\alpha + \frac{1}{12}a_1^{\alpha-1}x + \frac{1}{12}x^{\alpha-1}a_1 + \frac{1}{4}x^\alpha - \frac{1}{2}a_1^\alpha\right)$$
$$\leq K^q \left(\frac{-8a_1^\alpha + 2a_1^{\alpha-1}x + 2x^{\alpha-1}a_1 + 4x^\alpha}{12}\right) \tag{11}$$

sımılarly

$$\int_0^1 \left(a_2^\alpha - \left((1-t)a_2^\alpha + tx^\alpha\right)\right)\left|g'\left((1-t)a_2 + tx\right)\right|^q dt$$
$$\leq \int_0^1 \left(a_2^\alpha - \left((1-t)a_2^\alpha + tx^\alpha\right)\right)[(1-t)|g'(a_2)|^q + t|g'(x)|^q]dt$$
$$= |g'(a_2)|^q \left(\frac{a_2^\alpha - x^\alpha}{6}\right) + |g'(x)|^q \left(\frac{a_2^\alpha - x^\alpha}{3}\right)$$
$$\leq K^q \left(\frac{a_2^\alpha - x^\alpha}{2}\right) \tag{12}$$

consequently, theorem (7) follows easily from (8)-(12).

3.APPLICATIONS

Let $a_1, a_2 > 0$ with $a_1 \neq a_2$. Generalized logarithmic mean $L_{(\alpha,r)}(a_1, a_2)$, logarithmic mean $L(a_1, a_2)$, the arithmetic mean $A(a_1, a_2)$ of a_1 and a_2 are defined by

$$A(a_1, a_2) = \frac{a_1 + a_2}{2},$$

$$L(a_1, a_2) = \frac{a_2 - a_1}{\log a_2 - \log a_1},$$

and

$$L_{(\alpha,r)}(a_1, a_2) = \left[\frac{\alpha({a_2}^{r+\alpha} - {a_1}^{r+\alpha})}{(r+\alpha)({a_2}^\alpha - {a_1}^\alpha)}\right]^{\frac{1}{r}},$$

respectively.

Specifically, considering the functions $g(x) = x^r$ and $g(x) = \frac{1}{x}$, Then corollary 3 immediately leads to the following inequalities involving arithmatic and logarithmic menas.

If we consider the function $g(x) = x^r$, then we have

$$g\left(\frac{a_1 + a_2}{2}\right) = \left(\frac{a_1 + a_2}{2}\right)^r = [A(a_1, a_2)]^r$$

and

$$\int_{a_1}^{a_2} g(s) d_\alpha s = \Gamma(\beta + 1) \frac{a_2^{r+\alpha} - a_1^{r+\alpha}}{(r + \alpha)}.$$

Theorem *Let* $r > 1$, $\alpha \in (0,1]$ *and* $\beta > 0$. *Then we have the inequality*

$$\left|\frac{[A(a_1, a_2)]^r}{\Gamma(\beta + 1)} - \frac{\left[L_{(\alpha,r)}(a_1, a_2)\right]^r}{\Gamma(\beta + 1)}\right|$$
$$\leq \frac{r(a_2 - a_1)}{2(a_2^\alpha - a_1^\alpha)\Gamma(\beta + 1)} \left[\left(\frac{2a_1^{\alpha-1} a_2 - 10a_1^\alpha + a_1 + a_2}{24}\right) |a_1|^{r-1}\right.$$
$$+ \frac{a_1}{12} |a_1|^{r-1} [A(a_1, a_2)]^{\alpha-1} + |A(a_1, a_2)|^{r-1} \left(\frac{5a_1 + 3a_2 - 12a_1^\alpha}{24}\right)$$
$$+ \frac{a_1}{12} |A(a_1, a_2)|^{r-1} [A(a_1, a_2)]^{\alpha-1} + \frac{1}{6} a_2^\alpha |a_2|^{r-1} - \frac{1}{6} [A(a_1, a_2)]^\alpha |a_2|^{r-1}$$
$$\left.+ \frac{a_2^\alpha}{3} |A(a_1, a_2)|^{r-1} - \frac{1}{3} |A(a_1, a_2)|^{r-1} [A(a_1, a_2)]^\alpha\right].$$

If we consider the function $g(x) = \frac{1}{x}$, then we have

$$g\left(\frac{a_1 + a_2}{2}\right) = \left(\frac{a_1 + a_2}{2}\right)^{-1} = [A(a_1, a_2)]^{-1}$$

and

$$\int_{a_1}^{a_2} g(s) d_\alpha s = \Gamma(\beta + 1) \frac{a_2^{\alpha-1} - a_1^{\alpha-1}}{(\alpha - 1)}.$$

Theorem *Let* $r > 1$, $\alpha \in (0,1]$ *and* $\beta > 0$. *Then we have the inequality*

$$\left|\frac{[A(a_1, a_2)]^{-1}}{\Gamma(\beta + 1)} - \frac{\left[L_{(\alpha,-1)}(a_1, a_2)\right]^{-1}}{\Gamma(\beta + 1)}\right|$$
$$\leq \frac{a_2 - a_1}{2(a_2^\alpha - a_1^\alpha)\Gamma(\beta + 1)} \left[\left(\frac{2a_1^{\alpha-1} a_2 - 10a_1^\alpha + a_1 + a_2}{24}\right) |a_1|^{-2}\right.$$
$$+ \frac{a_1}{12} [A(a_1, a_2)]^{\alpha-1} |a_1|^{-2} + \left(\frac{5a_1 + 3a_2 - 12a_1^\alpha}{24}\right) |A(a_1, a_2)|^{-2}$$
$$+ \frac{a_1}{12} |A(a_1, a_2)|^{-2} [A(a_1, a_2)]^{\alpha-1} - + \frac{1}{6} a_2^\alpha |a_2|^{-2} - \frac{1}{6} [A(a_1, a_2)]^\alpha |a_2|^{-2}$$
$$\left.+ \frac{a_2^\alpha}{3} |A(a_1, a_2)|^{-2} - \frac{1}{3} |A(a_1, a_2)|^{-2} [A(a_1, a_2)]^\alpha\right].$$

4.CONCLUSIONS

The well-known Ostrowski inequality is the subject of numerous results. Numerous applications of this inequality can be found in numerical analysis. Results for Ostrowski inequality for *M*-fractional integrals are presented in this study, along with their applications to means. Firstly, we establish an identity related to the *M*-fractional integrals Ostrowski inequality. We derive many findings for the inequality utilizing this identity, convexity of several classes of functions, and other well-known inequalities. In particular situations, the inequalities derived here are also shown to correspond to certain known results. Finally, we also show case applications from Formans. The hypothesis could lead to additional studies in the M-fractional integral theory field.

REFERENCES

1. Alomari, M., Darus, M., Dragomir, S.S., Cerone, P., Ostrowski type inequalities for functions whose derivatives are s-convex in the second sense, Appl. Math. Letter, Vol:23, No:9, 1071--1076, 2010.
2. Kavurmaci H, Özdemir ME, New Ostrowski type inequalities for *m*-convex functions and applications, Hacettepe Journal of Mathematics and Statistics, Vol:40, No:2, 135-145, 2011.
3. Matłoka M., Ostrowski type inequalities for functions whose derivatives are *h*-convex via fractional integrals, J Sci Res Rep., Vol:2014, 1633-1641, 2014.
4. Ozdemir ME, Kavurmaci H, Set E., Ostrowski's type inequalities for (α, m)-convex function. Kyungpook Math J., Vol:50, No:3, 371-378, 2010.
5. Tunç M., Ostrowski-type inequalities via *h*-convex functions with applications to special means, J Inequal Appl, Vol:2013, No:1,1-10, 2013.
6. Set E., New inequalities of Ostrowski type for mappings whose derivatives are *s*-convex in the second sense via fractional integrals, Comput Math Appl., Vol:63, No:7, 1147-1154, 2012.
7. Muhammad, Adil Khan, Sumbel, Begum, Yousaf, Khurshid Yu-Ming, Chu, Ostrowski type inequalities involving conformable fractional integrals, Journal of Inequalities and Applications, Vol:70, 1-14, 2018.
8. Anastassiou, G. A., M-fractional integral inequalities, J. Comput. Anal. Appl, Vol:29, No:6, 1153-1158, 2021.
9. Dragomir, S. S.,, A functional generalization of Ostrowski inequality via Montgomery identity. Acta Math. Univ. Comenian (N.S.), Vol:84, No:1, 63-78, 2015.
10. Dragomir, S.S., The Ostrowski integral inequality for mappings of bounded variation, Bull. Aust. Math. Soc., Vol:60, 495–508, 1999.

11. Dragomir, S.S., Refinements of the generalised trapezoid and Ostrowski inequalities for functions of bounded variation, Arch. Math., Vol:91, No:5, 450–460, 2008.
12. Dragomir, S.S., A companion of Ostrowski's inequality for functions of bounded variation and applications., Int. J. Nonlinear Anal. Appl., Vol:5, No:1, 89–97, 2014.
13. Alomari, M.W., A companion of Dragomir's generalization of the Ostrowski inequality and applications to numerical integration., Ukr. Math. J., Vol:64, No:4, 491–510, 2012.
14. Cerone, P., Cheung, W.S., Dragomir, S.S., On Ostrowski type inequalities for Stieltjes intergals with absolutely continuous integrands and integrators of bounded variation. Comput. Math. Appl., Vol:54, No:2, 183–191, 2007.
15. Tseng, K.-L.,Improvements of the Ostrowski integral inequality for mappings of bounded variation II, Appl. Math. Comput., Vol:218, No:10, 5841–5847, 2012.
16. G. A. Anastassiou, Fractional Left Local General M-Derivative. Intelligent Analysis: Fractional Inequalities and G. A. Anastassiou, Fractional Right Local General M-Derivative. Intelligent Analysis: Fractional Inequalities and Approximations Expanded, 511-520, 2020.
17. G. A. Anastassiou, Ostrowski type inequalities, Proc. AMS, Vol:123, 3775-3781, 1995.
18. Chu, Y.-M., Zhang, X.-M., Wang, G.-D.: The Schur geometrical convexity of the extended mean values. J. Convex Anal. Vol:15, No:4, 707--718, 2008.
19. Agarwal RP, Luo M-J, Raina RK. On Ostrowski type inequalities. Fasciculi Math., Vol:56, 5-27, 2016.
20. Budak, H., Hezenci, F., Kara, H., On parameterized inequalities of Ostrowski and Simpson type for convex functions via generalized fractional integrals., Mathematical Methods in the Applied Sciences, Vol:44, No:17, 12522-12536, 2021.
21. Budak Hüseyin, Sarıkaya Mehmet Zeki, A new generalization of Ostrowski type inequality for mappings of bounded variation, RGMIA Research Report Collection, Vol:18, 2015.
22. Sarikaya, Mehmet Zeki, Samet Erden, and Hüseyin Budak, Some generalized Ostrowski type inequalities involving local fractional integrals and applications, Adv. Inequal. Appl, Vol:2016, 2016.

8th International Conference on Computational Mathematics and Engineering Sciences

17 – 19 May 2024,

Şanlıurfa – Türkiye